MEASUREMENTS IN THE BOUNDARY LAYER ON A SMOOTH FLAT PLATE IN SUPERSONIC FLOW

Thesis by

Donald Coles

In Partial Fulfillment of the Requirements

For the Degree of

Doctor of Philosophy

California Institute of Technology

Pasadena, California

1953

ACKNOWLEDGMENTS

A contemporary Texan, J. Frank Dobie, has said in another context that research is frequently a process of moving old bones from one graveyard to another. Those who have tried to find their way recently in the formidable literature of boundary layers may agree that the metaphor is often apt enough, but will perhaps be moved to excuse some redundancies in the present report.

It is obvious that many persons must have contributed to the success of the current boundary layer research. Among them, Hans Wolfgang Liepmann of the Guggenheim Aeronautical Laboratory has on many occasions provided both inspiration and encouragement. At the Jet Propulsion Laboratory, Frank Goddard has supported the research enthusiastically since its inception in 1950. Finally, solution of many problems of instrumentation would have been immensely more difficult without the services of Duncan Griffith, in whose hands tools become living things.

Summary

In Section I available measurements in low-speed turbulent boundary layer flow are compared with a simple analysis based on functional similarity, and the boundary layer is found to be unique within the accuracy of the experimental data. Some consequences of the mean equations of motion are obtained, including the distribution of shearing stress through the boundary layer, and an attempt is made to generalize the relationship known as the law of the wall to flows with variable density.

In Section II some problems encountered in the development and use of the floating surface element and other instrumentation are discussed in detail.

In Section III are presented measurements of mean and local surface friction carried out on a flat plate model in the 20-inch supersonic wind tunnel at the Jet Propulsion Laboratory. The boundary layer flow is studied for free stream Mach numbers of 2.0, 2.6, 3.7, and 4.5. The experiments, which involve nominal Reynolds numbers from 2×10^5 to 9×10^6, include a few measurements in laminar flow, but emphasize transition and the turbulent regime. The effectiveness of various tripping devices is mentioned, and the problem of defining an effective Reynolds number for the fully turbulent flow is discussed at length. Finally, turbulent boundary layer profile measurements are examined for consistency with low-speed data, with a generalized mixing length theory, and with the analysis of Section I of the present report.

Table of Contents

Figures

Tables

Table of Symbols

a	a constant
A	(1) a constant; (2) area of stream tube; (3) effective area of probe entrance
A_o	geometric area of probe entrance
b	a constant
C	a constant
C_1	velocity profile parameter defined by Eq. (29)
C_2	velocity profile parameter defined by Eq. (30)
C_D	(1) measured friction drag coefficient of a plate, defined by Eq. (1); (2) drag coefficient of a cylinder
C_f	ideal local friction drag coefficient of a plate, defined by Eqs. (8) and (12)
C_{f_i}	value of C_f for fluid of constant density
C_F	ideal mean friction drag coefficient of a plate, defined by Eqs. (9) and (15)
C_{F_i}	value of C_F for fluid of constant density
d	distance separating plates in channel calibration
D	measured friction drag of a plate
D_o	form drag of surface roughness
e	base of the natural logarithms, e = 2.71828.....
E	modulus of elasticity in bending
f	(1) an unspecified function in the law of the wall or elsewhere; (2) force on the floating element in the channel calibration
F	an unspecified function in the velocity defect law
g	dimension of gap around the floating element
h	distance implied by apparent shear in a pressure gradient

I moment of inertia in bending

k spring constant of the flexure system

l characteristic or mixing length in analysis of turbulent shear flow

m (1) energy parameter for compressible flow, defined by Eq. (38); (2) mass, in mass flow rate dm/dt

M Mach number

n exponent in power law velocity profile

p static pressure

p_c corrected static pressure in nozzle calibration

p_o' impact pressure

p_o'' pressure upstream of metering orifice

P a function of x defined by Eq. (102)

q free stream dynamic pressure, $\rho_1 u_1^2/2$

r (1) temperature recovery factor, $(T_w-T_1)/(T_o-T_1)$; (2) notation for velocity ratio u/u_τ

R (1) ideal Reynolds number defined in context, $u_1 \ell/\nu_1$; (2) gas constant in Eq. (98)

R' Reynolds number per inch

R_g Reynolds number of flow through element clearance gap

R_j Reynolds number for air jet tripping device, defined on page 141

R_s sublayer Reynolds number, defined by Eq. (42)

R_t ideal Reynolds number at point of maximum shearing stress

R_δ boundary layer thickness Reynolds number, $u_1 \delta/\nu_1$

R_θ ideal momentum thickness Reynolds number, $u_1 \theta/\nu_1$

R_Θ measured momentum thickness Reynolds number, $u_1 \Theta/\nu_1$

s most upstream value of x for fully developed turbulent boundary layer

S a function of x defined by Eq. (103)

T	static temperature
T_c	balance chamber temperature
T'_o	local stagnation temperature in boundary layer
u	streamwise velocity in boundary layer
u'	streamwise velocity fluctuation
u_τ	friction velocity defined by Eq. (20) or (78)
U	streamwise velocity modified by density factor, defined by Eq. (80)
v	normal velocity in boundary layer
v'	normal velocity fluctuation
V	normal velocity modified by density factor, defined by Eq. (80)
w	(1) a width dimension; (2) a weight in element calibration
W	weight of portion of floating element assembly
x	distance from plate leading edge
x_o	value of x at apparent origin of turbulent boundary layer
y	distance from the wall
z	a variable of integration
α	angle of attack, positive when surface pressure increases
γ	ratio of specific heats, C_p/C_v
δ	thickness of the boundary layer
$\delta+$	upper limit of integration for which integrand vanishes
δ^*	displacement thickness of the boundary layer, defined by Eq. (32) or (97)
Δ	(1) an increment; (2) value of Howarth variable at edge of boundary layer
η	Howarth variable, defined initially by Eq. (89) and finally by Eq. (94)
θ	ideal momentum thickness, defined by Eqs. (10) and (11)
Θ	measured momentum thickness, defined by Eq. (33) or (96)

θ_o apparent momentum thickness for form drag of roughness, defined by Eq. (14)

$\varkappa$ mixing parameter, first used in Eq. (23)

λ a length connected with surface shearing stress distribution, defined by Eq. (60)

μ viscosity; see Eq. (39)

ν kinematic viscosity, μ/ρ

ξ ideal analog of experimental length coordinate $(x-x_o)$

ρ density

ρ_v reference density in Eq. (80)

ρ_τ reference density in Eq. (78)

τ shearing stress

φ a function in the velocity profile, Eq. (23)

ψ a function of x and y defined by Eq. (59) or Eq. (85)

Subscripts:

o value at isentropic stagnation condition

s value at edge of sublayer

w value at wall

1 value in free stream

1,2 initial and final values of variable in question

I. The Problem of the Turbulent Boundary Layer

A. Introduction

Historically, experimental measurements of the magnitude of surface friction have usually preceded the development of adequate methods of prediction, and the present study of supersonic boundary layers is a case in point. Before undertaking the interpretation of the data obtained during the current research, therefore, it is desirable to examine the turbulent boundary layer problem in some detail from the experimental point of view, in an effort to identify the features which must eventually appear in any successful analysis of boundary layer flow.

If experimental measurements could be compared with an exact solution of the equations of fluid motion for the particular model geometry involved, any discrepancies could be assigned to error in the measurements or to failure of the equations to describe the behavior of the fluid in question. In practice, however, a comparison of physical and mathematical models for the case of viscous flow over a flat plate can be achieved only in an asymptotic sense, first because of mathematical approximations which are not uniformly valid in the entire flow field, and second because of physical imperfections which are idealized or ignored in the usual theoretical treatment.

The idea of an asymptotic correspondence between actual and assumed conditions is essential to any definition of the boundary

layer problem. For laminar shear flow this idea, which is explicit in the boundary layer concept of Prandtl (1), is acquiring an increasingly precise mathematical formulation, and the recent development of methods for improving the theoretical analysis in this respect is a conspicuous sign of current interest in the question (2, 3, 4, 5).

On the other hand, the present inadequate state of knowledge of turbulent shear flows requires the corresponding definition of the turbulent boundary layer problem to be almost completely heuristic, so that the validity of a particular analysis can only be tested in the light of experimental evidence. It is proposed to illustrate this difficulty by a brief discussion of the flat plate boundary layer, using an analysis which is frankly phenomenological and which is therefore less vulnerable to criticism of concept than an analysis which assumes one or another mechanism for the various turbulent transport processes.

The need for such a discussion is obvious in the present research program, whose primary objective is to establish experimentally the influence of compressibility on the turbulent boundary layer flow along a flat plate. While the review given here is designed to provide a point of departure for the study of compressible boundary layers, and while an attempt will be made later to generalize some of the relevant considerations to the case of a fluid of variable density, it should be remembered that the purpose of the discussion is to facilitate the interpretation of experimental data rather than to suggest or to support a particular

theoretical analysis of the turbulent boundary layer.

B. The Boundary Layer with Constant Density

1. General Considerations. The remarks of the present paper refer to steady two-dimensional mean flow past a flat plate at sufficiently large Reynolds numbers so that the boundary layer hypothesis may be assumed to apply. It is further assumed, unless otherwise specified, that there is no heat transfer between the plate and the fluid, and that the pressure, density, and velocity of the external flow are uniform.

Early experiments, particularly those carried out in towing tanks, were in most cases designed to determine a mean friction coefficient from its definition in terms of the dynamic pressure and of the drag per unit width of one side of a flat surface,

$$D(x) = q \times C_D(x) \tag{1}$$

while an alternative method makes use of the equivalence of the drag force and the rate of momentum change in the boundary layer or in the wake,

$$D(x) = \int_0^{\delta+} \rho u (u_1 - u)\, dy \tag{2}$$

Finally, the total drag may be equated to the sum of the downstream components of the integrated tangential and normal forces,

$$D(x) = \int_0^x \tau_w(x)\, dx + D_0(x) \tag{3}$$

where the second term on the right represents the form drag of any roughness elements which may be present on the plate surface.

The first two equations above are usually combined in the form

$$C_D(x) = \frac{2}{x}\,\Theta(x) \tag{4}$$

in which the boundary layer momentum thickness Θ is defined by the definite integral

$$\Theta(x) = \int_0^{\delta+} \frac{\rho}{\rho_1}\frac{u}{u_1}\left(1 - \frac{u}{u_1}\right) dy \tag{5}$$

The first and third equations in turn provide a relationship between drag and local friction,

$$C_D(x) = \frac{1}{x}\int_0^x \frac{\tau_w(x)}{q}\,dx + \frac{D_0(x)}{q\,x} \tag{6}$$

so that

$$\frac{\tau_w(x)}{q} = 2\frac{d\Theta}{dx} - \frac{1}{q}\frac{d\,D_0(x)}{dx} \tag{7}$$

The notation in these expressions is chosen deliberately in order to emphasize that x, τ_w/q, C_D, and Θ are experimentally measured quantities. The essence of most boundary layer research consists of the assumption that there exist corresponding uniquely defined quantities ξ, C_f, C_F, and θ, which may be associated with an ideal boundary layer, and of the attempt to determine the

latter quantities by necessarily imperfect experimental techniques. That is, by definition,

$$C_f = C_f(\xi) = \frac{d}{d\xi}\xi C_F(\xi) = 2\frac{d\theta}{d\xi} \tag{8}$$

$$C_F = C_F(\xi) = \frac{1}{\xi}\int_0^{\xi} C_f(\xi)\,d\xi = 2\frac{\theta}{\xi} \tag{9}$$

$$\theta = \theta(\xi) = \frac{1}{2}\xi C_F(\xi) = \frac{1}{2}\int_0^{\xi} C_f(\xi)\,d\xi \tag{10}$$

In order to establish a connection between the experimental and ideal quantities defined above, it is necessary to introduce an additional hypothesis. The assumption usually made is that the effect of conditions near the leading edge on the surface friction far downstream will eventually vanish, in the sense that the function $\Theta(x)$ for a smooth plate is the ideal relationship $\theta(\xi)$ subject to a possible displacement of the streamwise coordinate; in other words, downstream of a particular point $x = s$,

$$\Theta(x) = \theta(x - x_0) \tag{11}$$

While the experimental data will show that the hypothesis (11) may be sufficiently general in practice, a similar but less restrictive assumption may be made in terms of the local surface friction;

$$\frac{\tau_w(x)}{q} = C_f(x - x_0) \tag{12}$$

It follows from (12) that the ideal momentum thickness is given by the expression, obtained from Eqs. (4), (6), and (10),

$$\theta (x - x_o) = \textcircled{H}(x) - \textcircled{H}_o \tag{13}$$

where

$$\textcircled{H}_o = \frac{D_o}{2q} + \frac{1}{2}\int_0^s \frac{\tau_w(x)}{q}\,dx - \frac{1}{2}\int_0^{s-x_o} C_f(\xi)\,d\xi \tag{14}$$

The definition (14) assumes that the form drag D_o is independent of x downstream of $x = s$, as will be the case for example if D_o is associated with finite leading edge curvature or with the presence of boundary layer tripping devices on the surface of the plate.

Finally, Eqs. (8), (9), and (13) imply

$$C_F(x - x_o) = 2\,\frac{\textcircled{H}(x) - \textcircled{H}_o}{x - x_o} \tag{15}$$

$$C_f(x - x_o) = 2\,\frac{d\textcircled{H}}{dx} = \frac{\tau_w(x)}{q} \tag{16}$$

The remarks above apply to both laminar and turbulent boundary layers* for arbitrary surface heat transfer and free stream Mach

---

* The definition of momentum thickness in Eq. (5) above should be slightly modified for a turbulent boundary layer; see for example (6). However, since the usual experimental methods for measurement of mean velocity involve errors of comparable magnitude, no distinction will be made here. Note also that Eq. (14) with $\textcircled{H}_o = 0$ provides a relationship between the drag of a tripping device, D_o, and the position of the apparent origin of the boundary layer at $x = x_o$.

number. The analysis leading to Eqs. (13) - (16) is carried out here formally and in detail both because of its generality and because the considerations mentioned are fundamental to any evaluation of experimental data. The presence of the parameter $\mathcal{H}_o$ in Eq. (15) immediately raises the question of uniqueness, especially for the turbulent boundary layer, since the hypothesis (11) implies (12) while the converse is not true. The term uniqueness, in the sense used here, refers to the validity of a comparison of the ideal function $\Theta(C_f)$, obtained by eliminating the variable ξ between the functions $\Theta(\xi)$ and $C_f(\xi)$ of Eqs. (8) and (10), with its experimental analog $\mathcal{H}(\tau_w/q)$. The suggestion that the slope of the experimental curve $\mathcal{H}(x)$ may not imply a unique value of the ordinate $\mathcal{H}$ is precisely equivalent to the introduction of the constant of integration $\mathcal{H}_o$. Since Θ increases with ξ, it is apparent that sufficiently far downstream the parameters x_o and $\mathcal{H}_o$ will always become small compared to x and $\mathcal{H}$ respectively. However, the sense in which an asymptotic correspondence between the real and ideal boundary layers is defined by this property is not the sense in which the concept is most appropriate to the experimental problem, as will be emphasized later.

The question of uniqueness can be examined more closely for the laminar boundary layer, since the theoretical solution is known within the limitations of the boundary layer approximation (7, 8), and has been verified experimentally by Dryden (9), Liepmann (10), Dhawan (11), and others. The laminar equations are satisfied by a function of a single independent variable equivalent to $y/\sqrt{\xi}$. The consequent similarity of the various velocity profiles along

the plate implies that the boundary layer momentum thickness is inversely proportional to the slope of the velocity profile at the wall, so that the functional relationship $\theta(C_f)$ mentioned above is

$$C_f R_\theta = C \tag{17}$$

for the laminar boundary layer, with $R_\theta = u_1 \theta / \nu_1$. The value of the constant C depends on Mach number; for incompressible flow $C = (0.664)^2$.

The experimental problem for the laminar boundary layer is illustrated by some measurements of Maydew and Pappas (12) in supersonic flow which are found to be in good agreement with the relationship (17), although the apparent origin of the boundary layer is well upstream of the physical leading edge. The discrepancy between theory and experiment in this case may be visualized in terms of an initial increment θ_o in the momentum thickness, possibly caused by pressure drag on the slightly blunt leading edge, which is eventually absorbed in the boundary layer and appears finally as a coordinate displacement x_o after similarity is achieved. On the other hand, Dalitz (13) has investigated theoretically the influence of a sharpened leading edge on the development of the laminar boundary layer along a plate of finite thickness in incompressible flow; he finds an eventual approach to the condition of similarity, with a definite upstream displacement of the apparent origin. The same behavior of the boundary layer was also predicted earlier by Hansen (14) for a comparable

plate geometry, so that a mechanism which may account for the observed discrepancies is at least partly distortion of the ideal surface shearing stress distribution by local pressure gradients near the leading edge of a plate of finite thickness.

For the turbulent boundary layer, unfortunately, the question of uniqueness lies under a darker cloud than can be dissipated by physical arguments alone. Further consideration of this problem will therefore be deferred until it becomes convenient below to cite experimental evidence in support of an analysis, based on considerations of similarity, of the turbulent boundary layer.

2. Functional Similarity. In the early attempts of Prandtl (15), von Kármán (16), and Taylor (17) to formulate a theoretical treatment of turbulent shear flows, the molecular transport process of the laminar regime was used as a model for a hypothetical turbulent transport process. The first and third of these analyses have in common the concept of a mixing length, analogous to the mean free path in a gas, whose magnitude is estimated in terms of some physical characteristic of the mean flow.

Not only have the mixing length theories made possible a careful extrapolation of empirical knowledge of turbulent shear flows to conditions outside the contemporary range of experiment, but they have provided a framework within which the effects for example of wall roughness (18) could be fitted. However, it is now generally recognized that recent measurements of the detailed structure of turbulent flow are making tenancy of the mixing

length hypothesis progressively more uncomfortable (19, 20), although the primitive state of experimental research has so far prevented replacing the theory with one more satisfactory.

The mixing length analogy for turbulent flow will not be discussed further here, since many detailed summaries are available (21, 22, 23, 24). Neither will any review be attempted of the current experimental investigations of Laufer (25), Klebanoff and Diehl (26), Townsend (27, 28 - 32), and others, which it is to be hoped will lead first to a knowledge of the structure, and finally to an understanding of the mechanism, of turbulent flow.

In the absence of an adequate theory describing the turbulent mechanism, the present discussion will attempt to organize, rather than to explain, the experimental evidence which is available for the low-speed turbulent flat plate boundary layer. The general analysis is based on the principle of physical similarity, on certain demonstrable properties of the boundary layer, and on the equations of motion for the flow, and is later made specific by an appeal to experimental data.

The mean velocity distribution $u(y)$ through an incompressible turbulent boundary layer may be taken to depend on four local parameters δ, τ_w, ρ, and μ; a fifth parameter u_1 is of course implied as the value of u when $y = \delta$. The first two quantities, δ and τ_w, depend on a length coordinate ξ which is not written explicitly, since it will be found that the Reynolds number $R = \rho u_1 \xi / \mu$ for the ideal boundary layer is fixed for a given profile by the assumptions already made in this and in the pre-

ceding section.

The function of six variables

$$u = g(y, \rho, \mu, \delta, \tau_w) \tag{18}$$

may conveniently be written without loss of generality as

$$\frac{u}{u_\tau} = G\left(\frac{y u_\tau}{\nu}, \frac{y}{\delta}\right) \tag{19}$$

in terms of a characteristic velocity u_τ and two characteristic lengths δ and ν/u_τ, where

$$\tau_w = \rho u_\tau^2 \tag{20}$$

Suppose that Eq. (19) can be specialized for the region near the wall, on the ground of a certain similarity observed experimentally. Both the laminar sublayer profile and the adjacent turbulent mean velocity profile near the surface are found to be independent of the boundary layer thickness δ, so that

$$\frac{u}{u_\tau} = f\left(\frac{y u_\tau}{\nu}\right) \qquad y \to 0 \tag{21}$$

Suppose further that in the outer region of the boundary layer similarity is observed with respect to a coordinate system attached to the edge of the layer and moving with the free stream. It is not surprising, if the shearing stress in this region is maintained by a turbulent transport process, that the velocity

defect is found to be independent of the viscosity of the fluid. In fact, turbulent shear flows with a free boundary, such as wakes and jets, have in common with the boundary layer the property that near the free boundary the characteristic length, when considering the distribution of mean velocity measured with respect to the outer fluid, is the width δ of the shear layer. Measurements of the space correlation across a turbulent channel flow by Laufer (33), across a turbulent boundary layer by Schubauer and Klebanoff (34), and across a free jet by Corrsin and Uberoi (35), together with the observation that a velocity defect law of the kind treated here holds at least approximately for such flows, are convincing evidence that large eddies are important in the general turbulent shear flow, whether the boundaries are free or solid or both.

The characteristic velocity for the velocity defect distribution is less easily identified. In considering flows past a solid boundary, the friction velocity u_τ is the most obvious choice, particularly since the entire velocity profile must depend on the local rate of energy dissipation and therefore on the flow in the laminar sublayer. However, the turbulence itself contributes to the dissipation, and accounts for the whole if no solid boundaries are present, so that it is with some reservations that the velocity defect law is introduced in the usual form,

$$\frac{u_1 - u}{u_\tau} = F\left(\frac{y}{\delta}\right) \qquad y \to \delta \qquad (22)$$

If now it is assumed that there exists a finite region in which both (21) and (22) are valid, it is easily shown (36; see also 37, 38) that (19) in this region must have the form

$$\frac{u}{u_\tau} = \frac{1}{\kappa} \ln \frac{y u_\tau}{\nu} + \varphi\left(\frac{y}{\delta}\right) \tag{23}$$

or more specifically, in view of (21),

$$\frac{u}{u_\tau} = \frac{1}{\kappa} \ln \frac{y u_\tau}{\nu} + \varphi(0) \tag{24}$$

Note that the existence of Eq. (23) is a sufficient condition to insure the existence of Eq. (22) since, if (23) is valid throughout the outer part of the boundary layer,

$$\frac{u_1 - u}{u_\tau} = \varphi(1) - \varphi\left(\frac{y}{\delta}\right) - \frac{1}{\kappa} \ln \frac{y}{\delta} \tag{25}$$

That the condition is also necessary is less commonly recognized. Eq. (22), which is both plausible on dimensional grounds and is supported by experimental evidence, and Millikan's demonstration of necessity, already cited, are together a less ambiguous basis for Eq. (24) than derivations involving specific assumptions about the mechanism of turbulent shear flow. In particular, the constant κ is introduced during a separation of variables in a manner which suggests clearly that the parameter should not depend on the surface shearing stress or on the boundary layer thickness, although it may depend on the wall geometry.

Evaluation of Eq. (23) at the edge of the boundary layer

yields immediately the friction law

$$\frac{u_1}{u_\tau} = \frac{1}{\kappa} \ln \frac{\delta u_\tau}{\nu} + \varphi(1) \qquad (26)$$

which may be applied directly to pipe or channel flow on replacing the boundary layer thickness by the pipe radius or channel half width. For a boundary layer, however, it is necessary to have recourse to the momentum equation in order to eliminate the thickness δ in favor of the length ξ. In the absence of pressure gradient and roughness, the local friction coefficient and the momentum thickness for the ideal turbulent boundary layer may be taken to be related by

$$c_f = \frac{\tau_w}{\frac{\rho}{2} u_1^2} = 2\left(\frac{u_\tau}{u_1}\right)^2 = 2\frac{d\theta}{d\xi} = 2\frac{d}{d\xi}\int_0^{\delta+} \frac{u}{u_1}\left(1-\frac{u}{u_1}\right) dy \qquad (27)$$

according to Eqs. (8), (7), (20), and (5) above. In the present notation, using (22) and (26) in turn in (27),

$$\left(\frac{u_\tau}{u_1}\right)^2 = \frac{d}{d\xi}\left(\frac{u_\tau}{u_1}\right)^2 \delta \int_0^1 \left(\frac{u_1}{u_\tau} - F\right) F\, d\frac{y}{\delta}$$

$$= e^{-\kappa\varphi(1)} \frac{d}{d\frac{u_1 \xi}{\nu}}\left(\frac{u_\tau}{u_1}\right) e^{\kappa \frac{u_1}{u_\tau}} \int_0^1 \left(\frac{u_1}{u_\tau} - F\right) F\, d\frac{y}{\delta}$$

Integrating and dropping terms of order unity, the turbulent flat plate friction law for $C_f(R)$ is obtained in the implicit form first given by von Kármán (39),

$$c_f R = 2c_1 e^{-\kappa\varphi(1)} e^{\kappa\sqrt{\frac{2}{c_f}}} \left[1 - \left(\frac{2}{\kappa} + \frac{c_2}{c_1}\right)\sqrt{\frac{c_f}{2}} + \frac{1}{\kappa}\left(\frac{1}{\kappa} + \frac{c_2}{c_1}\right) c_f\right] \qquad (28)$$

where

$$C_1 = \int_0^1 F\left(\frac{y}{\delta}\right) d\frac{y}{\delta} = \frac{u_1}{u_\tau}\frac{\delta^*}{\delta} \tag{29}$$

$$C_2 = \int_0^1 F^2\left(\frac{y}{\delta}\right) d\frac{y}{\delta} = \left(\frac{u_1}{u_\tau}\right)^2\left(\frac{\delta^* - \theta}{\delta}\right) \tag{30}$$

and

$$R = \frac{u_1 \delta}{\nu} \tag{31}$$

$$\delta^* = \int_0^{\delta+} \left(1 - \frac{u}{u_1}\right) dy \tag{32}$$

$$\theta = \int_0^{\delta+} \frac{u}{u_1}\left(1 - \frac{u}{u_1}\right) dy \tag{33}$$

Finally, the expressions (29) and (30) constitute a relationship for the variation of the form parameter δ^*/θ with Reynolds number,

$$\frac{\delta^*}{\theta} = \frac{1}{1 - \frac{C_2}{C_1}\frac{u_\tau}{u_1}} \tag{34}$$

while (29) offers a convenient definition for the physically ambiguous boundary layer thickness δ in terms of the displacement thickness δ^* defined by Eq. (32).

It remains to discuss the mean friction coefficient implied by Eq. (28). The relationship of Eq. (9)

$$C_F R = \int_0^R C_f \, dR \tag{9}$$

is of course valid for any law of variation of C_f with R provided that the integral exists. In the case of the full von Kármán formula (28), difficulty in evaluating the integral at the lower limit can be avoided by taking this limit slightly downstream of the leading edge. More specifically, the indefinite integral vanishes at a Reynolds number $R = (2C_1/\kappa^2)\exp[-\kappa\psi(1) + \kappa C_2/C_1]$ which, anticipating numerical values to be determined later, is of order 40. Taking this value as the lower limit of integration, in the hope that the contribution of the local friction in the omitted region will be small in a physical sense if not in a mathematical one, Eqs. (28) and (9) imply the relationship,*

---

* Some discussion appears in the literature of a truncated form of Eq. (28),

$$1/\sqrt{C_f} = a + b \log_{10}(C_f R) \qquad (a)$$

which was suggested by von Kármán (16). In this case the integral (9) is logarithmically infinite at the lower limit. Avoiding this difficulty in the way suggested above, the equation corresponding to (35) is

$$C_F = C_f + (2/R)\,10^{-a/b}\,Ei(\ln 10/b\sqrt{C_f}) \qquad (b)$$

where the exponential integral defined by $Ei(z) = \int_{-\infty}^{z} e^t/t\,dt$ is tabulated for example in Tables of Sine, Cosine, and Exponential Integrals, Department of Commerce, Washington, D.C., 1940. This function has the proper behavior at small Reynolds numbers, and has an asymptotic expansion for large argument which leads to

$$C_F/C_f = 1 + 2(b\sqrt{C_f}/\ln 10) + 2(b\sqrt{C_f}/\ln 10)^2 + \ldots \qquad (c)$$

The last expression is identical with (36) up to the last term exhibited here if $b = (\ln 10)/(\kappa\sqrt{2})$, and resembles a relationship suggested by Fage (40), following Squire and Young (41).

Schoenherr (42, 43), has proposed an expression of the form (a) for the mean friction. Such a relationship can readily be constructed from (a) and (c); the result is

$$1/\sqrt{C_F} = a + b \log_{10}(C_F R/e) + O(\sqrt{C_F}) \qquad (d)$$

(footnote continued on next page)

(Continuation of Footnote)

Consequently the mean turbulent friction coefficient at a given Reynolds number is asymptotically equal to the local friction coefficient at a Reynolds number smaller by a factor $e = 2.718\ldots$. This rule may be useful in the supersonic case, since it holds for arbitrary values of a, b in Eq. (a) above. The corresponding factor for a power friction law, $C_f = AR^{-1/n}$ say, is obviously $(1 - 1/n)^{-n}$.

easily obtained by writing $c_f dR = d(c_f R) - R\,dc_f$,

$$c_F R = 2R_\theta = 2C_1 e^{-\kappa\varphi(1)} e^{\kappa\sqrt{\frac{2}{c_f}}} \left(1 - \frac{C_2}{C_1}\sqrt{\frac{c_f}{2}}\right) \quad (35)$$

and it follows that

$$\frac{c_F}{c_f} = 1 + \frac{2}{\kappa}\left(\frac{c_f}{2}\right)^{1/2} + \frac{2}{\kappa^2}\left(\frac{c_f}{2}\right) - \frac{2}{\kappa^2}\frac{C_2}{C_1}\left(\frac{c_f}{2}\right)^{3/2} + \cdots \quad (36)$$

It may be observed, in connection with the mathematical approximation apparently made in deriving Eq. (35), that the latter expression can alternatively be obtained by eliminating δ^*/δ between Eqs. (29) and (30), and eliminating θ/δ between this result and Eq. (26).

The two equations (28) and (35) above define the ideal local and mean turbulent friction coefficients for a flat plate in terms of four empirical velocity profile parameters κ, $\varphi(1)$, C_1, and C_2. These parameters may supposedly be determined by simultaneous local measurements of velocity profile and surface friction at a single Reynolds number, and extrapolation of the resulting friction formulae to arbitrary Reynolds numbers may then be undertaken with the same degree of confidence which is attached to the hypotheses of similarity underlying Eqs. (21) and (22). It may be noted that Eq. (35) is the analog of Eq. (17) in supplying, for the turbulent boundary layer, a connection between local friction coefficient and local momentum thickness Reynolds number which may be taken both as a definition and as a test for uniqueness.

3. Experimental Literature.* While the turbulent boundary layer on a flat plate has been the subject of a great deal of experimental research, it is not easy to find reliable measurements of mean velocity profile and surface shearing stress made under identical experimental conditions. Before discussing the available measurements, therefore, it is convenient to provide a short catalog of several special techniques which have been used for determining local surface friction.

The derivative $d\Theta/dx$ supposedly gives the surface shear directly, provided that the flow is uniform and two-dimensional. Since differentiation of experimental data is necessary, large errors may occur unless careful and complete measurements are made of the various velocity profiles. Alternatively, extrapolation toward the wall of the turbulent shear $-\rho\,\overline{u'v'}$ or of the sublayer laminar shear $\mu\,\partial u/\partial y$ implies unusual nicety of experimental technique. Direct measurement of the shearing force on a floating surface element, although it requires a considerable effort in the development of special instrumentation, appears to be the most reliable method available at present. Finally, a device based on a relationship between heat transfer and momentum transfer in the sublayer has been used successfully, but must be calibrated by comparison with a primary standard obtained by one of the more

---

* The writer is indebted to Dr. G. B. Schubauer and Mr. P. S. Klebanoff of the National Bureau of Standards, Washington; to Dipl.-Phys. W. Tillmann of the Max-Planck-Institut für Strömungsforschung, Göttingen, and to Dr. F. R. Hama of the State University of Iowa, Iowa City, for their courtesy in providing numerical data for some of the measurements cited here.

conventional methods of local friction measurement.

The floating element technique is conspicuous among these methods for the consistency of the data obtained. Omitting a discussion of a meteorological application by Sheppard (44), three papers describing direct measurements of surface shearing stress on a flat plate in low-speed flow have appeared in the boundary layer literature.

Kempf (45) in 1929 measured the surface friction at several stations on the flat bottom of a ship model. Each of the floating surface elements, suspended by wires from an overhead frame, was returned automatically to a null position by a motor-actuated tension spring whose elongation was recorded on a rotating drum. The presence of a standing wave system on the free surface of the towing tank introduced into the friction coefficient data a scatter which is apparently systematic in terms of the Froude number, but random in terms of the Reynolds number; no attempt has been made to remove this scatter in the data considered here for the first four stations. Kempf's measurements were made at sufficiently large values of x so that the influence of the parameter x_o should be negligible. A criticism of the data can, however, be based on the possibility of secondary flow in the boundary layer, since the ship hull in question, even though flat-bottomed, was relatively narrow in its lateral dimension. A further criticism of the measurements at the largest Reynolds numbers has been expressed by Falkner (46) on the ground that

the length of run may have been insufficient to guarantee steady flow near the aft end of the ship model.

Schultz-Grunow (17) later used similar methods to measure the friction on the floor of a wind tunnel. The horizontal floating element, free to rotate about a vertical axis some distance to one side, was returned to a null position by an adjustable torsion spring. Great care was taken to minimize pressure variations along and across the small gap provided for clearance around the floating element. The tunnel boundary layer was removed at an upstream slot, whose downstream lip formed the leading edge of the plate under investigation. Transition to turbulent flow occurred immediately downstream of the curved leading edge; however, there is some doubt about the magnitude of the parameter x_o, especially since the Reynolds number was apparently varied by changing the velocity at a fixed station along the plate.

More recently, Dhawan (11) has obtained further data on the turbulent skin friction on a flat plate by means of the floating element technique. A section of the surface was suspended from a rectangular four-bar flexure linkage to allow motion only in the direction of the airflow, and the deflection under load was indicated by a variable reluctance transformer. Dhawan was able to induce transition by means of leading edge curvature, and to confirm the existence of turbulent flow over most of the working surface by means of an axial impact pressure traverse near the plate surface.

The experimental data of Kempf, Schultz-Grunow, and Dhawan are collected in Figure 1. The measurements appear to define a single curve over the range of Reynolds numbers from 2×10^5 to 4×10^8, with a scatter so small as to be almost unprecedented in boundary layer research. In fact, it may be admitted that the present re-examination of the turbulent boundary layer problem was to a large extent inspired by the remarkable consistency of these local friction data.

The existence of a unique relationship between the ordinate and the slope of the momentum thickness distribution, $\Theta(x)$, has already been proposed as a criterion for uniqueness in the turbulent flat plate boundary layer. The immediate question is one of demonstrating that such a relationship exists for the experimental data, without necessarily identifying the resulting function for example with Eq. (35) above. In view of the wide variations which occur from one experiment to another in various factors which influence boundary layer transition, it is not obvious a priori that a state is ever reached in which the dependence of the turbulent boundary layer on its early history is no longer measurable in terms of the local mean properties of the flow.

With the restricted definition of uniqueness considered here, it is sufficient as a beginning to consider the momentum thickness distribution only. The measurements which are most useful for this purpose were made by K. Wieghardt in 1943, as part of an extensive research program carried out since 1939 in a boundary

layer tunnel at the Institut für Strömungsforschung at Göttingen. While this program has placed considerable emphasis on the determination of the drag of surface irregularities, including uniform roughness, and on the investigation of turbulent boundary layer flow in a pressure gradient, the case of a flat plate boundary layer has also been investigated in some detail. Measurements of local surface friction by Schultz-Grunow (47), using the floating element technique, are cited elsewhere in the present report, as are some data on the drag of slots obtained with the same balance equipment by Wieghardt (48) and by Tillmann (49). Mean friction measurements with artificial surface roughness have been reported by Wieghardt (50), who also investigated the effect of increased free stream turbulence on the turbulent boundary layer profile. Equivalent measurements in a flow with pressure gradient were carried out by Wieghardt (51), and analyzed by Wieghardt and Tillmann (52); some anomalous effects possibly caused in these experiments by secondary flows have been discussed by Tillmann in a report on further experiments with roughness and with pressure gradient (53), and clarified by Tillmann in his dissertation (54). More recently the same experimental environment has been employed by Ludwieg (55) and by Ludwieg and Tillmann (56) during the development of an instrument for the indirect determination of local shearing stress by means of heat transfer measurements.

Continuity in these German experiments is provided by two series of velocity profile measurements in uniform flow, carried out at free stream velocities of 17.8 and 33.0 meters per second respectively. In addition, Schultz-Grunow's experiments at 19.4

meters per second and a fourth unpublished series of profiles at 18.0 meters per second were obtained in the same channel. Of these data, Wieghardt's measurements at 17.8 meters per second, by virtue of early transition and almost immediate coincidence for the actual and apparent origins, will be found to be in good agreement with the properties of the ideal turbulent boundary layer. The local friction coefficients for this series, obtained by differentiating the experimental momentum thickness distribution, are plotted against R_θ in Figure 2.

Some recent measurements in a flat plate boundary layer at the National Bureau of Standards, reported by Klebanoff and Diehl (26), were undertaken in part to test the hypothesis of uniqueness for thick turbulent boundary layers produced for example by initial roughness. Figure 2 shows the relationship between $2\,d\theta/dx$ and R_θ observed in experiments with natural transition at a free stream velocity of 108 feet per second, and with initial sand roughness at 35, 55, and 108 feet per second. Except in the last instance, the most downstream data are in good agreement with Wieghardt's curve; the agreement is in fact better than might be expected considering the uncertainty in the local friction coefficients obtained by differentiation. Examination of the experimental velocity profiles shows that the present criterion for uniqueness is equivalent to the test proposed by Klebanoff and Diehl, of similarity in the velocity distribution, and serves equally well to identify the profiles which should be studied in detail.

Dhawan (11) has reported a single mean velocity profile,

obtained at a relatively small Reynolds number, for which the surface shearing stress was measured by the floating element technique as described in one of the paragraphs above. Schultz-Grunow (47) made profile surveys as well; however, the station of the floating element is not specified, and if the local friction coefficient $2\,d\Theta/dx$ at 5.3 meters is compared to the measured value of τ_w/ρ at the same Reynolds number $u_\infty x/\nu$, a discrepancy of about ten per cent is found.* In fact, the profile data of Schultz-Grunow in the plane ($2\,d\Theta/dx$, R_Θ), shown in Figure 3, differ noticeably from the experiments already cited of Wieghardt and of Klebanoff and Diehl, and from the ideal relationship to be obtained later.

Finally, Hama (57) has published some velocity profile measurements in turbulent boundary layers, and his experimental values for the distribution of $\Theta(x)$ have been used to obtain the local friction coefficients plotted in Figure 2. While the detailed profiles are not at present available, good agreement was obtained by Hama in his original paper with the particular logarithmic velocity formula discussed below.

Several velocity profiles which should be representative of the fully developed turbulent boundary layer are shown in Figure 4, in the coordinate system of Eq. (21), in order to exhibit the

---

* At 5.3 meters the velocity profile has been recovered in as great detail as possible and Schultz-Grunow's value of Θ verified by numerical integration; the value of δ^* for the same profile should be increased about seven per cent above the value reported in the original paper. In analyzing this profile, the arithmetic average of the two local friction coefficients has been used.

occurrence of a logarithmic relationship in the profile near the surface. According to Eq. (24), the value of the parameter κ is determined by the slope* of the straight line in the figure, and $\varphi(0)$ by the intercept at $y u_\tau/\nu = 1$.

In establishing a value for the boundary layer thickness δ, needed in determining the parameter C_1 from Eq. (29), it has been found convenient to plot $(1 - u/u_1)^{2/3}$ against y and to fit a straight line to the outer part of the profile in this coordinate system. The thickness δ is defined as the intercept on the y axis. This convention has no special significance; it is suggested by the mixing length theory of Prandtl when the shearing stress varies linearly with y and the mixing length is constant, but is justified only by its convenience as a well defined method for specifying the boundary layer thickness.

Figure 5 shows the profiles** of Figure 4 in the coordinate system required by the velocity defect law, Eq. (22). Again fitting a straight line with a slope determined by κ to the logarithmic region, the intercept at $y = \delta = \delta^* u_1 / C_1 u_\tau$ is $\varphi(1) - \varphi(0)$, according to Eqs. (24) and (26).

---

* It should be pointed out that the region in the neighborhood of $y u_\tau/\nu = 20$ is known to be characterized by large fluctuations in the instantaneous velocity (27, 25), so that impact probes may indicate too large a value of mean velocity in this region. While this problem complicates the determination of the slope of the logarithmic portion of the profile, the writer has found no reason to prefer another value for κ than the one originally suggested by Nikuradse (58), although the latter's interpretation of his pipe experiments has been criticized by several writers; e.g. (59).

** The profile with natural transition of Klebanoff and Diehl was not at first consistent with the others; when the displacement thickness δ^* was recalculated it was found to be more nearly 0.206 inches than 0.216 inches.

This analysis of the turbulent velocity profiles has been carried out for all the data available to the writer, using a value of κ of 0.40 and determining values for $\varphi(0)$, $\varphi(1)$, C_1, and C_2, the latter from Eq. (30). For Wieghardt's measurements at 33.0 meters per second a modified procedure was followed, the local friction coefficients being obtained from the expression (35) using the measured values of R_Θ and preliminary estimates for C_1, C_2, and $\varphi(1)$.

The collected values for the parameters C_1, $\varphi(0)$, and $\varphi(1)$ are plotted against R_Θ in Figure 6, and show a surprising degree of consistency. The behavior at low Reynolds numbers illustrates an earlier remark about the asymptotic nature of the boundary layer problem. For example, the parameter C_1 is evaluated from Eq. (29); however, the integral in the latter expression obviously neglects the dependence of the sublayer profile on Reynolds number, and so cannot be uniformly valid for all the experimental data considered above. The contribution of the sublayer flow to the integral defining the displacement thickness increases with decreasing Reynolds number, and the effect is exaggerated by squaring the integrand in Eq. (30) which defines C_2. On the other hand, it is not certain that the variation observed for these parameters at low Reynolds numbers is genuine, since the data in question were obtained in a slight pressure gradient in Dhawan's experiments and near a blunt leading edge in the measurements by Wieghardt.

This difficulty of course does not prevent the choice of particular values for the parameters κ, $\varphi(1)$, C_1, and C_2, in order

to complete the numerical analysis of the turbulent boundary layer. Recognizing the asymptotic nature of the treatment by emphasizing the data at the larger Reynolds numbers, then approximately

$$\kappa = 0.400$$
$$\varphi(0) = 5.10$$
$$\varphi(1) = 7.90$$
$$C_1 = 4.05$$
$$C_2 = 29.0$$

These parameters have been used to evaluate R, R_θ, C_F, and δ^*/θ as functions of C_f from Eqs. (28), (35), and (34), and the resulting data are collected in Table I. The values tabulated in the first and second columns have been plotted in Figure 1 above, and those from the first and fourth columns in Figures 2 and 3. The values tabulated in the fourth and fifth columns are compared with the experimental values of the shape parameter δ^*/θ in Figure 7, the agreement here of course being expected since these experimental data were used to determine C_2. It may be pointed out by way of contrast that the curves in Figures 1 and 2 above and in Figure 8 below are in no sense fitted to the measurements in question, since the ideal curves are based on detailed information about the velocity profiles, while the measurements are not. Furthermore, although experimental values for u_τ were used to eliminate the influence of Reynolds number in the analysis of the profiles, it was not necessary to know the magnitude of the Reynolds numbers in question. In fact, the discrepancies in Figure 1 are probably connected with the assumption

Table I

Suggested Properties
of the Ideal Turbulent Boundary Layer
in a Fluid of Constant Density

C_f	R	C_F	R_θ	$\frac{\delta^*}{\theta}$	$\frac{\mu_T}{\mu_1}$
8.0×10^{-3}	1.017×10^{4}	1.032×10^{-2}	5.25×10	1.828	.0632
7.8	1.143	1.005	5.75	1.809	.0624
7.6	1.291	9.78×10^{-3}	6.31	1.790	.0616
7.4	1.463	9.52	6.96	1.772	.0608
7.2	1.666	9.25	7.70	1.753	.0600
7.0	1.906	8.98	8.55	1.735	.0592
6.8	2.193	8.70	9.54	1.717	.0583
6.6	2.536	8.43	1.069×10^{2}	1.699	.0575
6.4	2.950	8.16	1.204	1.681	.0566
6.2	3.45	7.89	1.362	1.663	.0557
6.0	4.07	7.62	1.551	1.645	.0548
5.8	4.84	7.35	1.776	1.628	.0539
5.6	5.79	7.07	2.047	1.610	.0529
5.4	7.01	6.80	2.383	1.593	.0520
5.2	8.49	6.53	2.771	1.575	.0510
5.0	1.050×10^{5}	6.26	3.29	1.558	.0500
4.8	1.310	5.99	3.92	1.540	.0490
4.6	1.653	5.72	4.73	1.523	.0480
4.4	2.115	5.45	5.77	1.506	.0469
4.2	2.748	5.19	7.13	1.488	.0458
4.0	3.64	4.92	8.95	1.471	.0447
3.8	4.91	4.66	1.143×10^{3}	1.453	.0436
3.6	6.78	4.39	1.487	1.436	.0424
3.4	9.72	4.13	2.004	1.419	.0412
3.2	1.398×10^{6}	3.87	2.700	1.401	.0400
3.0	2.107	3.60	3.80	1.383	.0387
2.8	3.30	3.35	5.53	1.366	.0374
2.6	5.43	3.09	8.38	1.348	.0361
2.4	9.43	2.835	1.337×10^{4}	1.330	.0346
2.2	1.755×10^{7}	2.581	2.265	1.311	.0332
2.0	3.55	2.331	4.14	1.293	.0316
1.8	8.00	2.083	8.33	1.274	.0300
1.6	2.068×10^{8}	1.837	1.899×10^{5}	1.254	.0283
1.4	6.43	1.594	5.13	1.234	.0265
1.2	2.583×10^{9}	1.354	1.748×10^{6}	1.213	.0245
1.0	1.518×10^{10}	1.117	8.48	1.191	.0224

that the real and apparent origins coincide for the experimental boundary layers; compare Figure 2, where local quantities only are involved.

The ideal relationship between R_θ and R from Table I is shown in Figure 8, together with the experimental values of Wieghardt. The measurements at 17.8 meters per second are in excellent agreement with the ideal curve, even at a Reynolds number as low as 10^5. The measurements at 33.0 meters per second, however, suggest that the apparent origin of the turbulent boundary layer at this higher velocity is upstream of the actual leading edge by a displacement of about 1.5×10^5 in the Reynolds number R, and the appropriate ideal curve is shown. Also plotted in Figure 8 is the relationship between R_θ and R implied by the turbulent friction formula of Schoenherr (42),

$$\frac{1}{\sqrt{C_F}} = 4.13 \log_{10}(C_F R)$$

which was fitted in 1932 to the experimental mean friction data which were available at that time, and has since been widely used in ship and aircraft design. The collected data from Schoenherr's paper may be found in Figure 110 of Reference (23), and consequently need not be reproduced here.

Finally, Wieghardt's velocity profile data at a free stream velocity of 33.0 meters per second are shown in detail in Figure 9 in order to illustrate the degree of confidence which can be placed in the law of the wall, Eq. (21), and the velocity defect

law, Eq. (22).

Some comment should be made about experimental data which have not been included in the summary above. Although any distinction between the exercise of judgment and the suppression of evidence is a matter of personal definition, it is felt that there are valid reasons for omitting certain measurements from the discussion.

Some experiments in turbulent flat plate boundary layers by Hansen (14), by Peters (60), by Baines (61), and by Townsend (27) are unfortunately not reported in sufficient detail to be useful here. Dryden's data (9) are in the same catagory, except perhaps for a single velocity profile at 28.5 inches, obtained with a turbulence screen which increased the free stream turbulence to about 2.8 percent. If the local friction coefficient for this profile is deduced from the measured momentum thickness Reynolds number, the data are found to be in excellent agreement with Figure 4 near the wall, and to exhibit the same tendency toward thickening of the outer boundary layer which has been reported by Wieghardt (50) to occur when the free stream turbulence level was raised in the Göttingen tunnel.

Nikuradse (62) has constructed an elaborate treatment of some measurements in a turbulent flat plate boundary layer around the assumption

$$\frac{u}{u_1} = f\left(\frac{y}{\delta^*}\right) \qquad (37)$$

This treatment belongs in the same class as the traditional power law analysis, in that both fail to predict many of the observed properties of the boundary layer, including several connected with the influence of viscosity. For example, Eq. (37) obviously implies a constant value for the ratio δ^*/θ, contrary to the bulk of experimental evidence. Furthermore, Nikuradse performs an analysis of his data in which the assumption (37) is introduced so early that one series of experimental values of δ^*/θ is in fact found to be independent of Reynolds number. For this reason, it was felt that a further study of Nikuradse's data, for which the original measurements could not be recovered, would not be profitable.

Ashkenas, Riddell, and Rott (63) have recently reported some detailed measurements in a turbulent boundary layer, which yield the several points shown in Figure 3. The discrepancy between these experimental data and the measurements of others working in the field, together with an observed tendency for the turbulent shearing stress distribution to have a maximum away from the wall, make it questionable whether the flow conditions for these experiments are representative of the flat plate turbulent boundary layer.

It is to be regretted that the early measurements of van der Hegge Zijnen (64) were carried out in a relatively poor experimental environment. The presence of an axial pressure gradient, and the failure to make each series of measurements with uniform flow conditions, prevent the inclusion of these data in the present

review of experimental literature. A set of points for the series at 8 meters per second, with a turbulence screen, are shown in Figure 3 to illustrate the difficulty. Certainly, the use of hot wire instrumentation for mean speed measurements recommends itself after a study of these original experiments, and considerable reliance has in fact been placed on the sublayer measurements of van der Hegge Zijnen in estimating the sublayer velocity profile, for values of $y u_\tau/\nu$ up to say 50, in Figure 4 above.

4. Discussion. If the development of the preceding sections has demonstrated that the mixing length hypothesis is not necessary to an adequate quantitative analysis of the turbulent boundary layer, then one purpose of the writer has been served. Most of the ideas involved are not new; for example, Eq. (23) was postulated on empirical grounds, and Eq. (28) derived as a consequence, by von Kármán in 1932 (39); and Schultz-Grunow in 1939 (47) carried an analysis of his experimental data almost to the point where the numerical results of the present paper could have been obtained. More recent papers by Landweber (65), Rotta (66), and Baines (67) have discussed the representation of the turbulent boundary layer in terms of the law of the wall and the velocity defect law, but have not emphasized the physical interpretation of these formulae. The essential element of the present study is of course the demonstration that the two similarity laws together are sufficient to

imply a logarithmic region in the velocity profile. This demonstration, as first given by Millikan in 1938 (36), is an application of a discipline which may be called functional analysis, as distinguished from the less powerful method of dimensional analysis which is usually applied to the problem, and deserves a place among major contributions to the boundary layer literature.

It is to be hoped that the experimental evidence for similarity in the turbulent boundary layer is sufficiently convincing to provide motivation for a serious attempt to discover the physical mechanisms which are responsible. Certainly, the evidence that the turbulent boundary layer may be considered to be a unique phenomenon, at least for purposes of preliminary study, should simplify the interpretation of experimental data. For example, it is clear that an estimate of the surface shearing stress corresponding to a given velocity profile may be made in several ways without benefit of direct measurement; the two most obvious of these consist of observation of Φ and use of Eq. (35), and of observation of u(y) and use of Eq. (24). In this same connection, it is known that the law of the wall is insensitive to pressure gradient, to free stream turbulence, and even to the presence of a second boundary, while the velocity defect law depends strongly on these three factors but is insensitive to surface roughness.

In reviewing the asymptotic nature of the turbulent boundary layer problem against the background of the similarity laws, it seems likely that extrapolation of a local friction law based on

functional similarity to indefinitely small Reynolds numbers* is permissible only in a restricted sense. Apart from the fault of neglecting the sublayer in evaluating the momentum integral, a fault which is easily corrected at the cost of slightly more complicated formulae, it is not apparent that the two similarity laws cited here can be valid at low Reynolds numbers. For the region of common validity is marked by a logarithmic velocity profile, which obtains only for values of $y u_\tau / \nu$ greater than say 50. However, Figure 5 shows that the logarithmic law can describe the velocity profile only within the inner 20 percent of the boundary layer in any case, so that the smallest value of $\delta u_\tau / \nu$ which satisfies both criteria is about 250. But from Eq. (29), the corresponding $u_1 \delta^* / \nu$ is 1000, and consequently $u_1 \theta / \nu$ should not be smaller than about 700 in order for the velocity profile to satisfy the two requirements of similarity. Consulting the experiments, the approximate value of the abscissa in Figure 6, below which the parameters $\varphi(0)$ and $\varphi(1)$ appear to be no longer independent of Reynolds number, is $u_1 \Theta / \nu = 1500$.

It should be a matter of some interest to determine whether at low Reynolds numbers similarity is achieved earlier near the wall than near the free stream, as has been reported for pipe and channel flows (68, 69). The turbulent outer flow in a boundary layer is

---

* Note however that an examination of Wieghardt's data at 17.8 meters per second in Figure 8 shows that the corresponding values in Figures 2 and 6 would lie closer to the ideal curve or to the other measurements cited if the analysis were repeated with more realistic values of the local friction coefficients than the initial estimates of the writer.

known to be of an irregular and intermittent nature (27, 70), and the possible connection between intermittence and transition is an important aspect of the turbulence problem.

The widespread current revival of interest in the theoretical and experimental aspects of the boundary layer problem can hardly fail to lead to important discoveries, both in a knowledge of the structure of turbulent shear flows and in the formulation of an adequate theory. In the meantime, the discussion given here of the more rudimentary properties of one such flow may serve to allow the identification of a proper environment for further experimental research, and some remarks below about several consequences of the similarity laws may suggest a few of the many directions in which such research might proceed.

C. The Boundary Layer with Variable Density

1. Theoretical Literature. A bewildering number of theoretical papers treating the development of turbulent boundary layer on a semi-infinite flat plate in compressible flow have recently appeared in the literature of applied mechanics. Because the results obtained by the various authors differ widely, it is desirable to compare the assumptions made and to organize if possible the available information into a common structure which may then be examined experimentally. This service is cheerfully undertaken by the present writer*, and the result for the condition of zero heat transfer is

---

* Dr. Dean Chapman of the Ames Aeronautical Laboratory has contributed several comments in the preparation of the table and of the notes. Papers by Fediaevsky and Bloch, CAHI, Moscow, Rep. 516, 1940, and by Smith and Harrop, RAE TN Aero. 1759, 1946, are not available to the writer, and some variations by Rubesin, Maydew, and Varga, NACA TN 2305, 1951, have been omitted.

summarized in Table II.

In most cases the analysis is based on the von Kármán momentum integral, Eq. (2), and is a generalization of the similarity or mixing length theory of Prandtl (15) or von Kármán (16). The boundary layer velocity profile is either assumed or is developed through a phenomenological treatment of turbulent shear flow in a compressible fluid. The calculations implied by such a development are avoided by several writers by proceeding directly to the friction law, which is assumed to be unchanged if density and viscosity are evaluated at some characteristic temperature for the flow.

Without exception, all the writers cited assume constant static pressure and stagnation enthalpy in the boundary layer, and those who discuss turbulent shear flow assume constant total shearing stress and a mixing constant κ which is independent of Mach number. In the latter case, the momentum integral usually cannot be evaluated in closed form, and a uniform degree of approximation has therefore been used for the appropriate asymptotic series.

The comparison in Table II is made on the basis of two functions, one involving R and M and the other C_f and M, which replace R and C_f in the incompressible friction law. No distinction is made in the table between treatments which are essentially similar, but which differ in detail in the assumptions made for the variation of viscosity with temperature or in the modification of the surface temperature or wall viscosity to correspond to the partial temperature recovery which is observed experimentally for air. The parameter m

Table II

Formulation of the Compressible Turbulent Boundary Layer Problem

Source	Form assumed for: Shear / Correlation / Mixing length	Result obtained for generalized C_f / R	Remarks
(1) von Kármán (71) Tucker (72)		$\frac{T_w}{T_1} C_f$ $\frac{T_1}{T_w}\frac{\mu_1}{\mu_w} R$	Incompressible friction law is assumed to hold with density and viscosity evaluated at surface temperature.
(2) Tucker (73)		$\frac{1}{2}\left(1 + \frac{T_w}{T_1}\right) C_f$ $\frac{2}{1 + \frac{T_w}{T_1}} \frac{\mu_1}{\mu_{\frac{1+w}{2}}} R$	Incompressible friction law is assumed to hold with density and viscosity evaluated at arithmetic mean of free stream and surface temperatures.
(3) Cope (74)		$\frac{T_w}{T_1} C_f$ $\frac{I_n(0)}{I_n(m)}\left(\frac{T_1}{T_w}\right)^2 \frac{\mu_1}{\mu_w} R$	Power law velocity profile, $u \sim y^{1/n}$, is assumed to be independent of Mach number. For $I_n(m)$ see Note (a).
(4) Monaghan and Johnson (75,76) Cope (74)	$\tau = -\rho_w \overline{u'v'}$ $\overline{u'v'} = -l^2\left(\frac{du}{dy}\right)^2$ $l = \kappa y = \kappa \frac{du/dy}{d^2u/dy^2}$	$\frac{T_w}{T_1} C_f$ $\left(\frac{T_1}{T_w}\right)^2 \frac{\mu_1}{\mu_w} R$	Logarithmic velocity profile is assumed to be independent of Mach number and surface temperature. Result does not then depend on heat transfer.
(5) Kalikhman (77)	$\tau = -\rho \overline{u'v'}$ $\overline{u'v'} = -\frac{\rho_w}{\rho} l^2\left(\frac{du}{d\eta}\right)^2$ $l = \kappa\eta$	$\frac{T_w}{T_1} C_f$ $\frac{T_1}{T_w}\frac{\mu_1}{\mu_w} R$	Momentum integral is transformed to incompressible form by Howarth's transformation, $d\eta/dy = \rho/\rho_0$. For velocity profile this relationship is approximated by $\eta/y = \rho_w/\rho_0$. Result is equivalent to von Kármán's assumption in (1) above.
(6) Eckert (78)		$\frac{T_m}{T_1} C_f$ $\frac{I_n(0)}{I_n(m)}\left(\frac{T_1}{T_m}\right)^2 \frac{\mu_1}{\mu_m} R$	Generalization of Prandtl's pipe-plate transformation (79) to compressible flow. Pipe friction law is assumed to hold when based on mean velocity and on density implied by volume flow and mass flow in pipe. Boundary layer thickness is identified with pipe radius, and rate of change of momentum thickness with pipe shearing stress. For $I_n(m)$ see Note (a); for T_1/T_m see Note (b).

(7) Wilson (80) Frankl and Voishel (81) Rubesin, Maydew, Varga (82) Clemmow (83)	$\tau = -\rho\,\overline{u'v'}$ $\overline{u'v'} = -l^2\left(\frac{du}{dy}\right)^2$ $l = \kappa\,\frac{du/dy}{d^2u/dy^2}$	$\left(\frac{m}{\sin^{-1}m}\right)^2 \frac{T_w}{T_1}\,C_f$ $\left(\frac{\sin^{-1}m}{m}\right)^2 \frac{T_1}{T_w}\frac{\mu_1}{\mu_w}\,R$	Generalization of von Kármán's similarity theory (16) to compressible flow. Frankl and Voishel use expansion valid for small Mach numbers to evaluate momentum integral. Wilson and Rubesin, Maydew, Varga use quasi-numerical methods. Clemmow obtains an asymptotic representation valid for large R, for which see Note (c), but erroneously reports a result corresponding to $l = \kappa y$.
(8) Van Driest (84) Young (85)	$\tau = -\rho\,\overline{u'v'}$ $\overline{u'v'} = -l^2\left(\frac{du}{dy}\right)^2$ $l = \kappa y$	$\left(\frac{m}{\sin^{-1}m}\right)^2 \frac{T_w}{T_1}\,C_f$ $\left(\frac{\sin^{-1}m}{m}\right)^2 \left(\frac{T_1}{T_w}\right)^{3/2}\frac{\mu_1}{\mu_w}\,R$	Generalization of Prandtl's mixing length theory (15) to compressible flow. Young's paper gives velocity profile, but not skin friction.
(9) Clemmow (83) Van Driest (86)	$\tau = -\overline{(\rho u)'v'}$ $\overline{(\rho u)'v'} = -l^2\frac{du}{dy}\frac{d\rho u}{dy}$ $l = \kappa y$	$\left[\frac{m}{F_1(m)}\right]^2 \frac{T_w}{T_1}\,C_f$ $(1+m^2)^{1/2}\left[\frac{F_1(m)}{m}\right]^2 \frac{T_1}{T_w}\frac{\mu_1}{\mu_w}\,R$	Generalization of Prandtl's mixing length theory with density and velocity fluctuations given equal weight. For $F_1(m)$ see Note (d).
(10) Li and Nagamatsu (87)	$\tau = -\overline{(\rho u)'v'}$ $\overline{(\rho u)'v'} = -l^2\frac{du}{dy}\left(\rho\frac{du}{dy} + \alpha u\frac{d\rho}{dy}\right)$ $l = \kappa y$	$\left[\frac{m}{F_\alpha(m)}\right]^2 \frac{T_w}{T_1}\,C_f$ $\left[1+(2\alpha-1)m^2\right]^{1/2}\left[\frac{F_\alpha(m)}{m}\right]^2 \frac{T_1}{T_w}\frac{\mu_1}{\mu_w}\,R$	Generalization of Prandtl's mixing length theory with momentum transport by density fluctuations weighted by factor α. For $F_\alpha(m)$ see Note (d). Analysis includes results of (8) and (9) as special cases.
(11) Ferrari (88)	$\tau = -\rho\,\overline{u'v'} - u\,\overline{\rho'v'}$ $\overline{u'v'} = -l\sqrt{\overline{(v')^2}}\,\frac{du}{dy}$ $\overline{\rho'v'} = -\beta m\,\frac{\tau_w}{u_1}$ $l\sqrt{\overline{(v')^2}} = \kappa y u_\tau$	$\left[\frac{m}{G_\beta(m)}\right]^2 \frac{T_w}{T_1}\,C_f$ $\left(\frac{1}{1-\beta m}\right)\left[\frac{G_\beta(m)}{m}\right]^2 \frac{T_1}{T_w}\frac{\mu_1}{\mu_w}\,R$	Generalization of Moretti's formulation of mixing length theory (94) to compressible flow. Shear equation reduces for negligible density-velocity correlation to $u_\tau = (\rho/\rho_w)\,\kappa y\,(du/dy)$ rather than $u_\tau = (\rho/\rho_w)^{1/2}\,\kappa y\,(du/dy)$. For $G_\beta(m)$ see Note (e). Result for $\beta = 0$ is identical with Li's and Nagamatsu's case $\alpha = \frac{1}{2}$. Representation of velocity profile near the free stream is improved in a second paper (89) using the von Mises transformation, and flow in a positive pressure gradient is treated in a third paper (90).

Note (a) $I_n(m)$ is the ratio of momentum thickness to total thickness for a power law profile, $u/u_1 = (y/\delta)^{1/n}$.

$$I_n(m) = \frac{\theta}{\delta} = n(1-m^2)\int_0^1 \frac{z^n(1-z)\,dz}{1-m^2z^2}$$

Tucker (72, 73) has tabulated this and related functions for n = 5, 7, 9, 11 and for Mach numbers from zero to ten. Gompf (91) has obtained expressions in closed form for n = 1, 7; in particular

$$I_7(m) = \frac{7}{2}\frac{(1-m^2)}{m^8}\left[2 - \frac{m^2}{3} - \frac{m^4}{10} - \frac{m^6}{21} - \ln(1-m^2) - \frac{1}{m}\ln\left(\frac{1+m}{1-m}\right)\right]$$

Note (b) T_m is a mean temperature associated with the mean density obtained by dividing mass flow by volume flow for a pipe. With a power law profile,

$$\frac{T_1}{T_m} = \frac{\rho_m}{\rho_1} = \frac{(n+1)(2n+1)}{n}(1-m^2)\int_0^1 \frac{z^n(1-z^n)\,dz}{1-m^2z^2}$$

and for n = 7,

$$\frac{T_1}{T_m} = \frac{60}{7}\frac{(1-m^2)}{m^{14}}\left[2 + \frac{2}{3}m^2 + \frac{2}{5}m^4 + \frac{2}{7}m^6 - \frac{7}{9}m^8 - \frac{7}{22}m^{10} - \frac{7}{39}m^{12} - m^6\ln(1-m^2) - \frac{1}{m}\ln\left(\frac{1+m}{1-m}\right)\right]$$

Note (c) Clemmow (83) shows that the series obtained by repeated partial integration of

$$J(z,\psi_1) = \int_0^{\psi_1} f(\psi)\,e^{z\psi}\,d\psi$$

where $f(0) = f(\psi_1) = 0$ and $f(\psi)$ is regular for $0 \le \psi \le \psi_1$, is asymptotic in the sense of Poincaré (92) for large values of z;

$$J \sim -\frac{f'(\psi_1)\,e^{z\psi_1}}{z^2}\left[1 - \frac{f''(\psi_1)}{f'(\psi_1)}\frac{1}{z} + \ldots\right]$$

Note (d) $F_\alpha(m)$ is a definite integral arising in the quadrature of the velocity profile,

$$F_\alpha(m) = \int_0^m \frac{\left[1 + (2\alpha - 1)\, z^2\right]^{1/2} dz}{1 - z^2}$$

and is given in closed form for general m and α in the GALCIT paper by Li and Nagamatsu (87). In particular,

$$F_0(m) = \sin^{-1} m$$

$$F_{1/2}(m) = \frac{1}{2} \ln\left(\frac{1+m}{1-m}\right)$$

$$F_1(m) = \frac{1}{\sqrt{2}} \ln\left(\frac{\sqrt{1+m^2} + m\sqrt{2}}{\sqrt{1+m^2} - m\sqrt{2}}\right) - \frac{1}{2} \ln\left(\frac{\sqrt{1+m^2} + m}{\sqrt{1+m^2} - m}\right)$$

Note (e) For constant stagnation enthalpy in the boundary layer, Ferrari obtains the velocity profile by integrating

$$\tau_w = \rho \kappa^2 y^2 \left(\frac{du}{dy}\right)^2 \frac{\rho}{\rho_w} \left[1 - \beta \sqrt{1 - \frac{\rho_w}{\rho}}\right]^{-2}$$

where Li and Nagamatsu use

$$\tau_w = \rho \kappa^2 y^2 \left(\frac{du}{dy}\right)^2 \frac{\rho}{\rho_w} \left[1 + (2\alpha - 1)\left(1 - \frac{\rho_w}{\rho}\right)\right]$$

The function $G_\beta(m)$ is given by

$$G_\beta(m) = \ln\left[\left(\frac{1+m}{1-m}\right)^{\frac{1}{2(1+\beta)}} \left(\frac{1-\beta m}{1-m}\right)^{\frac{\beta}{1-\beta^2}}\right]$$

Ferrari's formulation for $\beta = 0$ is also discussed in an appendix by Clemmow (83) and in a paper by Thompson (93).

is a convenient pseudo-Mach number based on the maximum attainable velocity,

$$m^2 = \frac{u_1^2}{2 c_p T_0} = 1 - \frac{T_1}{T_0} = \frac{\frac{\gamma-1}{2} M^2}{1 + \frac{\gamma-1}{2} M^2} \qquad (38)$$

and consequently ranges from zero to unity as the free stream Mach number M ranges from zero to infinity. In physical terms, m^2 is the fraction of the available energy which is in the form of directed kinetic energy in the free stream.

The various formulations of the compressible turbulent boundary layer problem of Table II are compared graphically in Figure 10, which shows the ratio of the local friction coefficient at a Mach number M to the value at zero Mach number, both being evaluated* at a Reynolds number $u_1 \xi / \nu$, of 10^7.

Three sources of possible ambiguity, beyond the variation involved in taking a value for n other than 7, must be considered in the comparison of the various curves in Figure 10. First, the temperature recovery factor has been taken as unity in all cases, so that $T_w = T_0$ and $\mu_w = \mu(T_0)$. Since T_1/T_w and $(1 - m^2)$ are not identical in the formulae if the recovery factor is different from

---

* The method of calculation is clear from Table II; given the Reynolds number R for the compressible flow at Mach number M, an equivalent Reynolds number for constant density is computed from the second entry of the third column of the table. The known local friction coefficient at this equivalent Reynolds number is then identified with the first entry in the third column of the table and the compressible friction coefficient follows.

unity, the original papers should be consulted to determine where one or the other of these quantities should be specified. Second, T_o has been taken as 550 °R, which is a representative value for wind tunnel operation up to Mach numbers of say five. Ignoring the probable occurrence of air condensation at larger Mach numbers, the viscosity has been computed from the Sutherland formula,

$$\frac{\mu}{\mu_+} = \left(\frac{T}{T_+}\right)^{3/2}\left(\frac{T_+ + C}{T + C}\right) \qquad (39)$$

with C = 192 °R for T_r = 492 °F. Eq. (39) is a good approximation to the values of viscosity tabulated by Hirschfelder, Bird, and Spotz (Table XVI, 95) for dry air at temperatures between 180 °R and 1000 °R.

Finally, the calculation in terms of an equivalent Reynolds number for low-speed flow is highly sensitive to the form of the assumed local friction law at zero Mach number and low Reynolds number. For example, the calculation of C_f/C_{f_i} by Wilson's formulation at a Reynolds number of 10^6 and a Mach number of 4.5 requires a knowledge of the local friction coefficient for a low-speed turbulent boundary layer at a Reynolds number $u_e\theta/\nu$ = 70,000, far beyond the range of experimental definition. Even if the values of Table I above are accepted, it is not clear that the concept of a turbulent boundary layer has physical significance for values of $u_e\theta/\nu$ less than say 50, since the turbulent friction is then less than the laminar value, given the writer's extrapolation toward

small Reynolds numbers in Table I. While there is not a uniform correspondence between the coefficient of R in the third column of Table II and the relative position of the corresponding curve in Figure 10, each of the formulations cited provides a function M(R) for which the method of calculation becomes questionable in the sense defined above, and extrapolation to indefinitely large Mach numbers in Figure 10 is therefore not recommended.

In commenting on the energy which has been dissipated in providing the material for Table II and Figure 10, it should be remembered that most of the papers in question were published before any experimental data became available, so that in general neither the premises nor the conclusions could be compared with experiment. However, it will be noted in later paragraphs that the predominating factor in the compressible turbulent boundary problem is the effect of high temperature on the velocity profile near the wall, and therefore on the shearing stress. This idea was first advanced by von Kármán in 1935 (71), but has been somewhat neglected in favor of interpolation formulae or of elaborate generalizations of the mixing length hypothesis.

The known importance of laminar dissipation in the sublayer suggests that the effect of increasing the Mach number at a given Reynolds number should be similar to the effect of decreasing the Reynolds number at a given Mach number. It is intuitively clear, other things being equal, that the increased temperature at the surface in high-speed flow implies a larger viscosity coefficient and a smaller velocity gradient, so that the thickness of the laminar

sublayer increases; the same behavior is of course responsible for the observed increase in thickness of laminar boundary layers at high Mach numbers. An adequate theory of the compressible turbulent boundary layer should predict this effect and determine its consequences.

Working independently, attempts to formulate the compressible problem in terms of the sublayer flow have been made by Kirkwood (96), by Amano (97), and more recently by Donaldson (98).

Kirkwood assumes a power law velocity profile

$$\frac{u}{u_1} = \left(\frac{y}{\delta}\right)^{1/n} \tag{40}$$

for the purpose of computing the momentum thickness, so that in the present notation

$$c_f = 2 I_n(m) \frac{d\delta}{d\xi} \tag{41}$$

where $I_n(m)$ is defined in Note (a) of Table II above. In order to avoid the difficulty of an infinite velocity derivative at the wall, Kirkwood assumes a linear sublayer profile with $\partial u/\partial y$ equal to its value at the wall. The two velocity curves then intersect at a point (u_s, y_s) which is assumed to satisfy the relationship

$$R_s = \frac{u_s y_s}{\nu_s} = \text{constant} \tag{42}$$

Evaluation of (41) and

$$c_f = \frac{\mu_w}{\rho} \frac{u_s}{y_s} \tag{43}$$

with u_s and y_s eliminated by means of Eqs. (40) and (42) results in an ordinary differential equation for $\delta(\xi)$,

$$(K_s)^{\frac{2}{n+1}} \frac{dR_s}{dR} = \frac{1}{I_n(m)} \frac{\mu_w}{\mu_1} \left(\frac{\mu_1}{\mu_s} \frac{T_1}{T_s}\right)^{\frac{n-1}{n+1}} (R_s)^{\frac{1-n}{1+n}} \tag{44}$$

The dependence of μ_s/μ_1 and T_s/T_1 on R is neglected by Kirkwood in integrating Eq. (44); R_s is taken as independent of Mach number; and several mathematical approximations are made which limit the validity of the result to small Mach numbers. That T_s/T_1 is in fact a slowly varying function of Reynolds number is evident from the equation of energy for constant stagnation enthalpy in the boundary layer,

$$\frac{T}{T_w} = 1 - m^2 \left(\frac{u}{u_1}\right)^2 \tag{45}$$

which implies, in view of (42) and (43),

$$\frac{T_1}{T_s} = 1 - m^2 \left(1 - \frac{c_f R_s}{2} \frac{\mu_s}{\mu_w}\right) \tag{46}$$

Donaldson (98), on the other hand, begins with the mixing length representation of the turbulent shearing stress and considers a constant ratio, say C, of the total to the turbulent shear at the intersection of the sublayer profile and the outer profile,

$$\tau_w = \mu_s \frac{u_s}{y_s} = C \left[\rho \kappa^2 y^2 (du/dy)^2\right]_s \tag{47}$$

Eq. (47) is evaluated for a power law profile, yielding the result that the sublayer Reynolds number $R_s = u_s y_s / \nu_s$ is constant. However, Donaldson's analysis is equivalent to Kirkwood's, since it is easily shown that given a velocity profile $u/u_1 = f(y/\delta)$ and given the expression (47)*, then either of R_s = constant and $u_s/u_1 = (y_s/\delta)^{1/n}$ implies the other, and furthermore that $R_s = n^2/C\kappa^2$.

Donaldson, in preference to integrating Eq. (44), uses the parametric representation obtained from (43) and (46),

$$C_f (R_s)^{\frac{2}{1+n}} = 2 \left(R_s \frac{T_s}{T_1} \right)^{\frac{1-n}{1+n}} \left(\frac{\mu_s}{\mu_1} \right)^{\frac{2}{1+n}} \qquad (48)$$

and

$$\frac{T_1}{T_s} = 1 - n^2 \left(1 - \frac{C_f R_s}{2} \right) \qquad (49)$$

where μ_w does not appear since Donaldson uses μ_s rather than μ_w in Eq. (43).

Amano (97) writes two momentum equations, for the variation with ξ of the sublayer thickness y_s and of the full boundary layer thickness δ, and eliminates ξ between these expressions. The velocity distribution in the sublayer contains a transition term

---

* Donaldson writes the term $\mu_s u_s / y_s$ as $(\mu \partial u/\partial y)_s$, with the latter evaluated as $\mu_s u_s / n y_s$ for the power profile; C is then the ratio of laminar to turbulent shearing stress, although both are underestimated in approaching the point of discontinuity in $\partial u/\partial y$ from above. The final result is unchanged in any important detail.

which allows matching the derivative $\partial u/\partial y$ at the intersection with the power law profile; the shearing stress at this point is assumed to be wholly turbulent and is expressed by the mixing length formula (47). Several approximations in the momentum integrals limit the validity of the analysis to small Mach numbers, and the treatment is in general similar to that of Kirkwood.

It is instructive to compare several estimates of the magnitude of the sublayer Reynolds number R_s. Kirkwood, Donaldson, and Amano all cite Prandtl's evaluation of the constants in the integrated form of Eq. (44) to arrive at the value $R_s = 158$ for low-speed flow. Alternatively, the edge of the sublayer may be defined as the intersection of the two curves in Figure 4 of the present paper, at $u_s/u_\tau = y_s u_\tau/\nu = 11.3$, say, so that $R_s = 128$. Or the value of the stress ratio C may be anticipated from the data of Table III below as 1/0.54 at $y_s u_\tau/\nu = 11.3$, and using $\kappa = 0.4$ and $n = 7$ then $R_s = n^2/C\kappa^2 = 165$.

Equations (48) and (49) above allow an estimate of the variation with Mach number of the relative sublayer thickness. Computing y_s/δ from (40) and (42),

$$\frac{y_s}{\delta} = \left(\frac{R_s}{R_\delta} \frac{\mu_s}{\mu_i} \frac{T_s}{T_i} \right)^{\frac{n}{n+1}} \qquad (50)$$

and taking $R_s = 158$, $n = 7$, and $R_\delta = 5 \times 10^5$, the latter corresponding roughly to $R = 3 \times 10^6$ for zero Mach number, the approximate sublayer thickness at various Mach numbers is given by the table below.

M	y_s/δ
0	.007
2	.013
4	.035
6	.072
8	.121
10	.180

The values of y_s/δ tabulated here account in part for the writer's mistrust of generalizations of the conventional mixing length hypothesis to compressible flow, since these analyses emphasize the logarithmic region in the velocity profile, while in fact this region may become progressively less important at large Mach numbers.

It can be shown from Eqs. (48) and (49) that the local friction coefficient must decrease as the Mach number increases for fixed values of R_δ and R_s, and that the predicted change is in good agreement with recent measurements. At the same time, the local Mach number at the edge of the sublayer increases, since, from Eqs. (45) and (49),

$$M_s = M_1 \sqrt{\frac{c_f R_s}{2}}$$

In inquiring whether the sonic local Mach number is distinguished in a turbulent shear flow, no definite conclusions can at present be drawn from experiment. However, if it is assumed that large fluctuations in velocity will continue to characterize the flow near the edge of the sublayer at large free stream Mach numbers, it follows that a condition may eventually be reached say at Mach numbers of order 20 where the r.m.s. velocity fluctuations will

become sonic with respect to the local flow, and that radiation of energy into the ambient fluid may then dominate in determining the drag. On the other hand, at large Mach numbers it appears that the Reynolds number must also be large in order for a turbulent shear flow with a sublayer in the conventional sense to exist, so that the hypersonic boundary layer of technical interest may have few of the characteristics now attributed to turbulent flows at lower speeds.

2. Equations of Motion. The most conspicuous feature of the discussion so far is that it has been carried out without benefit of reference to the detailed differential equations of motion for the turbulent boundary layer. The writer feels that this omission is a serious one, and in attempting to repair it has been led to some interesting ideas in connection with the law of the wall, especially for compressible shear flow. Although the important results could be obtained directly, the development is most logically presented in the sequence in which the various aspects of the problem were originally considered, and so begins with the special case of incompressible flow.

The turbulent boundary layer equations* may be written, for

---

* No distinction is made in the first of these equations between the static pressure outside the boundary layer, denoted by p, and the statistical pressure within the boundary layer, which includes a contribution from the turbulent normal stresses. In any more sophisticated treatment of the role of the pressure, particularly in connection with the mechanism of production, transfer, and dissipation of turbulent energy near the wall, the discussion of the present section should be reexamined. However, a precedent may be found (19, see also 99) for connecting, for a free jet, the experimental mean velocity and turbulent shearing stress distributions through the equations of motion.

a fluid of constant density,

$$u \frac{\partial u}{\partial x} + v \frac{\partial u}{\partial y} = - \frac{1}{\rho} \frac{dp}{dx} + \frac{1}{\rho} \frac{\partial \tau}{\partial y} \qquad (51)$$

$$\frac{\partial u}{\partial x} + \frac{\partial v}{\partial y} = 0 \qquad (52)$$

$$\tau = \mu \frac{\partial u}{\partial y} - \rho \overline{u'v'} \qquad (53)$$

Schultz-Grunow (47) and others at Göttingen have investigated Eqs. (51) - (52) from the experimental point of view, making use of measurements of the velocity field u(x,y) in a turbulent flat plate boundary layer. In spite of obvious difficulties encountered in the differentiation of experimental data, the shearing stress profiles obtained are quite plausible. Strangely, the corresponding theoretical investigation of the kinematic properties of the turbulent shear flow near a wall, using the equations of motion and the information about the velocity distribution which is available in the similarity laws, has apparently never been carried out.

The present development begins with an investigation of the consequences of the assumption that the mean velocity profile in the region near the wall is given by the similarity law

$$\frac{u}{u_\tau} = f\left(\frac{y u_\tau}{\nu}\right) \qquad (21)$$

In fact, the experimental observation of Ludwieg and Tillmann (56) that Eq. (21) describes the velocity profile near the wall even

when the flow involves a pressure gradient, permits the consideration of the full Eq. (51) including the pressure gradient term.

Eq. (21) and the continuity equation (52) imply, with the boundary condition $v = 0$ at $y = 0$,

$$\frac{v}{u_\tau} = -\frac{\mu}{\tau_w}\frac{du_\tau}{d\xi}\frac{yu_\tau}{\nu}\frac{u}{u_\tau} \tag{54}$$

where ξ is written for x in order to preserve the notation of the paragraphs above, and x will be used throughout the sequel.

Furthermore, Eq. (51) can be integrated, with the aid of Eqs. (21) and (54) and the boundary condition $\tau = \tau_w$ at $y = 0$, to yield

$$\frac{\tau}{\tau_w} = 1 + \frac{y}{\tau_w}\frac{dp}{dx} + \frac{\mu}{\tau_w}\frac{du_\tau}{dx}\int_0^{yu_\tau/\nu}\left(\frac{u}{u_\tau}\right)^2 d\,\frac{yu_\tau}{\nu} \tag{55}$$

The derivation of Eqs. (54) and (55) is greatly simplified by the fact that certain terms involving derivatives of the function f either combine or cancel each other. In the belief that this happy circumstance is not entirely accidental, a fresh beginning may be made by examining Eq. (51) more closely in an attempt to determine necessary and sufficient conditions for the shearing stress distribution to have the particularly simple form given by Eq. (55). For this purpose it is convenient to write (51), with the aid of (52), as

$$\frac{\partial\tau}{\partial y} = \frac{dp}{dx} + \rho\frac{\partial uu}{\partial x} + \rho\frac{\partial uv}{\partial y} \tag{56}$$

so that

$$\tau - \tau_w = y \frac{dp}{dx} + \rho u v + \rho \int_0^y \frac{\partial u^2}{\partial x} dy$$

$$= y \frac{dp}{dx} - \rho u \int_0^y \frac{\partial u}{\partial x} dy + \rho \int_0^y \frac{\partial u^2}{\partial x} dy \qquad (57)$$

Replacing the independent variable u in the incomplete momentum integral Eq. (57) by u/u_τ, as suggested by the relationship $\tau_w = \rho u_\tau^2$, it follows that

$$\frac{\tau}{\tau_w} = 1 + \frac{y}{\tau_w} \frac{dp}{dx} - \frac{1}{\lambda} \int_0^y \left(\frac{u}{u_\tau}\right)^2 dy + \psi(x, y) \qquad (58)$$

with the function ψ given by

$$\psi(x, y) = \frac{1}{\lambda} \frac{u}{u_\tau} \int_0^y \left(\frac{u}{u_\tau}\right) dy - \frac{u}{u_\tau} \int_0^y \frac{\partial}{\partial x} \left(\frac{u}{u_\tau}\right) dy$$

$$- \frac{1}{\lambda} \int_0^y \left(\frac{u}{u_\tau}\right)^2 dy + \int_0^y \frac{\partial}{\partial x} \left(\frac{u}{u_\tau}\right)^2 dy \qquad (59)$$

The length $\lambda(x)$, connected with the distribution of surface friction*, is defined by

---

* A simple geometrical interpretation of the parameter λ is provided for a flat plate by Eq. (54), which may be written

$$v/u = y/\lambda$$

and it follows that the velocity vector through a point (x, y) intersects the surface a distance λ upstream.

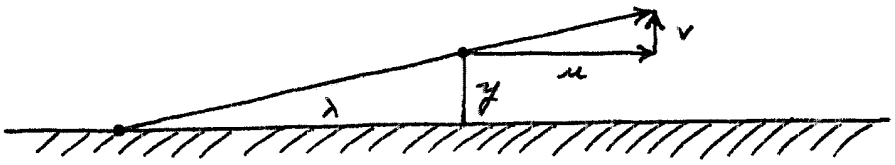

Furthermore, since λ is a function only of x, this property defines completely the direction of the velocity vector field at a given station along the plate; the streamlines thus follow directly from the surface shearing distribution, and conversely.

$$\frac{1}{\lambda} = -\frac{1}{u_\tau}\frac{du_\tau}{dx} \tag{60}$$

Comparing Eqs. (58) and (55) it appears desirable, since a necessary condition for Eq. (55) is being sought, to investigate further the properties of the differential equation obtained by putting

$$\psi\left(\frac{u}{u_\tau}, x, y\right) \equiv 0 \tag{61}$$

Differentiating Eq. (59) twice with respect to y, eliminating the definite integrals between $\partial\psi/\partial y = 0$ and $\partial^2\psi/\partial y^2 = 0$, and denoting the velocity ratio u/u_τ temporarily by r, the equation is obtained

$$\frac{\frac{\partial\psi}{\partial y}\frac{\partial^2\psi}{\partial x\partial y} - \frac{\partial\psi}{\partial x}\frac{\partial^2\psi}{\partial y^2}}{\left(\frac{\partial\psi}{\partial y}\right)^2} = \frac{\partial}{\partial y}\left(\frac{\partial\psi/\partial x}{\partial\psi/\partial y}\right) = -\frac{1}{\lambda} \tag{62}$$

Integrating once with respect to y and neglecting the arbitrary function of x since $\partial\psi/\partial x$ vanishes at the wall, then

$$\frac{\partial\psi}{\partial x} + \frac{y}{\lambda}\frac{\partial\psi}{\partial y} = 0 \tag{63}$$

The level curves, or more properly characteristic curves, of Eq. (63) are easily found by considering the curve r = constant, so that

$$d\psi = \frac{\partial\psi}{\partial x}dx + \frac{\partial\psi}{\partial y}dy = 0$$

and consequently

$$\frac{dy}{dx} = \frac{y}{\lambda(x)} \tag{64}$$

Substituting for $\lambda(x)$ from (60) and integrating, the characteristic curves of Eq. (63) are given by yu_τ = constant, and it follows that

$$+ = \frac{u}{u_\tau} = f\left(\frac{y u_\tau}{\nu}\right) \tag{21}$$

is the general solution of Eq. (61), $\psi(u/u_\tau, x, y) = 0$. The parameter ν is introduced here on the ground of dimensional homogeneity in the argument of the function f, since u/u_τ approaches yu_τ / ν for y approaching zero. That is, from the definition of τ_w as a particular case of Eq. (53),

$$\lim_{y \to 0} u = y\left(\frac{\partial u}{\partial y}\right)_w = \frac{y}{\mu}\tau_w = \frac{y u_\tau^2}{\nu} \tag{65}$$

To recapitulate, an expression has been obtained for the distribution of total shearing stress in a turbulent shear flow near a wall, in terms of a functional similarity observed experimentally for the velocity profile. In the absence of information about the velocity distribution, the same expressions may be obtained through consideration of a function $\psi(x, y)$ which appears in the integrated momentum equation. Since the only property of the turbulent field which has been used is the requirement that it vanish at the wall, thus excluding automatically the case of a rough wall,

it is not even necessary in the derivation to define the concept of turbulent shearing stress. Several arguments can be advanced to support the critical step in the analysis above, which is placing the function $\psi(x, y)$ equal to zero; the strongest of these is of course the fact that the law of the wall is obtained directly. However, if the use of a posteriori arguments to justify the treatment is to be avoided, it is necessary to look for convincing physical reasons for supposing that the shearing stress distribution has the form given in Eq. (55).

A beginning might be made by observing that the equations of motion (51) - (52) and the boundary conditions on the velocity at the wall together imply certain boundary conditions for the shearing stress distribution. For example, successive differentiation of Eq. (51) with respect to y leads to the series of expressions

$$\tau(x, o) = \tau_w(x) \tag{66a}$$

$$\tau_y(x, o) = \frac{d\rho(x)}{dx} \tag{66b}$$

$$\tau_{yy}(x, o) = 0 \tag{66c}$$

$$\tau_{yyy}(x, o) = -2 \frac{\tau_w^2(x)}{\mu \nu \lambda(x)} \tag{66d}$$

and so on, where the subscript y indicates partial differentiation. Eq. (66d) in particular is valid if the shearing stress at the wall

is identified with the laminar value $\mu \partial u/\partial y$. But these expressions could also be obtained directly from Eq. (55), and it follows that at least the first three derivatives of the function ψ vanish at the wall; in other words, no information about the first four terms in a hypothetical partial Taylor series expansion for $\tau(y)$ is lost by putting $\psi \equiv 0$. However, this process cannot be continued without more complete knowledge of the turbulence, since higher derivatives at the wall of the mean velocity cannot in general be identified with the appropriate derivatives of the shearing stress τ unless the turbulent shear correlation $-\overline{u'v'}$ in Eq. (53) has a derivative of the proper order which vanishes at the wall. It is clear that some such distinction must be recognized or there would be nothing in the development to distinguish between a laminar sublayer and a fully laminar boundary layer. On the other hand, it is easily shown that an expression of the form (21) is not compatible with the laminar similarity parameter $y/\sqrt{x}$ except for the trivial case of a linear velocity profile.

Similar considerations prevent any attempt to show rigorously whether Eq. (21) is an integral of the equations of motion for turbulent shear flow near a wall. For if it were, the two alternative derivations given above for the shearing stress distribution, Eqs. (55) and (58), would require the function ψ to be identically zero, so that if $\psi(x, y)$ has a partial Taylor expansion about $y = 0$, the coefficients could be computed by repeated differentiation of Eq. (59) or of Eqs. (58) and (51), and would necessarily be zero for all orders. That this computation is not possible

without more information about the turbulent field has already been shown.

The remarks above are related to a less obvious property of Eq. (21), which is that the physical scale for flow near a wall is determined by the kinematic viscosity of the fluid rather than by the proximity of a second free or solid boundary. An example for which experimental data are available (44) is the velocity profile in the wind near the ground. The difficulty in visualizing an origin or a second boundary for the large scale meteorological system does not prevent the application* of Eq. (21) to determine one of the quantities τ_w, ρ, μ, u, or y when the others are given.

It is possible that the physical scale for the turbulent shear flow near a plane is in fact connected with the region of validity of a particular formulation of the turbulence problem, and in this sense may depend on the nature of the other boundaries of the flow. To be explicit, one may consider a correspondence between some properties of the turbulent field behind a grid and of the turbulent shear flow near a wall. This comparison was recently suggested to the writer by Professor H. W. Liepmann, and had already been discussed by Lin and Shen (100). Both systems are characterized by the presence of large eddies, which are responsible for accepting energy from a prime mover, and by the presence of small eddies,

---

* The effects of surface roughness or thermal instability may not be negligible in such applications; see the discussion below of variable density.

in which viscous dissipation accompanies an approach to isotropy; in each case two distinct scales enter provided that the Reynolds number of the flow is sufficiently large. In the boundary layer the large eddies are manifested in the phenomenon of intermittence, in the velocity defect law, and in the macroscale of the space correlation. These large eddies are essentially independent of viscosity, but are fundamental in determining the shear field; that is, the shearing stress depends on the entire history of the turbulent flow and therefore on the scale in the large. The small scale turbulent structure in a boundary layer, on the other hand, is dependent on the local flow conditions, since both laminar and turbulent dissipation are large near the wall (25).

In this connection it is interesting to note that the turbulent flat plate boundary layer in a uniform stream has in common with the uniform turbulent channel flow the important property that the characteristic length for the logarithmic velocity distribution is ν/u_τ, while the characteristic length in the same region for the total shearing stress is very nearly δ. From Eq. (55), either

$$\frac{\partial \tau/\tau_w}{\partial y u_\tau/\nu} = -\frac{\nu}{\lambda u_\tau}\left(\frac{u}{u_\tau}\right)^2 \qquad (67)$$

or

$$\frac{\partial \tau/\tau_w}{\partial y/\delta} = -\frac{\delta}{\lambda}\left(\frac{u}{u_\tau}\right)^2 \qquad (68)$$

It is easily shown, for example with the velocity profile $u/u_\tau = A(yu_\tau/\nu)^{1/n}$, that the right hand side of (68), considered as a function of x and y/δ, is much more nearly independent of x than is the right hand side of (67) considered as a function of x and yu_τ/ν. That is, for the power friction law implied by the velocity profile in question, λ is proportional to x from Eq. (60), while C_F is a constant multiple of C_f and θ/δ is a constant. It follows from Eq. (68) that

$$\frac{\partial \tau/\tau_w}{\partial y/\delta} \sim (C_f)^{\frac{n+3}{n}} (R)^{\frac{2}{n}} (y/\delta)^{\frac{2}{n}} \qquad (69)$$

for values of yu_τ/ν outside the sublayer but within the region of validity of the law of the wall. However, the quantity $(C_f)^{\frac{n+3}{2}} \times (R)$ does not depend on R for a power friction law (23), and the right hand side of (68) is therefore a function only of (y/δ), even in a region where the velocity distribution depends on yu_τ/ν. That the channel also has this property is obvious but by no means trivial, since the interpretation must be that the shearing stress distribution depends strongly on the large scale eddy motion and thus on the history of the flow, while the local velocity near the wall depends on the small scale turbulent motion, and in particular on the local dissipation. It is clear that the traditional theories cannot predict this property for a turbulent shear flow when the shearing stress is assumed constant, particularly since the differential equation for the velocity distribution, e.g. Eq. (47) above, is homogeneous in y and therefore independent of the choice of scale for this coordinate.

It would appear at first glance that the channel flow is not included in the development above, since the properties of the flow do not depend on x in a given channel and so Eq. (61) is obviously satisfied by virtue of (60). Eq. (21) reduces, for practical purposes, to $u = f(y)$, and no quarrel is likely to arise as to whether this is an integral of the equations of motion for a uniform channel; it is therefore convenient to consider the flow in a channel as a limiting case of a flow between diverging or converging walls, or to rely on the limiting expression (65). The fact that the channel or pipe is not distinguished from the boundary layer in the analysis given above is consistent with the experimental observation that near the wall the same velocity profile obtains in all three cases, and so lends support to the view that a general flow with pressure gradient should be characterized by the same law of the wall as that discussed above. The important boundary conditions here are certainly connected with the presence of the wall, e.g. Eqs. (66a) - (66d), rather than with conditions in the external flow.

On the other hand, it is probable that there is a difference in kind as well as in degree between the sublayer flows in a channel and in a boundary layer. The kinematic behavior of the mean turbulent shear flow, to the extent that it implies the law of the wall, show that in the absence of a pressure gradient the turbulent correlation $\overline{u'v'}$ varies like y^3, or like u^3, near the wall; but in the presence of a pressure gradient there is an additional variation like y, or like u. The essential difference is the nature of the energy reservoir, which contains unlimited kinetic energy in one case and unlimited pressure energy in the other; the dynamics

of the turbulent fields apparently must also differ either in the magnitude of the velocity fluctuations or in the correlation coefficient $\overline{u'v'} / \sqrt{\overline{u'^2}}\sqrt{\overline{v'^2}}$ very near the wall.

The fact that the law of the wall is experimentally independent of these differences in dynamics, and the observation that this law is inherently incapable of predicting the magnitude of the surface shearing stress, which depends on the large scale structure and thus on considerations of energy, should be kept in mind later when it becomes necessary to discuss the thermodynamics of fluids of variable density.

Finally, it is interesting to note that Eq. (55) implies that the total shearing stress can have a maximum away from the wall if and only if the pressure is increasing and the surface shearing stress decreasing in the direction of flow, thus establishing a necessary condition for a turbulent boundary layer approaching separation.

In order to implement the remarks above, more detailed experimental evidence in favor of the law of the wall is required. Figure 11 shows three velocity profiles which include data for the sublayer flow. The measurements by Laufer (25) were carried out in a 10-inch diameter pipe, for which the surface shearing stress was obtained from the observed pressure gradient. For values of yu_τ/ν greater than 150 the mean velocity was obtained from pitot tube measurements, and for smaller values from hot wire data. Dr. P. S. Klebanoff has provided some as yet unpublished measurements for a

free stream velocity of 50 feet per second in the same boundary layer already mentioned (26); these data were likewise obtained with pitot tube and hot wire instrumentation. The friction coefficient estimated by Klebanoff for his flat plate measurements has been decreased by 8 percent to agree with the values already presented in Figure 2. Finally, one of van der Hegge Zijnen's profiles (64), for a local free stream velocity of 8 meters per second at x = 0.7 meters, is included in Figure 11; these data were obtained with a hot wire anemometer. For Zijnen's measurements C_f was chosen to provide agreement in the coordinate system (u/u_τ, yu_τ/ν) with the logarithmic region of Figure 4, and lies about midway between the values of $\mu(\partial u/\partial y)_w/q$ and $2d\Theta/dx$. Of the experiments cited here, Laufer's measurements may well be taken as definitive in view of the implied accuracy in the friction coefficient.*

Table III shows a set of tentative values for the four functions**

---

* Laufer's channel data (33), and some later measurements of Skinner (101) in the same apparatus, do not agree with the curve of Figure 11, lying appreciably above the data shown. After several discussions with Dr. Laufer of possible anomalies in his channel experiments, a decision of nolle prosequi was handed down.

** Measurements of turbulent shearing stress in a boundary layer approaching separation have been made by Schubauer and Klebanoff (34). In attempting to apply the relationships above to these data, the writer has found it necessary to concur in the opinion of Goldschmied (6) and of Ross and Robertson (102) that the published values of shearing stress are too large. If the velocity profile data are required to agree with Eq. (24), then the friction coefficients should be taken as 65 to 70 percent of the published figures.

Table III

The Law of the Wall in Detail

for a Fluid of Constant Density

$\frac{y u_\tau}{\nu}$	$\frac{u}{u_\tau}$	$\frac{u}{u_\tau}\,\frac{y u_\tau}{\nu}$	$\frac{d\,u/u_\tau}{d\,y u_\tau/\nu}$	$\int_0^{y u_\tau/\nu} \left(\frac{u}{u_\tau}\right)^2 d\,\frac{y u_\tau}{\nu}$
0	0	0	1.000	0
1	.99	1	.984	0
2	1.96	4	.960	3
3	2.90	9	.925	9
4	3.80	15	.880	20
5	4.65	23	.828	38
6	5.45	33	.771	63
7	6.19	43	.712	97
8	6.87	55	.651	140
9	7.49	67	.591	192
10	8.05	81	.536	252
12	9.00	108	.427	398
14	9.76	137	.350	575
16	10.40	166	.300	778
18	10.97	198	.267	1007
20	11.49	230	.240	1260
24	12.34	296	.190	1830
28	12.99	364	.140	2473
32	13.48	431	.109	3180
36	13.88	500	.092	3920
40	14.22	569	.079	4720
44	14.51	638	.068	5540
50	14.87	744	.050	6840
60	15.33	920	.042	9130
80	16.04	1283	.031	14040
100	16.60	1660	.025	19480
150	17.61	2642	.017	34100
200	18.33	3670	.013	50200
300	19.34	5800	.008	85800
400	20.06	8020	.006	124700
500	20.62	10310	.005	166200
600	21.08	12650	.004	209700
800	21.79	17430	.003	302000
1000	22.35	22350	.003	399000
1500	23.36	35000	.002	661000
2000	24.08	48200	.001	943000
3000	25.09	75300	.001	1549000
4000	25.81	103200	.001	2197000
5000	26.37	131900	.001	2879000
6000	26.83	161000		3590000
8000	27.54	220300		5060000
10000	28.10	281000		6610000

$$\frac{u}{u_\tau} = f\left(\frac{y u_\tau}{\nu}\right) \tag{21}$$

$$\frac{\lambda u_\tau}{\nu}\frac{v}{u_\tau} = \frac{y u_\tau}{\nu}\frac{u}{u_\tau} \tag{54}$$

$$\frac{\lambda u_\tau}{\nu}\left(1 - \frac{\tau}{\tau_w}\right) = \int_0^{y u_\tau/\nu} \left(\frac{u}{u_\tau}\right)^2 d\,\frac{y u_\tau}{\nu} \tag{55}$$

$$\frac{\tau}{\tau_w} + \frac{\overline{u'v'}}{u_\tau^2} = \frac{d\,u/u_\tau}{d\,y u_\tau/\nu} \tag{53}$$

which depend only on the argument yu_τ/ν in the absence of roughness and pressure gradient. For these conditions the friction parameter $\lambda u_\tau/\nu$ may be obtained from the information of Table I, since from Eqs. (60), (26), (29), and (30),

$$\frac{\lambda u_\tau}{\nu} = \frac{2\kappa}{c_f} R_\theta \left(1 + \frac{c_2}{c_1}\frac{c_f}{2\kappa}\frac{\delta^*}{\theta}\right) \tag{70}$$

If there is no pressure gradient, an analysis similar to that above may be carried out for the velocity defect law,

$$\frac{u_1 - u}{u_\tau} = F\left(\frac{y}{\delta}\right) \tag{22}$$

and leads first, through the continuity equation (52), to a defect law for the normal velocity component;

$$\frac{v_1 - v}{u_\tau} = \frac{d\delta}{dx}\left(\frac{u_1 - u}{u_\tau}\right)\frac{y}{\delta} + \left(\frac{d\delta}{dx} - \frac{\delta}{\lambda}\right)\int_{y/\delta}^{1}\left(\frac{u_1 - u}{u_\tau}\right) d\,\frac{y}{\delta} \tag{71}$$

where $v = v_1$ at $y = \delta$ and

$$\frac{v_1}{u_1} = \frac{d\delta^*}{dx} \tag{72}$$

as is easily shown from the continuity equation for a quite general velocity distribution u(y).

It is not surprising, in view of what has gone before, that the assumption that the two equations (71) and (54) for v(x, y) have a common region of validity requires the velocity distribution u(x, y) in this region to have precisely the form* of Eq. (24), and further implies Eqs. (23) and (26).

The writer has not found an alternative form for the expression (71) which is mechanically simpler than the one given above; the same is true for the shearing stress which follows from (22), (71), and (51);

$$\begin{aligned}\frac{\tau}{\tau_w} = {} & \left(\frac{d\delta}{dx} - \frac{\delta}{\lambda}\right)\left(\frac{u_1}{u_\tau} + \frac{u_1 - u}{u_\tau}\right)\int_{y/\delta}^{1}\left(\frac{u_1 - u}{u_\tau}\right) d\frac{y}{\delta} \\ & - \left(\frac{d\delta}{dx} - 2\frac{\delta}{\lambda}\right)\int_{y/\delta}^{1}\left(\frac{u_1 - u}{u_\tau}\right)^2 d\frac{y}{\delta} \\ & - \left(\frac{d\delta^*}{dx} - \frac{y}{\delta}\frac{d\delta}{dx}\right)\frac{u_1}{u_\tau}\left(\frac{u_1 - u}{u_\tau}\right)\end{aligned} \tag{73}$$

Practical calculation of the turbulent shearing stress distribution for a boundary layer with zero pressure gradient is expedited

---

* The detailed kinematic conditions imposed on the flow by the equations of conservation of mass and momentum are of course not necessary to the proof.

by the relationship, from Eq. (26),

$$\frac{d\delta}{dx} = \frac{\delta}{\lambda}\left(1 + \kappa \frac{u_1}{u_\tau}\right) \tag{74}$$

together with two auxiliary formulae. The first, from (29) and (74), is

$$\frac{d\delta^*}{dx} = \kappa C_1 \frac{\delta}{\lambda} \tag{75}$$

and the second, from (70), (26), (35), and (34), is

$$\frac{\lambda}{\delta} = C_2\left(1 - \kappa \frac{u_1}{u_\tau}\right) + \kappa C_1 \left(\frac{u_1}{u_\tau}\right)^2 \tag{76}$$

It should be noted that Eqs. (75) and (76) are not exact in the sense that (74) is exact, since the appearance of the parameters C_1 and C_2 means that the defect law (22) has been assumed to apply in the sublayer. Table IV, which is based on the experimental data of Figure 5 above, lists some tentative values for several functions of the argument y/δ which appear in Eqs. (71) and (73).

Although the possible consequences of the equations of motion have by no means been exhausted, it is not clear that there is an immediate profit to be gained from a further study of the defect law at the present time. The phenomenon of intermittence, while it does not invalidate Eqs. (51) - (53) if the concepts of average velocity and average shearing stress are clearly defined, must also

Table IV

The Velocity Defect Law in Detail
for a Fluid of Constant Density

$\frac{y}{\delta}$	$\frac{u_1 - u}{u_\tau}$	$\int_{y/\delta}^{1} \left(\frac{u_1 - u}{u_\tau}\right) d\frac{y}{\delta}$	$\int_{y/\delta}^{1} \left(\frac{u_1 - u}{u_\tau}\right)^2 d\frac{y}{\delta}$
.010	14.31	3.79	24.45
.015	13.30	3.72	23.40
.020	12.58	3.66	22.56
.025	12.02	3.60	21.81
.030	11.57	3.54	21.11
.040	10.85	3.43	19.86
.050	10.29	3.32	18.75
.060	9.83	3.22	17.73
.080	9.11	3.03	15.95
.100	8.56	2.86	14.39
.150	7.54	2.46	11.17
.200	6.70	2.10	8.64
.250	6.00	1.78	6.63
.300	5.37	1.50	5.01
.350	4.79	1.25	3.73
.400	4.25	1.02	2.70
.450	3.73	.82	1.91
.500	3.23	.65	1.30
.550	2.76	.50	.86
.600	2.31	.37	.53
.650	1.89	.27	.31
.700	1.50	.18	.17
.750	1.14	.11	.08
.800	.82	.07	.03
.850	.53	.03	.01
.900	.29	.01	0
.950	.10	0	0
1.000	0	0	0

be taken into account in an analysis of experimental data in order to insure that the quantities measured correspond to the accepted definitions. This remark is particularly relevant to the averaging properties of the measuring instruments used, and to the application of a Lagrangian concept of turbulent mixing to an Eulerian frame of reference. This is not to say that a study, for example, of the equations of motion with a generalized velocity defect law, including a pressure gradient parameter such as $\delta(dp/dx)/\tau_w$, might not shed some light on the validity of the single-parameter hypothesis for turbulent boundary layers.

It is the development involving Eqs. (57) - (65) which holds some promise of providing a generalization of the law of the wall to flows in which changes in density are not negligible. The discussion is simplified by omitting the pressure gradient term in the equations of motion and by assuming constant surface temperature, so that the reference density may be taken to be independent of x.

Since most engineering applications of boundary layer theory make use of the conventional definitions of drag coefficient and Reynolds number in terms of free stream quantities, Eqs. (1) - (3) may be retained with the stipulation that the free stream viscosity and static density are to be used. That is, in the absence of pressure gradient and surface roughness for an otherwise ideal boundary layer.

$$c_F = 2\frac{\theta}{x} = \frac{2}{x}\int_0^{\delta+} \frac{\rho}{\rho_1}\frac{u}{u_1}\left(1-\frac{u}{u_1}\right)dy \qquad (4)$$

$$c_f = 2\frac{d\theta}{dx} = \frac{\tau_w(x)}{\rho_1 u_1^2/2} \tag{7}$$

$$R = \frac{\rho_1 u_1 x}{\mu_1} \tag{31}$$

Under these circumstances, the definition of a friction velocity u_τ is still subject to some ambiguity. If the relationship chosen is $C_f = 2(u_\tau/u_1)^2$, then from Eq. (7), $\tau_w = \rho_1 u_\tau^2$. On the other hand, Eq. (65) may be generalized in view of Eq. (53) to

$$\lim_{y\to 0} u = y\left(\frac{\partial u}{\partial y}\right)_w = \frac{y}{\mu_w}\tau_w = \frac{y}{\nu_w}\frac{\tau_w}{\rho_w} \tag{77}$$

so that very near the wall the relationship $u/u_\tau = yu_\tau/\nu_w$ is valid only if $\tau_w = \rho_w u_\tau^2$. In order to distinguish between these alternatives, an unidentified reference density ρ_τ will be introduced by means of the expression

$$\tau_w = \rho_\tau u_\tau^2 \tag{78}$$

A second reference density, ρ_v say, is suggested by the fact that variations in density require a distinction to be drawn between the volume flow vector $\vec{q}$ and the specific momentum vector $\rho\vec{q}$ (5). Defining these vectors by their components as

$$\vec{q} = (u, v) \tag{79}$$

$$\rho \vec{q} = (\rho u, \rho v) = (\rho_v U, \rho_v V) \tag{80}$$

the boundary layer equations in terms of mean quantities may be written

$$\frac{\partial \rho u}{\partial x} + \frac{\partial \rho v}{\partial y} = \frac{\partial U}{\partial x} + \frac{\partial V}{\partial y} = 0 \tag{81}$$

$$\frac{\partial \tau}{\partial y} = \rho u \frac{\partial u}{\partial x} + \rho v \frac{\partial u}{\partial y} = \rho_v \left(\frac{\partial U u}{\partial x} + \frac{\partial V u}{\partial y} \right) \tag{82}$$

so that the more general form of Eq. (57) is

$$\tau - \tau_w = -\rho_v u \int_0^y \frac{\partial U}{\partial x} dy + \rho_v \int_0^y \frac{\partial U u}{\partial x} dy \tag{83}$$

Introducing the independent variables u/u_τ and U/u_τ in the two integrals, with u_τ defined by Eq. (78),

$$\frac{\tau}{\tau_w} = 1 - \frac{1}{\lambda} \frac{\rho_v}{\rho_\tau} \int_0^y \left(\frac{U u}{u_\tau^2} \right) dy + \psi(x, y) \tag{84}$$

where λ is defined by Eq. (60) above and

$$\begin{aligned} \frac{\rho_\tau}{\rho_v} \psi = {} & \frac{1}{\lambda} \frac{u}{u_\tau} \int_0^y \left(\frac{U}{u_\tau} \right) dy - \frac{u}{u_\tau} \int_0^y \frac{\partial}{\partial x} \left(\frac{U}{u_\tau} \right) dy \\ & - \frac{1}{\lambda} \int_0^y \left(\frac{U u}{u_\tau^2} \right) dy + \int_0^y \frac{\partial}{\partial x} \left(\frac{U u}{u_\tau^2} \right) dy \end{aligned} \tag{85}$$

A comparison of successive derivatives of the shearing stress,

from Eqs. (82) and (84), shows that ψ, $\partial\psi/\partial y$, $\partial^2\psi/\partial y^2$, and $\partial^3\psi/\partial y^3$ vanish at the wall as in the case of constant density, and that this result is valid for arbitrary heat transfer and for an arbitrary equation of state as long as the existence of a sublayer is assumed, so that the surface friction is Newtonian, Eq. (77). However, since there appears at present to be no way to show rigorously that $\psi \equiv 0$ follows from the equations of motion and the boundary conditions, thus requiring a certain similarity in the velocity profiles near the wall, neither can it be shown that Eq. (84) with $\psi = 0$ is the proper generalization to compressible flow of Eq. (55). With the understanding that the further development is completely speculative, the equation $\psi = 0$ may be considered in detail.

Proceeding to elimination of the definite integrals between the derivatives with respect to y of $\psi = 0$, it is easily shown that

$$\frac{\partial}{\partial y}\left(\frac{\partial r/\partial x}{\partial r/\partial y}\right) + \frac{1}{\lambda} + \frac{\frac{\partial r}{\partial x}\frac{\partial}{\partial y}\left(\frac{\rho}{\rho_r}\right) - \frac{\partial r}{\partial y}\frac{\partial}{\partial x}\left(\frac{\rho}{\rho_r}\right)}{\frac{\rho}{\rho_r}\frac{\partial r}{\partial y}} = 0 \quad (86)$$

where $r = u/u_\tau = r(x, y)$ as before.

A particularly simple integral of Eq. (86) may be found if the density and velocity are taken to be related by the Crocco energy integral (8, 24),

$$\frac{T}{T_w} = \frac{\rho_w}{\rho} = 1 + \left(\frac{T_0}{T_w} - 1\right)\frac{u}{u_1} + \left(\frac{T_1}{T_0} - 1\right)\frac{T_0}{T_w}\left(\frac{u}{u_1}\right)^2 \quad (87)$$

where T_o is the stagnation temperature of the external flow, T_1 is the static temperature, and T_w is the temperature of the wall; all are at present required to be independent of x. Eq. (86) becomes, after one integration with respect to y,

$$\frac{\partial f}{\partial x} + \frac{\partial f}{\partial y}\left[\frac{y}{\lambda} - \frac{1}{\lambda}\frac{u_\tau}{u_1}\left(\frac{T_o}{T_w} - 1\right)\int_0^y \frac{\rho}{\rho_w} f' dy - \frac{2}{\lambda}\left(\frac{u_\tau}{u_1}\right)^2\left(\frac{T_1}{T_o} - 1\right)\frac{T_o}{T_w}\int_0^y \frac{\rho}{\rho_w} f'^2 dy\right] = 0 \quad (88)$$

The appearance of certain definite integrals in Eqs. (84) and (88) suggests that the space coordinate y should be subjected to the Howarth transformation (103, 5),

$$\eta(x, y) = \int_0^y \frac{\rho}{\rho_w} dy \quad (89)$$

and when this operation is carried out,* Eq. (88) becomes simply

$$\frac{\partial f}{\partial x} + \frac{\eta}{\lambda}\frac{\partial f}{\partial \eta} = 0 \quad (90)$$

Thus the generalization of the law of the wall to compressible flow with heat transfer is of the form

$$\frac{u}{u_\tau} = f(\eta u_\tau) \quad (91)$$

---

* As is usual in transformation of this kind, consider $f(\xi, \eta)$, so that $r_x = r_\xi \xi_x + r_\eta \eta_x = r_\xi + r_\eta \eta_x$ and $r_y = r_\xi \xi_y + r_\eta \eta_y = r_\eta \eta_y$ when $\xi \equiv x$; r_x is of course not the same as r_ξ, since y is constant in the first case but η is constant in the second. Substituting in Eq. (88), differentiating the coefficient of $\partial f/\partial \eta$ with respect to y, and using the energy equation (87), several terms cancel by virtue of Eq. (88), and (90) follows.

with $\eta(x, y)$ given by Eq. (89) and $u_\tau(x)$ by Eq. (78).

In order to obtain a useful form of (91) it is necessary to satisfy the limiting expression (77), with the result that (91) should be written

$$\frac{u}{\sqrt{\tau_w/\rho_\tau}} = f\left(\frac{\rho_\tau}{\mu_w}\sqrt{\frac{\tau_w}{\rho_\tau}}\int_0^y \frac{\rho}{\rho_w}\,dy\right) \tag{92}$$

where f is the function of Eq. (21) and Table III above.

In seeking to determine which of the several restrictions already imposed might be relaxed, it may be noted that the reference density ρ_v is irrelevant, since it may be given an arbitrary value in Eqs. (84) and (86), and does not appear explicitly in Eq. (92); thus ρ_v may be considered for example as an isentropic reservoir density which is at least piecewise constant. Neither is the reference density ρ_τ involved in any of the mathematical manipulation required in deriving and solving (86), so that the restriction of zero pressure gradient may be dropped except for its possible bearing on the use of the Crocco energy integral (87) when there is heat transfer.

The remarkable result of the present synthesis is the fact, readily verified by substitution, that the arbitrary function $r(\eta\, u_\tau)$ of Eq. (91), with η defined by Eq. (89), satisfies (86) identically, whatever the equations of state and energy may be, and is valid for arbitrary pressure gradient, for arbitrary heat transfer, and for arbitrary surface temperature. It is of course necessary that the combination $\rho_\tau/\rho_w\mu_w$ be independent of

x, since the dependence of u/u_τ on x and y is already defined by (91). Thus the introduction of the Crocco energy relationship is superfluous, and is included here only to show why the writer's attention was directed specifically to the Howarth transformation. Finally, the combination $\rho_w \mu_w$ is closely proportional to pressure for many gases, so that the reference density ρ_τ which appears in the definition of u_τ may be nearly independent of x in a flow at constant pressure, even when large variations occur in ρ_w because of non-uniform surface temperature.

Given the applicability of the boundary layer equations, therefore, the conditions which are sufficient to require the velocity distribution to have the form (92) are first that the turbulent field vanishes at the wall, with Newtonian friction there, and second that the shearing stress distribution has the form

$$\frac{\tau}{\tau_w} = 1 + \frac{y}{\tau_w}\frac{dp}{dx} - \frac{1}{\lambda}\int_0^y \frac{\rho}{\rho_\tau}\left(\frac{u}{u_\tau}\right)^2 dy \qquad (93)$$

The first of these conditions is entirely plausible, but the second is a heuristic generalization of a recognized but not clearly understood property of the low-speed flow. It is therefore vital in future work to discover the physical reasons for the validity of the law of the wall, Eq. (21), for flows with constant density, and to determine whether these reasons can be adduced in flows with variable density to require the stress distribution (93). In the meantime, it is possible to test (92) and its various consequences by reference to experimental measurements.

Among these consequences, one or two are of particular interest. For example, most of the existing treatments of compressible turbulent shear flow predict that the generalized law of the wall should incorporate a distortion of the velocity distribution while the space coordinates remain unchanged, whereas the present formula states that the y-coordinate must, and the velocity may, undergo distortion when the density of the fluid is not constant.

The effect of temperature in increasing the thickness of the sublayer at large Mach numbers, discussed on page 48 above, may be demonstrated using the Howarth coordinates. By definition,

$$\eta = \int_0^y \frac{\rho}{\rho_w}\, dy \quad , \quad \Delta = \int_0^\delta \frac{\rho}{\rho_w}\, dy \qquad (94)$$

and it follows that

$$\left(\frac{\partial \eta/\Delta}{\partial y/\delta} \right)_{x,M} = \frac{\rho/\rho_w}{\int_0^{} \frac{\rho}{\rho_w}\, d\frac{y}{\delta}}$$

is less than unity near the wall if ρ/ρ_w increases monotonically with y/δ . The sketch shows how the physical sublayer thickness is magnified by the effect of high temperature at the wall, when flows with fixed and variable density are assumed to have coinciding velocity distributions in the coordinate η/Δ .

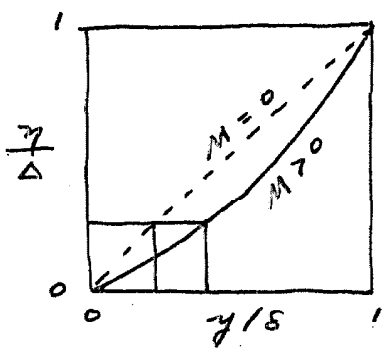

Unfortunately, the relationships given immediately above were obtained late in the present research effort, and it has not been possible to undertake a responsible analysis of the experimental data which are available for flows with variable density. Since the relationships in question are based entirely on kinematic grounds, with the density entering only as it affects local mass flow or local momentum, there is no reason to identify variations in density with variations in temperature until an equation of state is introduced. The development thus far should be equally applicable, for example, to vertical turbulent free convection given an obvious modification for body forces, to the wind near the ground, and to the turbulent boundary layer in supersonic flow. There occurs an arbitrary element in the reference density ρ_r, and further investigation is needed to determine criteria for selecting this parameter. Finally, it is clear that the velocity profile in physical coordinates depends on variations in density, and is therefore dependent on the energy distribution, although the same velocity profile in the Howarth coordinates is invariant.

The writer is hopeful that the detailed discussion of this section, of one aspect of the problem of turbulent shear flow near a wall, will demonstrate that this problem has not in fact been solved in any real sense in the past, and simultaneously will suggest that a solution may not be impossible in the future.

II. Instrumentation and Experimental Techniques at JPL

A. Introduction

The remaining portions of this report will be devoted to a presentation of some measurements by the writer in the boundary layer on a plate in supersonic flow, together with a discussion of several experimental methods which were used during the research.

The floating element technique, which attempts to measure directly the friction drag on a portion of a body in a fluid flow, was first successfully used in 1929 by Kempf (45), and later by Schultz-Grunow (47). An early but largely unproductive effort to apply the technique to supersonic flow was that of Ginsburgh (104). Beginning in 1948, H. W. Liepmann at GALCIT undertook the development of a floating element instrument for high-speed flow, and this work has been carried forward by Dhawan (11) and by Hakkinen (105). More recently the method has been used, with variations, by the writer, by Weiler and Hartwig at the University of Texas (106), by Eimer at GALCIT (107), by Bradfield, DeCoursin, and Blumer at the University of Minnesota (108), and with conspicuous success by Chapman and Kester at the Ames Laboratory of the NACA (109), the last two of these investigations being made with bodies of revolution rather than with a flat plate model.

The research at JPL, while inspired by the success of Liepmann and his group, is an independent attack on the flat plate drag problem, designed to take full advantage of the size and range of

the 20-inch supersonic wind tunnel at the Jet Propulsion Laboratory and of Liepmann's experience with the floating element technique. Design of the instrumentation and of the flat plate model was begun in early 1951, and the experiments reported here were carried out in the spring of 1952.

B. The Flat Plate Model

1. Model Installation. Figures 12 and 13 show the flat plate model installed in the test section of the 20-inch supersonic wind tunnel at the Jet Propulsion Laboratory. The plate completely spanned the tunnel, in order to isolate the working surface from pressure disturbances originating elsewhere on the model, and was supported by both side plates as shown in Figure 14. Part of the lift force on the plate was transmitted to the north door by means of a key and keyway; the remaining air loads were carried by the south door. With this arrangement for supporting the plate, the north door could be opened at any time to provide access to the model.

Two arguments suggested the selection of the lower surface of the plate for the present experiments. The floating element instrumentation described below could be most conveniently serviced and calibrated in this position. More important, it was felt that both the instrumentation and the surface finish were better insured against damage with the working surface on the bottom of the plate.

The leading edge of the model was located at Station (-6.5)

inches in the standard nozzle coordinate system, in which the window centerline is Station (-20.0). Three small windows of half inch plate glass were installed in each door, so that flow over the plate surface and leading edge could be observed using the tunnel Schlieren system. These windows were oriented with their direction of maximum taper parallel to the airflow, and uniform response to movement of a horizontal knife edge was obtained for the three pairs of windows.

Preliminary measurement of the width of the test section at the upstream and downstream edges of the 27 inch diameter window opening showed that on evacuating the test section these figures decreased by 0.015 inches and 0.022 inches respectively, and a conservative allowance was therefore made for tunnel deflection in specifying the plate width. Since the solid rubber seals provided along the edges of the plate were visible for part of their length, it was possible to verify that no leakage or interference occurred between the plate and side walls during operation.

For technical reasons connected with convenience in model installation rather than with advantages visualized in operation, provision was made in the design for changing the angle of attack of the model during a test. On loosening the bolts which normally clamped the flat plate rotation disc to the south door, the atmospheric air load on the disc was transferred through the key to a thrust bearing in the north door. The plate could then be

pitched through a total angle of twelve degrees by changing the length of a turnbuckle bolted between the disc and the south door, as shown in Figures 13 and 14. The plate angle of attack was indexed by a series of dowels in the north door.

2. General Instrumentation. Although the length of the flat plate was 33 inches, only the first 25 inches could be viewed with the tunnel Schlieren optical system, and the instrumentation was consequently confined to this region.

Three floating element instruments were mounted in the plate, on the tunnel plane of symmetry, at $x = 5.5$, 13.0, 24.0 inches from the leading edge. Since a factor of from four to eight was always available in the tunnel stagnation pressure, it was possible in most cases to measure surface friction at a given nominal Reynolds number with more than one of the friction instruments.

A series of 27 static pressure orifices was provided on the plate surface 2.75 inches south of the tunnel centerline. In addition, each of the floating element instruments incorporated three orifices for static pressure measurement; one of these orifices was the gap around the element itself.

Three copper-constantan thermocouples were soldered to stainless steel buttons which were buried in the plate surface 1.19 inches south of the tunnel centerline at $x = 9.25$, 16.75, 20.25 inches. The temperature was also measured in the floating element balance chambers.

All metal components exposed to the airstream on the working surface of the plate were fabricated of 410 stainless steel,* heat treated to a hardness of 35 on the Rockwell C scale before final machining. Particular attention was paid to working surface finish and to the sharpness of the leading edge, which was a wedge of 15 degree included angle. Various methods of estimating the leading edge radius indicated that the value finally achieved was less than one half thousandth of an inch.

Pressure, temperature, and friction instrumentation were carried outside the tunnel through the rotation disc shown in Figures 13 and 14, and all electrical and pressure leads were checked before installation of the model in the tunnel. The plate and rotation disc, which were permanently assembled, could be mounted in a calibration jig to allow access to either surface of the plate for assembly, inspection, and calibration of the instrumentation.

C. The Floating Surface Element

1. Flexure Assembly. The skin friction instrument described in these paragraphs is similar in principle to the floating element mechanism of Liepmann and Dhawan (11). The most important difference, aside from size and range, is the use at JPL of the null technique in measuring applied forces.

The basic components of the instrument are shown in Figures 15 - 17. The inner flexure system, consisting of the table, two flexlinks, and the ring, allows a deflection of the floating element

---

* SAE 51410 general purpose martensitic stainless steel.

under an applied load. The deflection is measured indirectly as the displacement which must be given to the table in order to return the element to a standard null position with respect to the surrounding structure. Motion of the upper table is effected by means of a precision micrometer, acting through a piano wire push rod clamped at both ends, and is constrained by the second or outer flexure system shown in the figures.

The null position of the floating element is detected by a Schaevitz variable reluctance transformer (110) whose coil is fixed on the instrument structure and whose core is attached to the element ring, so that no physical contact between the gauge and element is present to interfere with measurement of the small forces involved. Two dashpots are provided for damping in the inner flexure system, and are constructed with sufficiently small clearances so that capillary attraction prevents loss of fluid when the instrument is turned upside down.

The skin friction instrument, including the flexure systems, damping device, and Schaevitz gauge, is assembled on a stainless steel disc four inches in diameter and 5/16 inch thick. Installation in the flat plate for wind tunnel tests is accomplished by means of sixteen leveling screws which are alternately tapped into the disc and into the plate. Experience has shown that the discontinuity in surface level at the four inch parting circle can be reduced to less than 0.00005 inches without difficulty, and that a standard dial test indicator is adequate for measurement

of the discrepancy. It follows that one skin friction instrument can be exchanged for another in a relatively short time, and that repairs need not involve serious interruption to a particular wind tunnel experiment.

The choice of a rectangular surface element was made in order to approximate a local measurement, and the corresponding rectangular hole was fabricated by a combination of milling, machine filing, and broaching operations. Various methods have been tried for locking the floating element during lapping; the one finally adopted consists of filling the gap with glyptal* which is allowed to harden before lapping and is removed with acetone or other solvents after a smooth flush surface is obtained. It is believed that this technique avoids the possibility of elastic deformations in the flex-link structure, which could lead to serious misalignment when the element is released. The interference pattern of Figure 18, obtained with an optical flat and light of 5461 Å wave length, is typical in showing the alignment which can be expected after final installation. During the period of test, a sensitive dial indicator was used frequently to verify that the floating element remained flush with the surrounding metal within a few wave lengths.

2. Micrometer. The micrometer shown in Figure 17 is designed around a standard commercial lead screw of 0.025 inch pitch. The lead screw is keyed to prevent rotation and is actuated

---

* Glyptal clear varnish or red enamel, General Electric Co., Schenectady, New York.

by a rotating nut which is driven through a 25:1 worm and worm gear. Consequently, one revolution of the input shaft represents 0.001 inch of translation at the lead screw. A counter and graduated dial on the micrometer input shaft indicate the position of the element table in millionths of an inch.

A typical micrometer calibration, obtained by direct comparison with a Pratt and Whitney Standard Measuring Machine, is presented in Figure 19. The observed error has the same period as the spindle rotation, and is probably caused by misalignment of the spindle bearings or by departure of the lead screw or nut from a uniform helix. In any case, the maximum micrometer position error does not exceed 0.5 percent and can be neglected in the present measurements.

3. Electrical Components. The displacement-sensing device used in the present instruments is a Schaevitz differential transformer (110), whose properties were first exploited by Liepmann and Dhawan (11). Figure 20 shows a schematic view of the Schaevitz gauge, Figure 21 shows a schematic diagram for the input and output circuits for this gauge, and Figure 22 shows a wiring diagram of a three-channel power and isolation amplifier, not commercially available, which was developed to prevent electrical interference between the several gauge circuits.

A single pair of Hewlett-Packard vacuum tube voltmeters was used to measure input and output voltage, being connected to any one of the three gauges by a rotary gang switch mounted on the

flat plate model structure. The auxiliary 100 kc/s crystal oscillator and oscilloscope shown in Figure 21 were added to the system when it was found that the Hewlett-Packard audio-oscillator, used as a primary signal source, had relatively poor frequency stability. Although various input frequencies have been used, most of the present measurements were made at 20 or 25 kc/s, and the performance of the electrical equipment was judged to be entirely satisfactory. In particular, the writer has been impressed by the potentialities of the Schaevitz instrument as a highly sensitive device for measuring small displacements; in fact, evidence will be cited below to show that this gauge can detect even under field conditions motion through a distance equal to a small fraction of a wave length of light.

4. Technique of Use. The major components of the Schaevitz variable reluctance transformer have been shown schematically in Figure 20, and a typical output signal from the gauge is plotted in Figure 23 as a function of micrometer position. In theory, the difference between the opposing voltages induced in the two secondary coils is proportional to the displacement of the iron core. Consequently, after balancing the secondary circuit for a minimum null signal and adjusting the position of the coil so that this signal occurs approximately at the center of the element travel, the output voltage as a function of micrometer position should consist of the four straight line segments shown in Figure 23. Since this pattern should not depend on the load acting on the element, various functional disorders in the instrument can readily be diagnosed in

terms of changes in the output signal.

In the example of Figure 23, the motion of the element is delayed as the upper table moves upstream until a sufficiently large force is applied by the flexures to break a thin liquid film which is present in the gap. The element is then free to follow the motion of the table through the null position. A slight effect of residual magnetism is apparent in the figure before the final contact occurs, although in the present case neither the magnetism nor the presence of a fluid film is serious enough to interfere with use of the instrument. It should be noted that the presence of dust, lint, or other solid particles in the clearance gap is immediately apparent in operation, since the magnitude of the voltage at contact will decrease.

As perfect symmetry in the magnetic and electrical elements of the secondary circuits is not likely to be achieved, the null signal will not be perfectly sharp. In the present experiments the null was taken as the arithmetic mean of the two micrometer readings when the output voltage passed through a particular value, say ten millivolts. In general, under steady conditions, the null position defined in this way could be repeated within one or two millionths of an inch using ordinary care to avoid backlash in the micrometer mechanism. Failure to obtain the sensitivity mentioned could usually be traced to the presence of foreign material in the clearance gap.

The most important single characteristic of Figure 23 in

assuring proper functioning is the physical separation of the two micrometer readings for the specified value of output voltage. This distance, which is about 790 millionths in the present example, should not change when the element is under load. In the present experiments the gauge input voltage and frequency were carefully controlled, and the effects of temperature on the output pattern were found to be small. However, it was observed during early tests that the value of 0.79 thous increased with the tunnel stagnation pressure. The balance chamber was found to be improperly sealed, so that excess pressure in the chamber caused a small amount of air flow through the clearance gap around the element. The friction measurements in question were repeated after improving the balance chamber seals, and the performance of the instrument was found to be entirely satisfactory. It may be remarked that no aerodynamic or electrical interference between the floating element instruments was observed during the present tests.

5. Calibration and Estimate of Accuracy. In determining the surface shearing stress from the displacement under load of the floating element, it is assumed that the only force applied to the element is the local surface friction, and that the presence of the measuring instrument does not affect the quantity to be measured. It is further assumed that the deflection of the element with respect to the inner flexure system is proportional to the applied load, and that the constant of proportionality is independent of the point of application. Finally, it is assumed that the deflection mentioned can be exactly compensated for by a second

deflection of the support system. Each of these assumptions must be examined in detail.

It was discovered early in the development that residual magnetism in the element assembly and in the adjacent structure could cause a very erratic behavior, and this magnetism was removed as far as possible in the final assembly. The technique of null measurement is believed to eliminate any remaining effect, and the same remark applies to any axial force between the core and coil of the Schaevitz gauge.

The assumption of zero flow velocity will not be satisfied over the gap, where there will be a system of standing vortices. The energy dissipated in these vortices must be extracted from the external flow, and consequently will affect the mean friction or total drag downstream.

In the present design the floating surface element is 0.244 by 1.492 inches, and the rectangular hole is 0.250 by 1.500 inches, so that the clearance gap is about three percent of the total surface area. Since turbulent boundary layer flows are known to be insensitive to surface irregularities which are small compared to the sublayer thickness, as is the case for the gaps in most of the present measurements, it is to be expected that disturbances in the shear distribution will be negligible. Dhawan (11) found no measurable waves for either laminar or turbulent supersonic flow over a typical slot. Dhawan also investigated low speed flow over a slot whose width was about one-fourth of the boundary layer thick-

ness, and found no measurable effect of the slot on the wall shearing stress, as measured in the sublayer with a hot wire anemometer, in the immediate vicinity of the slot.

On the other hand, Tillmann (49) and Wieghardt (48) used Schultz-Grunow's wall drag balance (47) to measure directly the drag of slots normal and parallel to the flow in a turbulent low speed boundary layer. For the first case, the drag of a slot whose width was less than the boundary layer thickness was found to be independent of the slot depth, suggesting a shear rather than a pressure drag, and was found to have a magnitude of two or three times the surface friction on the same element of area. For the second case, the drag was found to depend on the slot depth, and to be about five to fifteen times the surface friction on the same area. These experiments, however, were carried out in boundary layers whose sublayer was of small thickness compared to the slot width, and so provide what is probably an upper bound on the slot drag.

In the data reduction for the present experiments, the actual element area was used to determine the shearing stress. If half of the slot drag were to be subtracted from the measured element load, and this drag were to be taken as twice the local shearing stress, the friction coefficients would be reduced by an amount not exceeding two or three percent. Because of the relatively small gap width involved here, this estimate of error is felt to be conservative.

In the same context, errors associated with misalignment of

the element with respect to the surrounding surface are probably negligible, in view of the data presented below for a turbulent boundary layer at a Mach number of 2.6, which data are believed to be free of variations in surface friction caused by local pressure gradient over the elements.

A detailed analysis of the elastic properties of a flexure system such as that used here is available in the engineering literature (111). It appears that, even within the limitations of slender beam theory, the deflection is neither strictly proportional to the applied load nor completely independent of the point of application. If it is assumed that the four unstiffened flexures are subjected to exactly the same loading, the approximate expression is obtained,

$$\frac{W}{kB} = 1 + 2\frac{b}{B} - \frac{\cosh\sqrt{\frac{Wb^2}{2EI}} + \sqrt{\frac{8EI}{WB^2}}\sinh\sqrt{\frac{Wb^2}{2EI}}}{\cosh\sqrt{\frac{Wb^2}{2EI}} + \sqrt{\frac{WB^2}{8EI}}\sinh\sqrt{\frac{Wb^2}{2EI}}} \qquad (95)$$

where k is the spring constant; W is the weight of the element, ring, etc.; B is the length of the stiffener; and E, I, and b are respectively the modulus of elasticity, moment of inertia, and free length of the unstiffened portion of the flexures. Estimated values* for the present design are

---

* In computing the moment of inertia, the width and thickness of the spring steel flexure are taken as 0.625 inches and 0.00205 inches respectively. The length/radius of gyration ratio for the flexures is about 250, so that failure may be assumed to occur by buckling. The ultimate normal pressure load is eight atmospheres, or about six times the maximum value expected in a high density emergency shutdown of the tunnel. It should be mentioned that difficulty with compound curvatures, or oil-canning, was encountered early in the instrument development, so that it was found necessary to place rigid specifications on the final alignment of the flexure systems.

$W = 43.5$ grams

$B = 0.825$ inches

$E = 29 \times 10^{6}$ pounds per square inch

$I = 4.5 \times 10^{-10}$ inches^4

$b = 0.150$ inches

Eq. (95) then yields the estimated value $k = 0.455$ pounds per inch.

In practice, two independent methods were used for the determination of the actual spring constant. As indicated in Figure 17, static calibration of the flexure system was carried out after final assembly and installation, using a nylon monofilament running over three jewel mounted pulleys to transmit loads from a weight pan to the element ring. Considerable difficulty with friction in the pulleys was encountered, and it was found necessary to use a vibrator on the pulley bracket. For each measurement the pan was unloaded and the zero return verified. The relationship between force and deflection for the three instruments is shown in Figure 24, and the spring constants are listed in the table below. In the interval between Tests 43 and 44, the floating elements were permuted to the stations indicated by the numbers in parentheses in the table, and were relapped and recalibrated. During this operation the elements C and D were rotated 180°, so that the direction of loading was reversed for the second column of the table.

A second method of calibration, which does not require the use of pulleys, is suggested by Eq. (95). If the element displacement due to gravity, x, is measured for various angles of attack,

α , the spring constant can be determined from

$$\frac{W}{k} = \frac{x}{\sin\alpha} \doteq \frac{x}{\alpha}$$

provided that the weight W is known. A second set of observations, with the weight of the element increased by a known increment, w, allows the determination of $Wb^2/2EI$ and $(W + w)b^2/2EI$, and therefore W/w, from Eq. (65), assuming that B and b are accurately known.

The latter calibration has been carried out* for the three elements used in the present experiments, and the result is shown in the third column of the table. In general, the second method of calibration is to be preferred from the standpoint of speed and convenience.

Spring constant, pounds per inch

Element	Pulley Calibration Tests 11-43	Pulley Calibration Tests 44-80	Gravity Calibration
B	0.387 (2)	0.381 (1)	0.381 (1)
C	0.411 (3)	0.416 (2)	0.412 (2)
D	0.433 (1)	0.432 (3)	0.431 (3)

Finally, a more complete analysis of the elastic flexure system than that leading to Eq. (95) has been carried to the point

---

* The additional weights w were 50, 10, and 20 grams respectively for elements B, C, and D, and the values found for W were 43.8, 44.8, and 45.3 grams.

where an estimate could be formed of the errors associated with the non-linearity and with the discrepancy between the points of application of static and dynamic loads; these effects are believed to be completely negligible for the present application.

The remaining source of error which should be mentioned here is electrical zero shift, caused principally by changes in temperature of various electrical components, especially the Schaevitz gauge. In order to investigate this point, several tests were made in the wind tunnel during which the floating surface elements were shielded from the airflow by small cover plates. A typical record of zero position against time, and also of balance chamber thermocouple output against time, is shown in Figure 25. It appears that the technique, common to all the experiments discussed in the present report, of using the post-run zero measurement in the data reduction should minimize errors from this source. The residual error, of perhaps 20 millionths of an inch, is only partly accounted for by the observed elastic deflection of the plate under aerodynamic load or by the possible effects of vibration. It is obvious that the zero error demonstrated here is negligibly small compared to element displacements of from 5 to 15 thousandths of an inch, normally encountered in turbulent boundary layers at large Reynolds numbers during the present experiments.

6. The Null Principle. Experience at JPL has confirmed several advantages which were visualized in using the null principle of force measurement.

First, the clearance which must be provided around the floating surface element is not dependent on the range and sensitivity. The surface condition can be made to approach arbitrarily close to an uninterrupted plane, subject to the necessity for being able to inspect and to clean the clearance gap. In fact, the null principle is desirable if more than one of the instruments is to be used, unless a large clearance is provided or precautions are taken to insure that all elements are free in both the loaded and unloaded condition for the angles of attack encountered in operation.

Second, the double flexure assembly is a true null system, in that deflections both parallel and normal to the airstream are compensated for during the measurement. Furthermore, the floating element should remain flush with the surface over a reasonable range of temperatures, since dimensional changes in the two flexure systems compensate each other.

Third, the accuracy is nearly independent of the range, in the sense that the initial and final displacements can be determined with the same accuracy whether the load is large or small. This point is important in the present application because the surface friction force on a given element may vary by a factor of 30 or more in a single test. In the same connection, it is apparent that the absolute accuracy of the electrical equipment is not relevant to the absolute accuracy of the friction instrument, and that input frequency and voltage can be varied from one test to another if desired, or the sensitivity varied by changing

the range of the voltmeter in the output circuit, without recalibration.

Finally, malfunctioning of the mechanical system can be detected at any time by routine electrical measurements. In particular, unusual restraints applied to the floating element by contact with the adjacent structure or with foreign particles deposited in the clearance gap by the airstream can be detected without special precaution or preparation.

D. The Channel Calibration

1. Pressure Gradient and Apparent Shear. Some of the local friction measurements in the 20-inch tunnel were made in the presence of an axial pressure gradient over the floating element. Since any unbalance of static pressure at the leading and trailing edge gaps may be expected to produce a force in the direction of decreasing pressure, it is necessary to estimate the magnitude of the errors involved. Furthermore, circulation of air into and out of the balance chamber may cause appreciable disturbances in the boundary layer flow near the gaps.

To investigate the feasibility of shear measurements in a pressure gradient, a calibration was carried out in a narrow channel, one wall of which was formed by the flat plate model and the other by a ground and lapped auxiliary plate. The two plates were separated by a shim, and the enclosed air space was ported through the auxiliary plate to a collector pipe at each end of the channel. Air flow was maintained by a vacuum pump; a valve at the air inlet

acted as a sonic orifice, and steady flow at low pressures was readily obtained.

For fully developed two-dimensional channel flow of an incompressible viscous fluid, the shear and pressure drop are related by the expression, independent of the velocity profile,

$$\tau_w = - \frac{d}{2} \frac{dp}{dx}$$

where d is the height of the channel. Symmetry about a mid plane has been assumed, so that local disturbances to the flow have not been taken into account.

Referring to Figure 26 for the notation used, it may be assumed that there exists a distance, h, normal to the surface, over which the variable pressure in the gap is effective in producing a streamwise force. Computing the apparent shear when the pressure changes uniformly in each gap from the value in the chamber to the value at the surface, the relationship is obtained

$$\frac{f}{\tau_w} = 1 + \frac{h}{d}$$

where f is the total apparent shear obtained from the element deflection.

Shims of 1/32, 1/16, and 1/8 inch nominal thickness were used in the calibration, and each was run at several mass flow rates. The pressure gradients were obtained from the slope of a plot of

p^2 against x, which is a linear function for fully developed flow (112). The distance d was measured for each element by a micrometer head which was retracted flush with the surface of the auxiliary plate when not in use. Individual zero readings were taken for the three elements for each operating condition. The channel flow is believed to have been laminar for all of the calibration measurements described here.

Values obtained for the hypothetical distance h are presented in Figure 26 against the background of the element geometry viewed normal to the flow direction. The abscissa is the Reynolds number of the gap flow, which is defined below. Except for small values of R_g, where the flow mechanism assumed here may not be valid, the values obtained for the distance h are consistent with the nominal physical dimension of 0.020 $\pm$ 0.003 inches for the part of the element exposed to pressure forces. In fact, if a value had been assumed for the distance in question on the basis of the element geometry, the channel calibration could conveniently have been used to establish the spring constant for the element. The data of Figure 26 involve shear values of from 0.00007 to 0.00116 pounds per square inch, and ambient pressures of from 0.3 to 5.7 centimeters of mercury, and correspond to conditions encountered in the wind tunnel at high Mach numbers. No definite trend with channel height, surface shearing stress, or pressure level was observed for the apparent shear due to pressure gradient, either here or in an earlier calibration carried out at atmospheric pressure. In the absence of

other evidence, it follows from a simple calculation that the necessary correction to shear measurements in the wind tunnel can be adequately represented by the expression

$$\Delta \frac{\tau_w}{q} = \frac{h}{\gamma M^2} \left(\frac{1}{p} \frac{dp}{dx} \right)$$

with say h = 0.019 inches.

2. Balance Chamber Pressure. The mechanism assumed above for the flow in the element gaps has been validated to some extent by an independent measurement. A linear pressure drop through the gap is consistent with a parabolic velocity profile there, and implies the same relationship between vertical pressure gradient and shear as has already been postulated for the channel itself. The gap flow Reynolds number based on the width and on the average velocity for the gap can easily be shown to be

$$R_g = \frac{\rho g^3}{12 \mu^2 h} |\Delta p|$$

where g is the gap dimension and Δp is the pressure difference between the chamber and the surface. This Reynolds number is essentially the mass flow through the clearance space, and for steady conditions must have the same value for the upstream and downstream gaps. Neglecting small variations in viscosity and density in the neighborhood of the element, a simple relationship is implied between element position and balance chamber pressure.

The solid line in Figure 27 shows this relationship for a typical condition of flow in the channel, involving a shear stress of about 0.001 pounds per square inch. The limiting values of chamber pressure were obtained from the observed pressure distribution. Also shown in the figure are the chamber pressures determined by experiment; two sets of data were taken because of the sensitive measurements required. The abscissae for the measured points were deduced from the element voltage output pattern, which has already been described in Section II, Part C4. Aside from a possible constant error of perhaps 100 millionths of an inch in the element position, the agreement with the predicted values is quite satisfactory.

3. Balance Chamber Leakage. Advantage was taken during the channel calibration of the opportunity to investigate the influence of balance chamber leakage on the instrument reading. Figure 28 is a record for several operating conditions of the relative downstream load, denoted by f, as a function of the excess chamber pressure, Δp; both have been made dimensionless by dividing by τ_w. One curve was also obtained in a laminar boundary layer at a Mach number of 2.0 and a Reynolds number of about 1.8×10^6 at Station 1.

It is clear from the figure that the effect of leakage probably cannot be predicted, either in magnitude or in sign, without more elaborate investigation, and errors from this source may therefore be minimized by requiring that the pressure in the balance chamber should not differ from the proper value by more than the magnitude

of the shearing stress on the element. The evidence given here confirms the experience of Dhawan (11) in demonstrating that the balance chamber must be sealed with extreme care. In the present instrument solid rubber compression seals were installed in grooves beneath the various cover plates, and satisfactory sealing was apparently achieved by this means.

E. The Low Pressure Multimanometer

As part of a routine effort to define the experimental environment for the research discussed here, a low pressure multimanometer was designed and constructed in early 1952. Since the interpretation of the turbulent friction measurements in particular would have been much more difficult without the information obtained from this instrument, several comments should be made about the design and use of the multimanometer.

The static pressures anticipated in the experiments ranged from 2 to 150 millimeters of mercury absolute, and it was thought necessary to provide instrumentation for obtaining sufficient pressure data to define the plate pressure distribution, particularly the local pressure gradients over the floating elements. The writer's experience with the problem, in connection with research in the GALCIT hypersonic wind tunnel, suggested the use of a multiple manometer of more or less conventional design, but using a light fluid and a low reference pressure. Figures 29 and 30 show the general arrangement of the manometer components.

In compromising the desirable properties of low viscosity, low

volatility, and uniform wetting characteristics, one of the silicone fluids* with a viscosity of about 10 centistokes appears to be quite satisfactory. The specific gravity of this fluid apparently is not closely controlled by the manufacturer, and should be measured under the conditions of use; the value obtained by the writer was 0.9306 ±0.0005 at 75 °F with a decrease of 0.0005 for each 1 °F increase in temperature.

The vapor pressure of the silicone fluid at room temperature has not been determined, but reference pressures of about 20 microns or 0.02 millimeters of mercury, as read by a McLeod gauge connected to the manometer through a dry ice and acetone trap, were easily obtained for the multimanometer described here in spite of the presence of several hundred O-rings and some dozens of flared fittings which were exposed to an atmospheric pressure differential.

Each of the 40 tubes in the manometer is provided at the top with a two-way sliding valve, shown in Figure 31, so that any tube may be connected either to the reference vacuum (equalized position) or to the tunnel pressure (reading position). The sliding valves can be operated by remote control through individual pneumatic pistons, which are supplied with air at 125 psig through a solenoid valve. The sliding valves are spring loaded to assume the equalized position when the actuating air pressure is less than about 80 psig, and the valves can also be operated manually and locked in either position when desired.

---

* DC-200 fluid, manufactured by Dow Corning Corporation, Midland, Mich.

Experience with low pressure manometers has suggested several precautions for preventing damage to the manometer in case one or more of the tubes is exposed to a pressure higher than the range of the instrument, in the present instance 110 millimeters of mercury absolute. Banks of ten tubes are manifolded together to a single fluid reservoir and the four reservoirs are in turn interconnected through a system of valves. The manifolds however are slanted, as shown in Figure 30, and are placed at the rear of the manometer at a position well above the lowest point of the individual tubes. Thus if air enters the manifolding system under pressure through a tunnel line, the path of least resistance is upward into the reservoir and there is no tendency to force manometer fluid into the tunnel from other manometer tubes. In practice, if one tube is exposed say to atmospheric pressure, a silicone-air emulsion forms immediately in the vertical line from the manifold to the reservoir, and the lowered density of this emulsion acts to siphon fluid out of the other nine tubes of the bank in question. After equalizing all tubes of the manometer, the reference vacuum may be restored and the manometer made ready for use in about half an hour. It is essential to provide adequate drainage into the reservoir or glass tubes for the valve system passages, since dissolved air may occasionally carry liquid into the valve block when the manometer is being evacuated.

One other feature of the manometer should be described. Provision is made for connecting any one of the model pressure lines to an auxiliary vacuum pump or to a source of pressure through an auxiliary passage in the valve block, so that model lines may be checked for leakage or identified.

Under steady conditions and with reasonable care in reading fluid

levels, the difference in pressure between the reference vacuum and a given model orifice may be read with an accuracy of about 0.3 millimeters of silicone fluid, or 0.02 millimeters of mercury. For pressures greater than 10 millimeters of mercury the reference pressure of 20 microns can be neglected for most purposes, and the manometer is an absolute pressure instrument. Care should be taken, when measuring pressures in this lower range, to establish equilibrium between the pressures at the manometer and at the model. The time required to reach equilibrium may be of the order of ten minutes, and since two or three minutes are sufficient to read the manometer fluid levels visually, it appears that photographic recording of data at low pressures is not always advantageous and may even involve a sacrifice in accuracy without a compensating saving in time. For the present experiments, the low pressure manometer was read manually in all cases.

F. The Mass Flow - Impact Probe and Flow Meter

1. Principle of Operation. The mean dynamic and thermodynamic states at a point in a supersonic boundary layer are adequately defined by three quantities; these are the velocity, pressure, and temperature (or density) of the fluid. Boundary layer research is commonly carried out, however, using a single measurement and two assumptions. The static pressure is assumed to be constant through the boundary layer, and the temperature is assumed to be a quadratic function of the velocity. The first of these propositions allows the local Mach number to be deduced from measurements of impact pressure in the stream and of static pressure at the adjacent wall; the latter quantity is sometimes inferred for the free stream through an assumption of isentropic expansion from a real or hypothetical reservoir. The use

of an impact pressure instrument has occasionally been replaced or supplemented by measurement of local density through interferometric or x-ray absorption techniques, although considerable finesse is required in the use of these methods.

The relationship between velocity and temperature in real fluids is a matter of fundamental importance in high-speed aerodynamics, and several instruments have been proposed to assist in measurement of this relationship. Conspicuous among these instruments is the stagnation temperature probe, which has been used with various degrees of success by Spivack (113), by Wegener (114), by Monaghan and Cooke (115), and by many others. The most obvious check on the accuracy of such an instrument is verification of the fact that the total energy in the flow must remain constant for steady flow without heat transfer;

$$\int_0^{\delta+} \rho u \left(T_o' - T_o \right) dy = 0$$

where T_o is the free stream or reservoir stagnation temperature, and T_o' is the local stagnation temperature in the boundary layer.

In considering obvious difficulties in the determination of local specific energy in high speed airflows, it has occurred to the writer that measurement of mass flow rate serves the same purpose as measurement of local stagnation temperature. Consider that the impact and static pressure together determine the local Mach number and therefore the local dynamic pressure,

$$\rho u^2 = \gamma p M^2$$

independent of the relationship between velocity and temperature. If now the local mass flow rate

$$\rho u = \frac{dm/dt}{A}$$

could be determined for a stream tube of area A, the velocity and density, and hence the static and stagnation temperatures, could be calculated immediately.

If the flow is supersonic, one may visualize a sharp-edged hollow probe with a sufficiently low internal pressure so that an attached shock system exists at the entrance; the nose area A then defines the stream tube being studied, and the mass flow rate may be measured at leisure further downstream. Closing off the internal passage converts the instrument to a conventional impact probe, and thus allows the necessary measurements to be carried out at precisely the same point in the flow.

The development of a mass flow-impact probe was undertaken at JPL as part of the instrumentation for the present boundary layer research. In the final analysis the performance of the instrument in a boundary layer was found to be unsatisfactory; however, there is sufficient promise for the technique so that the experience at JPL should be made available to others working in the field.

2. Probe Construction. The original probes were machined cylinders with a straight or slightly diverging bore and an external nose half-angle of about ten degrees. The internal channel is obviously equivalent to the test section, second throat, and subsonic

diffuser of a conventional supersonic wind tunnel, and the usual rules must be followed in estimating the minimum permissible area in the throat formed by the internal boundary layer. A preliminary calibration was carried out using a probe with an entrance diameter of 1/16 inch, and it was found that the measured and predicted mass flow rates agreed within one percent in a uniform flow at a Mach number of 2.2. That the entering flow was supersonic was verified by observing the internal probe pressure very close to the entrance; the value found was nearly the static pressure in the free stream.

Because machining difficulties were anticipated in making a cylindrical probe small enough to be useful in boundary layer research, several rectangular probes were fabricated of tubing and razor blades with the objective of maintaining the mass flow rate at a useful value while reducing the vertical dimension of the probe. Figures 32 and 33 show two views of such a probe; the entrance, as measured with an optical comparator, was about 0.009 by 0.053 inches. This probe is typical of several which were used by the writer, and the rectangular design is quite satisfactory. The method of fabrication was to relieve a piece of hardened steel tubing to accept the razor blade segments, which were arranged to form a straight internal channel; after soldering, the sides of the probe were ground to the shape shown in the figure.

Several compromises must be made in the design of the mass flow-impact probe. Since the internal channel must eventually diverge, the probe may not approach a wall as closely as if impact measurements

alone were intended. This is not in practice a serious disadvantage, since the writer has found that impact pressure measurements in supersonic flow made closer to the wall than about twice the height of a rectangular probe should be viewed with suspicion; if this criterion is accepted, the probe body diameter may be made four times the entrance height without real sacrifice in performance.

Another limitation arises in the fact that the nose wedge angle of commercial razor blades is invariant between various makes, and has a value of about 14 degrees. Thus, a straight internal channel means that shock detachment will occur at Mach numbers below about 1.6. Again, the disadvantage may not be apparent in turbulent boundary layer research, since $M = 1.6$ usually occurs very close to the wall for free stream Mach numbers of the order of 3 or 4.

3. Flow Meter. Mass flow rates were measured by two methods. The first consisted of operating the probe exactly like a blowdown wind tunnel, exhausting into an evacuated receiver for a measured time interval; the mass flow transferred was deduced from the initial and final pressures and temperatures in the receiver. This method required a considerable time for preparing the system between blows, and was abandoned in favor of a calibrated sonic metering orifice and vacuum pump, so that the probe could be operated continuously.

The sonic orifice in question was a ruby watch jewel of 1.1 millimeter internal diameter, and a needle was provided to vary the area of the orifice. This needle was positioned by a commercial micrometer head, set at zero when the needle filled the orifice; the

needle was withdrawn completely at an axial displacement of 0.35 inches. The orifice was found to be rather sensitive to viscous effects, i.e. to changes in back pressure at low flow rates, especially when the needle was partially inserted, but was always used with the same pump and porting so that the calibration was repeatable. Flow rates could be measured to an accuracy of one percent or better in the range from 5×10^{-8} to 5×10^{-6} slugs per second. The former figure corresponds to a flow of one cubic foot of free air in about twelve hours.

4. Calibration and Performance. Figure 34 shows the ratio of effective entrance area to measured entrance area deduced from free stream mass flow measurements with a typical probe; the ordinate is also the ratio of measured to predicted mass flow.

The difficulty encountered in practice with this probe is apparent in the figure. At lower Reynolds numbers, below say 1000 based on the entrance height, the mass flow decreases markedly, indicating that the entering flow is not supersonic and that considerable spillage is occurring at the nose.

In order to determine whether the entrance flow was supersonic at larger Reynolds numbers, the probe internal pressure was varied and changes in mass flow rate observed. Figure 35 shows several examples of this measurement which establish that the mass flow rate was usually independent of internal pressure as long as the latter was less than say half of the impact pressure at the point in question.

The probe was always operated at the largest available compression ratio when measuring flow rate.

The presence of viscous effects at low Reynolds numbers may have been the major cause of failure to obtain useful measurements with this instrument, although the presence of fluctuations in local flow direction in the turbulent boundary layer may also have been a factor, leading to a chronic state of shock detachment from one or another surface of the probe. The values of the product ρu obtained in practice invariably became smaller than the predicted values as soon as the probe was well into the boundary layer, so that the stagnation temperature appeared to rise indefinitely as the wall was approached.

The difficulties encountered here might well be avoided by restricting the application of the technique to flows in which the probe Reynolds number is not less than several thousand, and the use of larger probes may provide a useful comparison for experiments with stagnation thermocouples or resistance thermometers in measurements of temperature distributions in supersonic streams or in boundary layers which are thicker than those studied here.

5. Double Sonic Orifice Thermometer. Following a suggestion by Wildhack (116) and by Blackshear (117), that values for stagnation temperature in a fluid might be inferred from the reservoir conditions for two sonic orifices in series, some calibration was carried out with a slightly modified mass flow probe. For two sonic orifices in series, the equivalence of mass flow requires

$$\frac{p_o'}{\sqrt{T_o'}} A' = \frac{p_o''}{\sqrt{T_o''}} A''$$

where the single prime refers to conditions upstream of the first orifice and the double prime to conditions upstream of the second. If the first orifice occurs just downstream of a normal shock, then p_o' is the impact pressure. Since p_o'' and T_o'' are easily measured upstream of the second orifice, the stagnation temperature T_o', which is conserved through the shock, is determined if the ratio A''/A' is known as a function of Mach number and Reynolds number.

Since the sharp-edged probe has only two stable operating conditions, with the entering velocity either well above or well below the sonic value, a blunt shroud was provided around the entrance to insure that sonic flow would occur there for sufficiently low internal pressure.

Figure 36 shows a typical free stream calibration, giving the relative effective area of the entrance in terms of the Mach number and probe internal pressure at the point in question.

An attempt was made to use this instrument in the boundary layer, without success. It is believed that the difficulty here is a fundamental one, and that the method is not likely to be useful in flows with large velocity gradients. The reason appears to be connected with large curvature of the nose shock wave; in a gradient the streamline which corresponds to the observed mass flow does not coincide

in position with the streamline which corresponds to the observed impact pressure, and the discrepancy is likely to be present even in a uniform supersonic stream if the instrument is not aligned with the flow direction. This objection does not of course apply to use of the technique in gases which are at rest or moving slowly.

6. Use as Impact Probe. One or two comments are in order concerning the writer's experience with the measurement of impact pressure. Since the pressures encountered in the present experiments were always large enough to offer no problem in measurement, it is necessary only to consider whether these pressures can be properly interpreted.

The experience of many investigators has shown that an impact probe in a boundary layer is an instrument subject to several sources of error. The presence of the probe may influence the development of the original boundary layer through upstream propagation of pressure disturbances, especially in the case of the laminar flow. The existence of a velocity gradient and the proximity of a wall will cause distortion of the normally symmetrical flow pattern around the probe. On the other hand, the use of small probes in an effort to minimize the problems already mentioned may introduce new errors associated with viscous dissipation near the probe nose. Finally, the effect of velocity and density fluctuations on the pressure indicated by the probe may not be negligible.

Figure 37 shows two turbulent Mach number profiles as obtained with an impact probe fabricated of razor blades, and with the same

probe equipped with a close-fitting rectangular shroud to increase the nose area. The two configurations register the same pressure, within the accuracy of the measurements, except when the larger probe approaches the wall closer than twice the probe height. This experience is consistent with that of Wilson and Young (118), although the present probes are of rectangular rather than circular cross section.

Figure 38 illustrates the method used to detect contact of the probe body with the wall. Since contact is first made about 0.3 inches behind the probe entrance, the direction of motion of the latter will be reversed upon contact, and the observed impact pressure will begin to increase.

The four profiles shown were obtained at a Mach number of about 4.5 during an investigation of flow with a pressure gradient, and are typical in exhibiting the repeatability of the probe positioning mechanism. The distance from the probe entrance to the wall was taken as half of the separation of the probe from its reflection in the plate surface as determined with a cathetometer.* Errors caused by imperfections in the reflecting surface were minimized by making the same measurement from several points of observation.

Figure 38 also shows the variation of impact pressure with distance for a hypothetical sublayer without pressure gradient; the

---

* Wild NIII precision level, manufactured by Henry Wild Surveying Instruments Supply Company, Ltd., Heerbrugg, Switzerland.

velocity gradient is assumed to have the constant value implied by the known shearing stress and viscosity at the wall, and the speed of sound is taken constant at the wall value. This calculation should suggest the nature of an extrapolation to the wall which might be attempted for the experimental data.

In an analysis undertaken in Section III below for these profile data, it will be pointed out that there is some evidence for the proposition that wall interference may result in too low an estimate of velocity for the last few points near the wall, even with the unshrouded probe; it is also possible that errors caused by fluctuations of velocity may be present for measurements near the edge of the sublayer.

III. Measurements in a Flat Plate Boundary Layer at JPL

A. General Discussion

1. Tunnel Operation. Although a description of the 20-inch supersonic wind tunnel at the Jet Propulsion Laboratory is available in a report by Schurmeier and Riise (119), several features of the facility which make it especially suitable for boundary layer research should be mentioned here. A precise calibration of the test section airflow is available for a series of nominal Mach numbers from 1.33 to 4.50, so that experiments may be carried out in an ambient flow whose properties are supposedly known. Moreover, the continuously variable test section Reynolds number makes it possible to study both laminar and turbulent boundary layer flow, and in particular to investigate some properties of the laminar flow regime for large Mach number and small Reynolds number; of the turbulent boundary layer for relatively large Reynolds number; and of the boundary layer transition.

The flexible nozzle of the 20-inch wind tunnel is supported by 22 pairs of electrically driven jacks, whose positions are remotely controlled by a cam bank operated from the control console. Any pair of jacks may be adjusted individually, within the limitations of allowable bending stress in the nozzle plates, and this adjustment can in most cases be made without interrupting the supersonic flow in the test section. A typical pressure influence curve, calculated by the method of characteristics for an extension of 0.020

inches of Jack 3* at a nominal Mach number of 4.50, is shown in Figure 39. Also shown is the increment in pressure observed experimentally on the surface of the flat plate model for a slightly different condition, the nozzle being initially distorted to provide a uniformly decreasing pressure along the plate surface.

During the calibration of the 20-inch wind tunnel, static pressures were measured on both surfaces of a horizontal wedge traversing the tunnel centerline. The lower wedge surface pressures, corrected to zero flow inclination, are shown in Figure 40 for the Mach numbers of current interest. The pressure distributions in question have been displaced upstream to account for the location of the flat plate model surface one-half inch below the tunnel centerline, and therefore supposedly represent the pressures which would be observed in the absence of a boundary layer on the plate. Also noted are the special jack corrections applied to the flexible nozzle for the present tests, and the corresponding computed pressure distributions. The waves which are present at the two lowest Mach numbers are caused by failure of the flexible plate to reproduce the discontinuity in wall curvature which exists at the inflection point in the theoretical nozzle contour, and this problem is discussed in detail in the JPL report by Schurmeier and Riise.

In making quantitative use of the calibration data, it should be remembered that the tunnel Mach number decreases with decreasing

---

* Jack numbers increase when proceeding upstream from the test section. Jack 0 controls the position of the top and bottom test section walls, and successive jacks are spaced 6.5 inches apart along the arc length of the nozzle.

stagnation pressure because of an increase in nozzle wall boundary layer thickness, and slight changes can therefore be expected both in absolute magnitude and in axial location for the pressure distributions of Figure 40.

During the early experiments it was found that the flat plate model could be pitched, after starting the tunnel with zero angle of attack, through the range $-2^{\circ} \leq \alpha \leq +2^{\circ}$ at M = 2.0; $-6^{\circ} \leq \alpha \leq +6^{\circ}$ at M = 3.7; and $-3^{\circ} \leq \alpha \leq +4^{\circ}$ at M = 4.5. Except for one test to determine the effect of angle of attack on transition at a Mach number of 2.6, and one experiment with a laminar boundary layer at a Mach number of 4.5, however, all measurements were made with the plate pitched 0.17 degrees nose down.

Starting the tunnel offered no difficulty except at the lowest Mach number, where the test section was blocked by the model. In order to run at the nominal Mach number of 1.97 at which the nozzle had been calibrated, it was found necessary to start the tunnel at M = 2.05; flow could then be maintained at zero angle of attack with Mach numbers as low as 1.86 before blocking occurred. The balance sector windshield remained in the tunnel supersonic diffuser for all tests.

The Reynolds numbers which could be realized in operation were limited on one hand by allowable casing pressure or by the power available in the compressor system, and on the other hand by the capacity of the pumps used to reduce the tunnel stagnation pressure. When operating at low pressure levels, accumulation of wet air was

prevented, and pressure regulation improved, by allowing a continuous flow of dry air into the tunnel circuit. On one or two occasions temporary separation of the air flow from the plate surface was observed when the diffuser pressure was disturbed by the admission of makeup air. In general, however, the range and flexibility of the 20-inch tunnel were found to be quite as good with the flat plate model installed as with the test section empty, and this range was exploited fully during the tests.

2. Experimental Program. The experimental measurements of the present research are discussed in detail in the sections below, and the test schedule given here therefore serves the more general purpose of providing continuity for the various aspects of the research. It may be remarked that the measurements were made in three periods of testing. The first of these, in October 1951, provided experience in tunnel operation and defined the operating limitations of the tunnel-model combination. The second period, in March 1952, yielded most of the useful information obtained on the magnitude of local and mean friction, and included an attempt to measure local mass flow rates in supersonic boundary layers. The third period, in May 1952, was an investigation of flow in a pressure gradient and of the effect of various tripping devices on boundary layer transition.

B. Local Surface Friction

The essence of the present experimental research is presented

Table V

Test Schedule
Flat Plate Boundary Layer Research
20-Inch Supersonic Wind Tunnel, JPL

Test* Number	Mach Number	Date	Remarks
409 - (1)	3.67	Oct. 18 1951	Shakedown of flat plate model without instrumentation. Determination of operating range of Mach number and Reynolds number and plate angle of attack. Test 10 omitted.
(2)	3.67	18	
(3)	3.67	18	
(4)	4.50	18	
(5)	4.50	18	
(6)	1.79	18	
(7)	1.97	Oct. 19 1951	
(8)	1.97	19	
(9)	3.67	19	
(10)			
(11)	3.67	Feb. 29 1952	Preliminary test of floating element instrumentation. Leading edge fence installed after Test 12; balance chamber seals improved after Test 13. Data repeated in Tests 37, 35, and 16 respectively.
(12)	1.97	Mar. 3 1952	
(13)	1.97	Mar. 4 1952	
14	3.67	Mar. 5 1952	Measurements of local surface friction at three stations with fence trip. Probe installed at Station 3 after Test 17.
15	4.50	Mar. 6 1952	
16	1.97	6	
17	2.55	Mar. 7 1952	
(18)	2.55	Mar. 10 1952	Shakedown of probe instrumentation.
19	3.67	Mar. 11 1952	Measurement of profiles at x = 21.5 inches with fence trip. Calibration of mass flow probe. Shroud installed on probe after Test 30. Local friction measurements made, except in Test 19, at Stations 1 and 2.
20	3.67	11	
21	3.67	11	
22	4.50	Mar. 12 1952	
23	4.50	12	
24	4.50	12	
25	2.55	12	
26	2.55	Mar. 13 1952	
27	2.55	13	
28	1.97	13	
29	1.97	13	
30	1.97	13	

* No important measurements were made in tests indicated by parentheses.

Test Number	Mach Number	Date	Remarks
31	3.67	Mar. 14 1952	Calibration of double sonic orifice probe; measurement of profiles at x = 21.5 inches with fence trip. Fence removed after Test 32.
32	2.55	14	
33	4.50	Mar. 17 1952	Measurement of local surface friction at two stations with clean leading edge. Plate angle of attack changed in Test 38. Calibration of double sonic orifice probe. Shroud removed, probe moved to Station 2, and wire holder installed at Station 1 after Test 38.
34	2.55	17	
35	1.97	Mar. 18 1952	
(36)	3.67	18	
37	3.67	18	
38	2.55	Mar. 19 1952	
(39)	1.97	Mar. 20 1952	Investigation of wake behind heated wire outside boundary layer. Calibration of mass flow probe.
(40)	3.67	20	
(41)	3.67	20	
42	2.55	Mar. 21 1952	
(43)	2.55	Mar. 24 1952	
(44)	2.07	May 15 1952	Manipulation of flexible nozzle to provide positive and negative pressure gradients over flat plate. Tests 48 and 53 to determine effect of various air jet discharge rates on surface friction distribution.
(45)	2.07	May 16 1952	
(46)	4.50	16	
(47)	4.50	16	
48	4.50	May 19 1952	
(49)	4.50	19	
(50)	4.50	May 20 1952	
(51)	4.50	20	
(52)	4.50	20	
53	1.97	May 21 1952	
(54)	4.50	May 21 1952	Determination of floating element zero with elements shielded from airflow.
55	4.50	May 22 1952	Measurement of local surface friction at three stations with air jet trip and various pressure gradients. Sand strip installed after Test 59.
56	4.50	22	
57	4.50	May 23 1952	
58	4.50	23	
59	4.50	May 26 1952	
60	4.50	May 26 1952	Measurement of local surface friction at three stations with sand strip trip. Probe installed at Station 3 after Test 60 and profile measured at x = 21.5 inches; sand removed after Test 61.
61	4.50	May 27 1952	

Test Number	Mach Number	Date	Remarks
62	4.50	May 27 1952	Measurement of profiles at x = 21.5 inches with air jet trip and various pressure gradients.
63	4.50	27	
64	4.50	May 28 1952	
65	4.50	28	
66	4.50	28	
(67)	3.67	May 28 1952	Calibration of mass flow probe.
(68)	2.55	28	Probe moved to Station 2 after Test 68.
(69)	1.97	May 29 1952	
(70)	3.67		
71	1.97	May 29 1952	Measurement of profile at x = 10.5 inches with air jet trip.
72	4.50	May 29 1952	Measurement of profiles at x = 10.5
73	4.50	June 2 1952	inches with air jet trip and various
74	4.50	2	pressure gradients. Profile with
75	4.50	2	clean leading edge obtained in Test
76	4.50	2	76.
(77)	3.67	June 2 1952	Calibration of mass flow probe. Removed damping from element at Station 1 after Test 77.
78	2.55	June 3 1952	Measurement of profiles at x = 10.5
79	1.97	3	inches with clean leading edge.
(80)	1.97	June 3 1952	Attempt to observe behavior of undamped floating element in transition region.

in Figures 41 - 50 and in Table A. Both the ordinate τ_w/q and the abscissa $u_1 x/\nu_1$ have been deduced in an unambiguous way from measured physical quantities. In particular, the static pressure in the balance chambers, and therefore the pressure in the element clearance gaps, was used in all cases to determine the local free stream Mach number, temperature, velocity, and density. For this calculation the fluid was assumed to be a perfect gas expanding isentropically from the tunnel reservoir with $\gamma = 1.400$, and the Sutherland equation, Eq. (39), was used to relate temperature and viscosity.

Two corrections, always amounting to less than two percent in the shear, have been applied to the data of the figures. First, the apparent shear associated with the floating element in a pressure gradient has been compensated for on the basis of the channel calibration discussed in Section II, Part D1 above. Second, the turbulent friction data, which are relatively sensitive to variations in Mach number, have been corrected to the nominal Mach number of the figures by means of the approximate relationship $(\partial C_f/\partial M)_R = - m^2 C_f/M$; that is, the function C_f/C_{f_i} has been approximated by the quantity $\sqrt{T_1/T_o} = (1 + \frac{\gamma-1}{2} M^2)^{-1/2}$.

The probable random error in the local turbulent friction coefficients is felt to be less than two percent. Contributing to this error are the uncertainty in the element electrical zero position under dynamic conditions, and the uncertainty in both the element static calibration and in the micrometer calibration. In addition, there are obvious problems in the accurate measurement of tunnel

static pressures of the order of two to ten millimeters of mercury absolute. Both the pressure and zero position are of course relatively more uncertain at low Reynolds numbers. An exception to the estimate of probable error must be made in the case of measurements near the region of transition from laminar to turbulent flow, where large and apparently random fluctuations in the shear were usually observed. The only systematic error which is felt to be of importance is associated with the presence of the gaps around the floating surface elements, and this probably does not exceed three percent.

In the exploitation of the pressure and Mach number range of the 20-inch supersonic wind tunnel during these measurements, it was found that a period of approximately ten to fifteen minutes was usually necessary to reach an equilibrium operating condition and to record the plate pressure distribution and element deflections. In many cases slow fluctuations of perhaps one percent in stagnation pressure were encountered during the recording of data, and these fluctuations are responsible for some of the uncertainty in static pressure measurement. However, it was possible during the profile surveys which are discussed below to repeat some of the shear measurements at the first and second stations. These data are shown as flagged points in Figures 41-50, and in general indicate excellent reproducibility.

C. Mean Surface Friction

The execution of boundary layer research with impact probe instrumentation is a routine procedure, and so will not be discussed at greater length than is necessary to establish the approximations which

are necessary in reducing the data.

The quantities sought are the momentum thickness,

$$\Theta = \int_0^{\delta+} \frac{\rho}{\rho_1} \frac{u}{u_1} \left(1 - \frac{u}{u_1}\right) dy \qquad (96)$$

and the displacement thickness,

$$\delta^* = \int_0^{\delta+} \left(1 - \frac{\rho}{\rho_1} \frac{u}{u_1}\right) dy \qquad (97)$$

Figures 51 and 52 show the variation with y of the integrands in the two expressions above for two typical boundary layer profiles at a Mach number of 4.5. The quantity directly measured was of course the impact pressure, p_0'; the static pressure was assumed to correspond to isentropic expansion from the tunnel reservoir with $\gamma = 1.400$, and to be constant through the boundary layer. The latter assumption was in each instance confirmed by measurement of surface pressure near the probe station. From these pressure data the local Mach number in the boundary layer follows.

The stagnation temperature in the boundary layer has been assumed constant at the value in the tunnel reservoir. The local static temperature, density, velocity of sound, and fluid velocity were obtained from the usual equations of energy and state; in particular, the gas constant R has been taken as 1716 $(\text{lb./ft.}^2)/(\text{slugs/ft.}^3)(^\circ\text{R})$ in the state equation

$$p = R \rho T \qquad (98)$$

An inspection of the method of data reduction shows that errors in the velocity u and in the momentum ρu will be respectively in the same and opposite direction as the error in the local stagnation temperature, and will be of about half the magnitude. Although the calculation of the integrand in the momentum equation thus involves a cumulative error at a given point, it seems unlikely that the computed value of Θ might differ from the correct value by more than the probable uncertainty of one or two percent in the stagnation temperature which is typical for most of the boundary layer.

Table B lists the more important aerodynamic parameters for the fourteen turbulent boundary layer surveys made during the present research, and Table C gives the variation of velocity with distance for the various profiles, all but one of which were obtained at a distance of about 21.5 inches from the plate leading edge.

D. Surface Pressure Distribution

Before discussing the friction measurements in detail, it is convenient to describe a second technique which was found useful in establishing the nature of the boundary layer flow over the plate. During the present research relatively large static pressure disturbances, of the order of five percent, were observed on the plate surface, especially in the region of transition from laminar to turbulent flow. In fact, the experience at JPL suggests that accurate measurements of surface pressure on a plate in a well calibrated supersonic air flow might be a means for obtaining quantitative data on surface friction. Certainly, the influence of various disturbances on tran-

sition could be established by relatively simple means.

Only the experience at a Mach number of 3.7 will be discussed, since the plate surface pressures at Mach numbers of 2.0 and 2.6 are difficult to interpret because of the waves mentioned above in Section III, Part A1, and the measurements at a Mach number of 4.5 are subject to hazard because of the low static pressures involved. Even at M = 3.7, the maximum static pressure which could be reached was 22 millimeters of mercury, or about one fifth of full scale for the silicone multimanometer described above in the section on instrumentation.

Figures 53 and 54 show the pressure distributions observed during the friction measurements of Figures 45 and 46. The expansion downstream of the leading edge and the compression in the transition region are quite conspicuous when the observed pressures are compared to the empty test section pressure distribution.

In order to determine quantitatively the pressure disturbance associated with the boundary layer on the plate surface, several other sources of pressure variation must be eliminated. These are (a) the error in the wedge calibration data caused by the existence of a boundary layer on the wedge; (b) the change in pressure level associated with the slight negative plate angle of attack; and (c) the variation of test section Mach number with tunnel stagnation pressure because of changes in the nozzle boundary layer thickness. As an alternative to estimating these effects individually, their

net effect for a given stagnation pressure has been determined by means of the assumption that the pressure increment caused by the laminar boundary layer on the flat plate is a parabolic function of the distance from the leading edge.

Suppose that the unknown free stream static pressure is denoted by p_1, and the pressures observed in the test section during the tunnel calibration and on the flat plate surface during the friction measurements are denoted by p_c and p_w respectively. Writing

$$\frac{p_w}{p_1} - 1 = \frac{p_o}{p_1}\left(\frac{p_w - p_c}{p_o} + \frac{p_c - p_1}{p_o}\right) = \frac{A}{\sqrt{R}}$$

where p_o is the isentropic stagnation pressure, observation of p_w as a function of R allows the parameters A and p_1 to be determined independently for each value of p_o or of R'. As a check, the variation of local Mach number with R' for Test 37, computed from the pressure ratio p_1/p_o, has been compared with the variation indicated by an impact probe located outside the boundary layer at Station 3 on the plate, and excellent agreement found.

The pressure increment associated with the existence of a boundary layer on the plate is shown in Figure 55. The resemblance of the curves to those for the surface friction* is striking, and is of course not accidental, since the apparent body presented to the airflow should have a contour corresponding closely to the distribution of displacement thickness in the boundary layer.

---

* The figure suggests that the special nozzle corrections noted in Figure 40 may not have been used in these tests.

E. Interpretation of Experimental Measurements

1. Transition. The region of transition from laminar to turbulent flow may be identified by a minimum and a maximum in the curve of local shearing stress plotted against Reynolds number. The transition is not in general a unique function of the Reynolds number for the experiments reported here, and this fact increases the difficulty of determining the shear distribution from observations at three points. However, since a strong correlation has been observed between the shear and pressure distributions over the plate surface, the latter may be useful in interpolating between measured values of the friction coefficient at a given stagnation pressure.

Figure 56 - 62 show, for the tests with natural transition and with the leading edge fence, the Reynolds numbers of the minima and maxima in the shear and pressure distributions as obtained from Figures 41 - 48 and from pressure measurements like those of Figure 53. Some judgment has of course been exercised in estimating the Reynolds numbers for the pressure extrema, since the data are not always adequate to the demands imposed. Furthermore, for technical reasons the pressure measurements were made approximately three inches from the plane of symmetry, and it is not certain that the boundary layer flow was accurately two-dimensional. In spite of these defects in the pressure data, it appears that the minimum in the static pressure distribution corresponds closely in all cases to the position of maximum rate of change of the local friction coefficient. It should be remembered that both the friction and pressure measurements in the region of transition represent the response of a highly damped instrument to a

quantity which is fluctuating rapidly with time, and therefore that the present observations of transition may be peculiar to the particular wind tunnel and instrumentation involved.

Several other features of Figures 56 - 62 are of special interest. The Reynolds number per inch, R', is proportional to the tunnel stagnation pressure, and the movement of the natural transition toward smaller values of x but toward larger values of $u_1 x/\nu_1$ with increasing tunnel pressure is quite evident in the coordinate system of the figures. On the other hand, the fence tripping device apparently has the fortunate property at high stagnation pressures of causing transition to occur at a fixed Reynolds number increment from the leading edge. It is therefore possible that the tendency of the corresponding local friction measurements to define a single curve in the turbulent flow regime is not accidental; see for example Figure 44, where the measurements are probably free of errors caused by local pressure gradients. At low values of tunnel stagnation pressure the effect of the fence is entirely different. The large initial increment in ⑭ caused by wire drag apparently does not influence the slope of the velocity profile at the wall upstream of actual transition, as may be verified by a comparison of Figures 47 and 48. Furthermore, the transition at the lowest tunnel pressures may actually be moved to higher Reynolds numbers by the disturbance from the fence, from the evidence for example of Figures 61 and 62. These remarks serve to emphasize the lack of real understanding of the transition phenomenon, and show the need for caution in attempting to predict the influence of a given disturbance.

2. Effective Reynolds Number. Two reasons may be advanced in justification of an attempt to define, using experimental information about the boundary layer flow, the effective or ideal Reynolds numbers for the measurements in the turbulent regime. The first is the relatively detailed information on transition which is available. The second is the supposition that the measured local friction coefficients may be accepted as correct, and only the Reynolds numbers need be determined in order to obtain the properties of the ideal boundary layer.

The question of uniqueness has been discussed from the experimental point of view for the turbulent boundary layer with constant density in Section I. In keeping with the extensive experience in low speed flow, the fully developed compressible turbulent boundary layer may be characterized by a unique relationship between the slope and ordinate of the momentum thickness distribution $\Theta(x)$. Since there exists no sound theoretical organization of the problem, the analysis should be carried out as far as possible using experimental information about the boundary layer.

Figure 63 shows the experimentally determined relationship between τ_w/q and $u_1\Theta/\nu_1$ for various Mach numbers, from the data of Table B, together with the corresponding curve for zero Mach number from Table I. It appears that the boundary layer is fully developed according to the present criterion except perhaps for the points which are farthest to the left in the figure at the lower Mach numbers.

If the data are now required to be internally consistent in

terms of the relationship

$$R_{\theta_2} - R_{\theta_1} = \int_{R_1}^{R_2} \frac{dR_\theta}{dR} dR = \frac{1}{2} (\tau_w/q)_{avg} (R_2 - R_1)$$

then the quantity $(R_2 - R_1)$ may be computed for any pair of observations at the same Mach number. For this purpose an acceptable average local friction coefficient may be obtained by assuming a power law for the variation of C_f with R_θ or with R within the interval in question; that is, $C_f = AR_\theta^{-1/n}$, and it follows that

$$C_{f\,avg} = \frac{1}{R_{\theta_2} - R_{\theta_1}} \int_{R_{\theta_1}}^{R_{\theta_2}} C_f \, dR_\theta$$

$$= \frac{(R_{\theta_2} C_{f_2} - R_{\theta_1} C_{f_1}) / (R_{\theta_2} - R_{\theta_1})}{1 - \ln (C_{f_1}/C_{f_2}) / \ln (R_{\theta_2}/R_{\theta_1})}$$

When these calculations are carried out, values for $(R_2 - R_1)$ like those below are obtained;

Mach No.	Tests	$R_2 - R_1$
2.6	27, 26	4,200,000
3.7	20, 19	4,650,000
4.5	23, 22	4,600,000
4.5	76, 62	3,400,000

where the second entry for $M = 4.5$ involves two profiles at different plate stations at the same pressure, and the remaining data involve two profiles at different pressures at the same station.

The effective Reynolds numbers for the measurements in supersonic

flow may now be related to the curve for $M = 0$. In Figure 63, a straight line which slopes up and to the right at 45° is a line on which C_f/C_{f_i} and R_θ/R_{θ_1} are equal, and may be assumed initially to be also a line of constant Reynolds number. The values of R obtained for the experimental data by reference to the low-speed data of Table I or Figure 8 are found to differ, for the paired profiles being considered here, by an amount larger than that implied by internal consistency.

This difficulty is met by assuming that lines of constant R in Figure 63 have a slope which is not 45°, but is at least independent of Reynolds number in the range being considered, and the problem is reduced to one of determining the proper slope so that the intercepts with the curve $M = 0$ are separated by the desired increment in R. Such lines are shown in the figure, and lead to the values of R, and of C_f/C_{f_i} and C_F/C_{F_i} at constant R, which are listed in Table B. The critical assumption in this procedure is that the quantity $(C_f/C_{f_i})/(C_F/C_{F_i})$ at constant R is nearly independent of Reynolds number, and in the writer's opinion does not constitute a severe restriction in the analysis.

Table B also lists values for C_f/C_{f_i} at constant $R_\delta = u_1 \delta/\nu_1$, using the values of C_{f_i} determined from Table I and Eqs. (30) and (34). In Figure 64 the measurements in the plane $(\tau_w/q, u_1\Theta/\nu_1)$ are connected to the curve for $M = 0$ by lines of constant R_δ, and in two cases several compressible profiles are observed to show consistent behavior with varying Mach number at a fixed value of R_δ.

In Figures 65 and 66 are shown the corrected friction data in the coordinate systems (C_f, R) and (C_F, R) as determined by the procedure outlined above of requiring the compressible data to be both self-consistent and compatible with the measurements at M = 0.

There is a cogent reason for citing the low-speed flow in the interpretation of supersonic measurements; the reason is connected with the convention for defining a Reynolds number R. The assumption of uniqueness implies a function

$$2\frac{dR_\theta}{dR} = g(R_\theta) \qquad (99)$$

which may be integrated to yield a relationship $R = G(R_\theta)$, on satisfying the initial condition R = 0 when $R_\theta = 0$. Since the surface shearing stress is supposedly always positive, R_θ is a monotonically increasing function of R, and the initial condition in question can always be satisfied.

However, the integration can be carried out, and an exact definition of R achieved, only if the function g is known for all positive values of R_θ. Given an analysis based for example on functional similarity and valid for large Reynolds numbers, an extrapolation to small values of R_θ is necessary in order to define a Reynolds number R, and it is fortuitous if the extrapolated function turns out to be integrable* at $R_\theta = 0$.

---

* The uniqueness function Eq. (99) for the turbulent boundary layer with constant density is Eq. (35) of Section I above. Not only is this function integrable, but R_θ vanishes for $C_f = 2(C_1/C_2)^2$; the mean and local friction coefficients are therefore finite, and are in fact equal, in the limit R = 0.

In compressible flow the definition of R likewise depends on the form assumed for the variation of C_f with R_θ; several writers have used a power law in the analysis of experimental data, while the present study attempts to relate compressible measurements to the better known state of affairs at $M = 0$. It is therefore obvious, in comparing various experimental reports in this field, that discrepancies in the final corrected data may not mean that one or another series of measurements is in error, but only that they are differently interpreted.

The method of correction given above has the considerable advantage that it is relatively insensitive to errors in measurement of either local or mean friction. This property of the analysis is a useful one, since there are measurable and systematic discrepancies in the data which have not yet been mentioned.

Figure 67 supposedly defines the function C_f (R) for the ideal turbulent boundary layer, at least in a restricted range of the variables. Within this range, it is possible to select two measurements of local friction made at successive stations along the plate at a fixed pressure, and to compare the ideal increment in Reynolds number with the known value of $u_1 \Delta x/\nu_1$ for the points in question. When this is done it is invariably found that the actual increment in R is smaller than the ideal increment by an appreciable amount. In terms of the friction coefficient, this means that τ_w/q as observed experimentally changes more rapidly with $u_1 x/\nu_1$ than would be predicted on the basis of the combined mean and local friction measurements.

The problem may be restated by considering an alternative interpretation of the local friction data. For the present measurements it has been observed that for a given Mach number the increment $u_1 \Delta x/\nu_1$ in Reynolds number, between the point of maximum surface shearing stress and the point of measurement, is a well-defined function of the measured local friction coefficient, whether transition is natural or forced. Figure 67 shows this relationship for Mach numbers of 2.6, 3.7, and 4.5; data at a Mach number of 2.0 is omitted because the presence of large local pressure gradients affects the local friction and simultaneously makes it difficult to identify the pressure disturbance at transition. The abscissa in Figure 67, denoted by $(R - R_t)$ and tabulated in Table A*, is the quantity $u_1 \Delta x/\nu_1$, where Δx is measured between the point of maximum shearing stress and the downstream element station for each operating condition.

But the local friction coefficient is now experimentally a unique function of $(R - R_t)$ and also by assumption a unique function of R. It follows that R_t can only be a function of R for a given Mach number; however, since the measurements at different stations at a fixed value of tunnel pressure should be characterized by the same value of R_t, the latter must be a constant for each of the three curves of Figure 67. This is very approximately to say that the end of the transition region occurs at a value of R_e which depends only on M whether transition is stimulated or not.

---

* Values of $(R - R_t)$ may be verified by subtracting the appropriate values of the Reynolds number of maximum shear, given as a function of stagnation pressure by the curves through the solid points in Figures 57 - 62, from the tabulated values of $u_1 x/\nu_1$ in Table A. Technical problems connected with management of the low pressure manometer instrumentation prevent discussing the data of Tests 44 et seq. in this context.

It may be observed, on comparing Figures 65 and 67, that there is no set of values of R_t which will lead to complete superposition of the supposedly ideal curves of the two figures, although magnitudes for R_t in the neighborhood of 1.5×10^6 are not unreasonable. The discrepancy in question may be identified as a tendency for R_θ to increase faster than the integral of τ_w/q. Fortunately the effect is not numerically large, amounting to perhaps a few percent in the shear.

It is possible that the flow in the 20-inch tunnel deviates sufficiently far from the two-dimensional condition to account for the inconsistency observed here. The practice of making an adjustment in the top and bottom nozzle contours, to account for the presence of a boundary layer on all four tunnel walls, leads inevitably to three-dimensional flow in the test section. The flow is slightly converging in the plan view and slightly diverging in the elevation; the two effects cancel as far as the pressure distribution along the tunnel centerline is concerned, yielding there a uniform value of static pressure. The calibration report by Schurmeier and Riise (119) discusses this problem in some detail, giving several pressure and flow inclination surveys off the nozzle centerline at a Mach number of 2.5 which definitely establish the presence of this peculiarity in the supposedly uniform flow.

An estimate may readily be formed of the errors which might be encountered in the present instance. Given an initial momentum thickness θ_1 and a specified shearing stress distribution, the momentum thickness downstream is

$$\theta_2 = \theta_1 + \frac{1}{2} \int_{x_1}^{x_2} \frac{\tau_w}{q} dx$$

However, if the width of the plate decreases uniformly from a value w_1 to a value w_2, the initial drag increment $w_1\theta_1$ remains constant but the contribution to the momentum thickness θ_2 at x_2 is larger by a factor w_1/w_2. Furthermore, each increment in θ undergoes the same kind of distortion in the converging flow, with the result that in fact

$$\theta_2 = \theta_1 \left(\frac{w_1}{w_2}\right) + \frac{1}{2} \int_{x_1}^{x_2} \frac{\tau_w}{q} \frac{w}{w_2} dx$$

or approximately

$$\theta_2 = \theta_1 \left(\frac{w_1}{w_2}\right) + \frac{1}{2} \left(1 + \frac{w_1}{w_2}\right) \frac{1}{2} \int_{x_1}^{x_2} \frac{\tau_w}{q} dx$$

An estimate of the rate of growth of the nozzle side wall boundary layer shows that the predicted effect is in the proper direction, but may not be large enough to account for the discrepancies in the present tests.* The discussion has of course assumed that the measurements are exact, and this assumption seems a liberal one even to the writer.

Of the alternative interpretations discussed here for the

---

* Mr. Weiler of the Defense Research Laboratory of the University of Texas, in a private communication, has informed the writer that the same kind of discrepancy appears in measurements of mean and local supersonic friction in the Dangerfield tunnel.

experimental data, it is probable that Figure 67 gives a lower bound to the ideal curves since the origin of the boundary layer is likely to be upstream of the point of maximum shearing stress. The original requirement of consistency between the mean and local friction measurements, although not completely compatible with the physical conditions actually encountered, yields corrected values which are quite plausible while giving proper emphasis to the profile data. It is therefore the writer's opinion that Figure 66 should be certified as representing the local surface friction in the ideal turbulent supersonic boundary layer.

3. Boundary Layer Profiles. Several generalizations of the incompressible mixing length theory to compressible flow have already been compared in Table II above. One of these (84), which is discussed here because of its computational simplicity, concludes that the dimensionless variables u/u_τ and yu_τ/ν should be replaced in compressible adiabatic flow by $(\sin^{-1}mu/u_1)/(m\sqrt{\tau_w/\rho_w}/u_1)$ and by $y\sqrt{\tau_w/\rho_w}/\nu_w$. Figure 68 shows three of the profiles of Table C, having nearly the same value of $u_1\delta/\nu_1$, in the generalized coordinate system; the appropriate low-speed profile is included for comparison.

It appears from Figure 68 that the influence of compressibility is probably taken into account to some extent by the formulation in question, although the agreement in the slope of the logarithmic portion of the profile is poor at the lower Mach numbers. It is questionable whether the mixing length theory, which emphasizes the logarithmic function, should be expected to describe adequately the effect of compressibility, since the logarithmic portion of the velocity

profile must become progressively less conspicuous as the Mach number increases for a fixed value of R_δ because of the increasing physical dimension of the sublayer.

In defense of the work of Van Driest, or for that matter of Wilson (80) since the two analyses are nearly equivalent in describing the measurements reported here, it should be said that the data in the coordinate system of the appropriate generalized velocity defect law are in fair agreement with low-speed measurements. In fact, the generalized velocity defect $(\sin^{-1}m - \sin^{-1}mu/u_1)/(m\sqrt{\tau_w/\rho_w}/u_1)$ is very closely a straight line, although not quite the same straight line for different values of M or R_θ, when plotted against $(1 - y/\delta)^{3/2}$, and the values of δ reported here have been determined by this method in order to be consistent with the analysis of Section I, Part B3 above.

An alternative formulation of similarity in compressible turbulent boundary layers has been suggested by the writer in Section I, Part C2 of the present report. By means of a frankly speculative generalization of an analysis of the low-speed problem, it is found that the relationship

$$\frac{u}{\sqrt{\tau_w/\rho_\tau}} = f\left(\frac{\rho_\tau}{\mu_w}\sqrt{\frac{\tau_w}{\rho_\tau}}\int_0^y \frac{\rho}{\rho_w}\,dy\right) \qquad (92)$$

may represent the velocity profile in compressible flow. The parameter ρ_τ is not defined during the analysis and may be chosen arbitrarily to provide agreement with the low speed data. Since ρ_w and μ_w do not depend on x for the present experiments, ρ_τ/ρ_w should be a function

only of Mach number.

It is convenient to write Eq. (92) as

$$\sqrt{\frac{\rho_T}{\rho_w}}\,\frac{u}{\sqrt{\tau_w/\rho_w}} = f\left(\sqrt{\frac{\rho_T}{\rho_w}}\,\frac{\sqrt{\tau_w/\rho_w}}{\nu_w}\int_0^y \frac{\rho}{\rho_w}\,dy\right) \qquad (100)$$

from which it is obvious that very close to the wall, where the function f is nearly equal to its argument, the coefficient $\sqrt{\rho_T/\rho_w}$ is immaterial; that is, for small values of y

$$\frac{u}{\sqrt{\tau_w/\rho_w}} \doteq \frac{y\sqrt{\tau_w/\rho_w}}{\nu_w}$$

Both of these quantities are tabulated in Table C, so that it is necessary only to compute

$$\eta = \int_0^y \frac{\rho}{\rho_w}\,dy \qquad (94)$$

as a function of y and to determine ρ_T/ρ_w for each of the boundary layer profiles in order to test Eq. (92).

The assumption of constant stagnation temperature leads near the wall to a value of the density which is too small, and near the edge of the boundary layer to a value which is too large. However, the use of a density computed in this way in Eq. (94), together with the use of an accurate value of ρ_w, will probably not seriously stultify the calculation of the Howarth coordinate η.

Values of ρ_T/ρ_w, chosen for a reasonable fit to the function

f of Table III in the region near arg f = 200, are given in Table B*, and the various profile data modified in accordance with Eq. (100) are listed in Table C.

The three boundary layer profiles of Figure 68 are shown in Figure 69 in the coordinate system of Eq. (92). It appears that the measurements may be adequately represented in terms of the new variables; the slight deterioration of the data nearest the wall is no better and no worse than is typical of impact probe instrumentation in low speed flow. If the effect of wall interference is to indicate too low a velocity, as suggested by Figure 37, and if the effect of large fluctuations in u and/or ρ is to indicate too large a velocity, the data are credible as they stand. The use of hot-wire instrumentation might resolve this issue, although a more critical test is the development of methods for predicting the proper value of the parameter ρ_τ.

F. Experience with Tripping Devices

1. Air Jets. The device of discharging air from small holes in a surface, for the purpose of stimulating transition to turbulent flow in the boundary layer, has been used by Fage and Sargent (120) and by Pfenninger (121). The most important property of such a tripping device, aside from the obvious advantage of control, is the low intrinsic drag of the jets, since the air is initially discharged normal to the external flow.

---

* The value of ρ_τ/ρ_w is quite sensitive to variation in τ_w/q, and the profiles at M = 2.0 are therefore not completely typical because of the presence of pressure gradients.

In order to establish a criterion for specifying the strength of the air jet tripping device, it is instructive to consider the increment in the mass flow in the boundary layer. Immediately upstream of the jets, from the definition of the displacement thickness,

$$\rho_1 u_1 (\delta - \delta^*) = \int_0^{\delta} \rho u \, dy$$

and downstream, denoting the appropriate density, velocity, and boundary layer thickness by primes,

$$\int_0^{\delta'} \rho' u' \, dy = \int_0^{\delta} \rho u \, dy + \frac{dm}{dt} = \rho_1 u_1 (\delta' - \delta^{*\prime})$$

so that, if $\delta' = \delta$,

$$\rho_1 u_1 (\delta^* - \delta^{*\prime}) = \frac{dm}{dt} = \rho_1 u_1 \Delta\delta^*$$

where dm/dt is the discharge per unit width in the lateral direction and corresponds to a decrease in the boundary layer displacement thickness. Forming a Reynolds number

$$R_j = \frac{dm/dt}{\mu_1} = \frac{u_1 \Delta\delta^*}{\nu_1}$$

it is obvious that the quantity R_j is independent of tunnel pressure level for a given tunnel temperature and air discharge rate, and so provides a convenient measure of air jet strength for the present tests.

The flat plate was modified, in the interval between Tests 43 and 44, by adding a row of holes 0.75 inches from the leading edge. These holes were 0.0135 inches in diameter (number 80 drill), spaced 0.25 inches apart, and led to a manifold on the upper surface and to a metering orifice outside the tunnel. The maximum mass flow of 10^{-5} slugs per second used in the experiments supplied a total of 65 discharge holes extending over 16 inches of the 18 inch plate width.

Tests 48 and 53 were carried out to determine the efficacy of the air jets as a tripping device at Mach numbers of 4.5 and 2.0 respectively, and the data from Stations 1 and 3 are shown in Figures 70 and 71, as surfaces of the function $\tau_w/q = \tau_w/q(R_j, u_1 x/\nu_1)$. The most conspicuous feature of the experiments at a Mach number of 2.0 is the existence of a critical discharge rate; for smaller rates than the critical value the air jets have a negligible effect on the surface friction, while for larger rates the effect is large and does not change appreciably with a further increase in the amount of air discharged. In fact it was not possible at a Mach number of 2.0 to adjust the air flow rate so as to obtain values of surface friction other than the two extremes of the figure. At a Mach number of 4.5 the boundary layer transition was less sensitive to discharge rate.

It is not known whether the values of R_j which critically affect transition would be appreciably altered by changes for example in the diameter, spacing, or streamwise position of the air discharge holes in the plate surface. The table below lists the criteria for

the present geometry.

Mach number	2.0	4.5
Maximum R_j	25	75
Critical R_j	10	25
Range of $u_1^j \delta^*/\nu_1$ at jets	700-2000	3000-5000
Critical increment in δ^*	0.5 - 1.4%	0.5 - 0.8%

It is of considerable interest to compare the measured friction data at the lowest tunnel pressure at a Mach number of 2.0, which are the points at the smallest values of $u_1 x/\nu_1$ in Figure 70, with the appearance of the physical boundary layer as revealed by Schlieren photographs. Figure 72 shows the boundary layer in question. The sudden increase in surface friction at Station 3 when R_j increases from 4.9 to 13.2 is consistent with the change in appearance of the boundary layer in the third window. The point of greatest interest, however, is the apparent superposition of laminar and turbulent boundary layer flow in the first and second windows in the photographs for R_j greater than the critical value of 10. It would appear that the observed slight increase of local friction at Station 1 corresponds to the occurrence of an ambiguous image of the boundary layer in the photographs, which were taken with an exposure of 1/200 second. The comment "unsteady" appears in the original data for the floating element friction measurements at the first and second stations, and it is likely that relatively high frequency random alternation between laminar and turbulent boundary layer flow actually occurred. Inspection of all Schlieren photographs taken during the present experiments suggests that the same phenomenon was present, although to a much less conspicuous extent, for natural transition at Mach numbers of 2.0 and 2.5. An investigation of the mechanism by which air dis-

charge stimulates transition would be of considerable interest as a problem in local instability, and might also shed some light on the connection which must exist between the transition phenomenon and the occurrence of intermittent turbulence in the outer part of the boundary layer farther downstream.

2. Angle of Attack. One of the factors which is known to affect boundary layer transition on a plate in subsonic flow is the position of the leading edge stagnation point. Hall and Hislop (122) found a pronounced variation in the Reynolds number of transition as a function of angle of attack for a thin plate with a sharp leading edge, and a smaller but similar variation for a thicker plate with an elliptic nose section. These observations suggest that transition in incompressible flow may be precipitated by large local pressure gradients and/or local separation at the leading edge, occurring possibly as a consequence of free stream velocity fluctuations near regions of large curvature.

Although a direct comparison of the JPL experiments with the experience of Hall and Hislop is difficult, in view of the asymmetric leading edge configuration for the present tests, no influence of angle of attack on transition was observed during the present investigation of supersonic boundary layers.

Qualitative evidence was obtained by means of Schlieren photographs for angles of attack of $\pm$ six degrees at a nominal Mach number of 3.7 and $\pm$ three degrees at a nominal Mach number of 4.5, and quantitative evidence was obtained at a nominal Mach number of 2.6

by observing changes in surface friction and pressure distribution. In view of the measurements of Figure 43, the tunnel pressure for the test at M = 2.6 was chosen so that the boundary layer was laminar at the first station and turbulent at the second for the normal angle of attack of -0.17 degrees.

Figure 73 shows the change in zero position with angle for element D, installed at the first station. The angle of attack of the plate was determined by observing with the Wild level the vertical separation of two sets of cross hairs scribed twenty inches apart on the side of the plate, and is probably accurate to about 10^{-4} radians.

The variation of friction coefficient with angle of attack is shown in Figure 74. The original values from Test 34 are verified within one or two percent and there is no significant change in the character of the boundary layer flow at either station for angles of attack over a range of about three degrees. The estimated curves shown are based on the assumption that the laminar friction is a function of Reynolds number alone, while the turbulent friction depends only on the Mach number. The actual small increase of turbulent friction coefficient at the second station, as the plate is pitched nose down, is probably associated with a decrease in effective Reynolds number as a result of the normal decrease in density behind the nose wave.

Further evidence is presented in Figure 75, which shows static pressure distributions along the plate observed at three angles of

attack, together with the appropriate tunnel calibration data. The pattern of pressure disturbances is seen to be independent of the plate angle of attack in Figure 75, and also in Figure 76, where the observed static pressures in the balance chambers are compared to the Prandtl-Meyer relationship for the variation of pressure with flow angle.

3. Fence and Sand Strip. Figures 77 and 78 show the physical appearance of the leading edge fence tripping device and of the sand strip. The latter will not be discussed here except to note that the sand, which in the present experiments extended approximately from $x = 0.8$ inches to $x = 1.2$ inches, proved to be relatively weak in stimulating transition. The intrinsic difficulty in defining the geometry of the sand strip is alone a great enough defect to disqualify the method for most applications.

The fence on the other hand has several virtues, among them the fact that relatively few parameters are needed to define the geometry, and that the initial momentum loss per unit span at the wires may be predicted from the known drag characteristics of cylinders in supersonic flow. The wires used were 0.014 inches in diameter, spaced 1/4 inch apart, and projected about 0.10 inches beyond the leading edge of the plate.

Figure 79 is a series of Schlieren photographs of the boundary layer flow, at various Mach numbers at the same Reynolds number, with the fence installed. The serrated pattern of waves apparently originating at the plate surface is typical of the fence configuration,

although no traces of these waves were found in the static pressure distribution measured at the surface.

Aside from some comments on page 128 above about the effectiveness of the fence trip, one remark about an aerodynamic property of the device should be made. The drag coefficient based on projected area for a cylinder is

$$C_D = \frac{D}{q L d}$$

and the initial momentum thickness change at the wires is therefore

$$\theta_o = \frac{D}{2 q w} = \frac{1}{2} C_D \frac{L d}{w}$$

Using d = 0.014, L = 0.10, and w = 0.25, then θ_o may be computed from

$$\theta_o = 0.0028 \; C_D \quad (\text{inches})$$

Given that the drag coefficient of a cylinder in compressible flow is nearly independent of Mach number and Reynolds number (123-126) for the range considered here, and assuming that a value C_D = 1.1 is typical even for Reynolds numbers as small as 10^3 based on cylinder diameter*, it follows from Table B that about 10 percent of the momentum thickness observed in the profile surveys was contributed

---

* The explanation for the non-occurrence of a critical Reynolds number at supersonic speeds is probably the fact that the potential flow about the cylinder already implies a large pressure drag, which is only slightly modified by movement of the separation point.

by the tripping device, and 90 percent by the surface friction. In view however of the discrepancies already noted in comparing the rates of growth of the boundary layer measured locally and in the large, no attempt has been made to verify the relative contributions of the fence and of the surface friction by integrating the latter over the plate length.

On comparing Figures 58, 60, and 62, it is apparent that as the Mach number increases there is a corresponding increase in the wire Reynolds number needed to affect the boundary layer transition. As in the case of the air jets, it is not known whether another geometry might be more effective, or whether an analysis in terms of some characteristic frequency of the tripping device might be useful.

Finally, the montage in Figure 80 shows the appearance of the boundary layer at a Mach number of 4.5 with natural transition and with the sand, jet, and fence trips. The friction measurements corresponding to the conditions of Figures 79 and 80 may be identified in Figures 41-50 or in Table A by using the specified Reynolds numbers per inch and values of x of 5.5, 13.0, and 24.0 inches for the three element stations; the latter are placed nearly at the downstream edges of the small windows in the Schlieren photographs.

G. Flow with Pressure Gradient

Several objectives were sought in the application of the technique of direct measurement of surface shear to a boundary layer

with pressure gradient, in spite of the limited scope of the investigation. Experimental verification of the momentum equation for a supersonic boundary layer, with an estimate of the effect of pressure gradient on the individual terms, would be a useful contribution to research in fluid mechanics. Furthermore, the floating element technique, once proved useful in a pressure gradient, might be applied to the investigation of more difficult problems such as the shock wave-boundary layer interaction. Finally, provision of a gradient by distortion of the nozzle walls was a relatively simple matter in the case of the 20-inch supersonic wind tunnel, so that a correspondingly small investment of time and effort was required to establish the desired environment for the measurements.

If the effect of curvature can be neglected, the momentum equation for a boundary layer can be written

$$\frac{d\theta}{dx} + P(x)\,\theta = S(x) \qquad (101)$$

where the functions P(x) and S(x) are given respectively by the extrinsic pressure field

$$P(x) = -\left(\frac{2 - M^2 + \delta^*/\theta}{\gamma M^2}\right)\frac{1}{p}\frac{dp}{dx} \qquad (102)$$

and by the surface shearing stress distribution,

$$S(x) = \frac{1}{2}\,\frac{\tau_w}{q} \qquad (103)$$

Experimental investigations of turbulent boundary layers in a pressure gradient have usually been designed to give information about the shear distribution S(x) from measurements of the pressure P(x) and the momentum thickness $\theta(x)$; however, theoretical knowledge of the problem is in a completely primitive state, and experimental difficulties have sometimes been encountered (6, 51-54).

It may be assumed that Eq. (101) is valid for a boundary layer provided that separation is not imminent, that pressure variations normal to the surface can be neglected, and that the external flow is isentropic. It is easily shown, for example by the substitution $\ln \varphi = \int P(x)dx$, that the integral of (101) between two stations along the plate is

$$\theta(x_2)\, e^{\int_{x_1}^{x_2} P(x)dx} - \theta(x_1) = \int_{x_1}^{x_2} S(x)\, e^{\int_{x_1}^{x} P(\xi)d\xi}\, dx \qquad (104)$$

Since the function P(x) vanishes for the case of zero pressure gradient, the last expression reduces to

$$\theta(x_2) - \theta(x_1) = \theta_2 - \theta_1 = \frac{1}{2}\int_{x_1}^{x_2} \frac{\tau_w(x)}{q}\, dx$$

and it is therefore convenient to normalize (104) in the form

$$\frac{\theta_2\, e^{\int_{x_1}^{x_2} P(x)dx} - \theta_1}{\theta_2 - \theta_1} = \frac{1}{\theta_2 - \theta_1}\int_{x_1}^{x_2} S(x)\, e^{\int_{x_1}^{x} P(\xi)d\xi}\, dx \qquad (105)$$

It should be noted that the function P(x) also vanishes when the quantity in parentheses in Eq. (102) changes sign. Figure 81 shows the variation of the quantity $(2 - M^2 + \delta^*/\theta)/\gamma M^2$ with Mach number, and therefore indicates the relative influence on the shearing stress of a given pressure gradient, the latter being expressed say as percent change in pressure per unit length. The curves for the laminar boundary layer are computed from the theory of Young and Janssen (127), and those for the turbulent boundary layer from the tabulated data of Tucker (72, 73) for a power law velocity profile. Also shown are typical experimental points obtained during the present research.

The significance of the change in sign of the pressure gradient parameter can be visualized by considering a fixed value of the quantity $d\theta/dx$ in Eq. (101). A positive value of dp/dx at low Mach numbers implies divergence of the streamlines in the ambient flow, together with a negative value of the parameter P(x). The contribution of the pressure forces to the fixed rate of momentum loss in the fluid is exaggerated by this divergence, and the resulting decrease in surface shearing stress may lead eventually to separation. On the other hand, at supersonic Mach numbers a positive value of dp/dx implies convergence of the streamlines in the ambient flow, so that the pressure contribution to the momentum loss is diminished; the net pressure force on a section of the boundary layer will finally become directed downstream when $(2 - M^2 + \delta^*/\theta)$ changes sign, and the skin friction will increase.

In view of Figure 81, measurements in a pressure gradient were carried out at the highest available nominal Mach number of 4.5* after several preliminary tests to establish nozzle contours which would provide a smooth and nearly linear pressure variation along the plate. Figure 82 shows the experimental evaluation of Eq. (105) for five conditions, with pressure gradients in the range ± two percent per inch. It is obvious that the momentum equation (101) is not in general valid for the boundary layer flow in question, and the difficulty is believed to be connected with the presence of three-dimensional ambient flow over the plate surface.

Figure 83 shows the static pressure distributions observed on the plate centerline, by direct measurement at or near the floating elements and by indirect measurement using the impact pressure observed outside the boundary layer. Also shown are the static pressures measured 2.75 inches from the plate centerline. Except for the flow without pressure gradient, there are large discrepancies between the two curves; the indication of later transition off the centerline is probably in error since the air jet directly in line with the static pressure orifices was later found to be plugged by a drill fragment.

It appears certain that the effort to determine the effect of pressure gradient on a supersonic turbulent boundary layer was aborted by failure to obtain the desired ambient flow conditions.

---

* An unsuccessful attempt was made to provide useful pressure gradients at M = 2.0; the short length of the test rhombus at this Mach number required that only the upper nozzle plate be distorted, in order that waves reaching the surface of the model after one reflection would not be superimposed on waves arriving directly from the lower nozzle plate.

It should be pointed out, however, that the flow with zero nominal pressure gradient in particular in Figures 82 and 83 has provided encouraging evidence of consistency between the present measurements of mean and local friction, since the momentum equation (101) was verified within three or four percent of the individual terms.

H. Assessment of the Research

The experimental results of the present research have been briefly reported at the 1952 summer meeting of the Institute of the Aeronautical Sciences in Los Angeles and at the Eighth International Congress for Theoretical and Applied Mechanics at Istanbul, and some preliminary data have been published in a short note (128). In the belief that the value of these experiments to others working in the field increases with the effort spent in interpretation, publication in detail has been delayed until several questions could be answered to the satisfaction of the writer.

In two years of wrestling with the problem of the turbulent flat plate boundary layer the writer has become convinced that existing empirical knowledge of the subject is capable of better organization than has been given it in the recent past. An effort has been made, at the risk either of duplicating or of differing with other contemporary discussion of the problem, to provide such an organization in the first three dozen pages of the present report. On the other hand, no description of the detailed structure of turbulent shear flows has been attempted, since except for general physical considerations such a description is not essential in the present study.

In Section I the writer has proposed a generalization to flows with variable density of the idea of functional similarity which has been found useful in discussing measurements in low-speed flow. Of this generalization it can be said that it is not contradicted by the writer's experimental measurements. An important result of the analysis is the appearance of a bulk or characteristic density, which accounts for non-uniformity in the streamwise convective transport of mass or momentum when the density is variable; the flow near a wall is thus no longer dependent only on the boundary conditions at the wall, as in low-speed flow. The value of the present analysis can only be determined by further comparison with experiments, and criticism is therefore invited from others working in the field. In the meantime it is possible to pursue further an investigation which is begun here of the joint consequences of functional similarity and of the equations of motion.

One of the original objectives of the JPL research program was to discriminate among several existing analyses of the compressible turbulent boundary layer. However, in the course of the experiments it has become apparent that failure to consider the flow in the sublayer must become a crippling defect at large Mach numbers. For this reason it is doubtful whether extrapolation of present knowledge of turbulent skin friction beyond a Mach number of five or to Reynolds numbers outside the range of observation can be undertaken with any confidence. In the writer's opinion, if an opinion is in order, the analysis of Donaldson, although rudimentary in a mathematical sense and not yet made properly quantitative, may describe the physical

problem of the supersonic turbulent boundary layer in sufficiently realistic terms to be useful for purposes of design.

Considerable emphasis is placed throughout this report on the asymptotic nature of the boundary layer problem, in an effort to define the problem in a way which may simplify the interpretation of experimental data. The attention which is paid from the beginning to the question of uniqueness leads naturally to a consideration of several physical and mathematical approximations which are commonly made, and is particularly useful when considering the question of defining a Reynolds number from the experimental point of view.

The writer's friction measurements have not been presented here in terms of the variation of friction coefficient with Mach number at constant Reynolds number, although this information is implied by Figures 65 and 66. A comparison with other measurements such as those of Wilson (80, 86), Rubesin, Maydew, and Varga (82), Chapman and Kester (109), or Hakkinen (105), should probably not be made in these terms, since the comparison would not then involve the measurements so much as the interpretation of the measurements. The investigations cited have all been carefully and accurately carried out, and deserve equal consideration with the data reported here. It is with the idea of emphasizing interpretation that the writer's measurements have been deliberately isolated, and it is with the expectation of continuing progress that the measured data are made available in tabulated form.

In conclusion, the most important point to be made is that the influence of compressibility on turbulent flat plate skin friction has been established experimentally in Section III for Mach numbers up to 4.5. If the discussion of instrumentation and techniques in Section II serves to inspire confidence in the accuracy of the measurements, and if the foundation laid in Section I serves to call attention to some ideas which are useful in discussing turbulent shear flows, then the publication of this report needs no further justification.

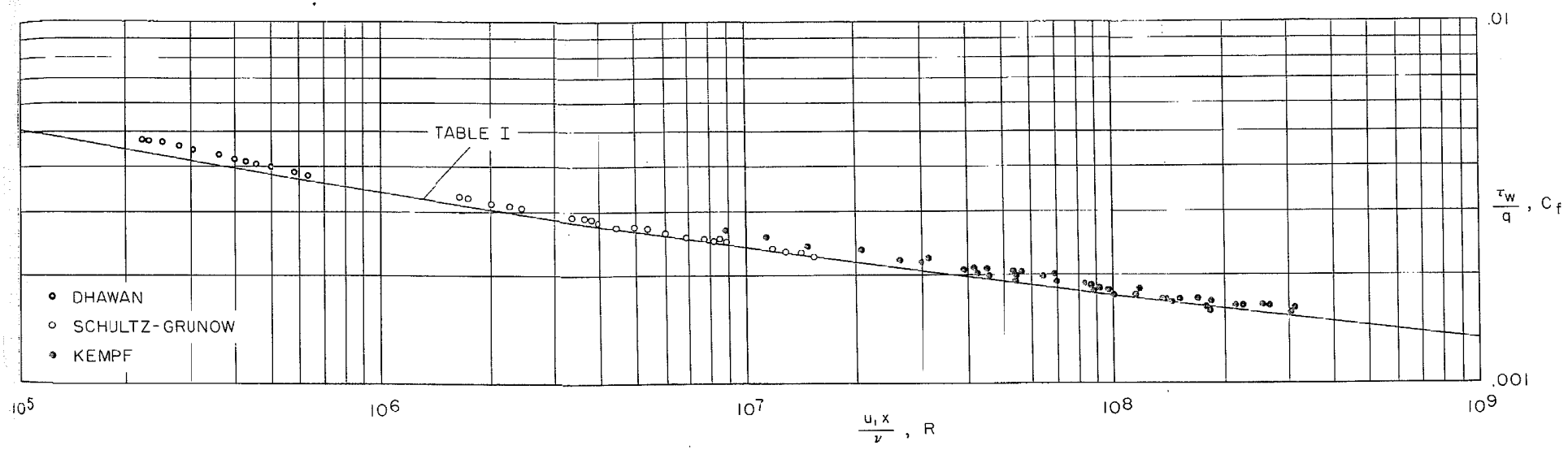

FIGURE 1 DIRECT MEASUREMENTS OF LOCAL TURBULENT FRICTION IN LOW-SPEED FLOW

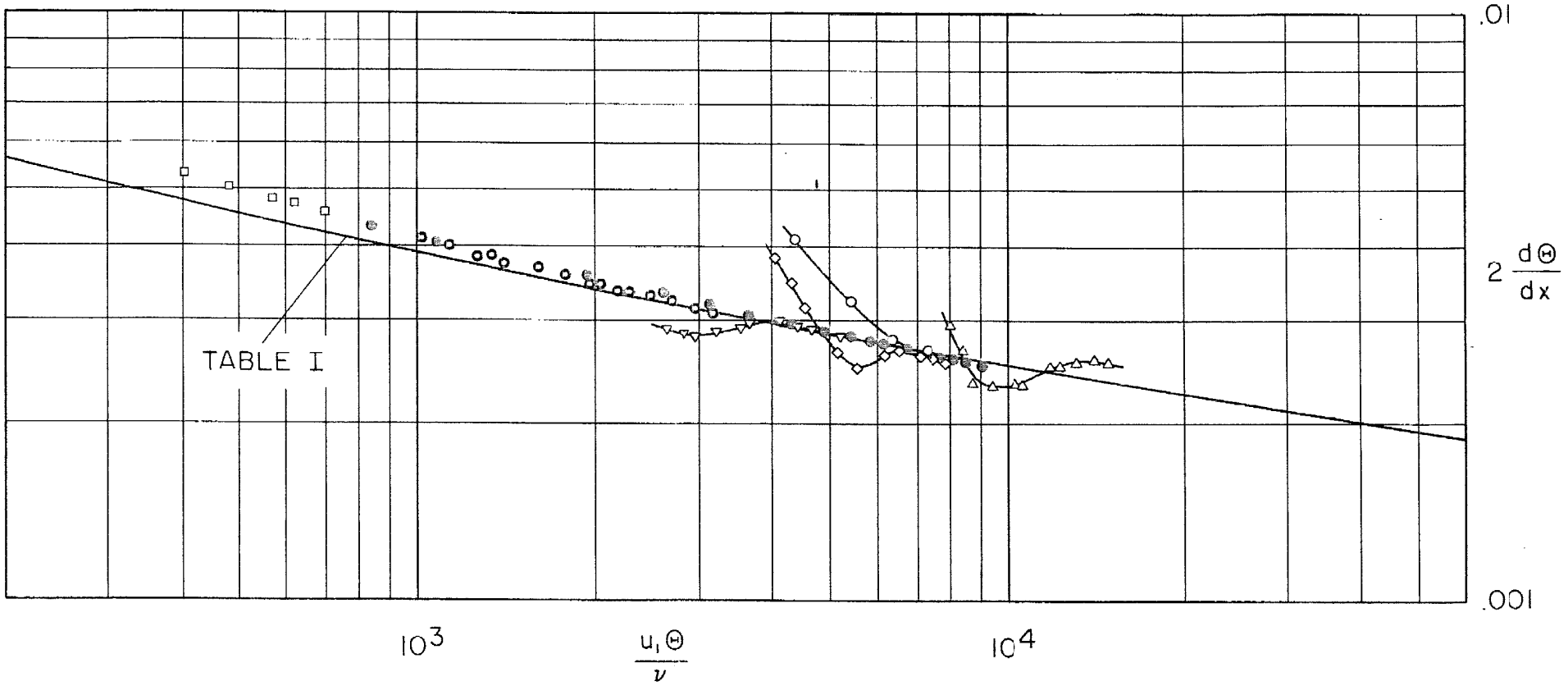

- ▫ HAMA, E SERIES
- ○ " , T SERIES
- ● WIEGHARDT, 17.8 m/s
- ▽ KLEBANOFF & DIEHL, sand, 35 ft/s
- ◇ " " , sand, 55 ft/s
- ○ " " , natural, 108 ft/s
- △ " " , sand, 108 ft/s

FIGURE 2

VELOCITY PROFILE FRICTION MEASUREMENTS IN LOW-SPEED FLOW

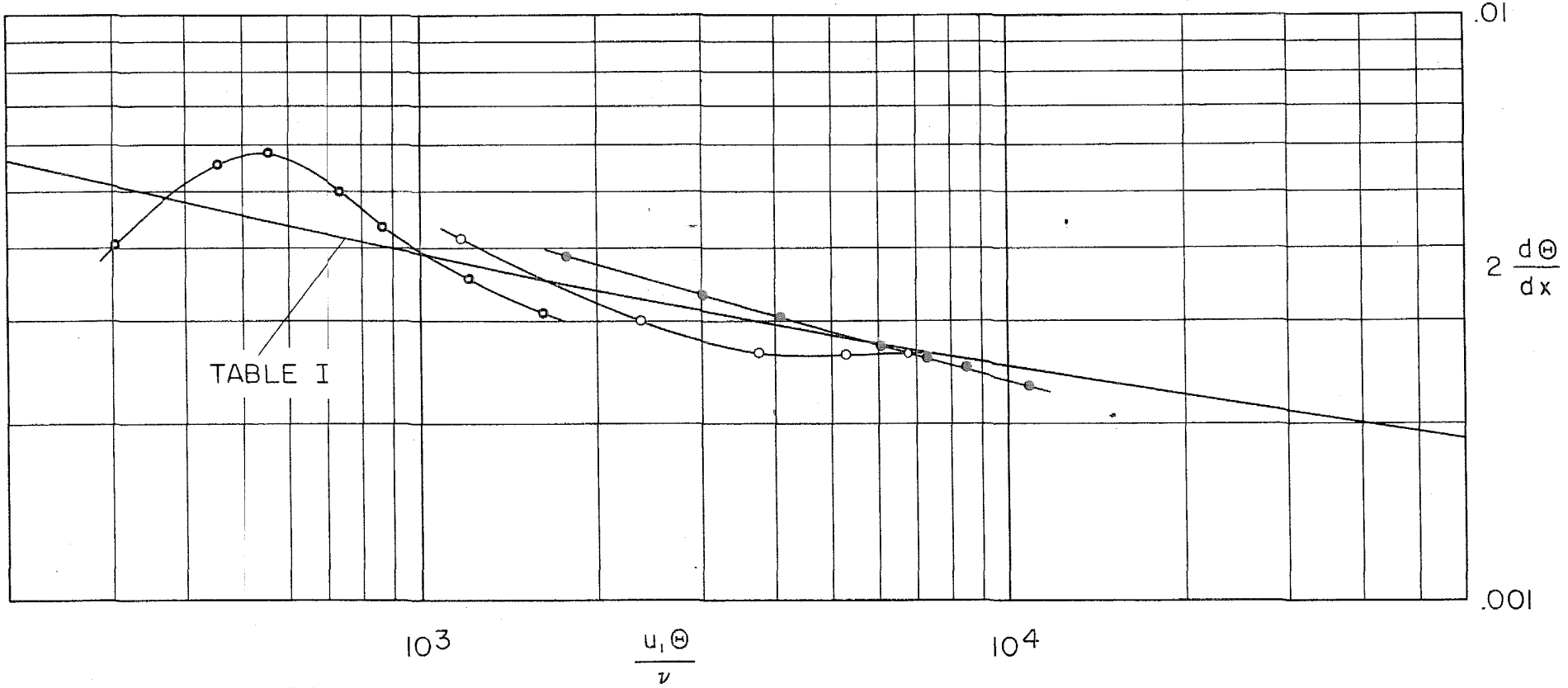

FIGURE 3

VELOCITY PROFILE FRICTION MEASUREMENTS IN LOW-SPEED FLOW

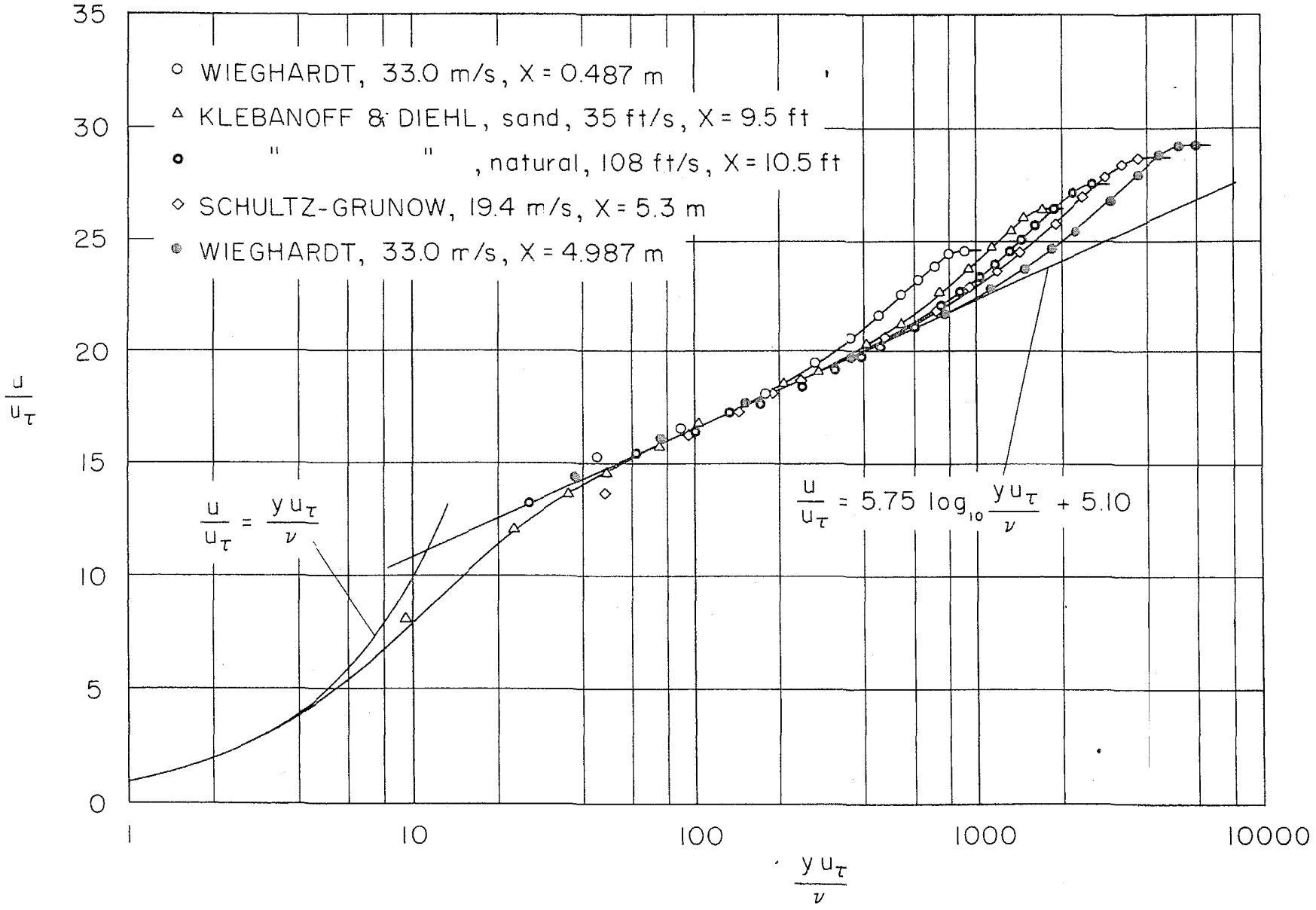

FIGURE 4 THE LAW OF THE WALL

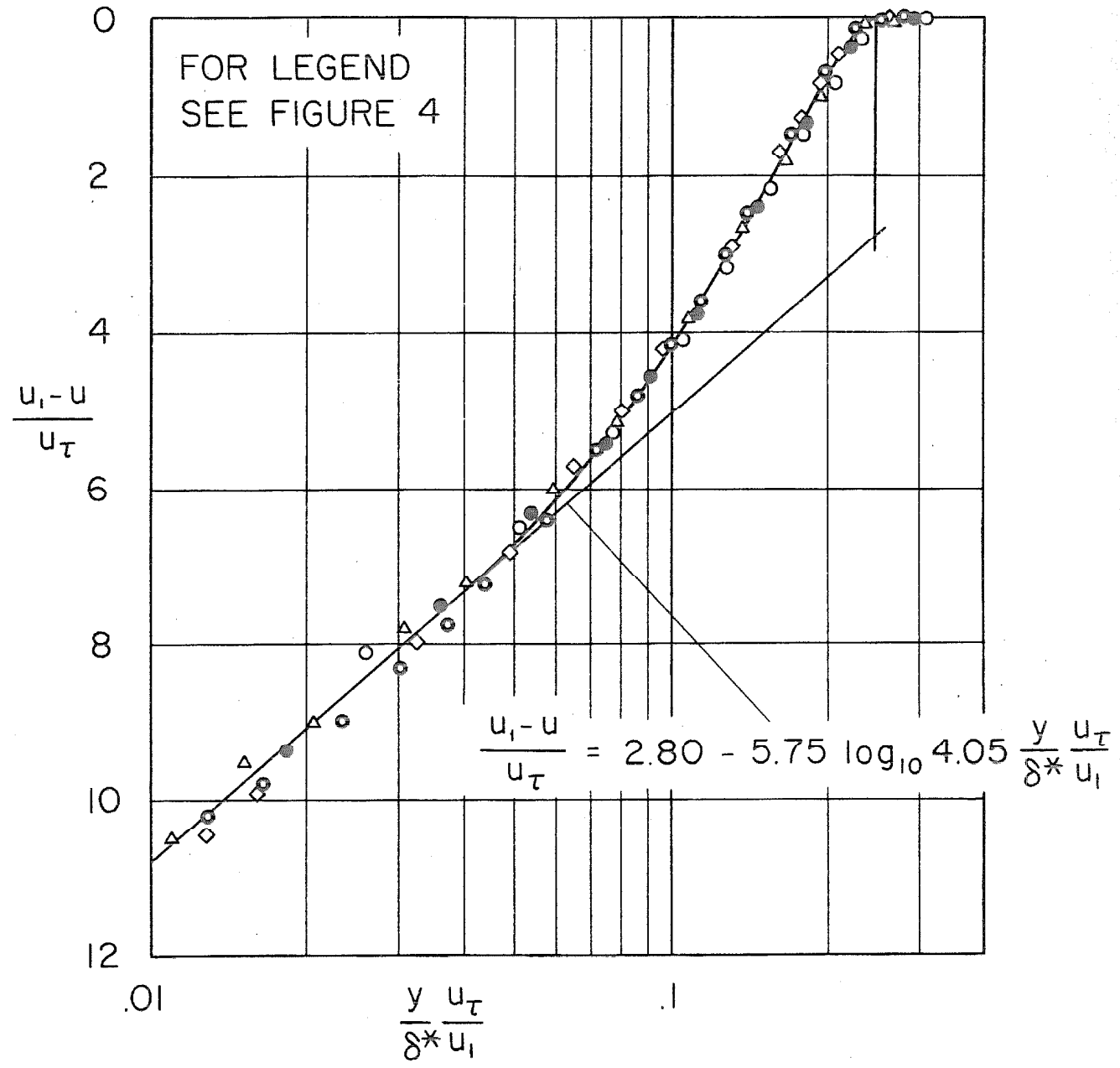

FIGURE 5 THE VELOCITY DEFECT LAW

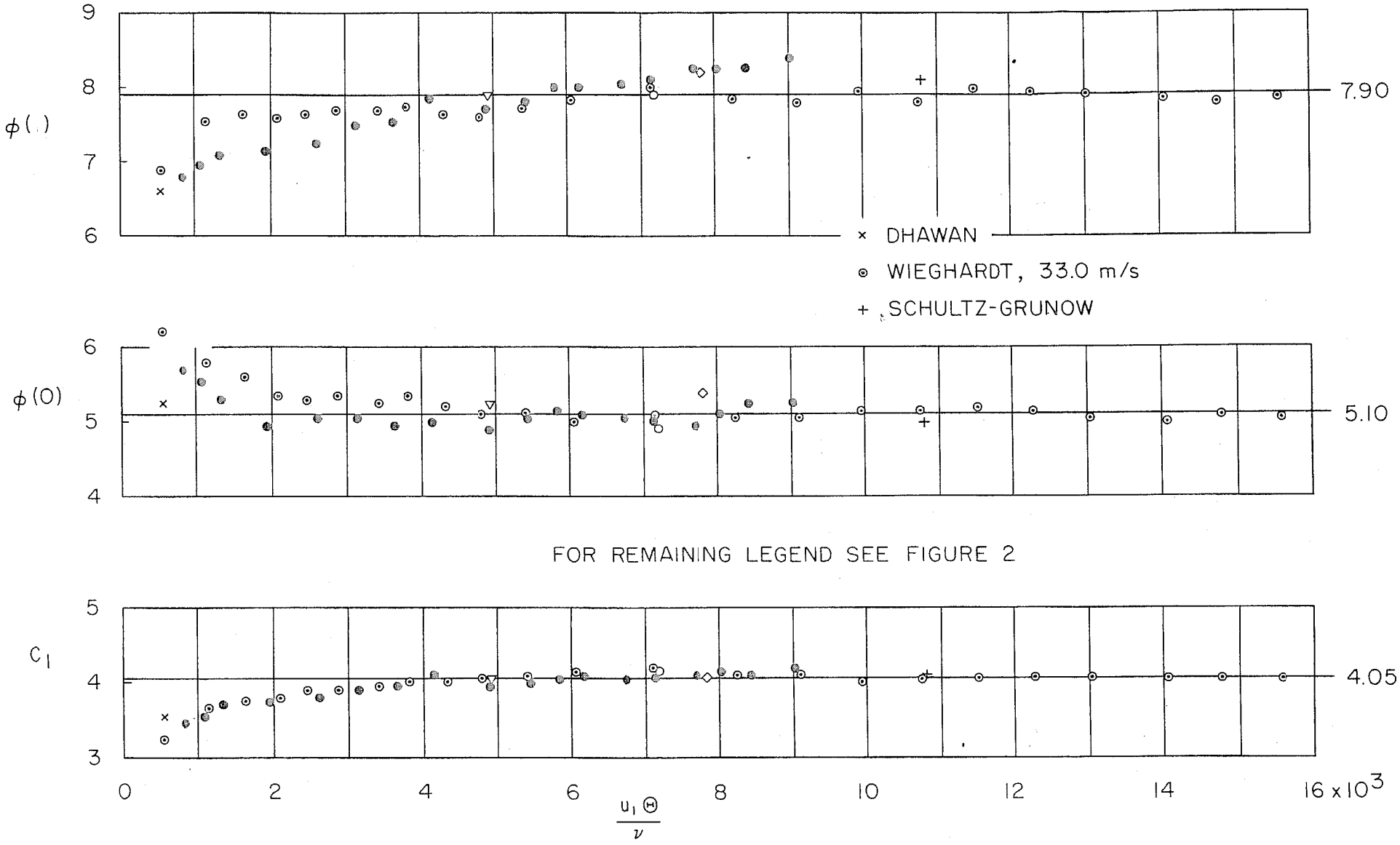

FIGURE 6 VELOCITY PROFILE PARAMETERS

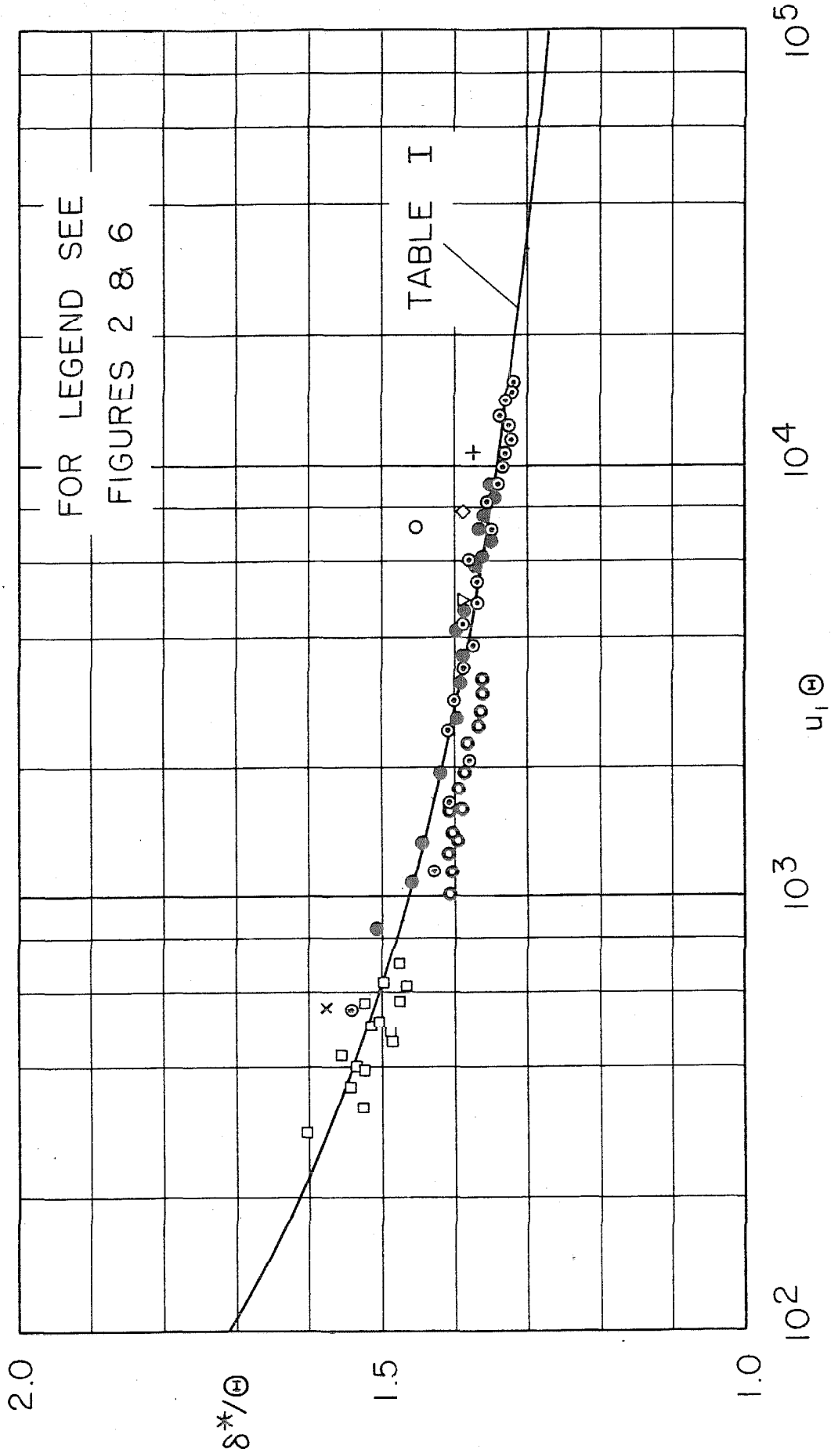

FIGURE 7 BOUNDARY LAYER SHAPE PARAMETER

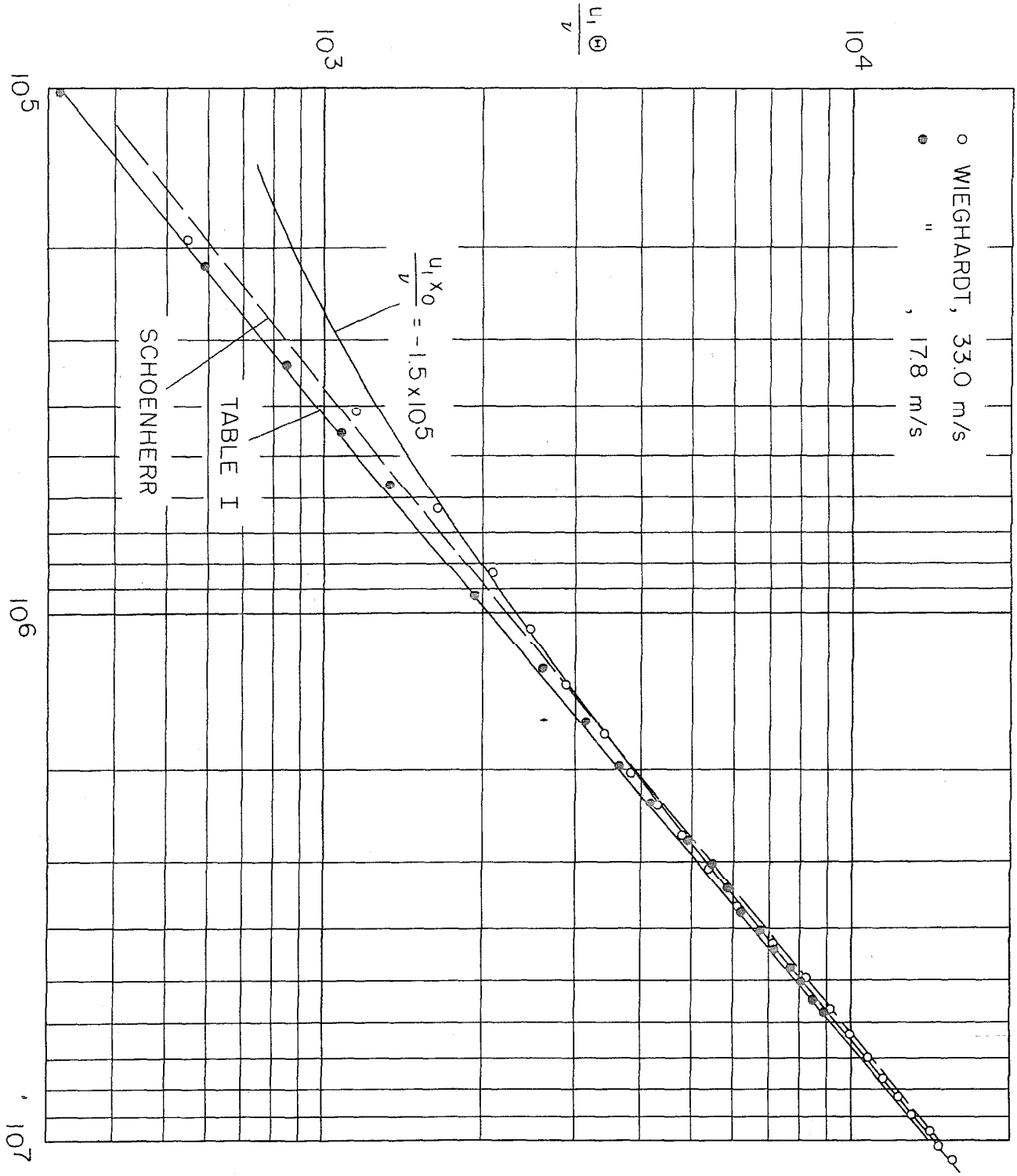

FIGURE 8 GROWTH OF THE BOUNDARY LAYER

FIGURE 9

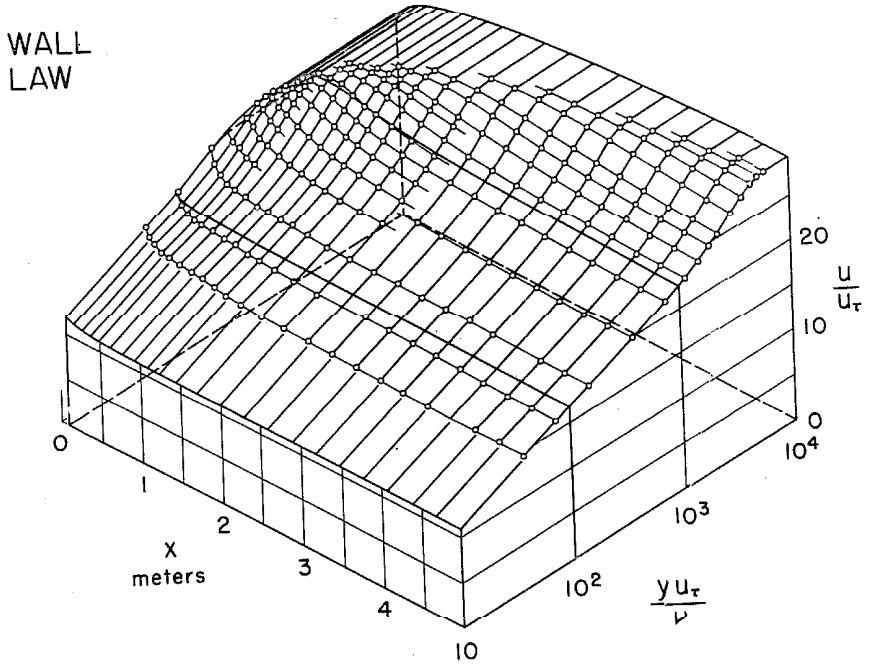
WALL
LAW
0
1
2
3
4
10
X
meters
10^2
10^3
10^4
$\frac{y u_\tau}{\nu}$
0
10
20
$\frac{u}{u_\tau}$

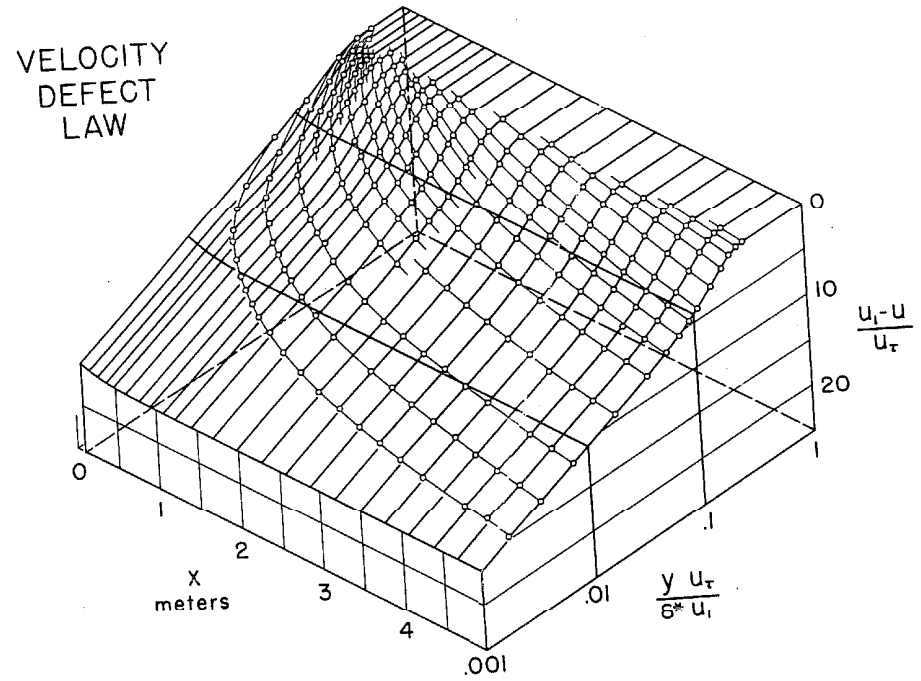
VELOCITY
DEFECT
LAW
0
1
2
3
4
X
meters
.001
.01
.1
1
$\frac{y\ u_\tau}{\delta^* u_1}$
0
10
20
$\frac{u_1 - u}{u_\tau}$

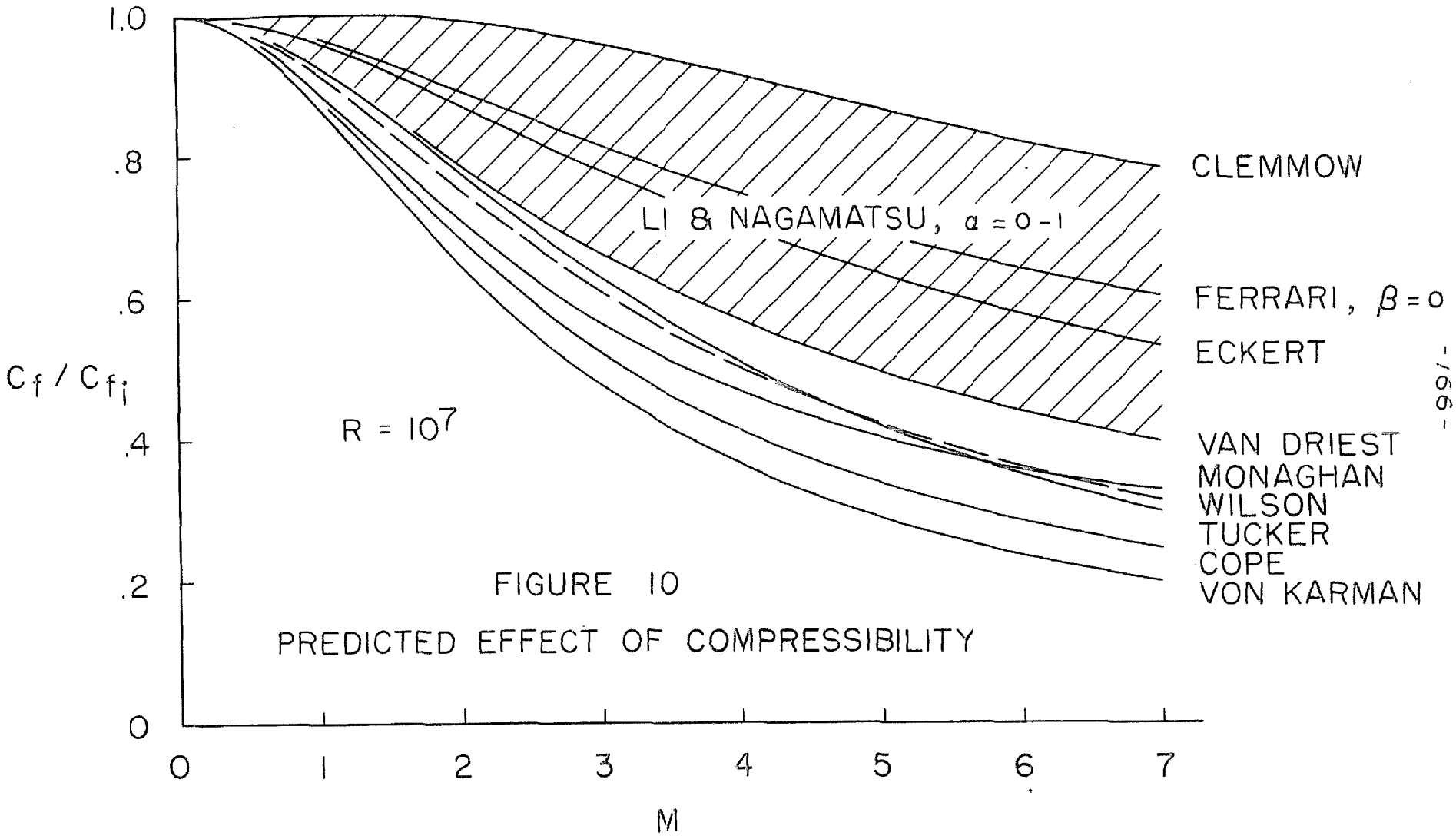

FIGURE 10

PREDICTED EFFECT OF COMPRESSIBILITY

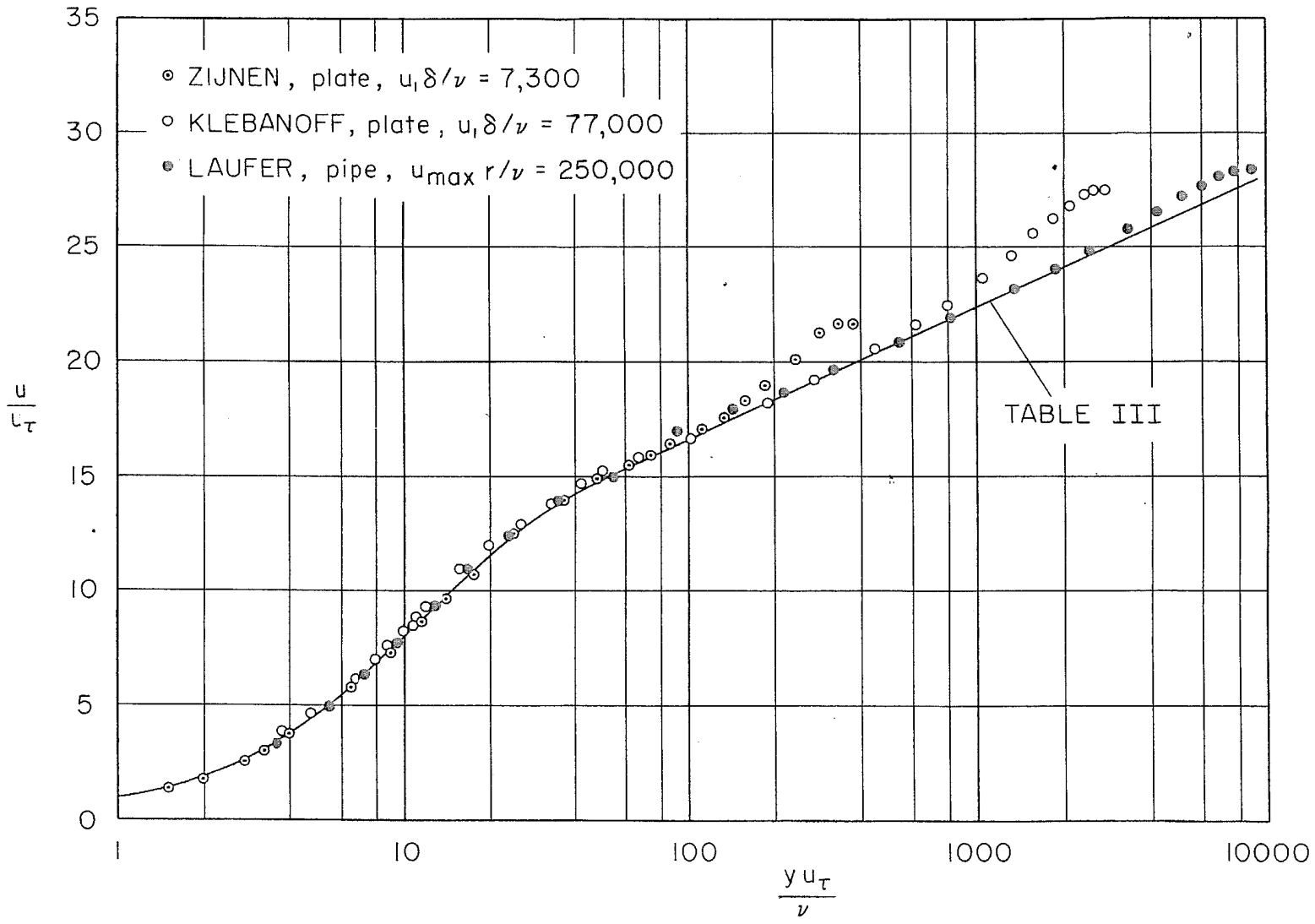

FIGURE 11 THE SUBLAYER PROFILE .

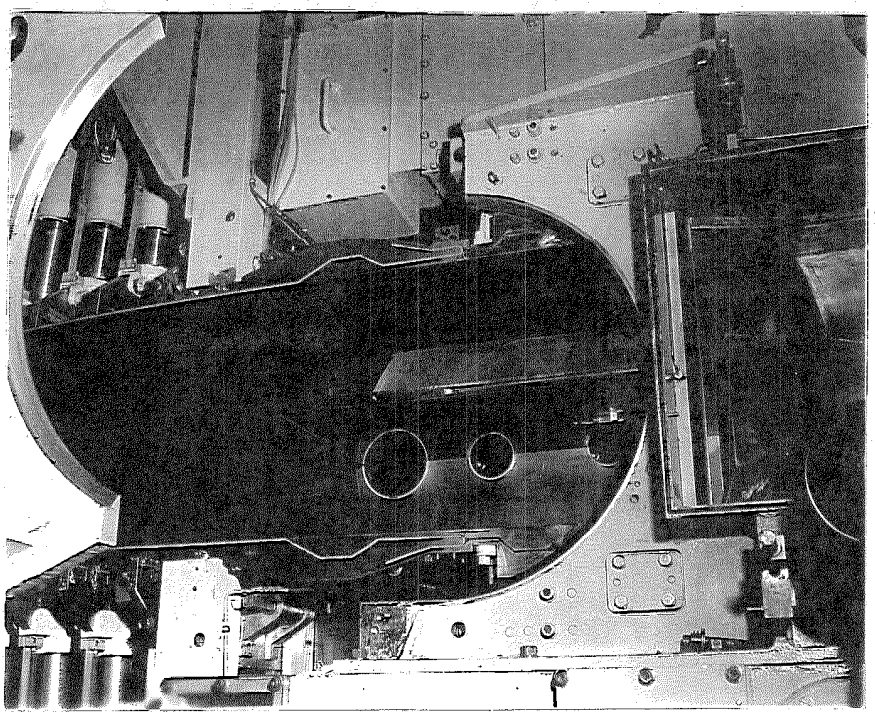

Figure 12 - The Flat Plate Model

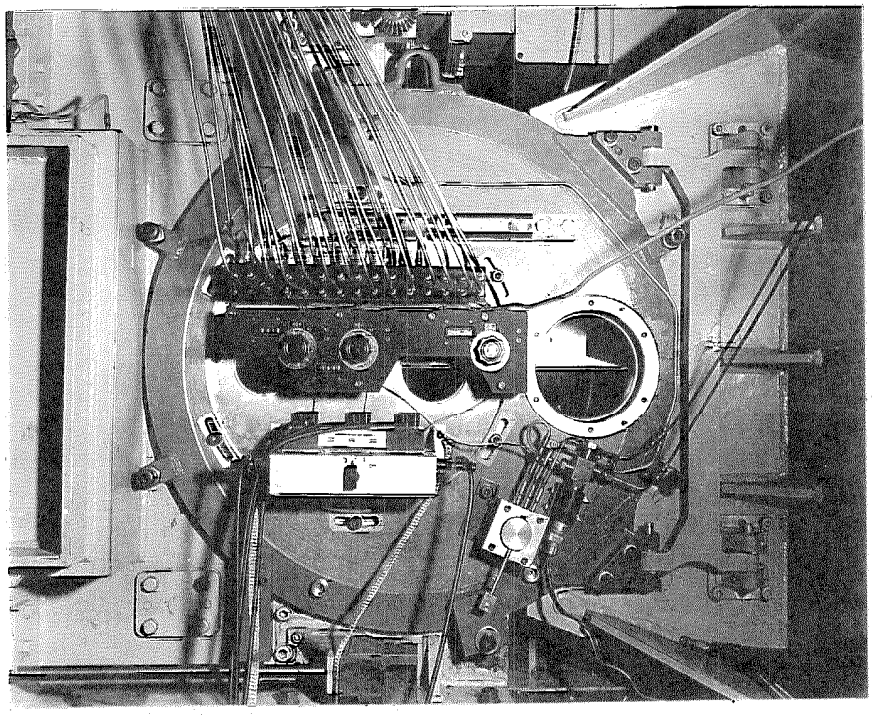

Figure 13 - External Instrumentation of the Flat Plate Model

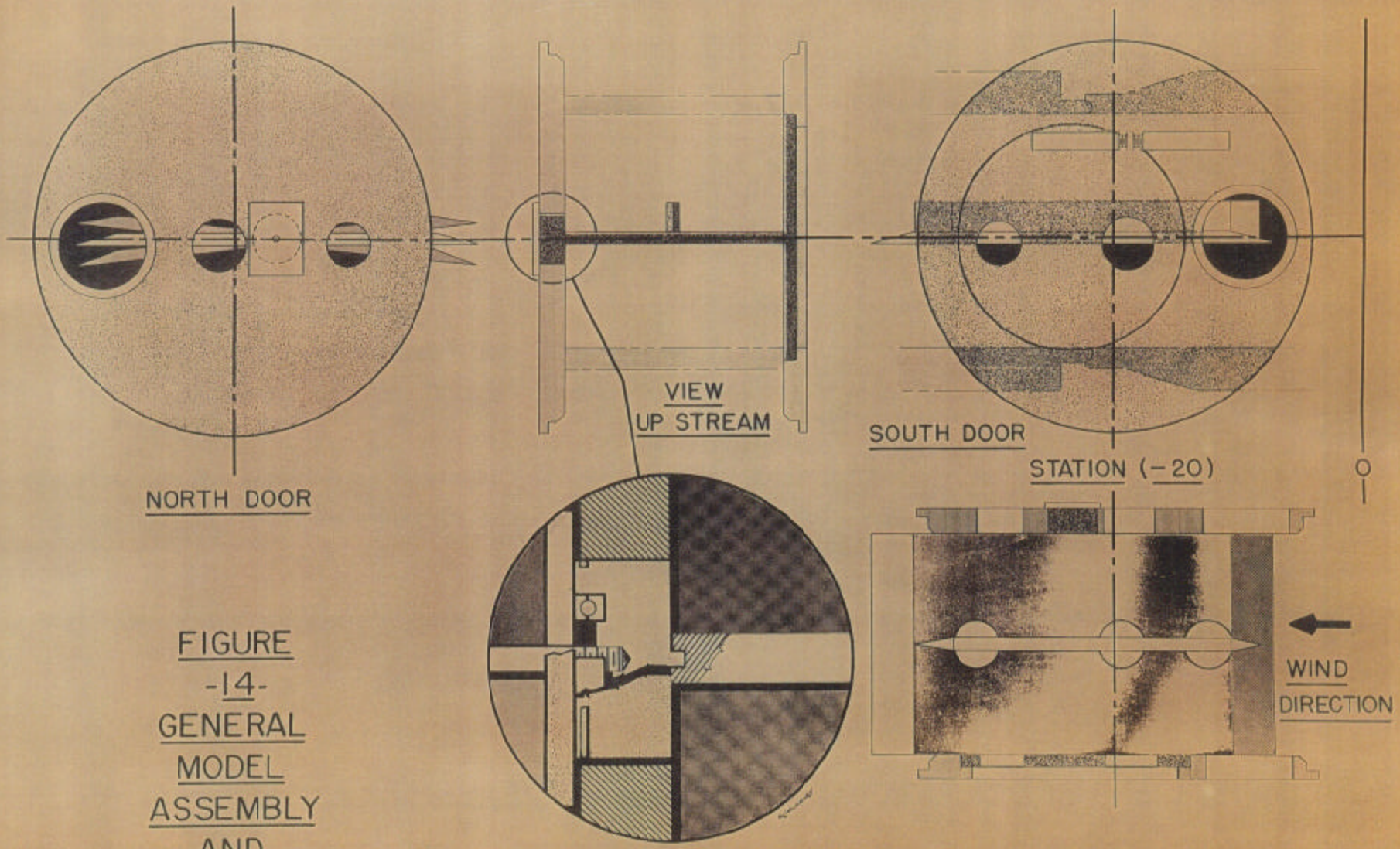

FIGURE
-14-
GENERAL
MODEL
ASSEMBLY
AND
INSTALLATION

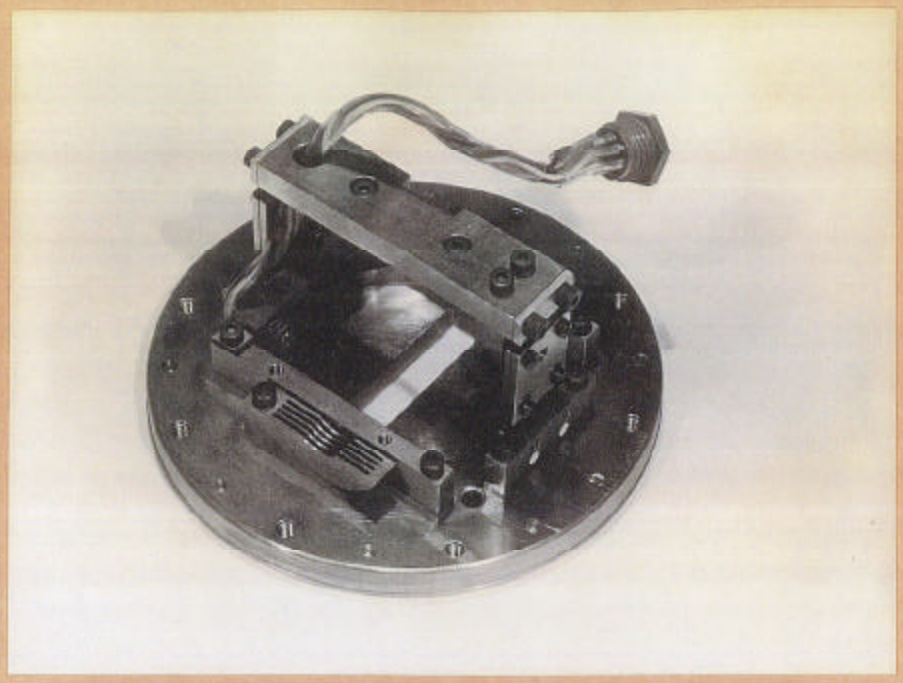

Figure 15 - The Outer Flexure System

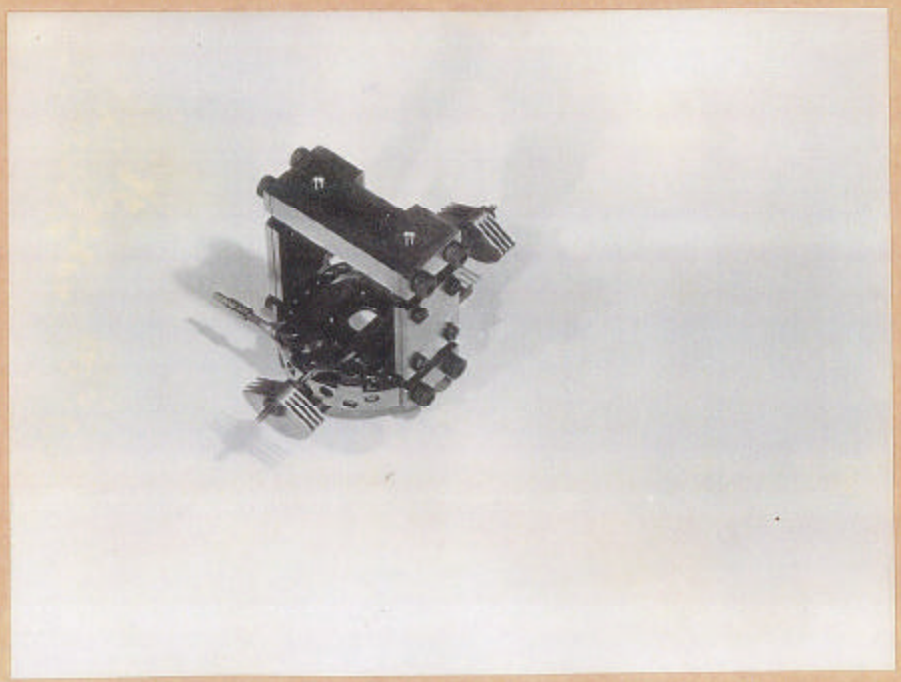

Figure 16 - The Inner Flexure System

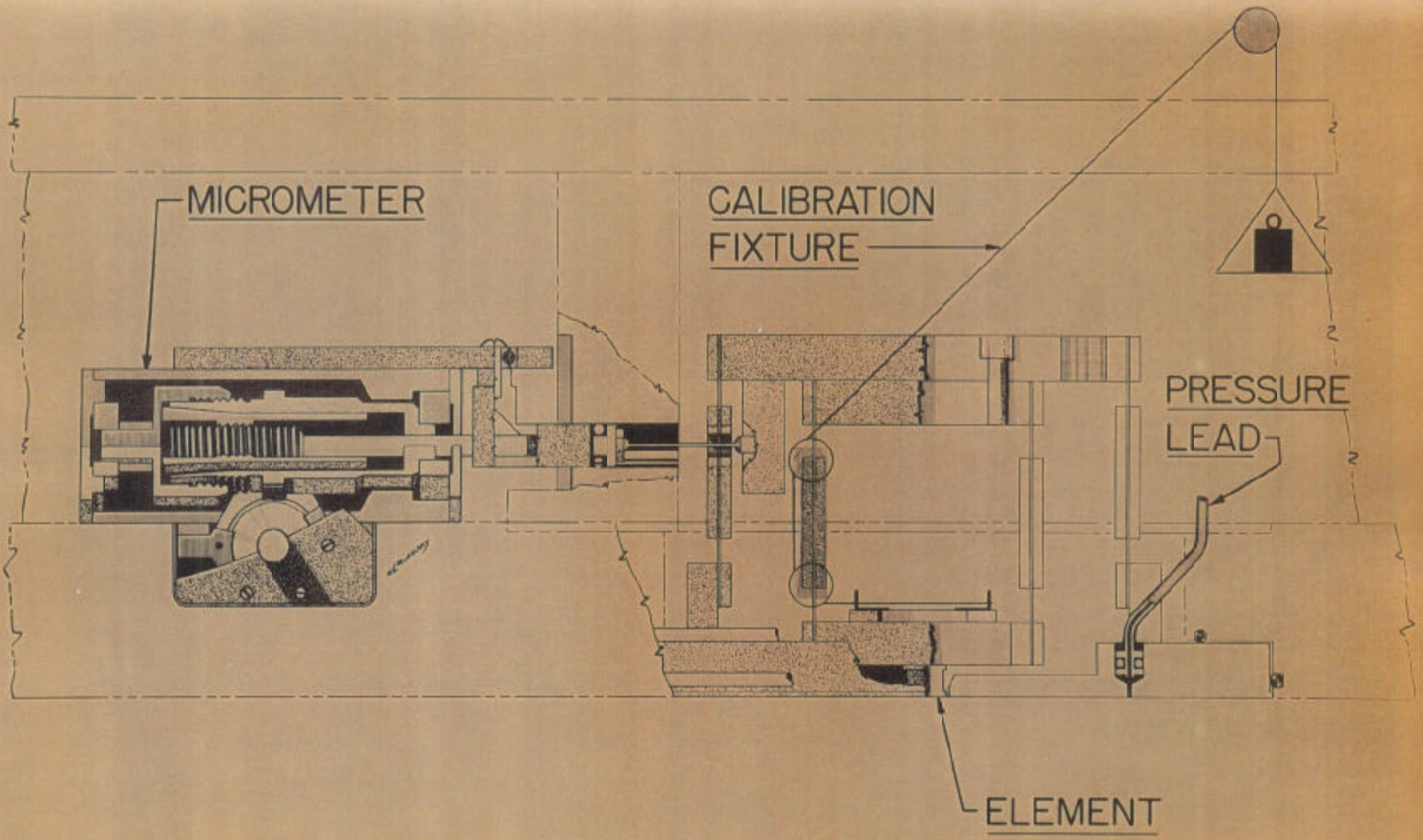

FIGURE 17 - THE FLOATING ELEMENT & MICROMETER INSTALLED IN THE PLATE

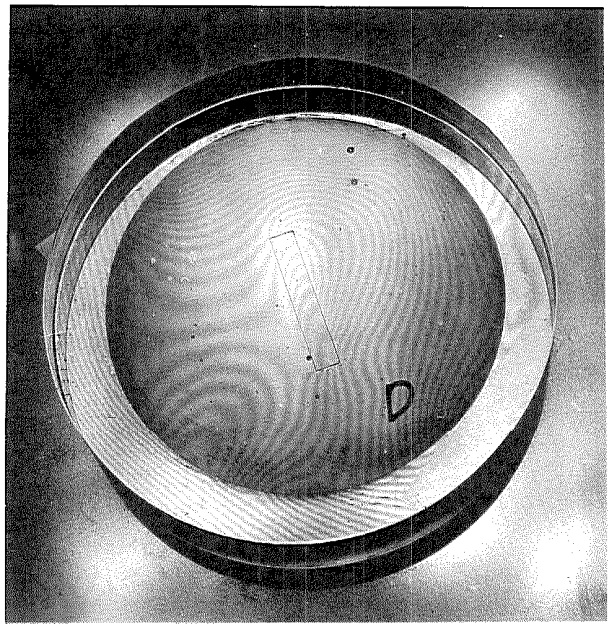

Figure 18 - Alignment of the Floating Element

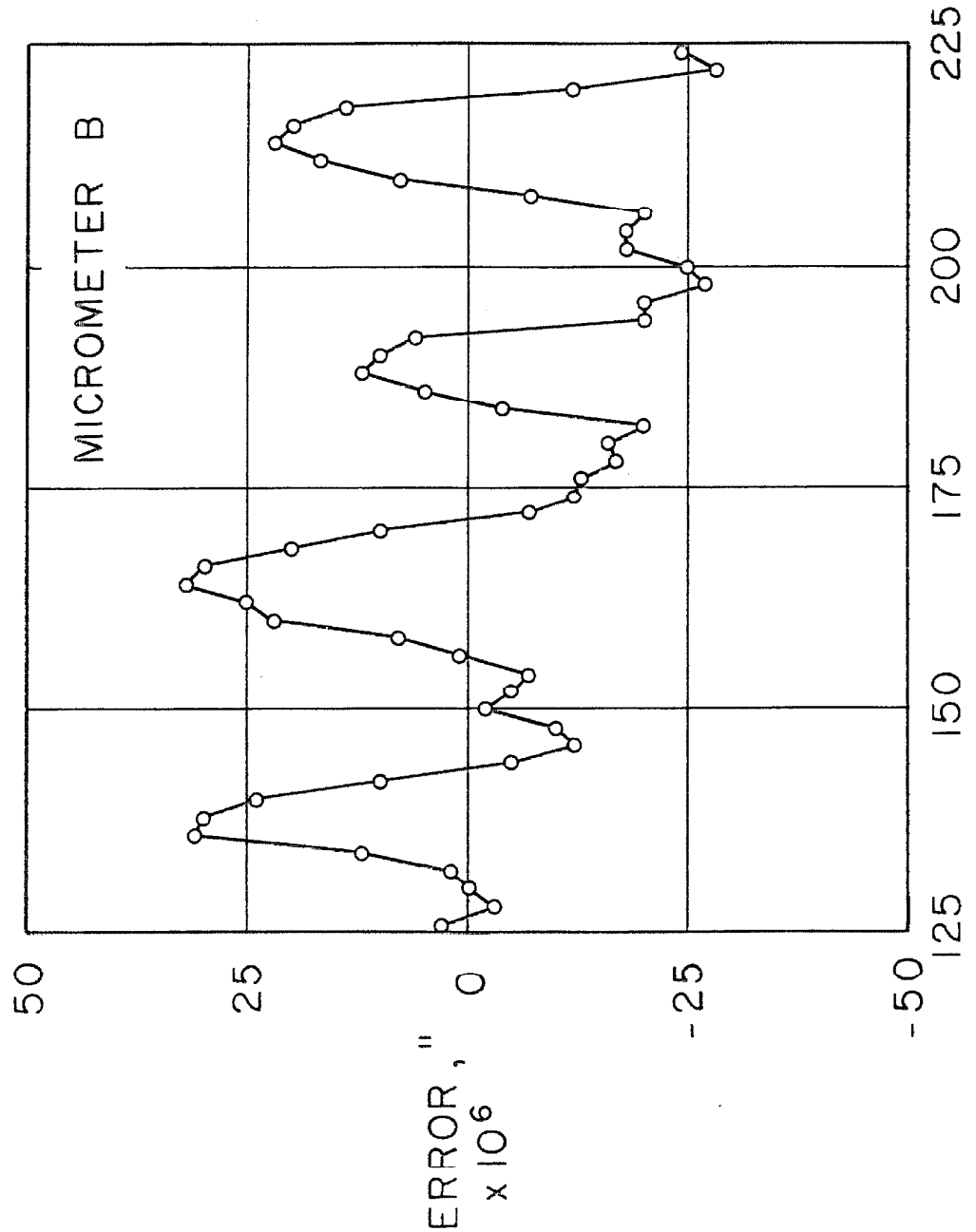

FIGURE 19 MICROMETER CALIBRATION

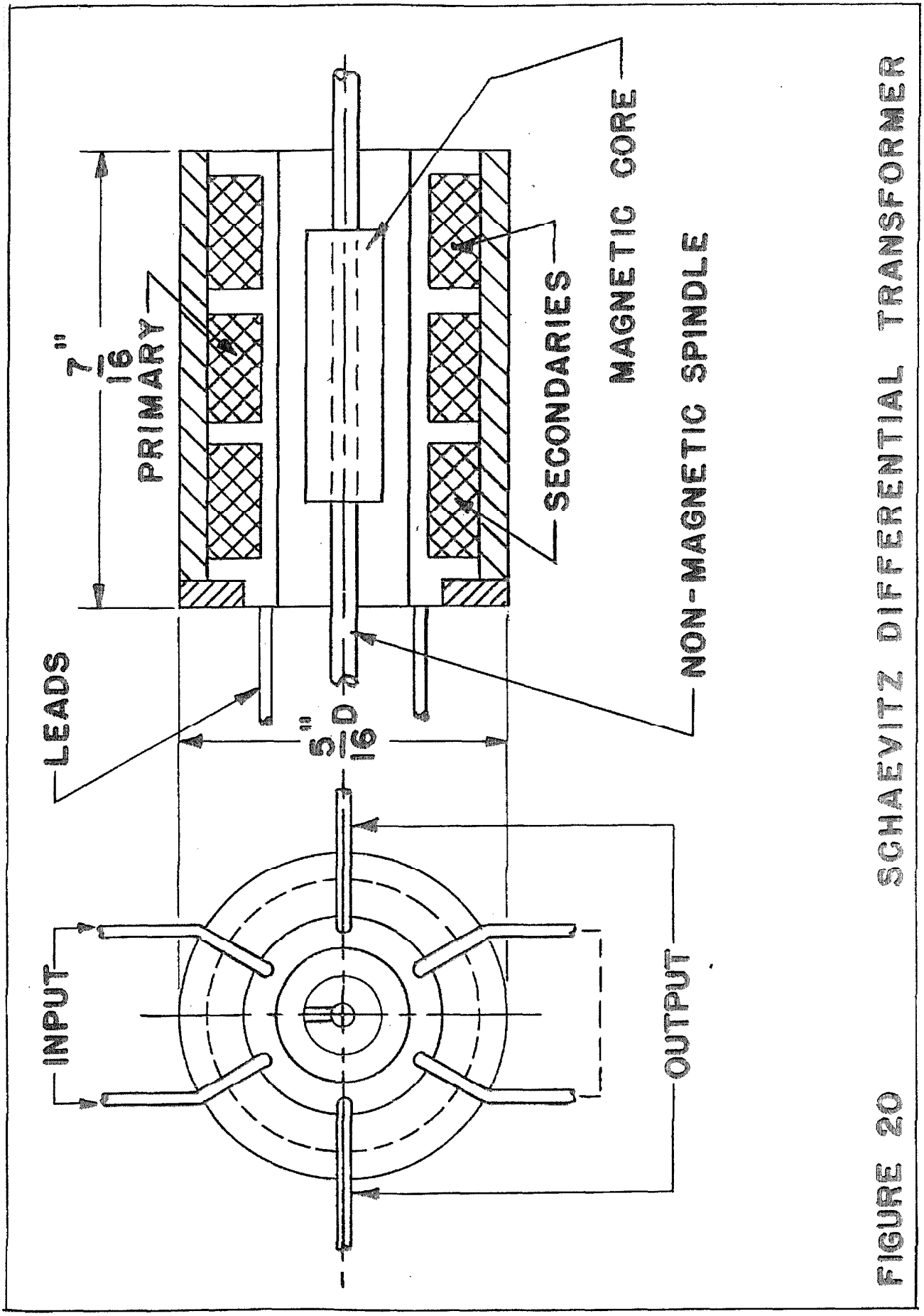

FIGURE 20 SCHAEVITZ DIFFERENTIAL TRANSFORMER

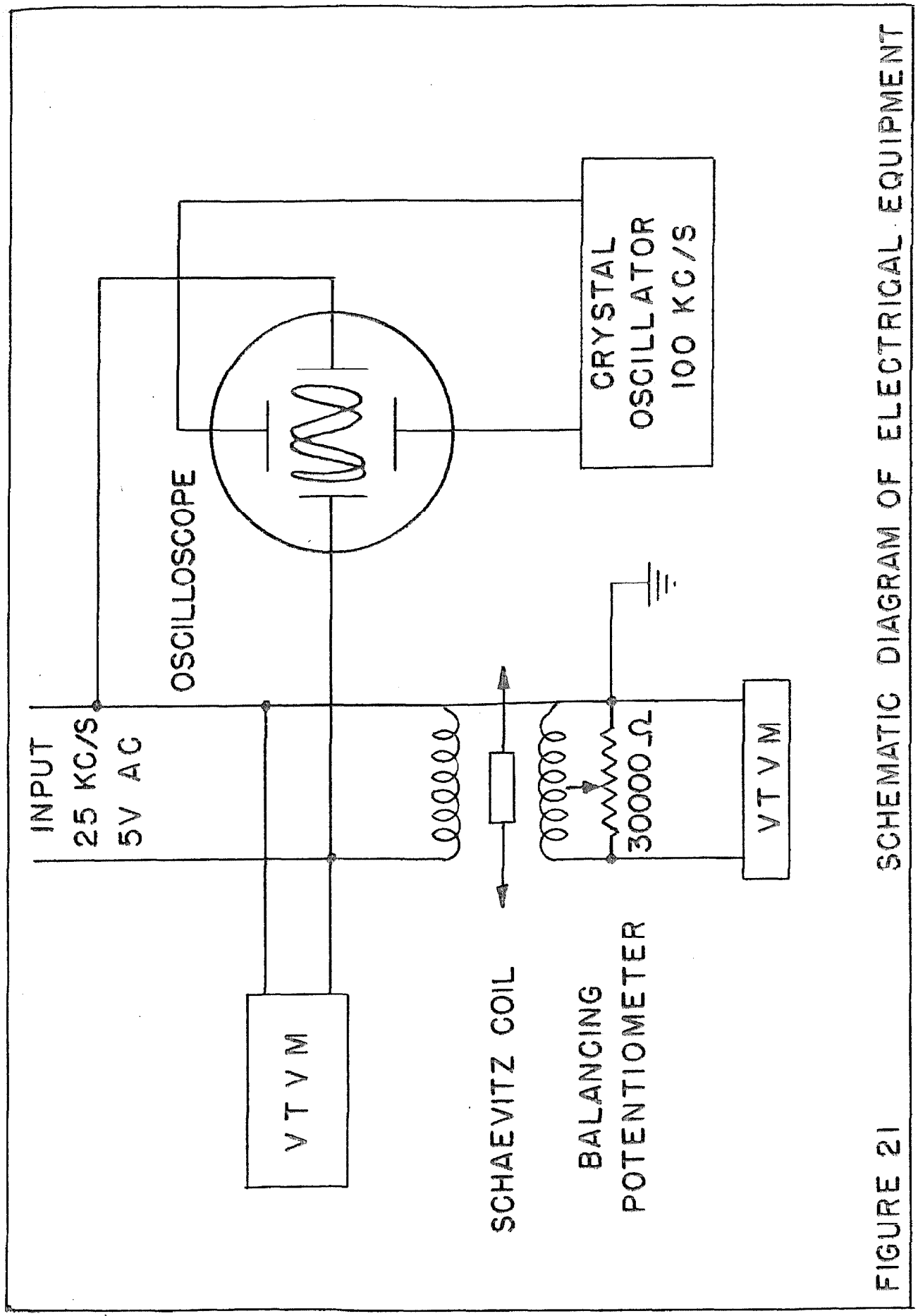

FIGURE 21 SCHEMATIC DIAGRAM OF ELECTRICAL EQUIPMENT

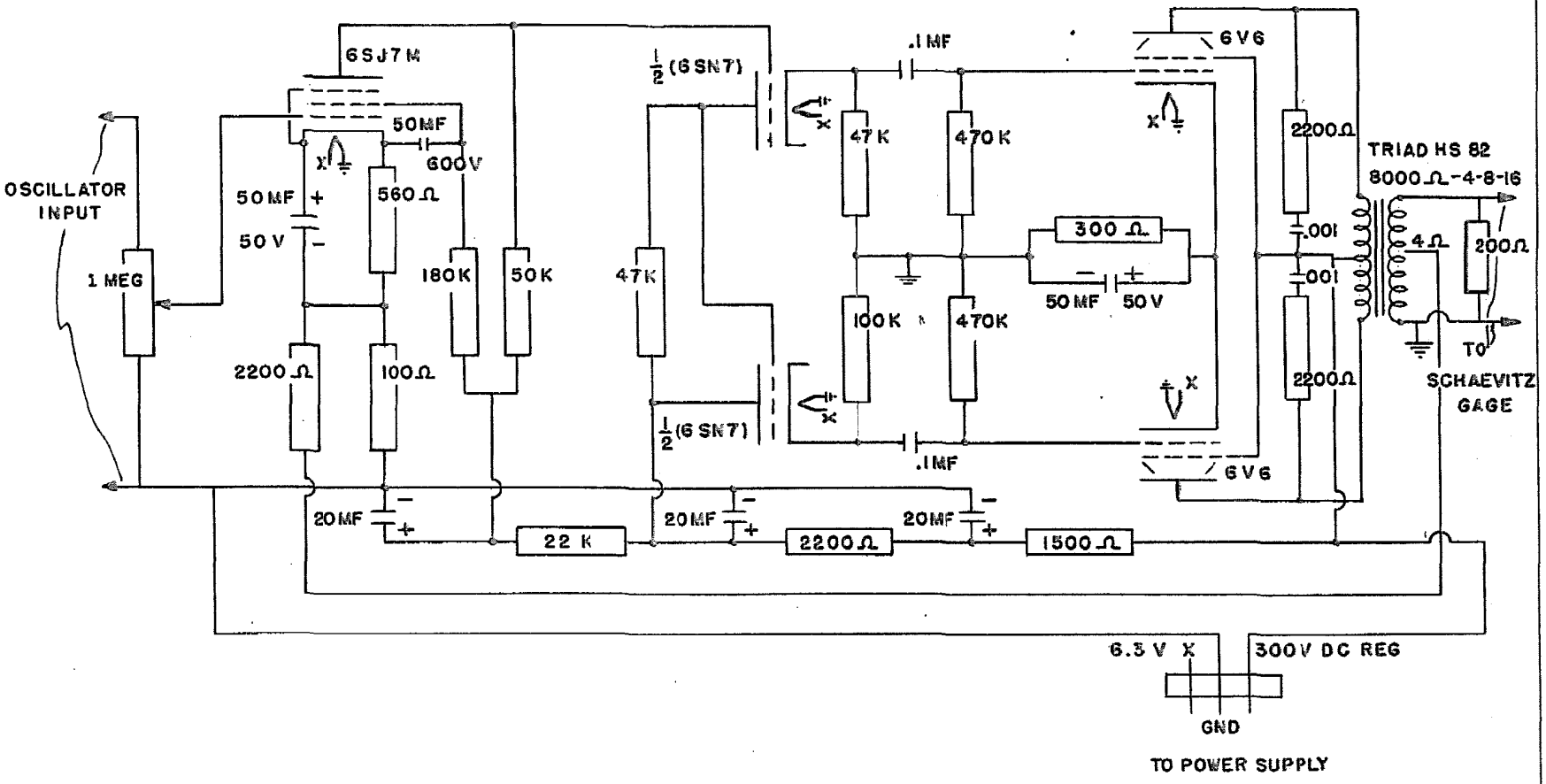

FIGURE 22 WIRING DIAGRAM FOR 3-CHANNEL AMPLIFIER

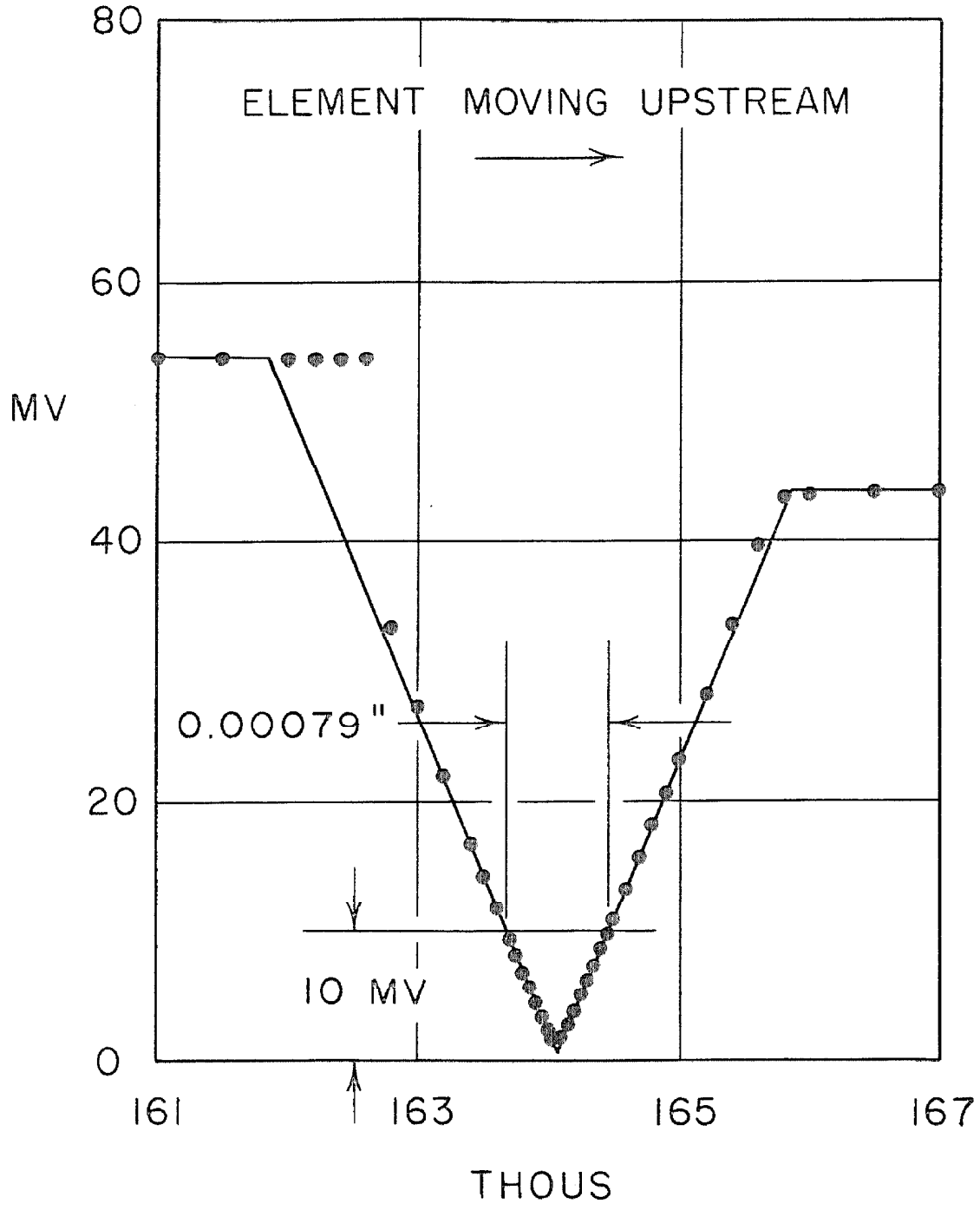

FIGURE 23 TYPICAL OUTPUT SIGNAL PATTERN

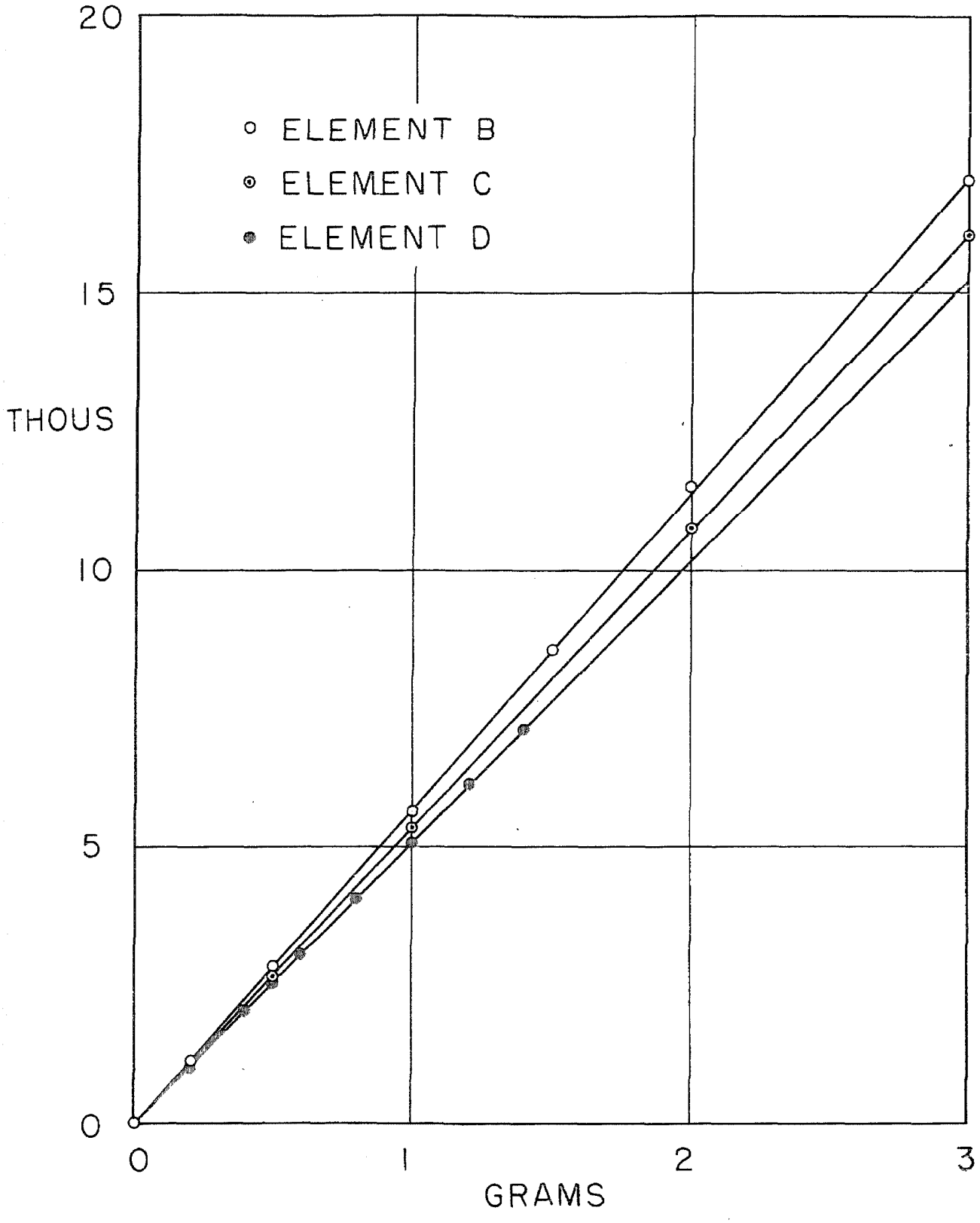

FIGURE 24 STATIC CALIBRATION

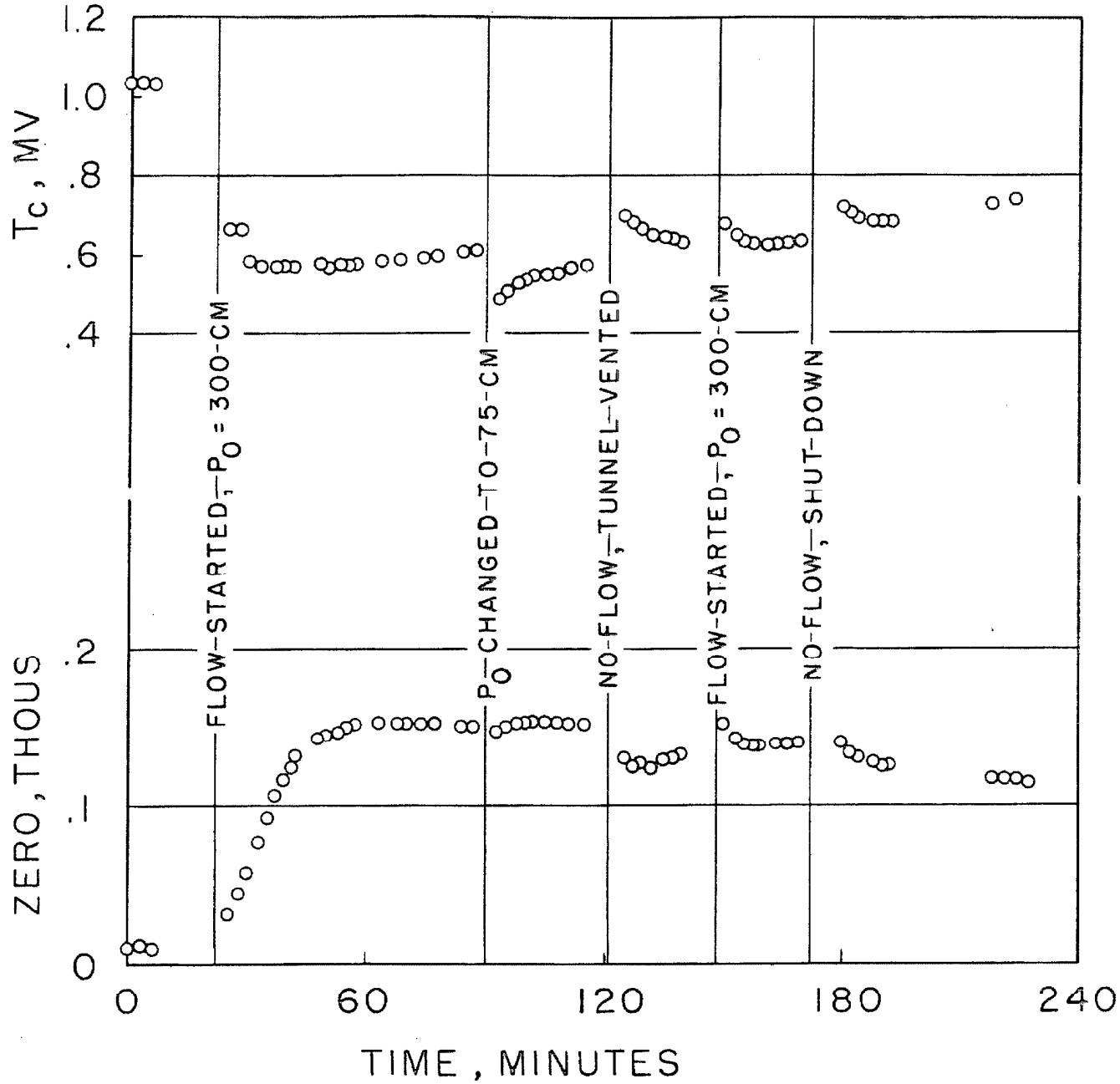

FIGURE 25 ZERO SHIFT IN USE

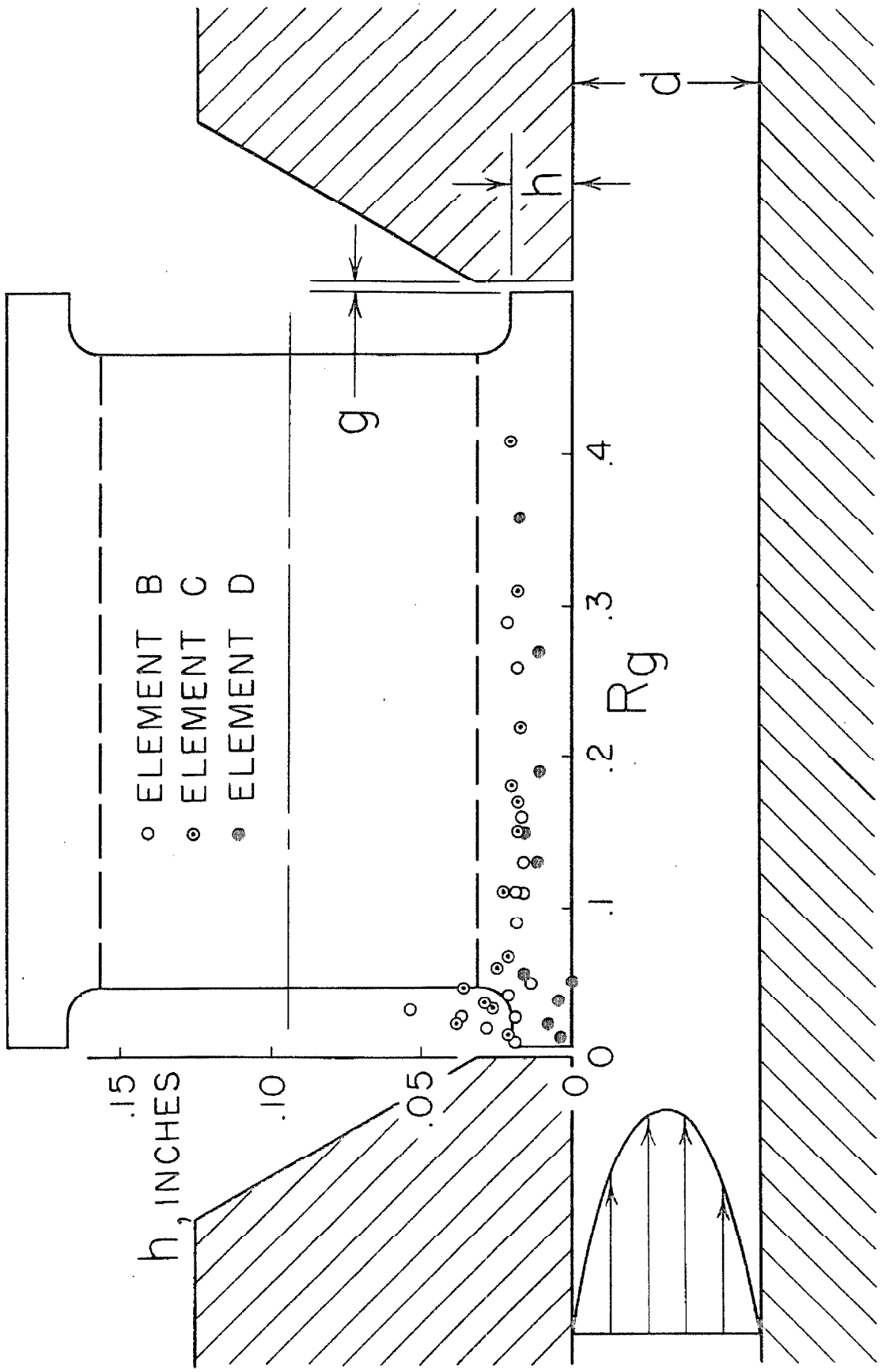

FIGURE 26 CHANNEL CALIBRATION

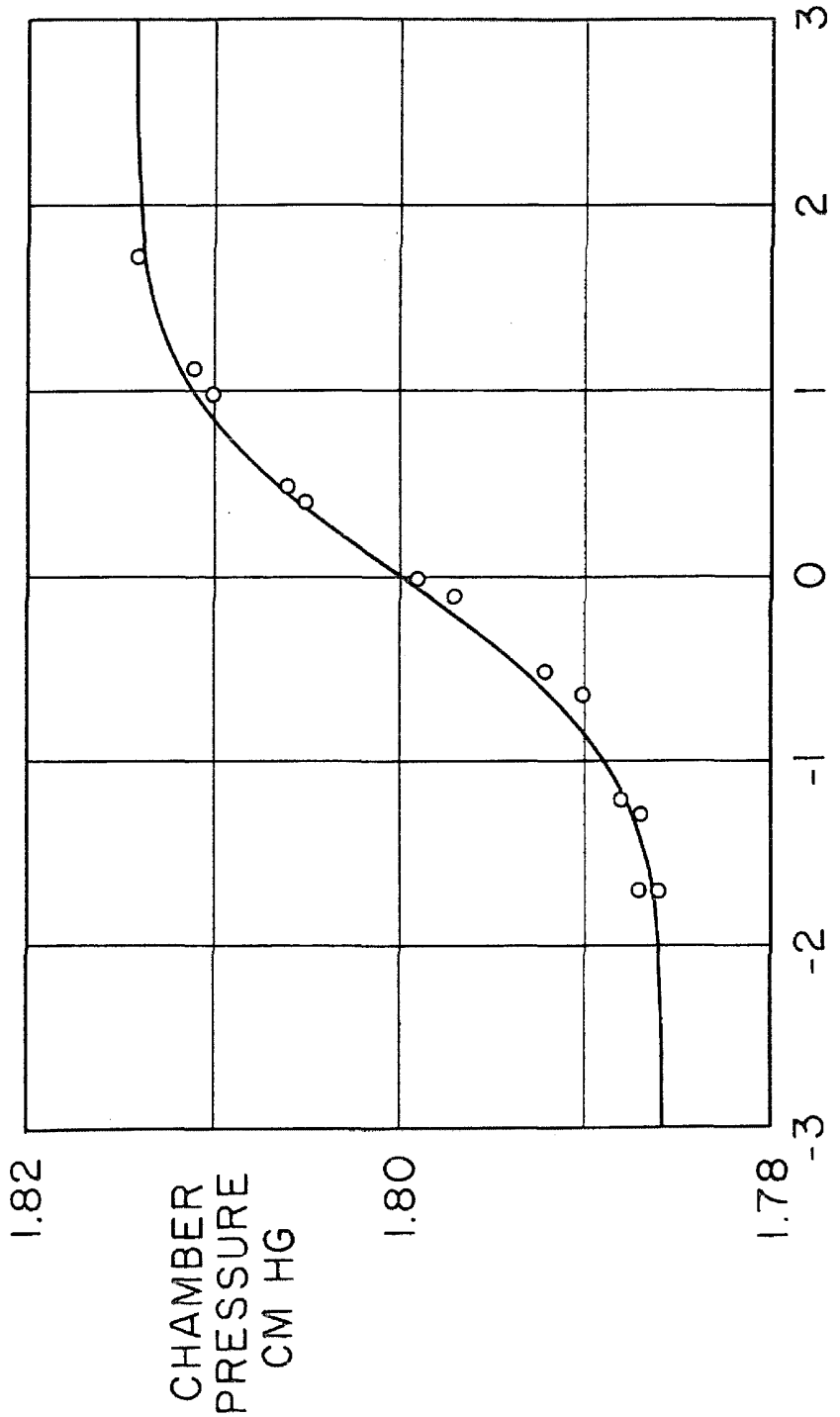

FIGURE 27 CHAMBER PRESSURE IN A PRESSURE GRADIENT

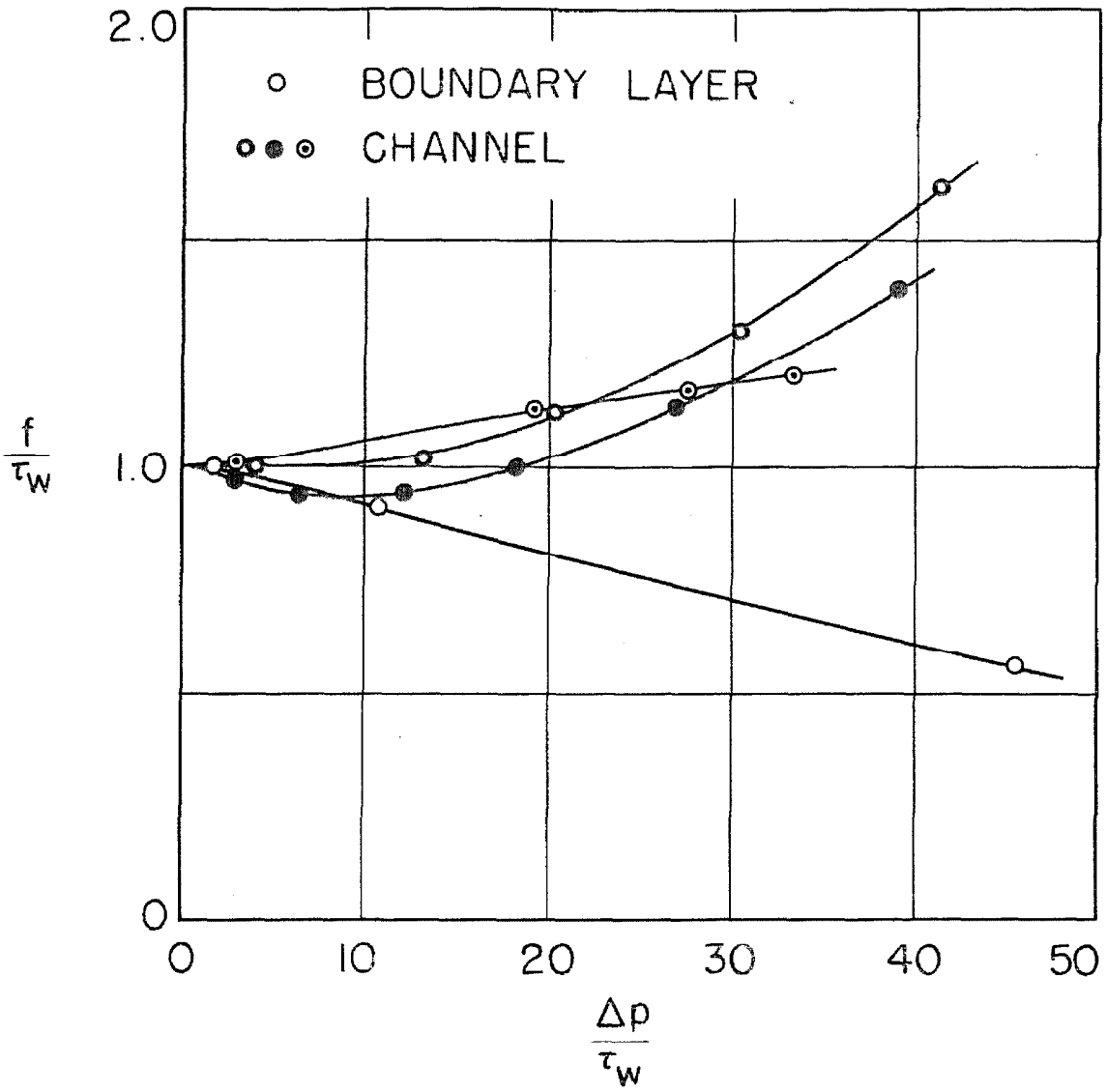

FIGURE 28. EFFECT OF CHAMBER LEAKAGE ON ACCURACY

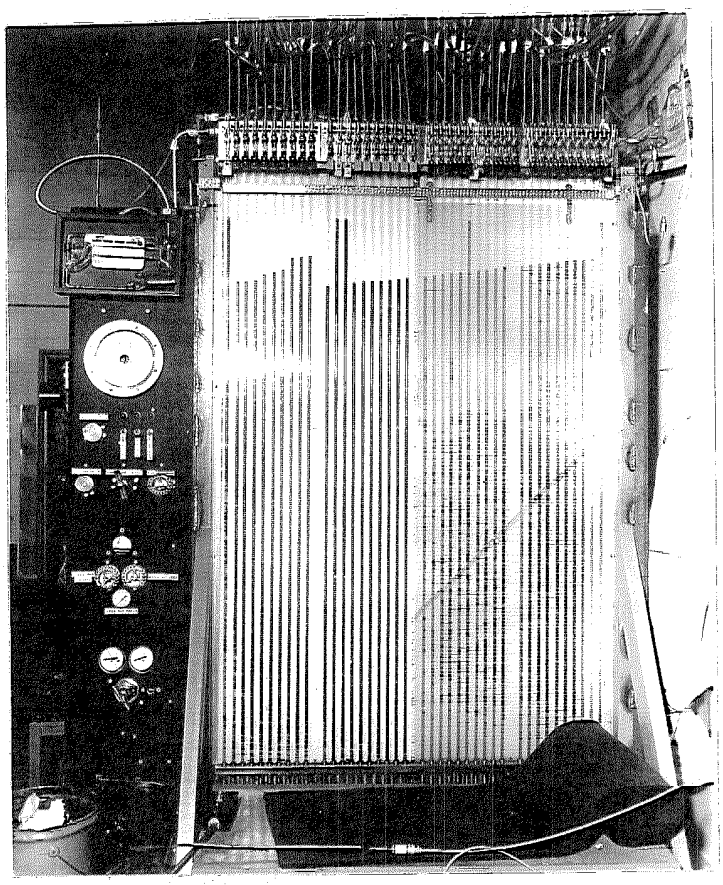

Figure 29 - The Low Pressure Multimanometer in Use

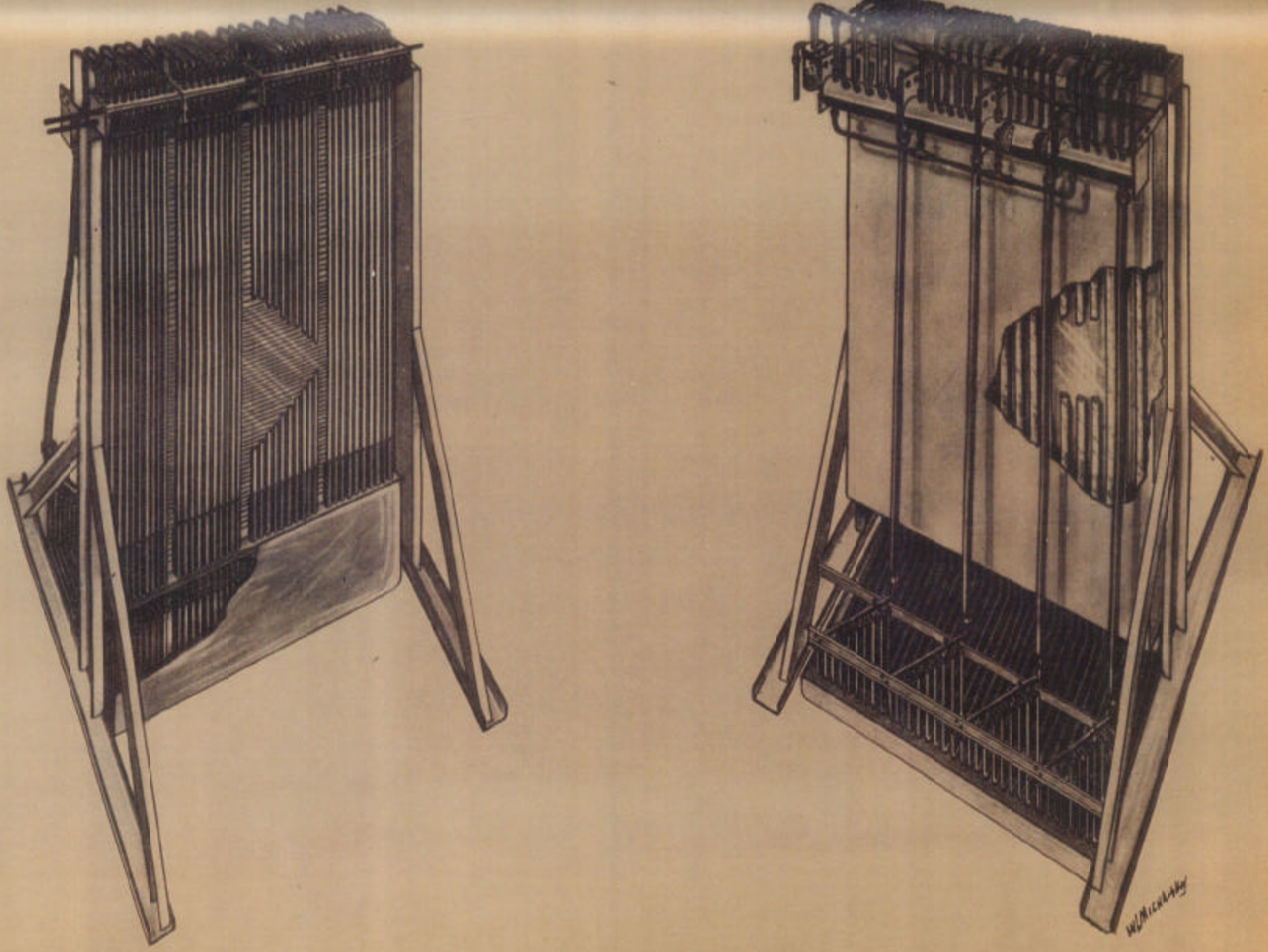

FIGURE 30 THE LOW PRESSURE MULTIMANOMETER

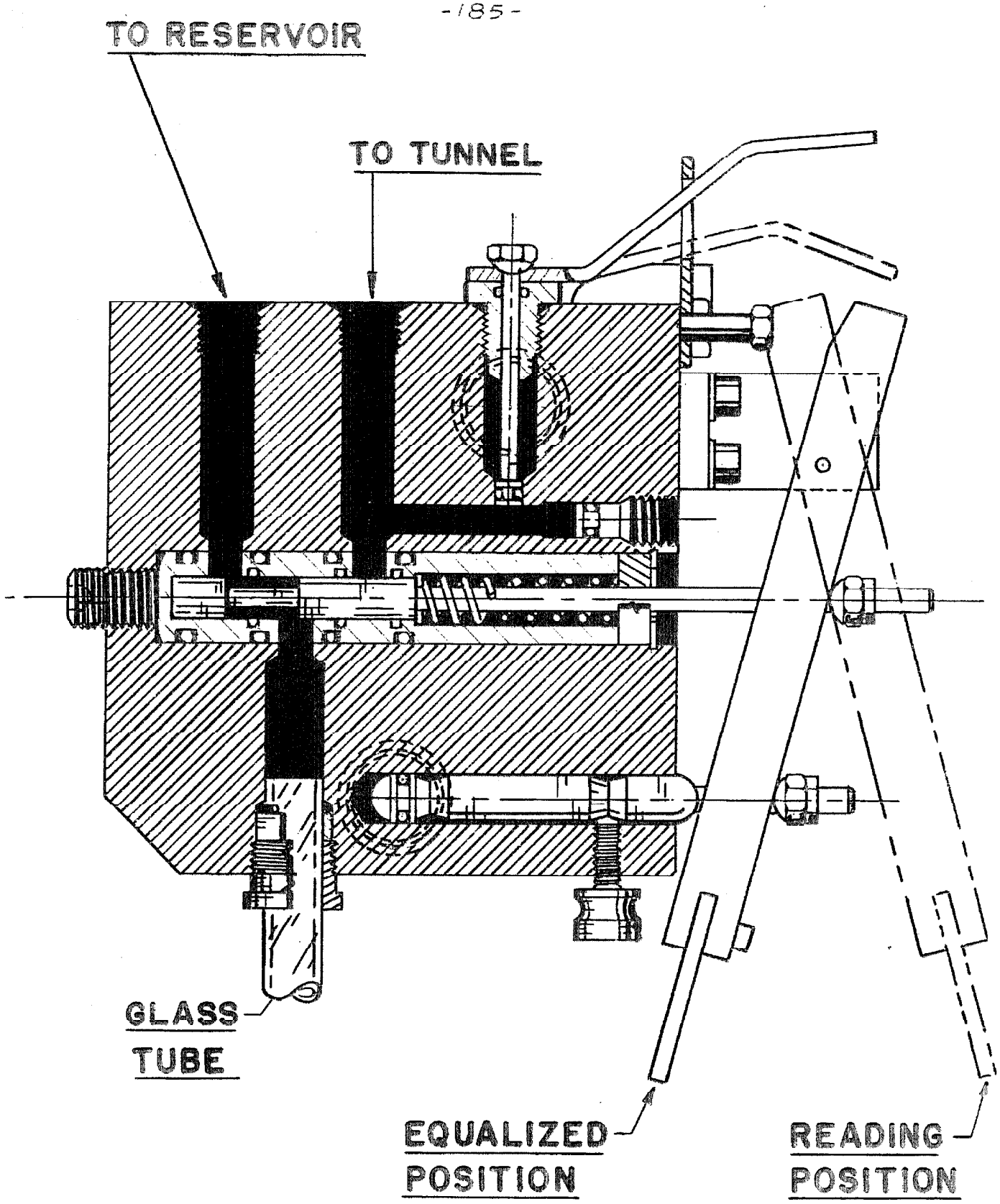

FIGURE 31

MANOMETER SLIDING VALVE AND PORTING

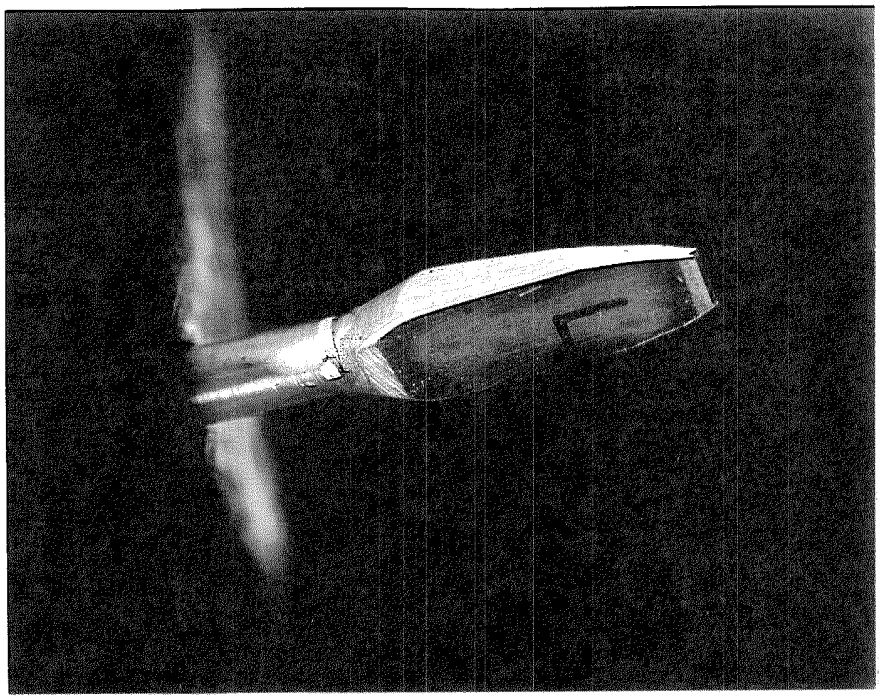

Figure 32 - The Mass Flow Probe

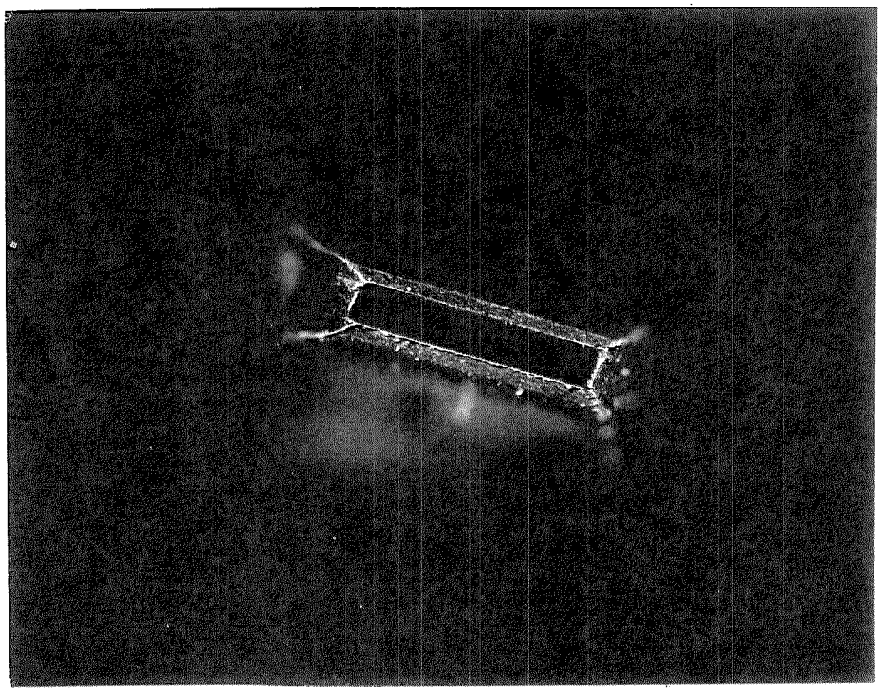

Figure 33 - Entrance of the Mass Flow Probe

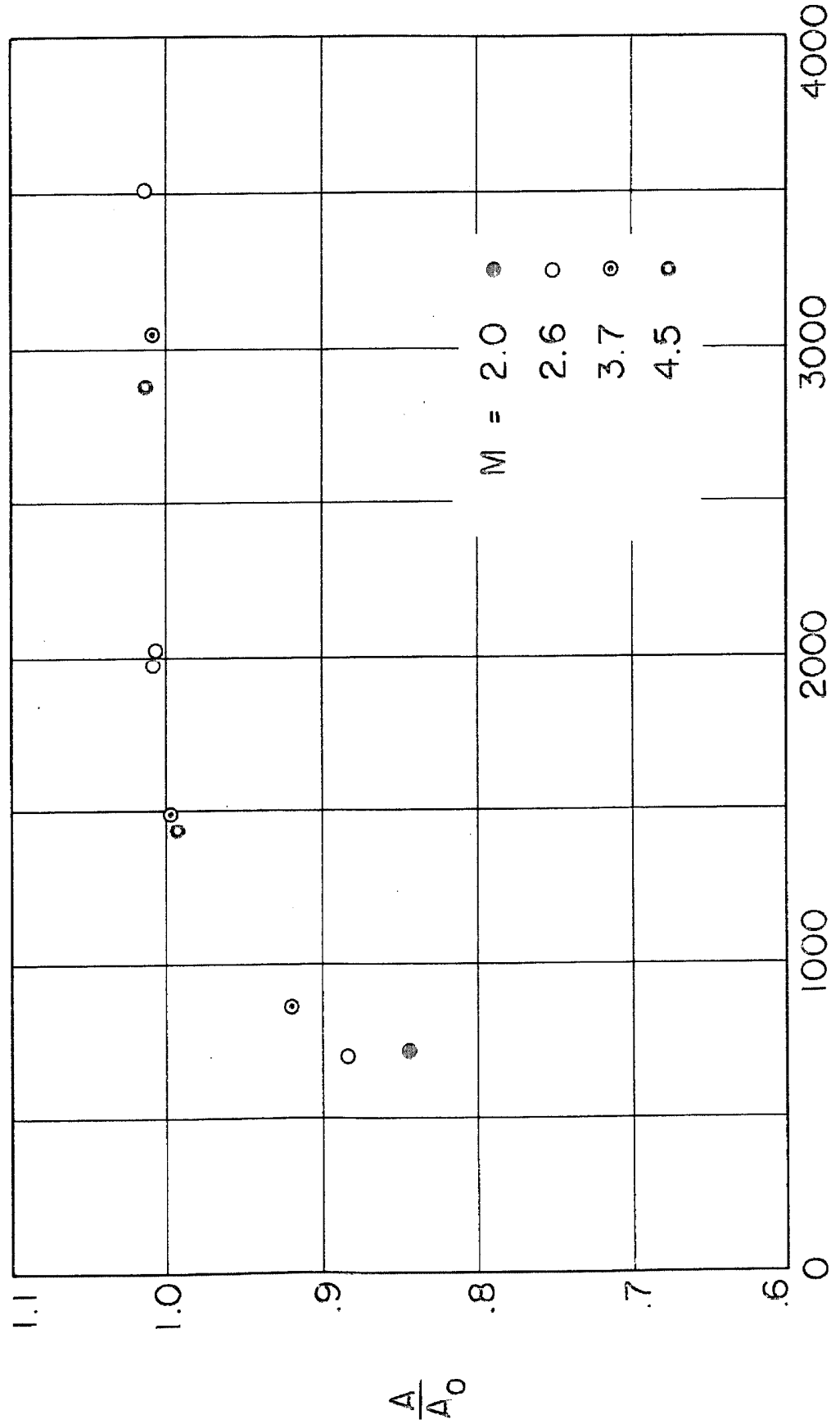

FIGURE 34. MASS FLOW PROBE CALIBRATION

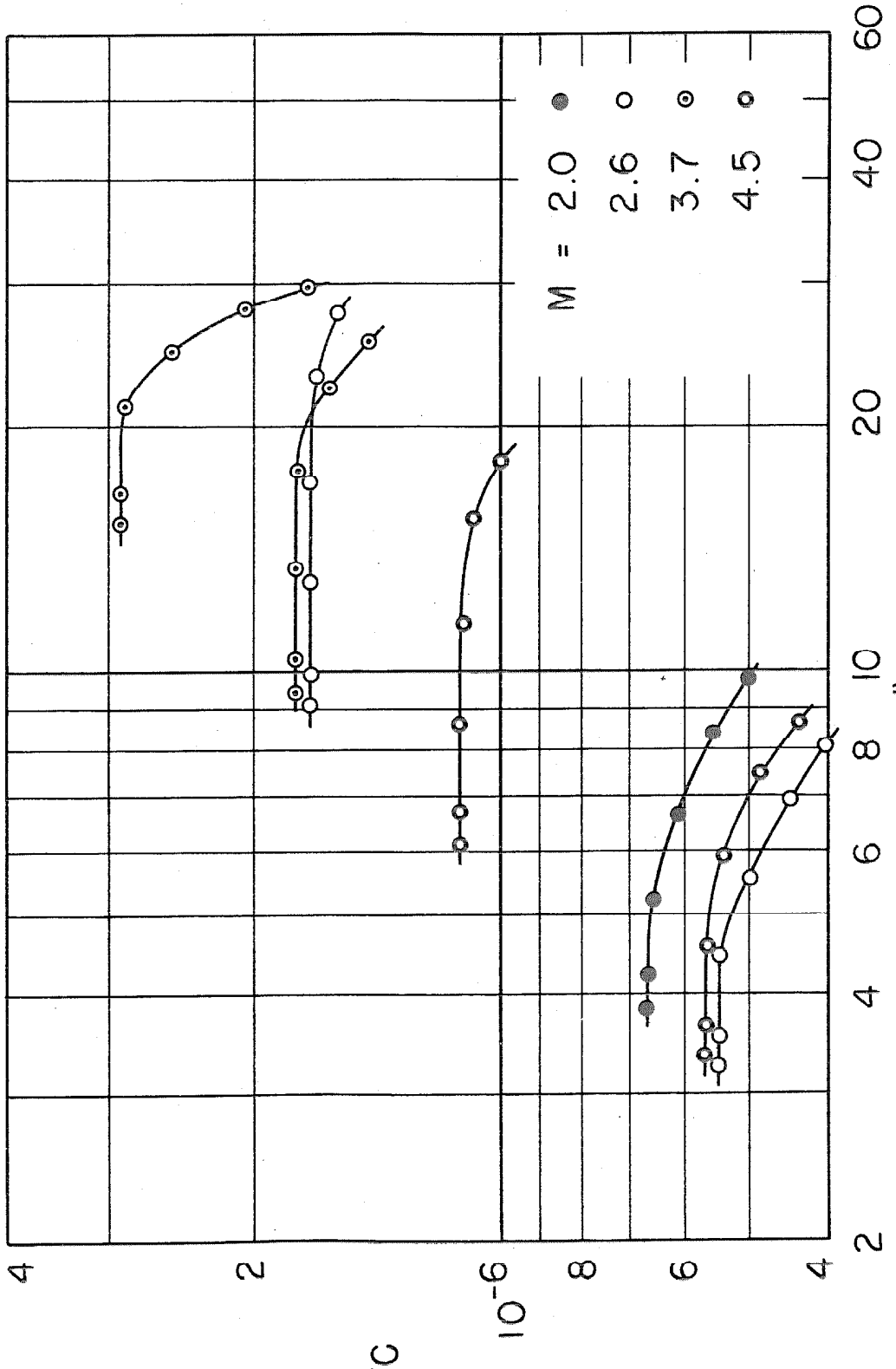

FIGURE 35. INDEPENDENCE OF MASS FLOW AND BACK PRESSURE

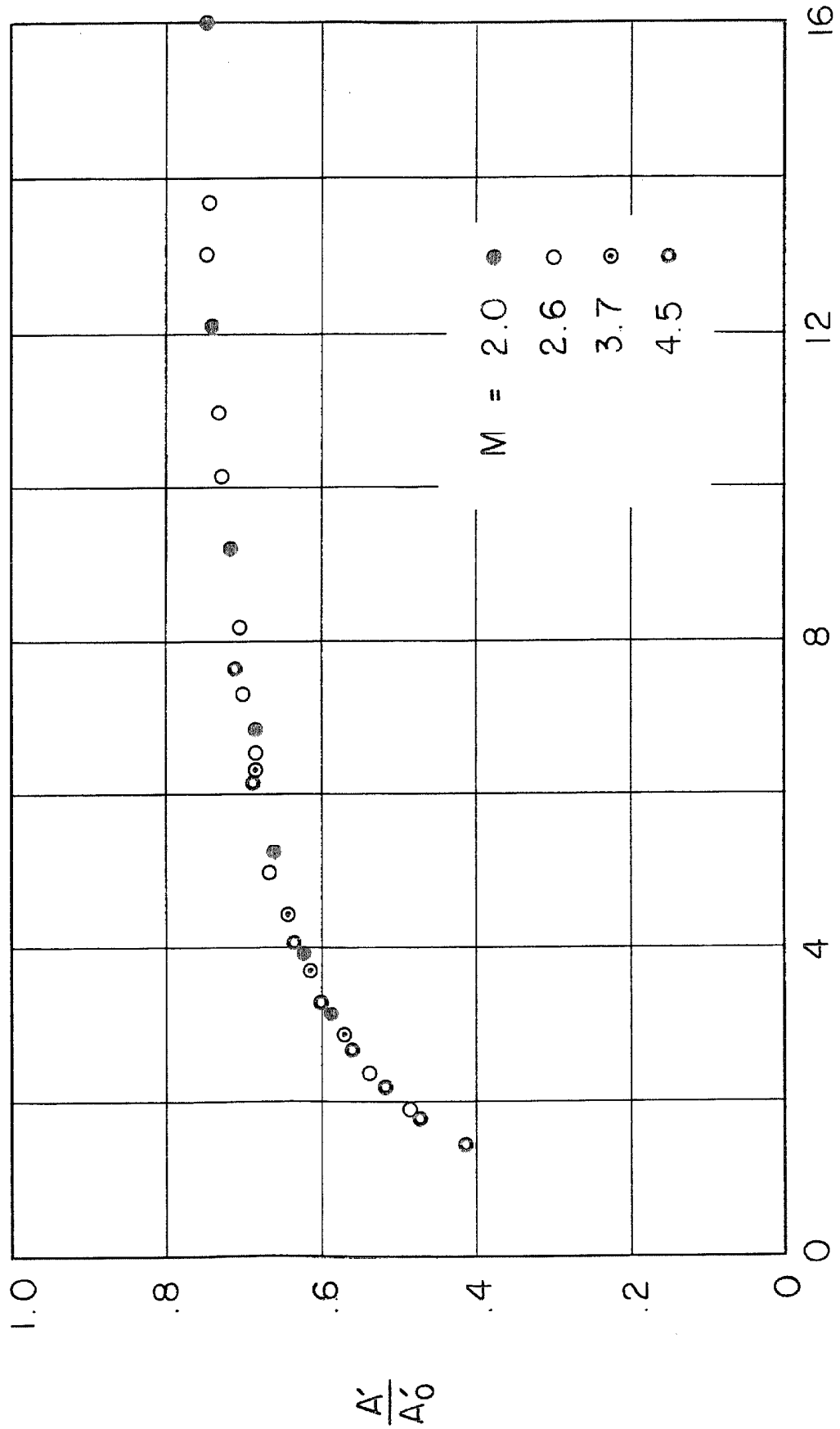

FIGURE 36. DOUBLE SONIC ORIFICE THERMOMETER CALIBRATION

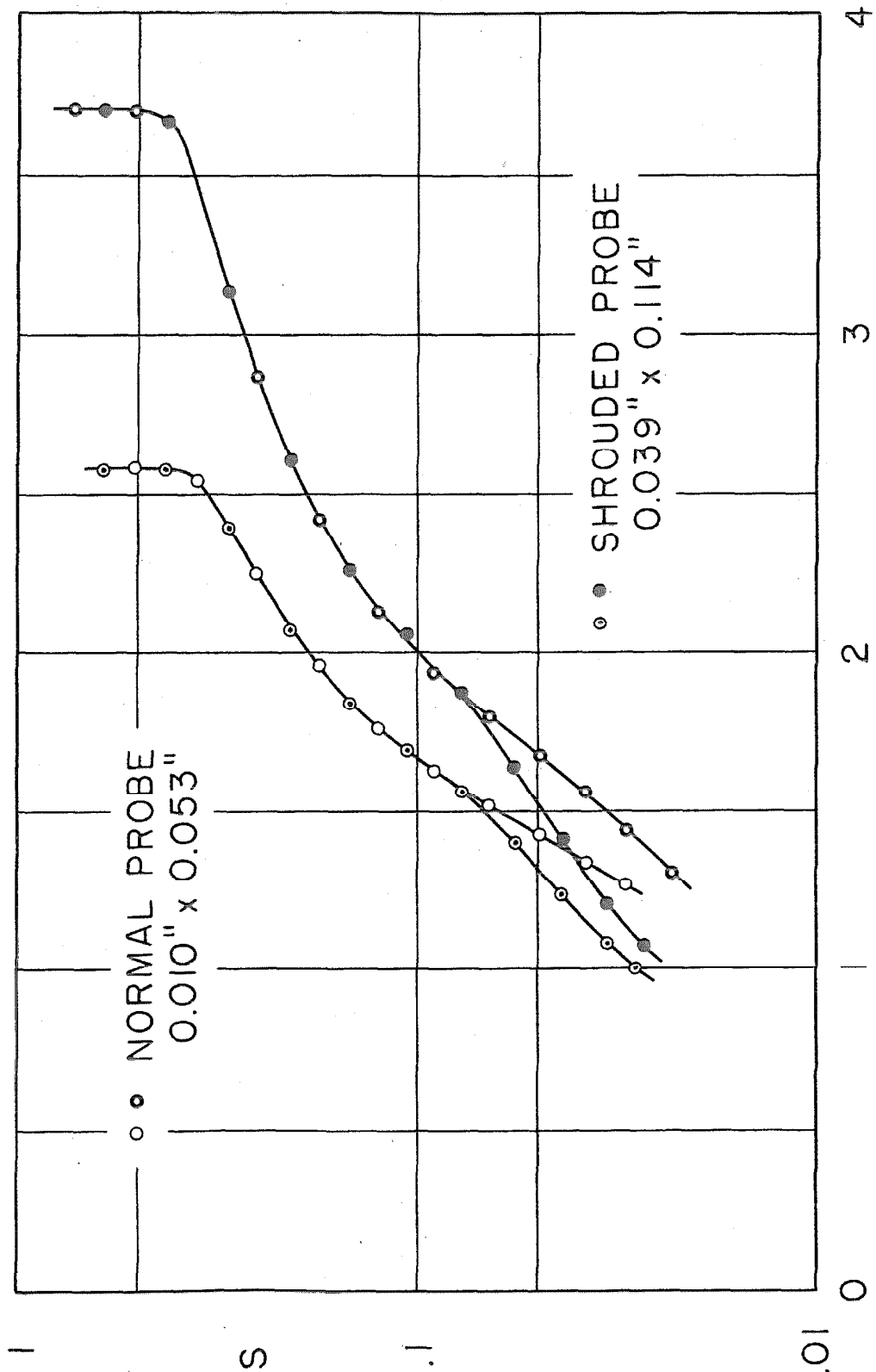

FIGURE 37 INTERFERENCE OF IMPACT PROBE AND WALL

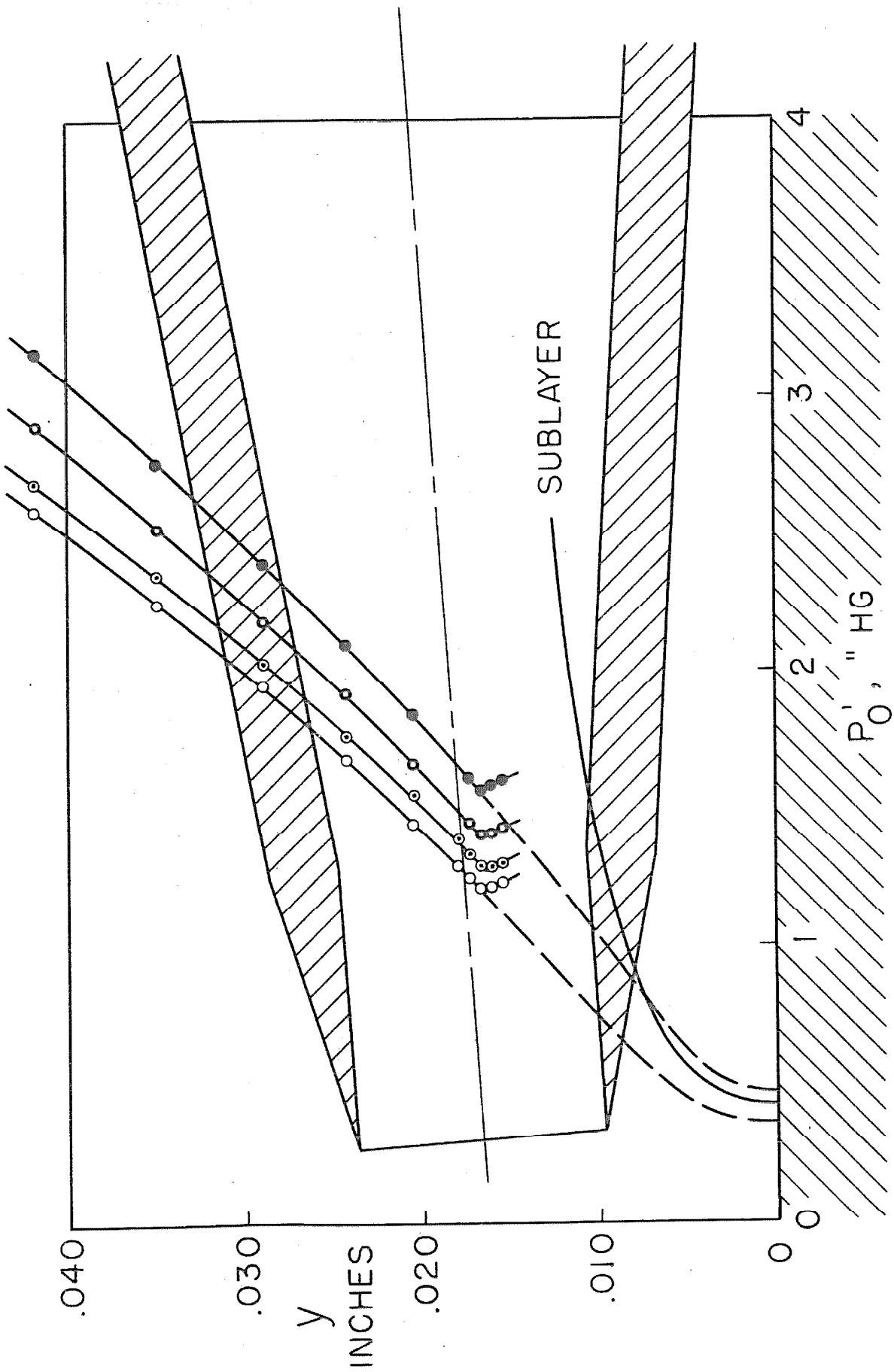

FIGURE 38 METHOD OF DETECTING PROBE CONTACT

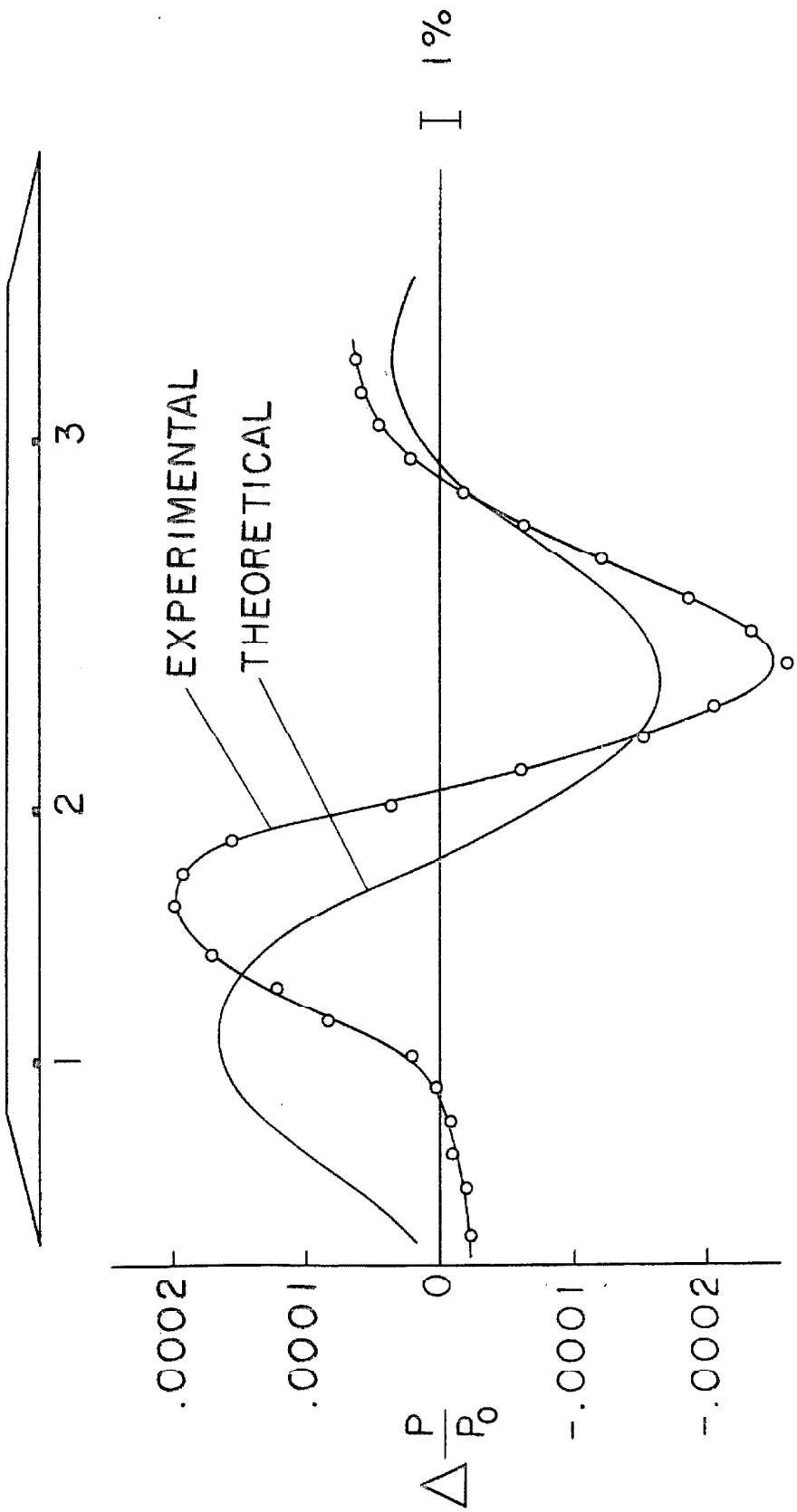

FIGURE 39. TYPICAL PRESSURE INFLUENCE CURVE

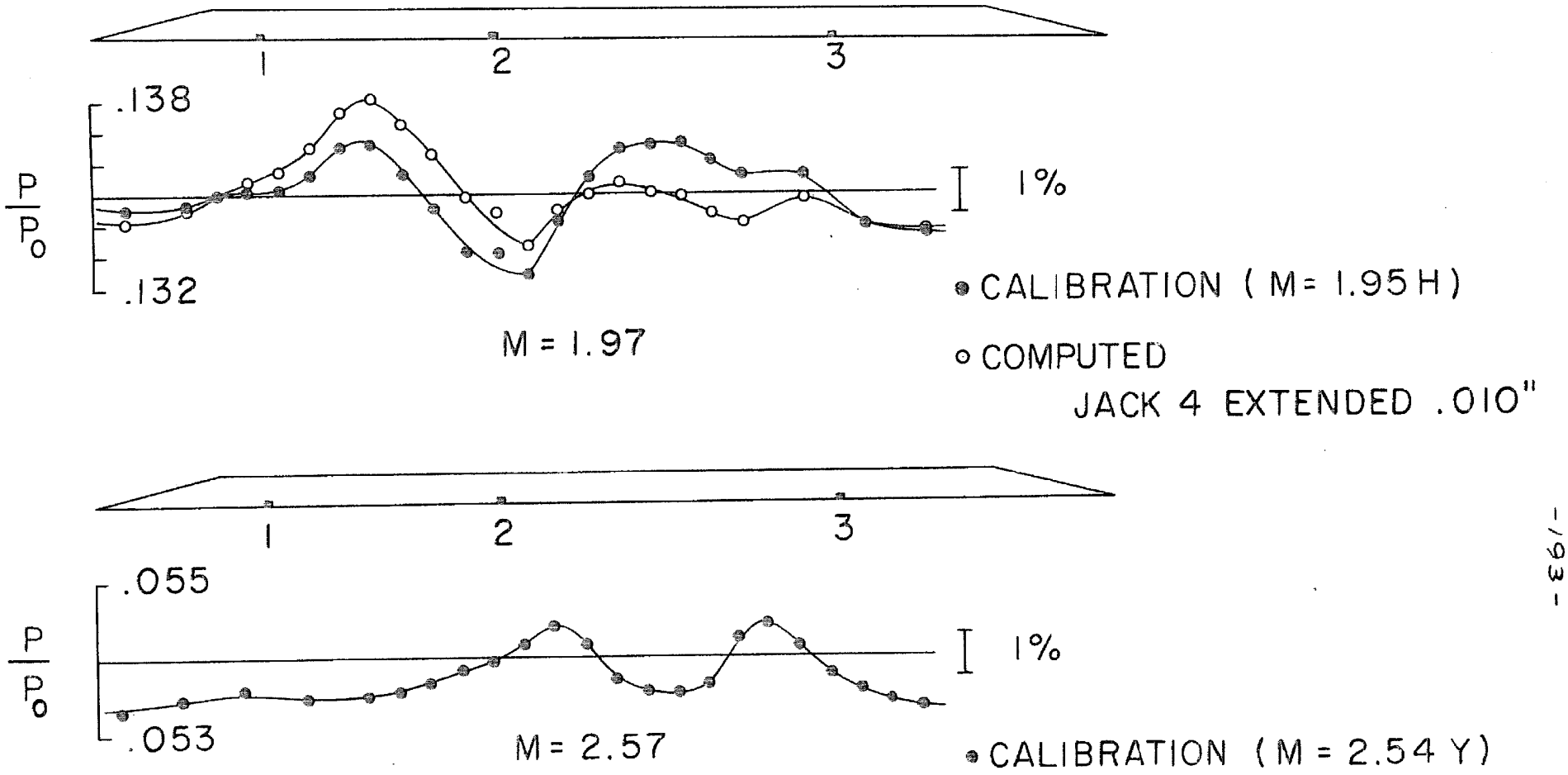

FIGURE 40. NOZZLE STATIC PRESSURE CALIBRATION

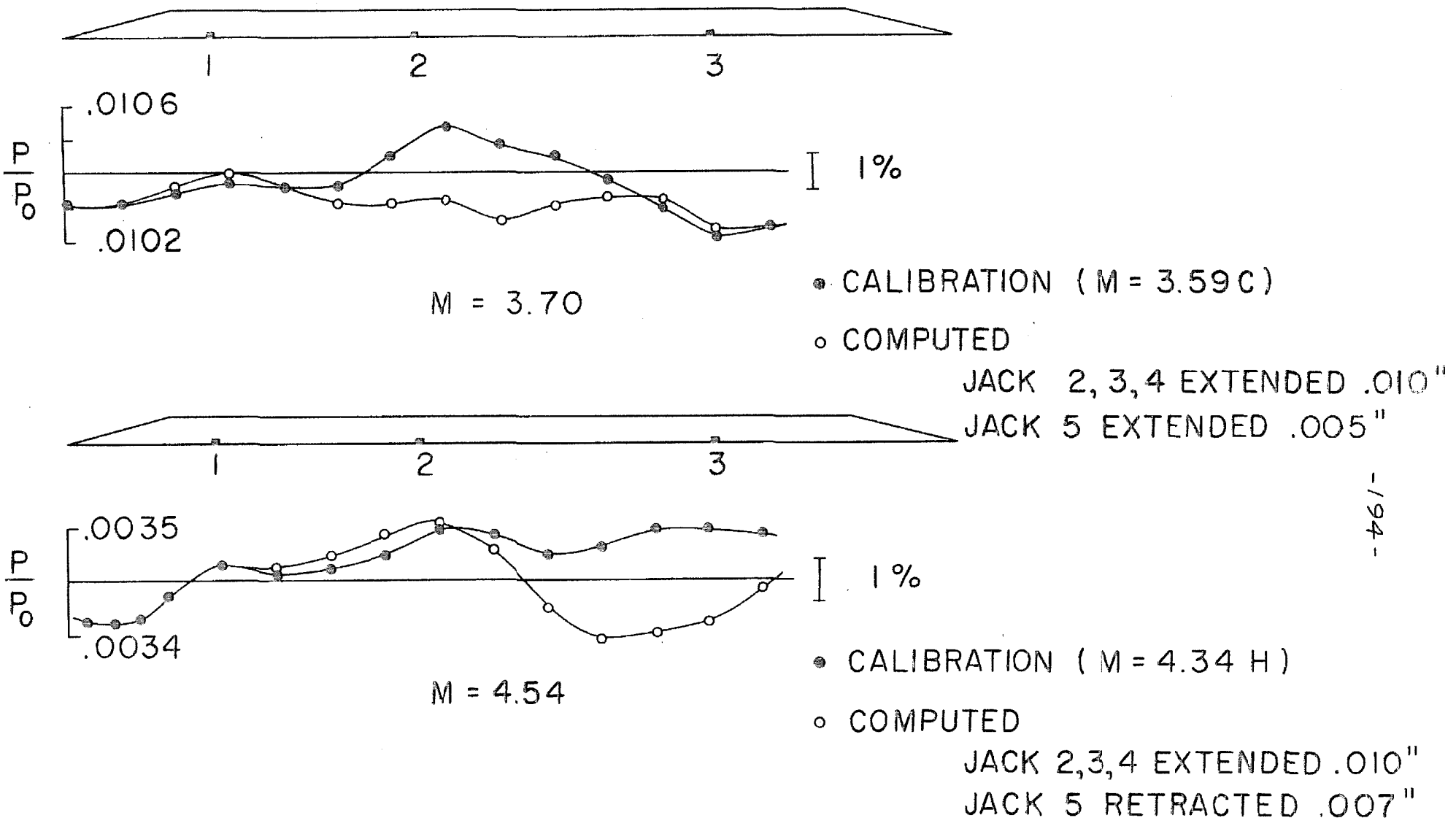

FIGURE 40 (CONT'D) NOZZLE STATIC PRESSURE CALIBRATION

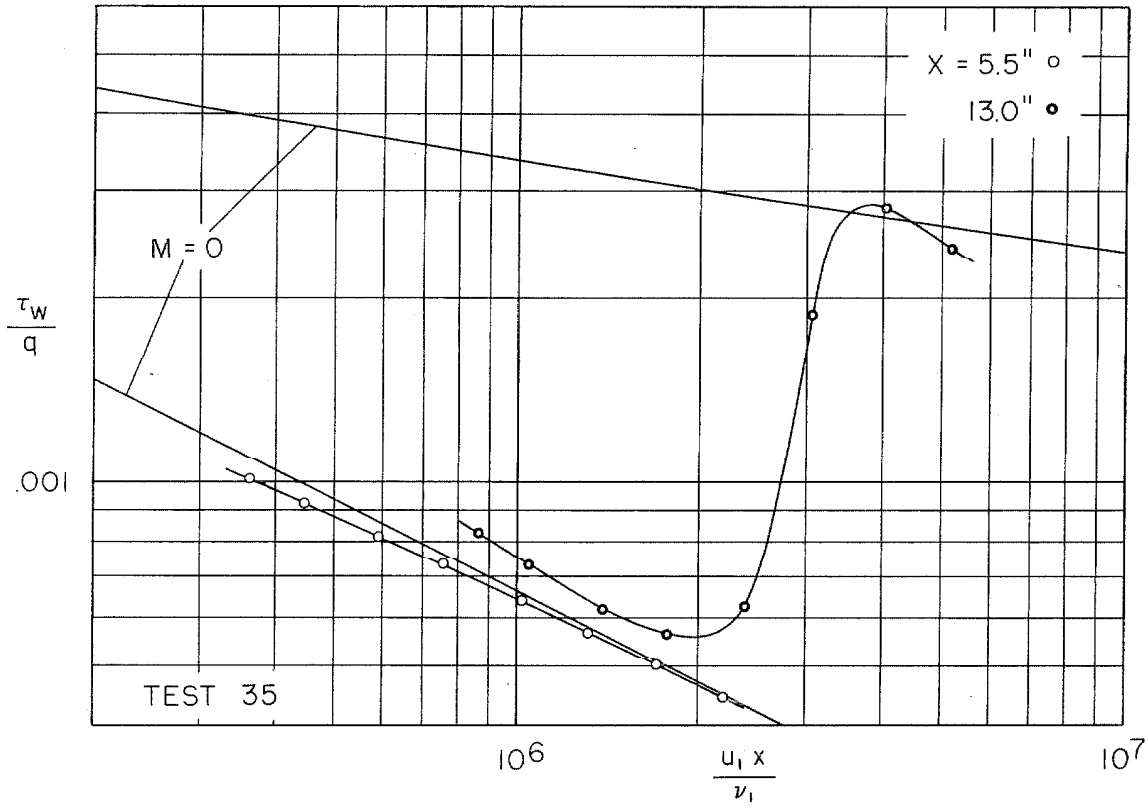

FIGURE 41 LOCAL FRICTION, NATURAL TRANSITION, M = 1.97

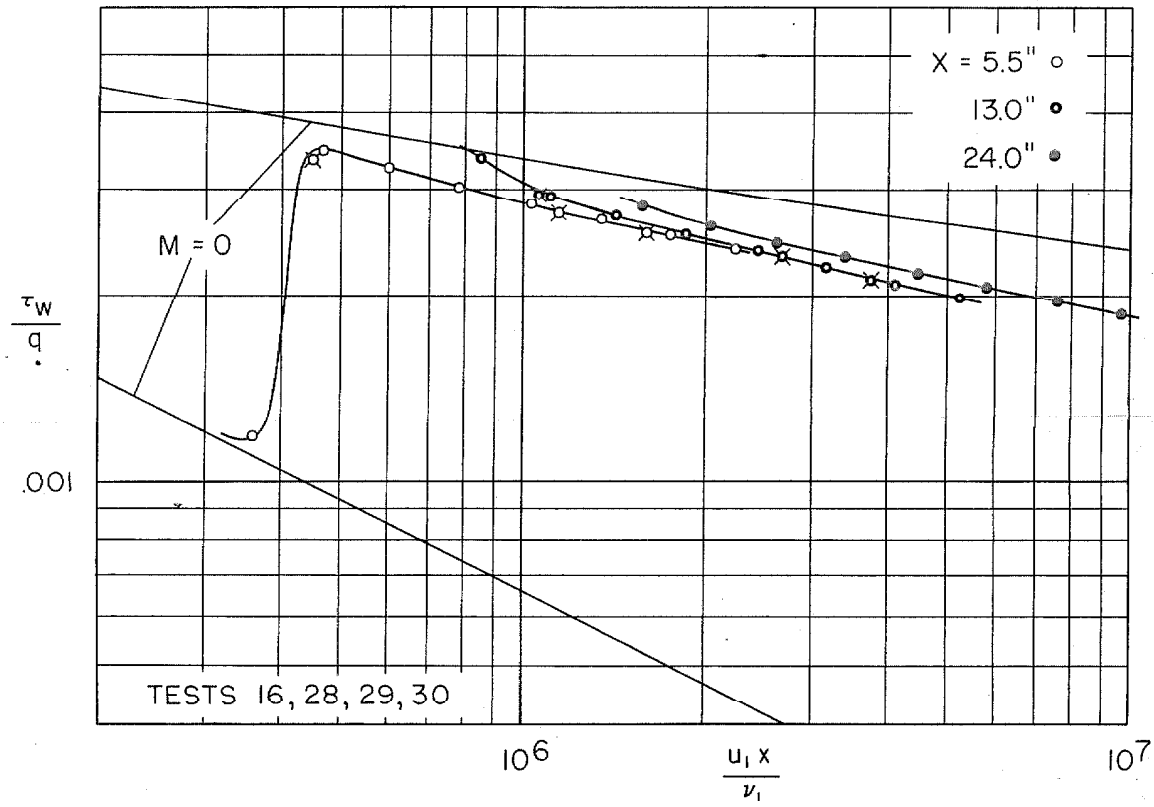

FIGURE 42 LOCAL FRICTION, FENCE TRIP, M = 1.97

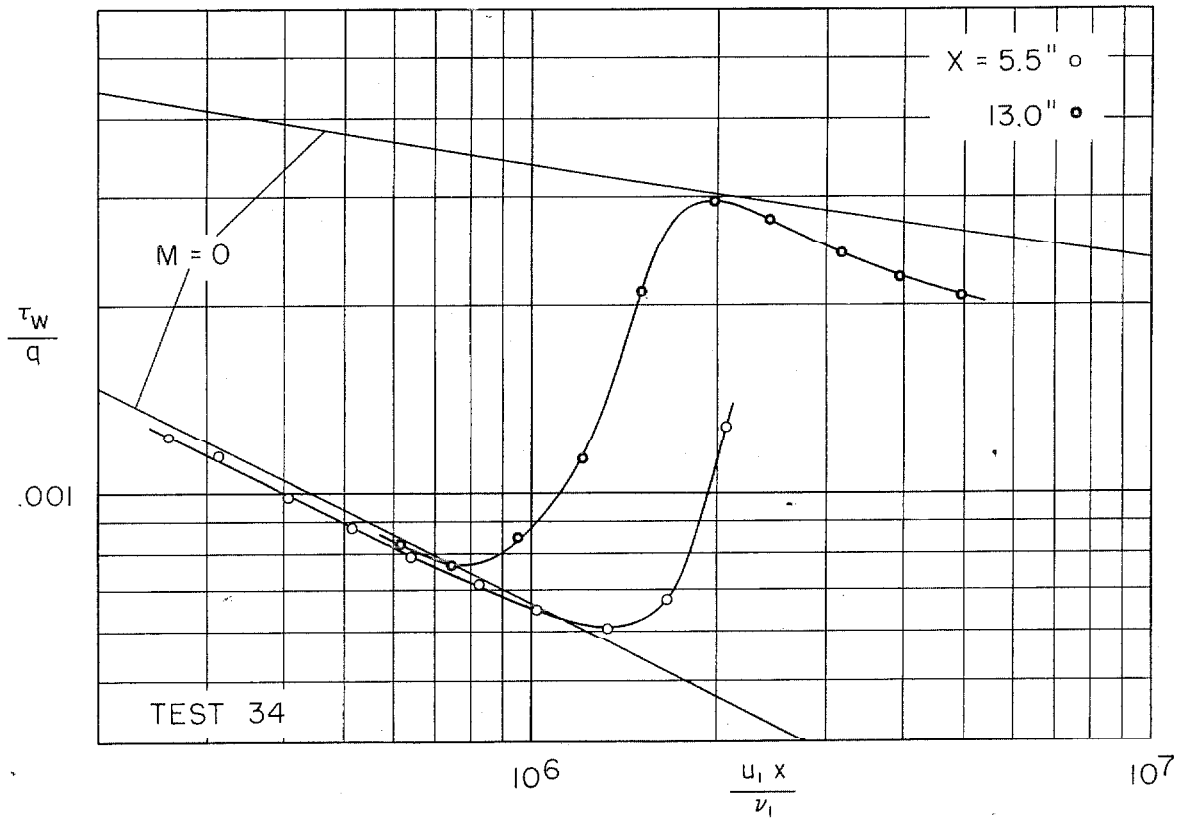

FIGURE 43 LOCAL FRICTION, NATURAL TRANSITION, M = 2.57

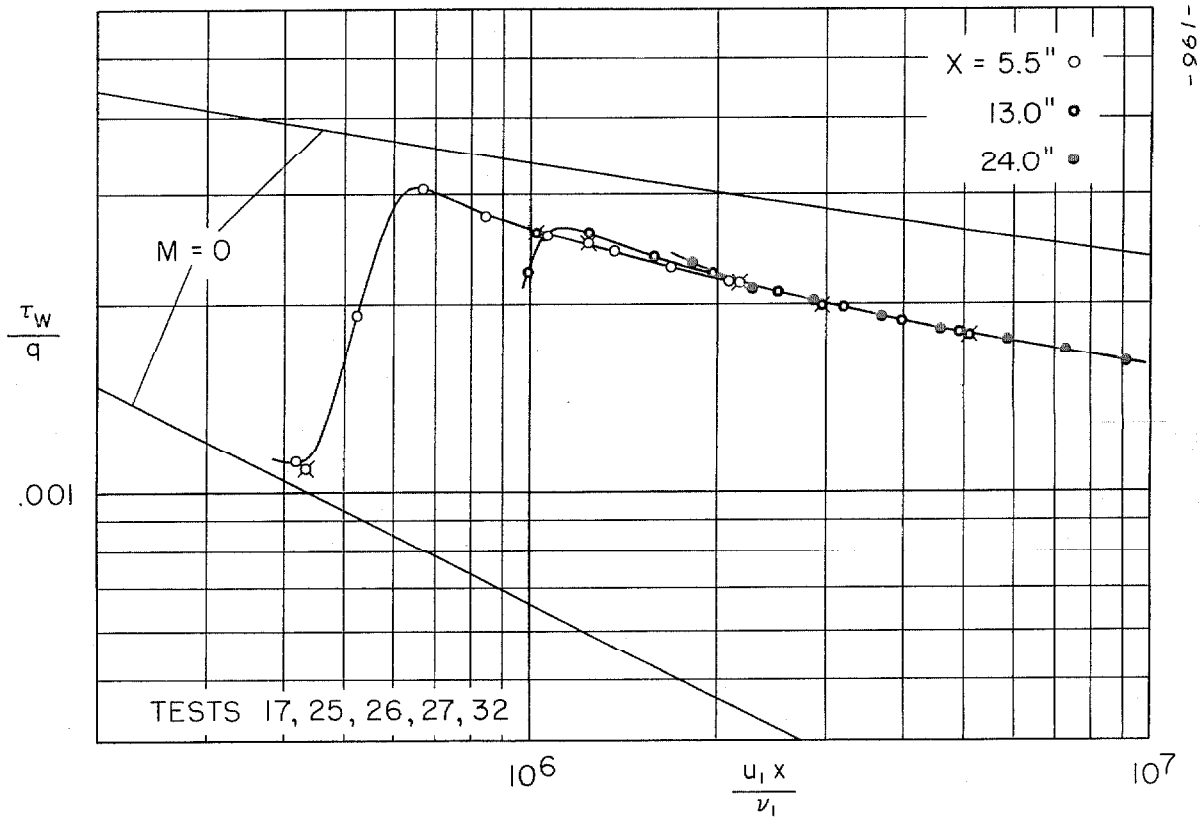

FIGURE 44 LOCAL FRICTION, FENCE TRIP, M = 2.57

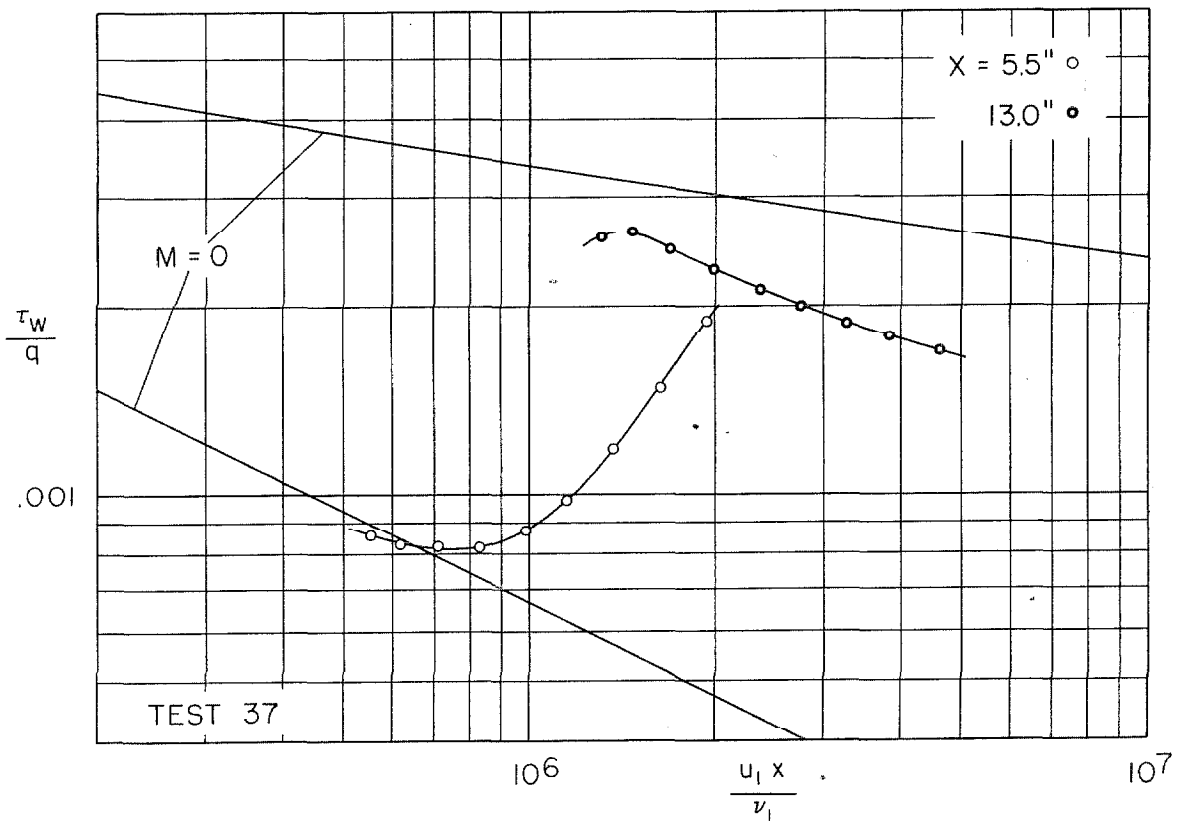

FIGURE 45 LOCAL FRICTION, NATURAL TRANSITION, M = 3.70

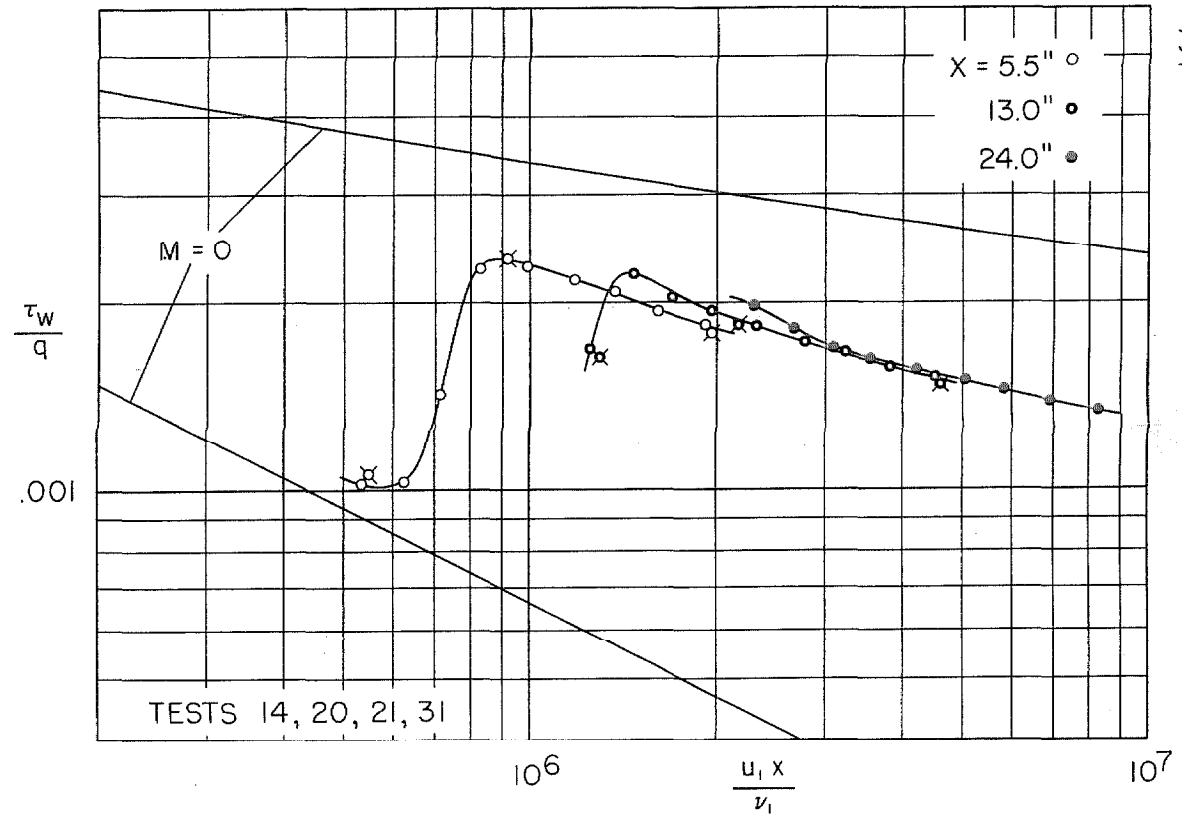

FIGURE 46 LOCAL FRICTION, FENCE TRIP, M = 3.70

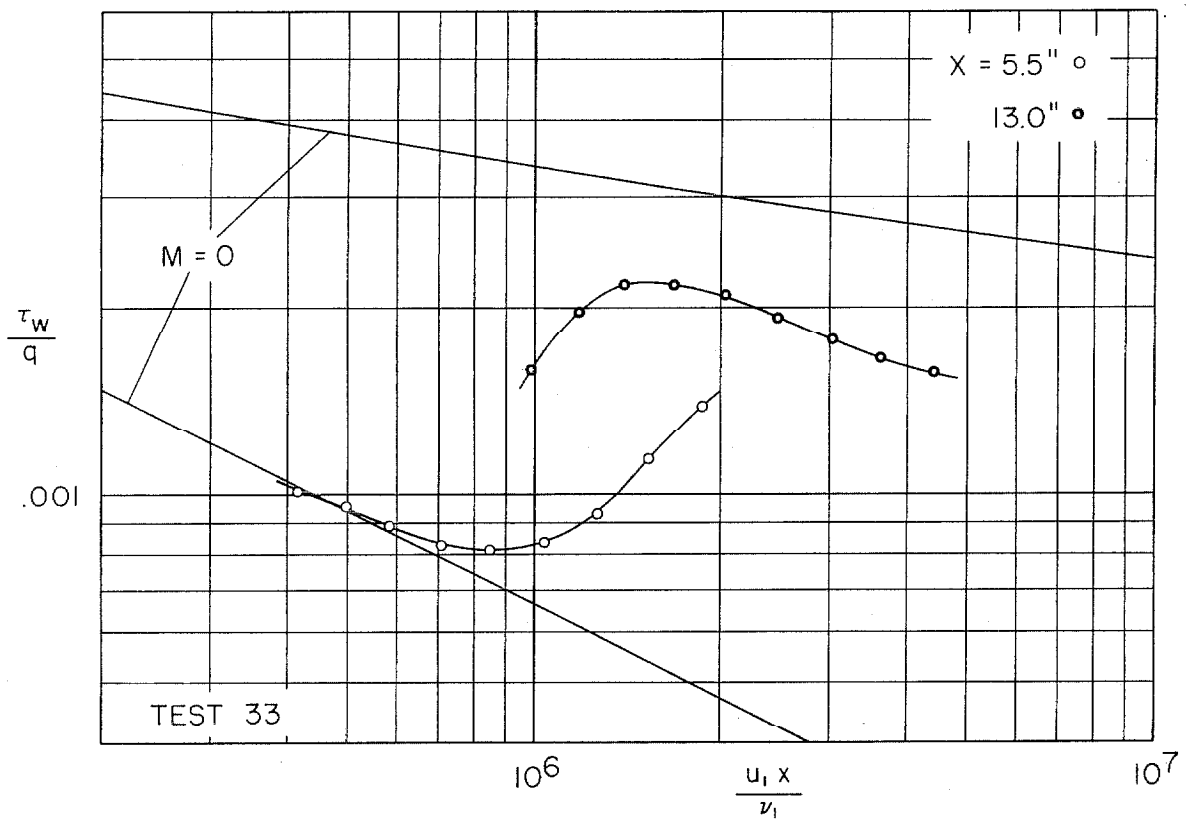

FIGURE 47 LOCAL FRICTION, NATURAL TRANSITION, M = 4.54

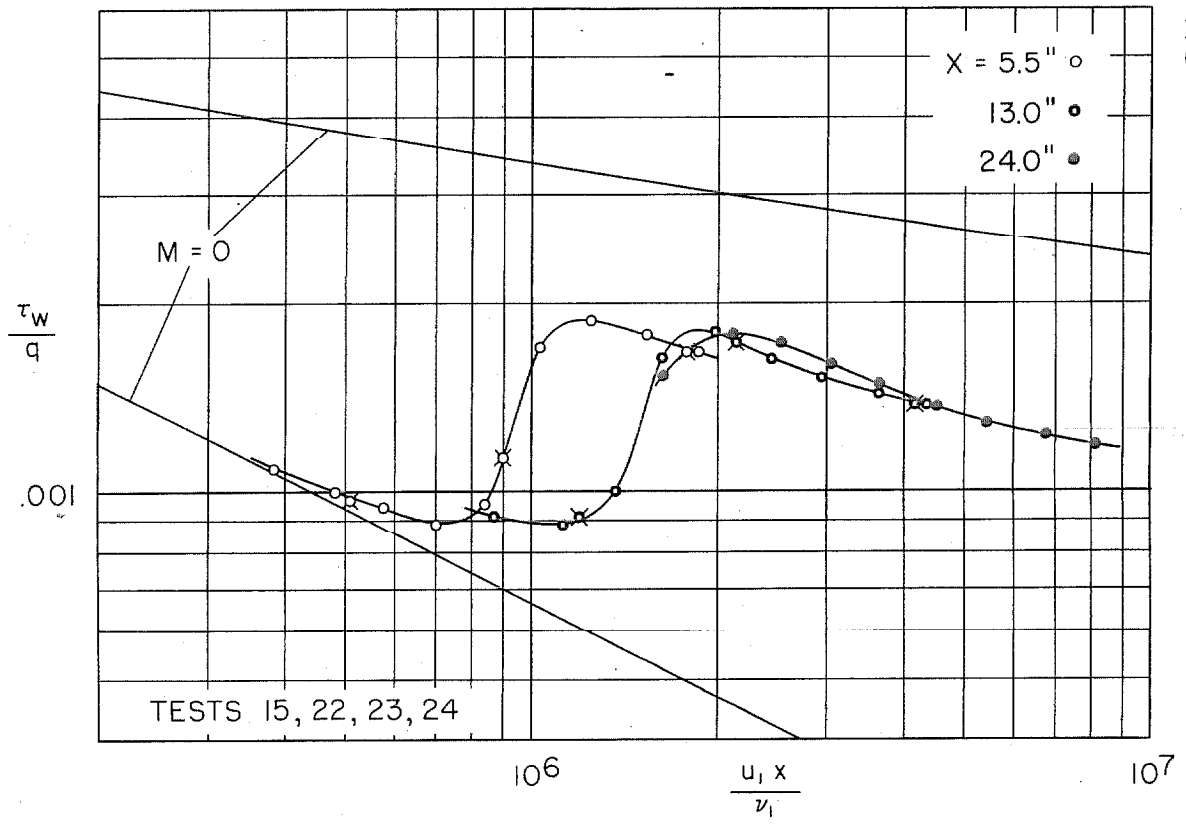

FIGURE 48 LOCAL FRICTION, FENCE TRIP, M = 4.54

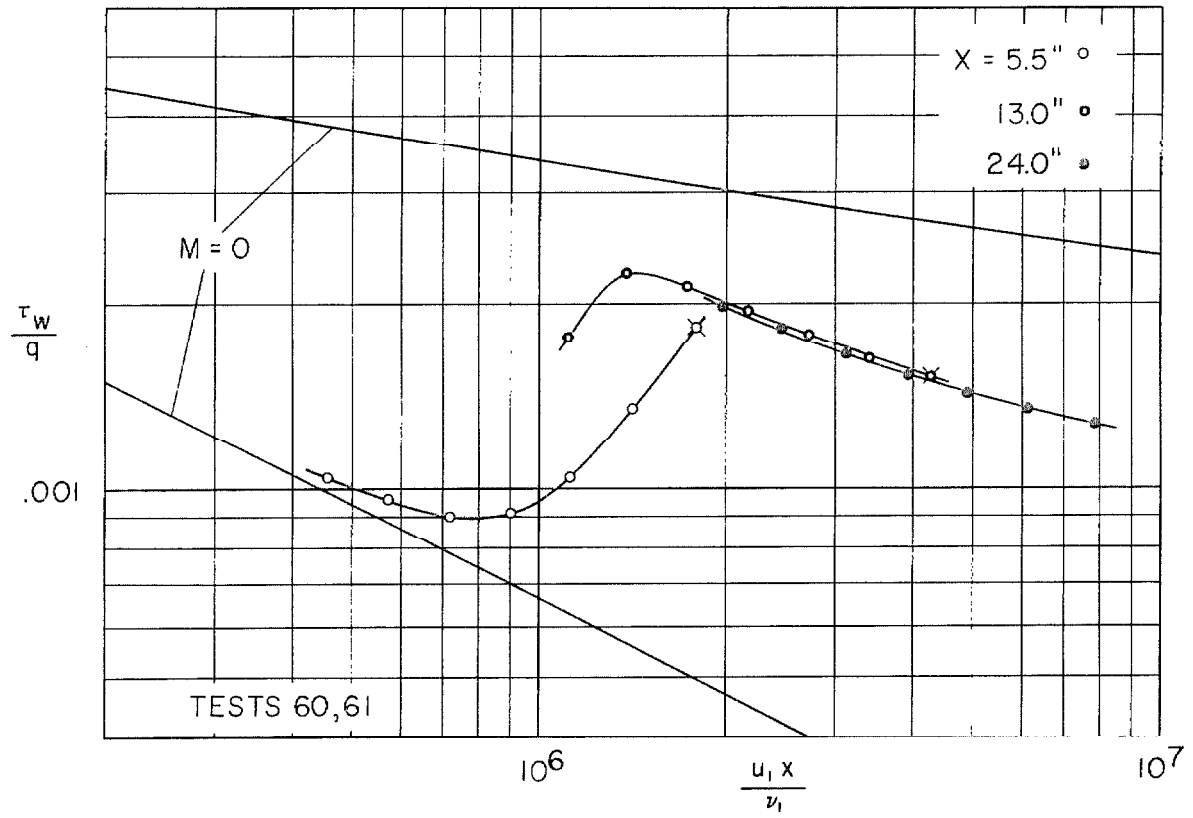

FIGURE 49 LOCAL FRICTION, SAND TRIP, M = 4.54

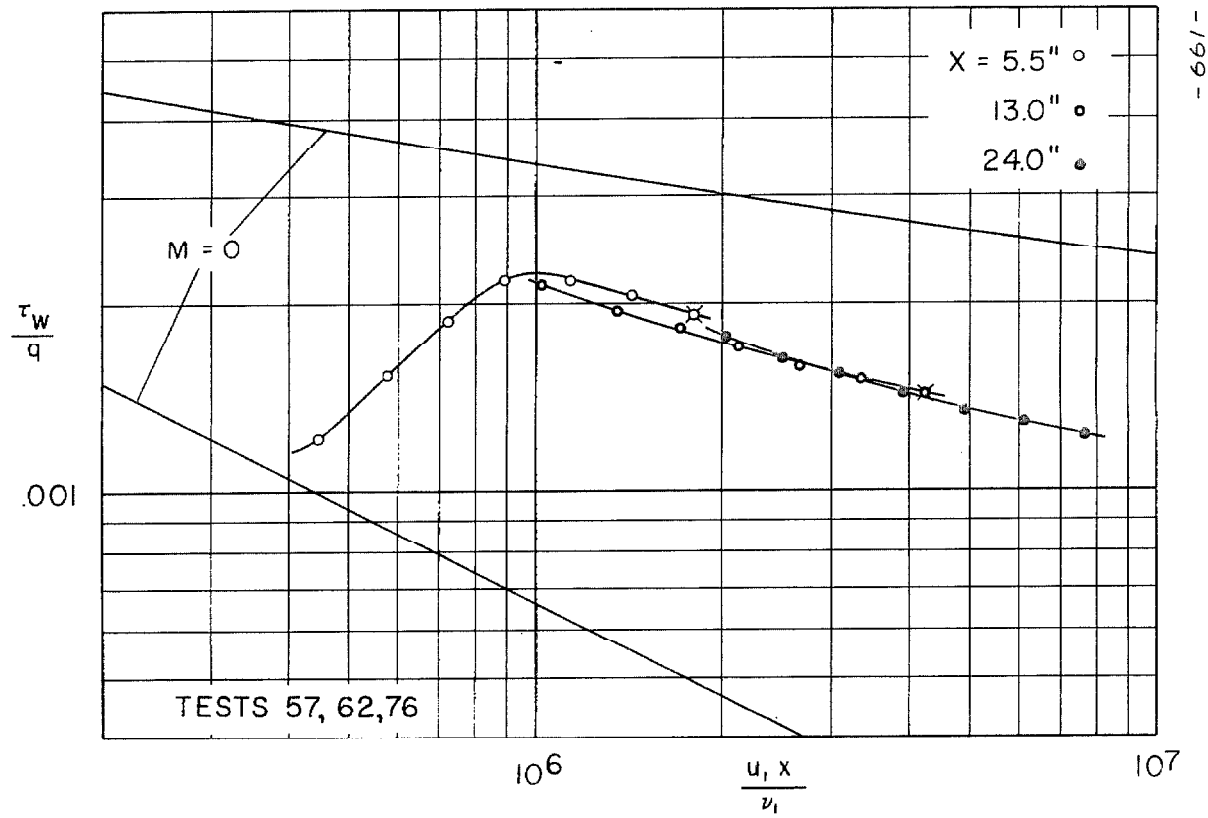

FIGURE 50 LOCAL FRICTION, AIR JET TRIP, M = 4.54

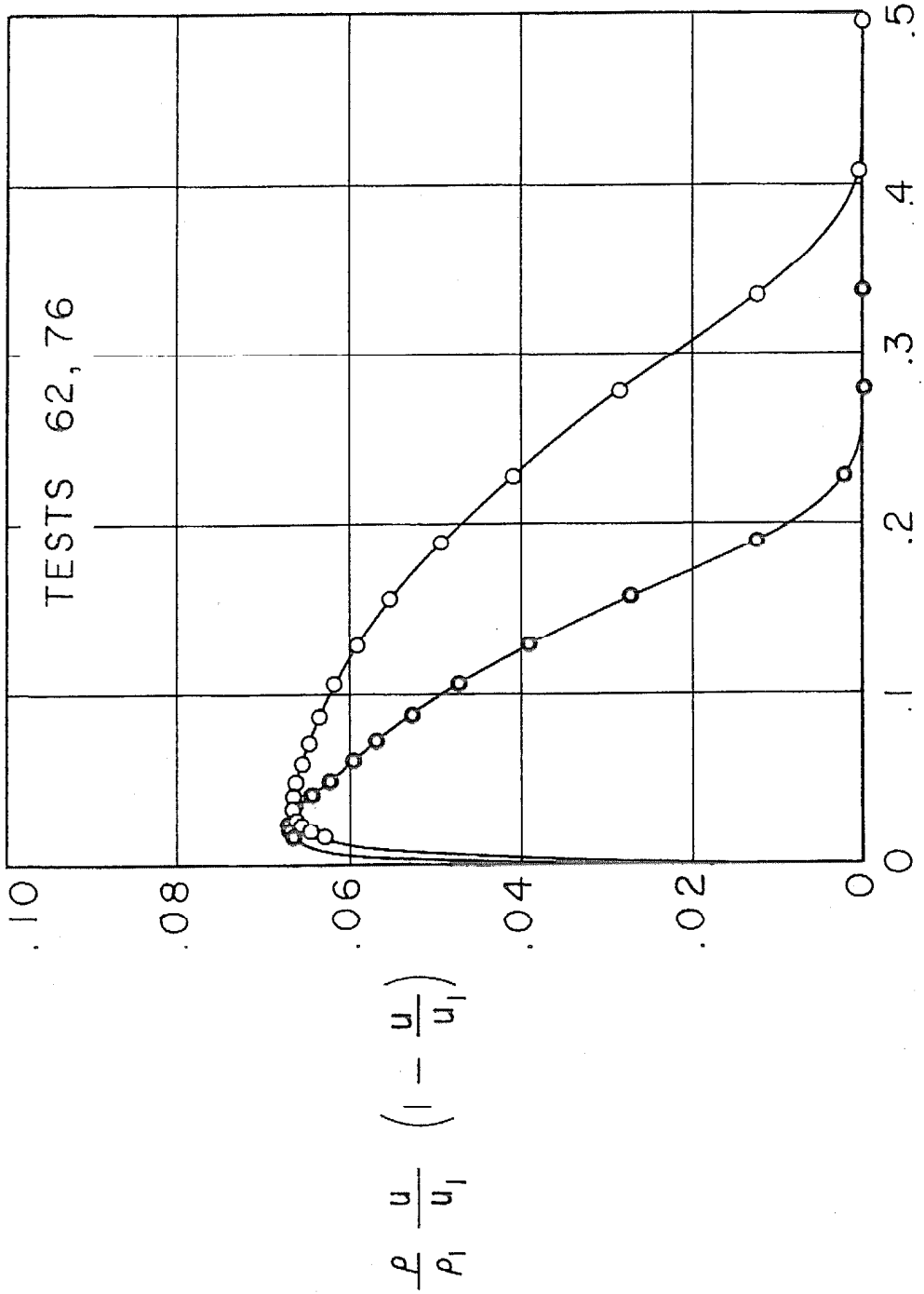

FIGURE 51. TYPICAL MOMENTUM THICKNESS DETERMINATION

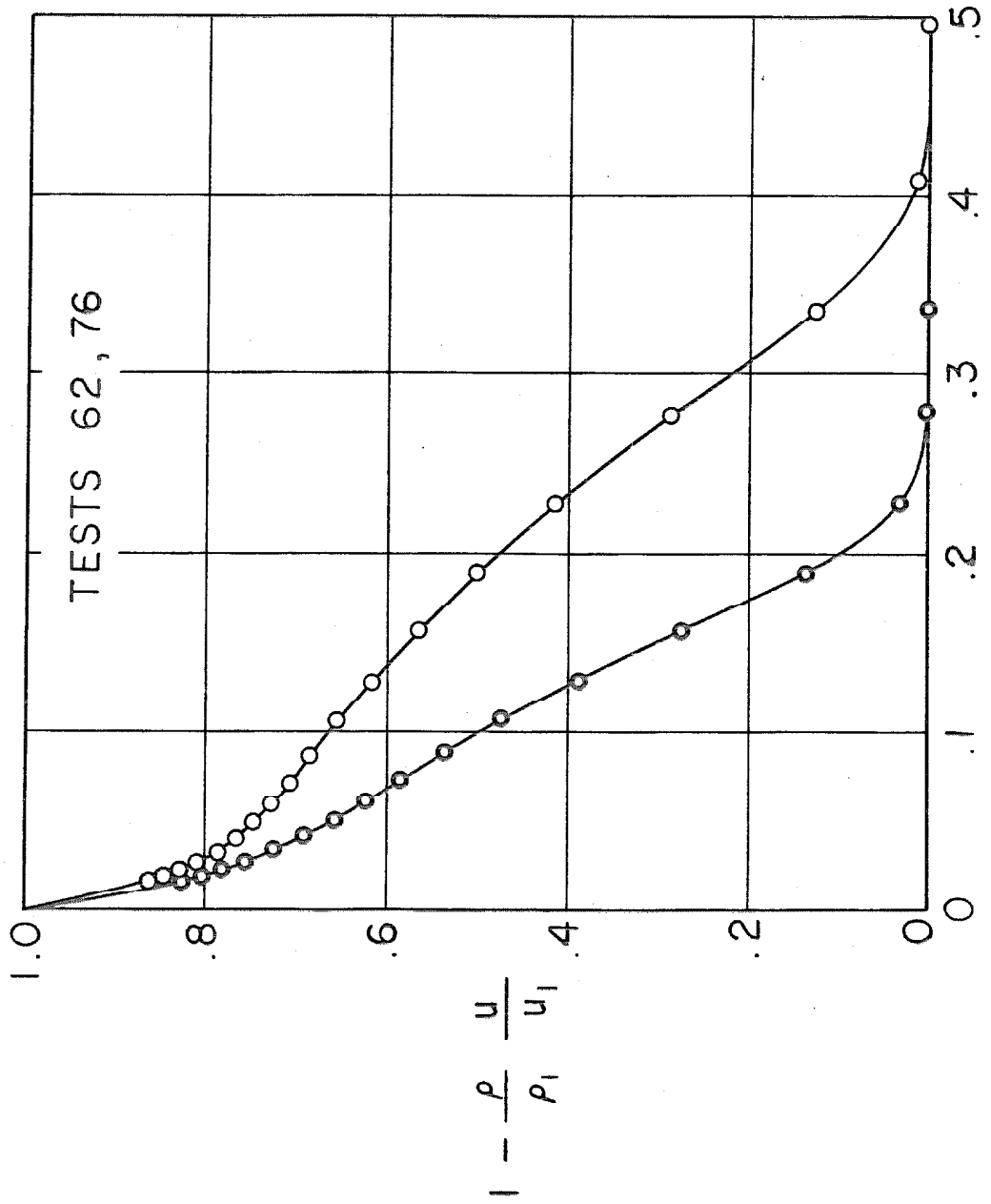

FIGURE 52. TYPICAL DISPLACEMENT THICKNESS DETERMINATION

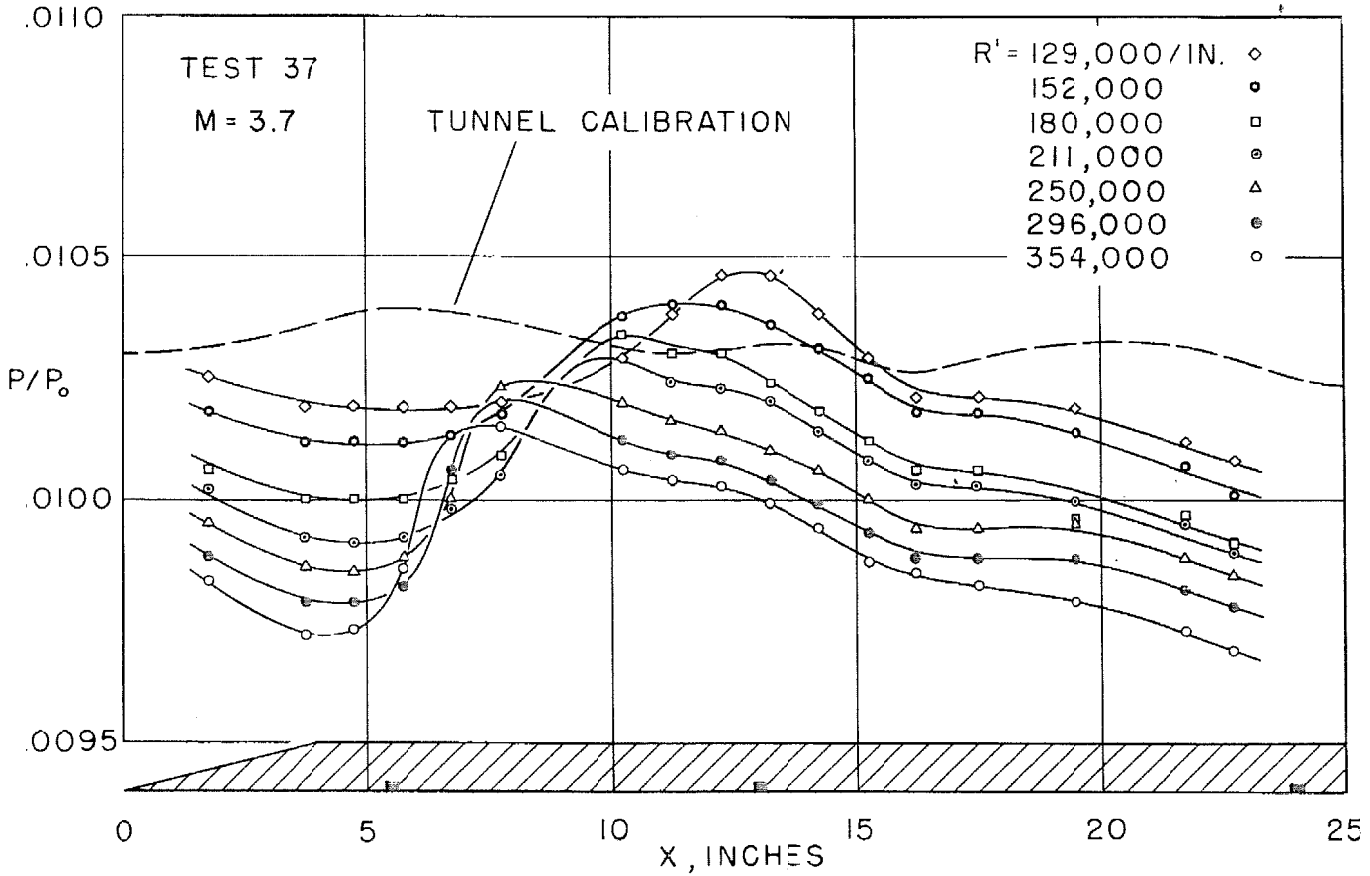

FIGURE 53. STATIC PRESSURE DISTRIBUTION WITH NATURAL TRANSITION, M = 3.7

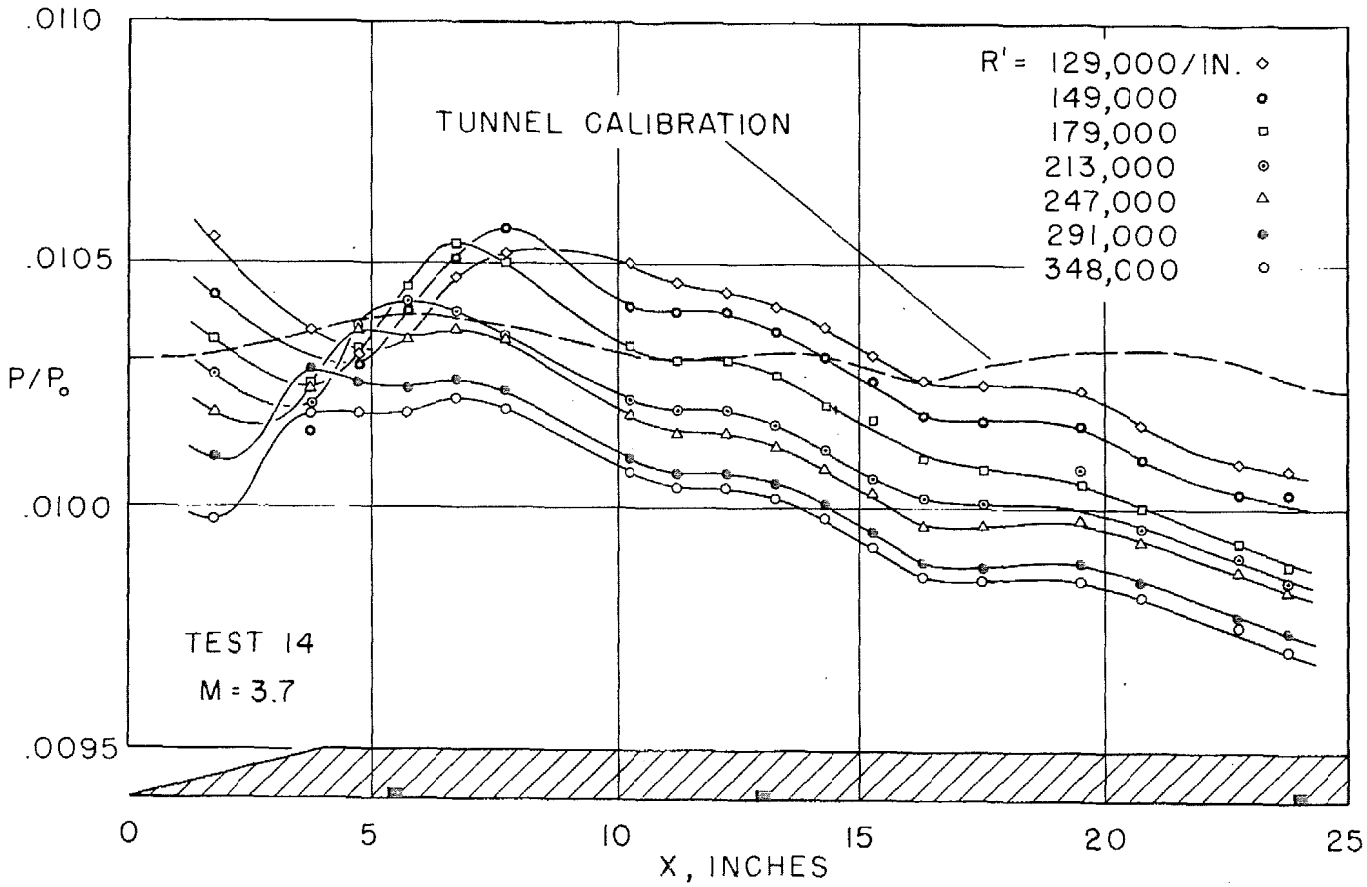

FIGURE 54. STATIC PRESSURE DISTRIBUTION WITH FENCE TRIP, M = 3.7

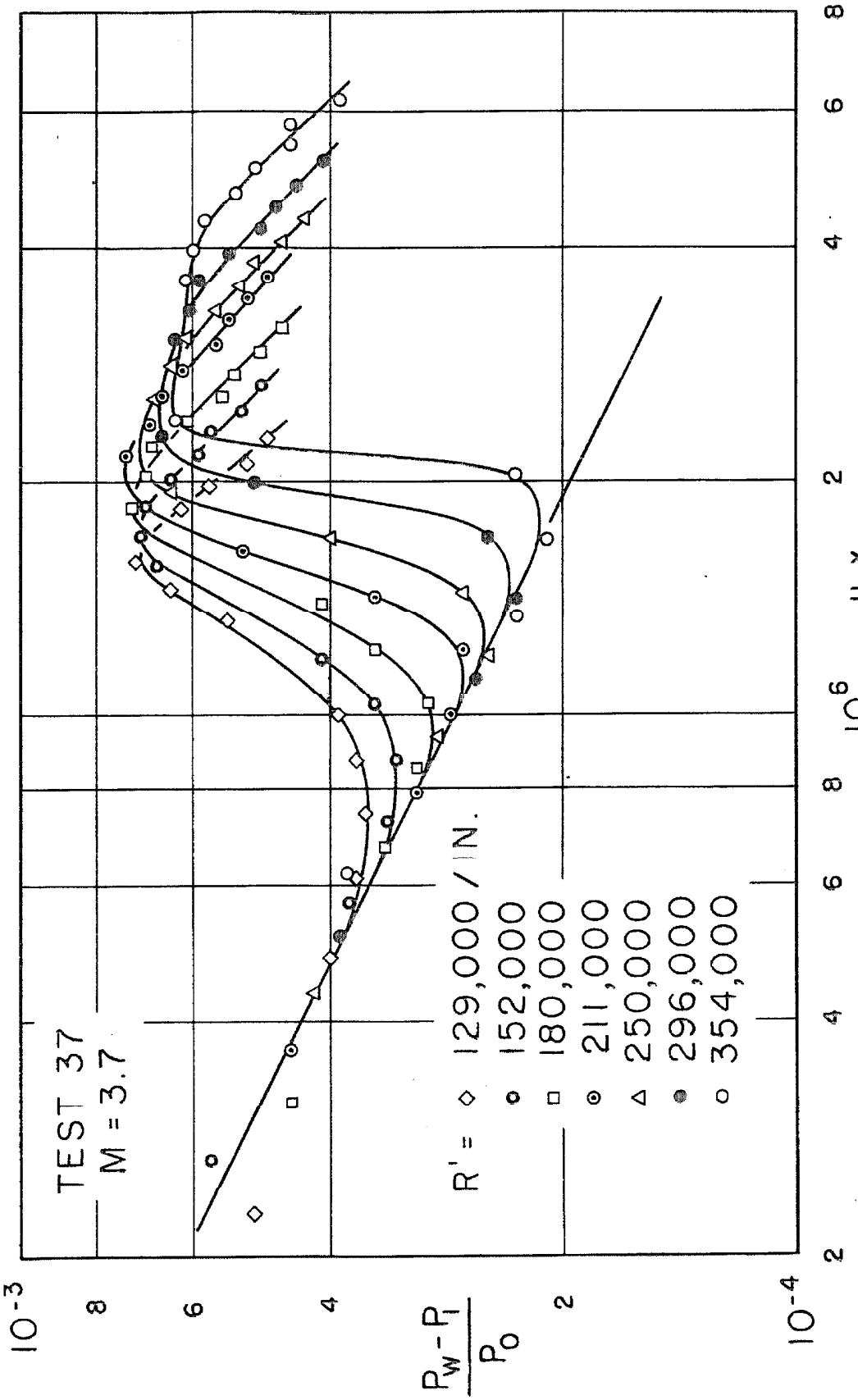

Figure 55. PRESSURE INCREMENT FROM BOUNDARY LAYER

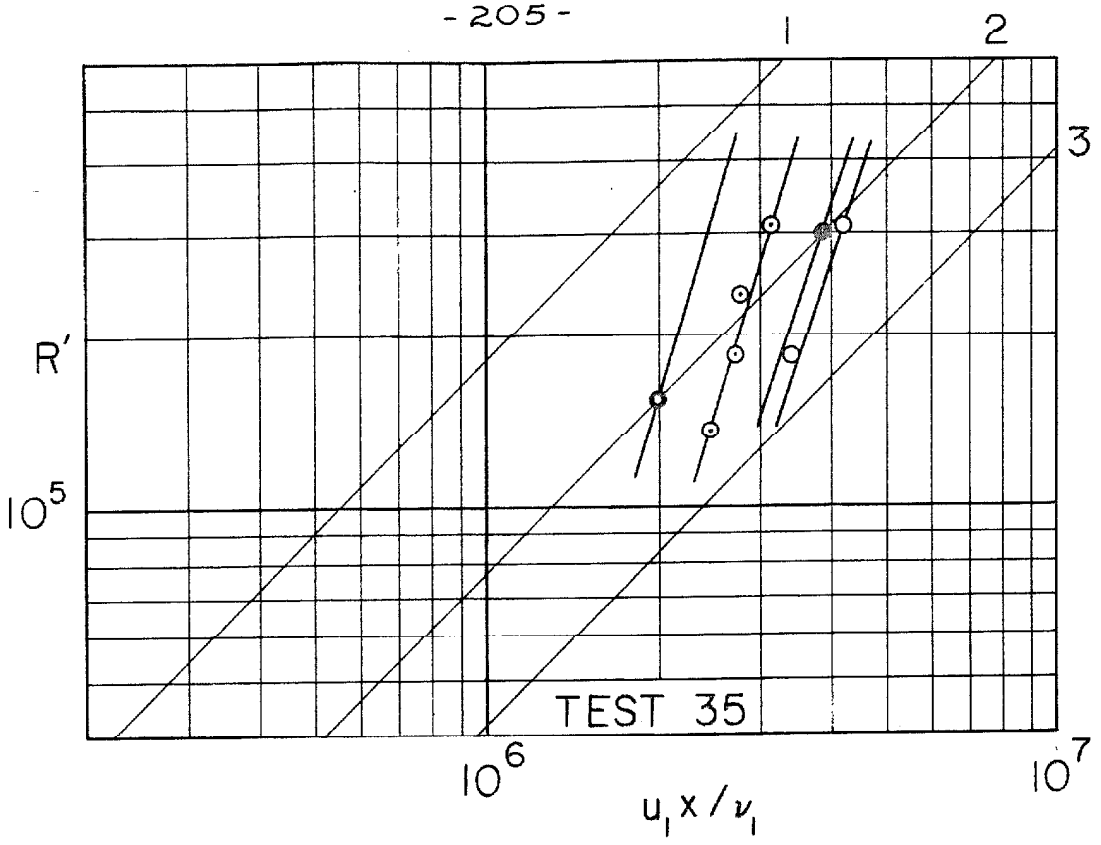

FIGURE 56. NATURAL TRANSITION, M = 1.97

- ◉ MINIMUM SHEARING STRESS
- ⊙ MINIMUM STATIC PRESSURE
- ● MAXIMUM SHEARING STRESS
- ○ MAXIMUM STATIC PRESSURE

FIGURES 56 - 62. OBSERVATIONS OF TRANSITION

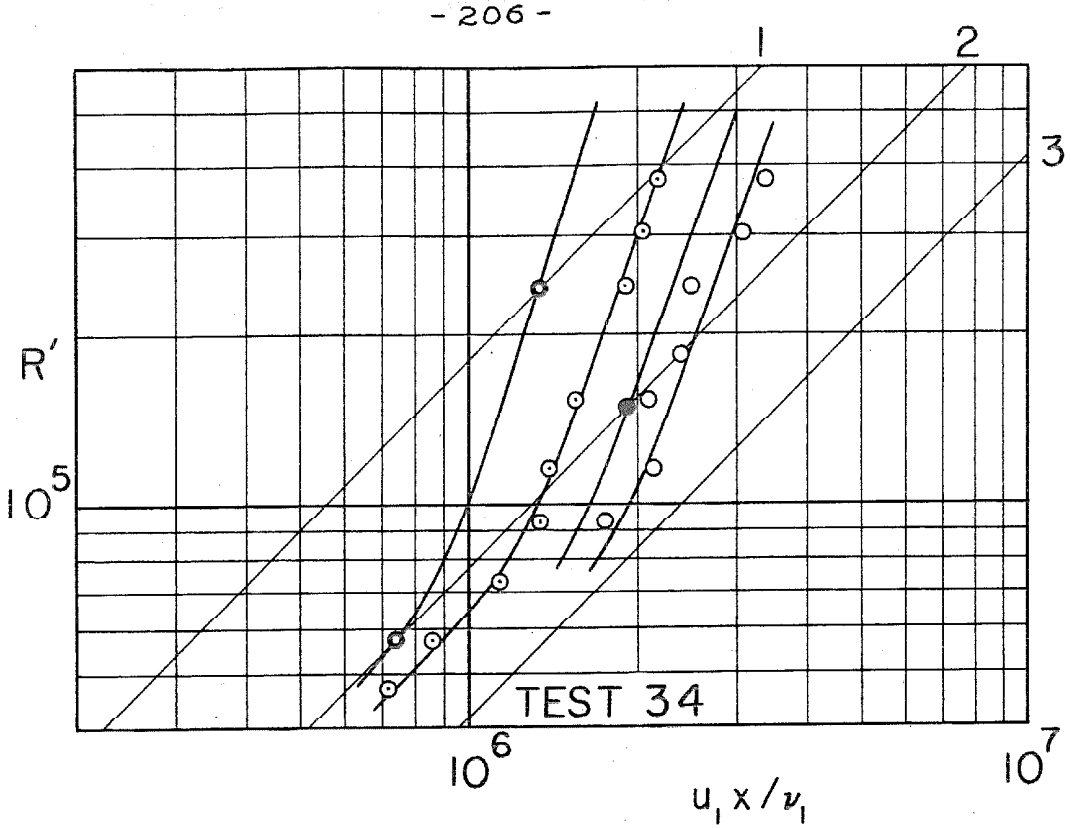

FIGURE 57. NATURAL TRANSITION, M = 2.57

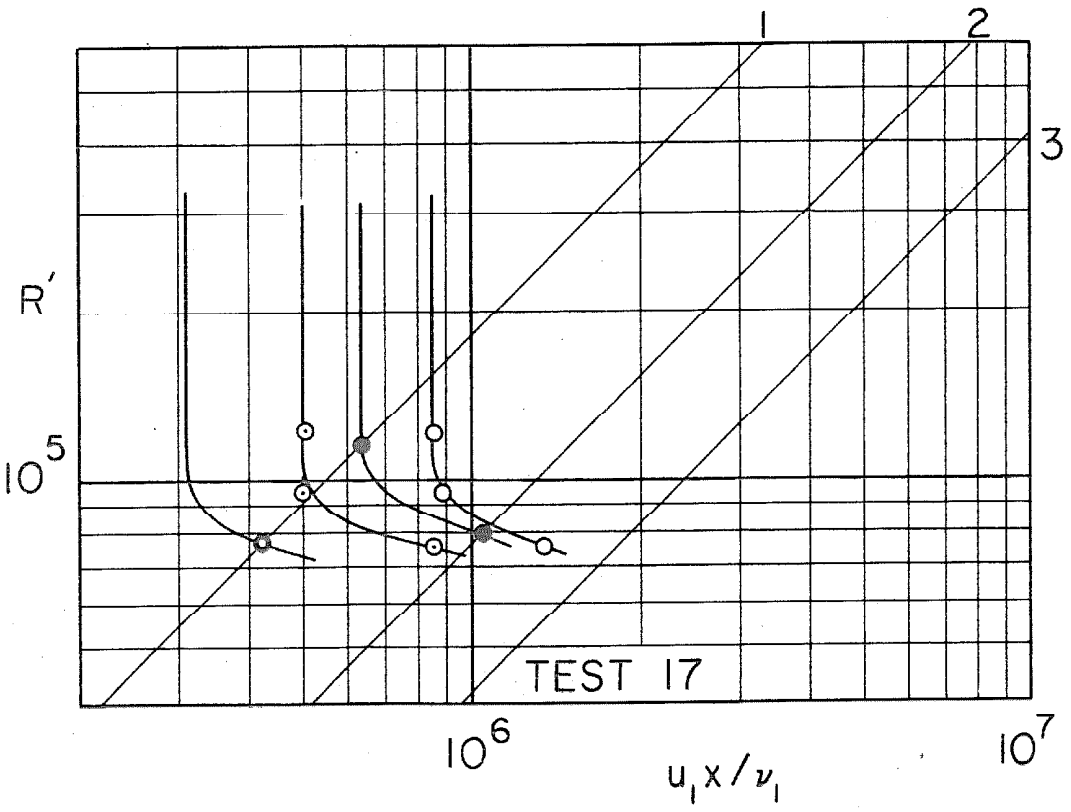

FIGURE 58. TRANSITION WITH FENCE TRIP, M = 2.57

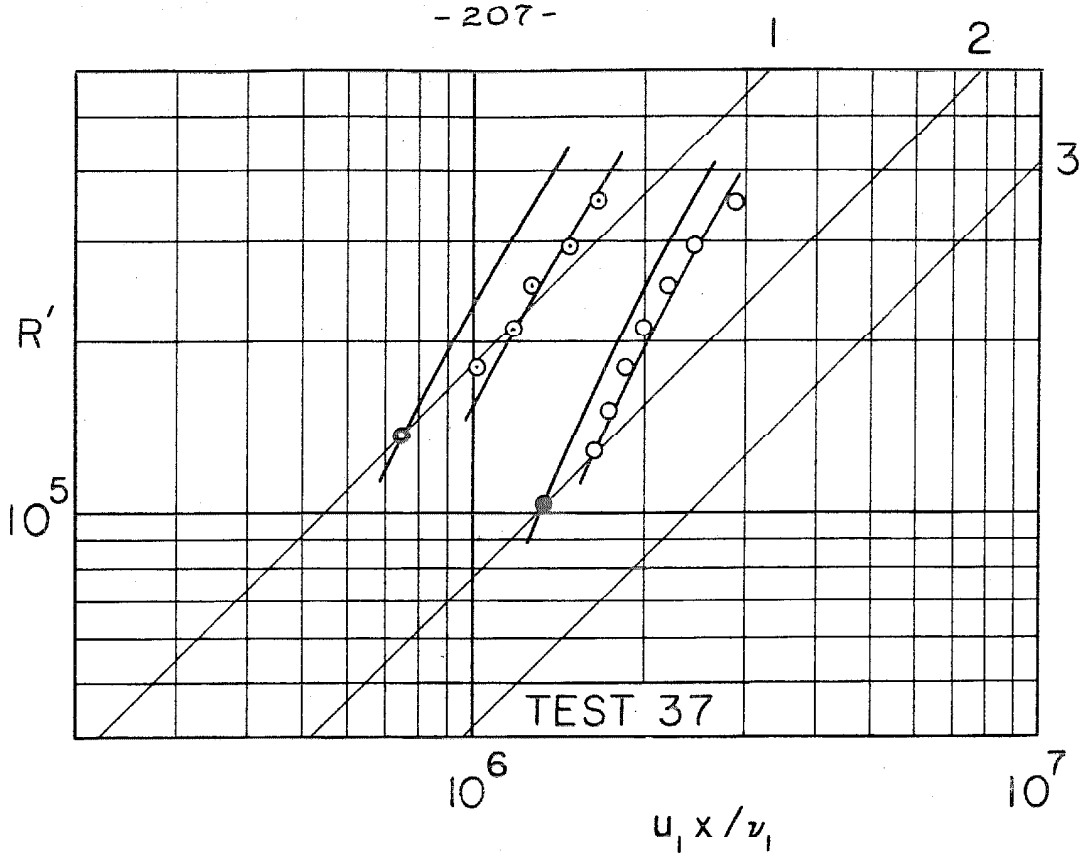

FIGURE 59. NATURAL TRANSITION, M = 3.70

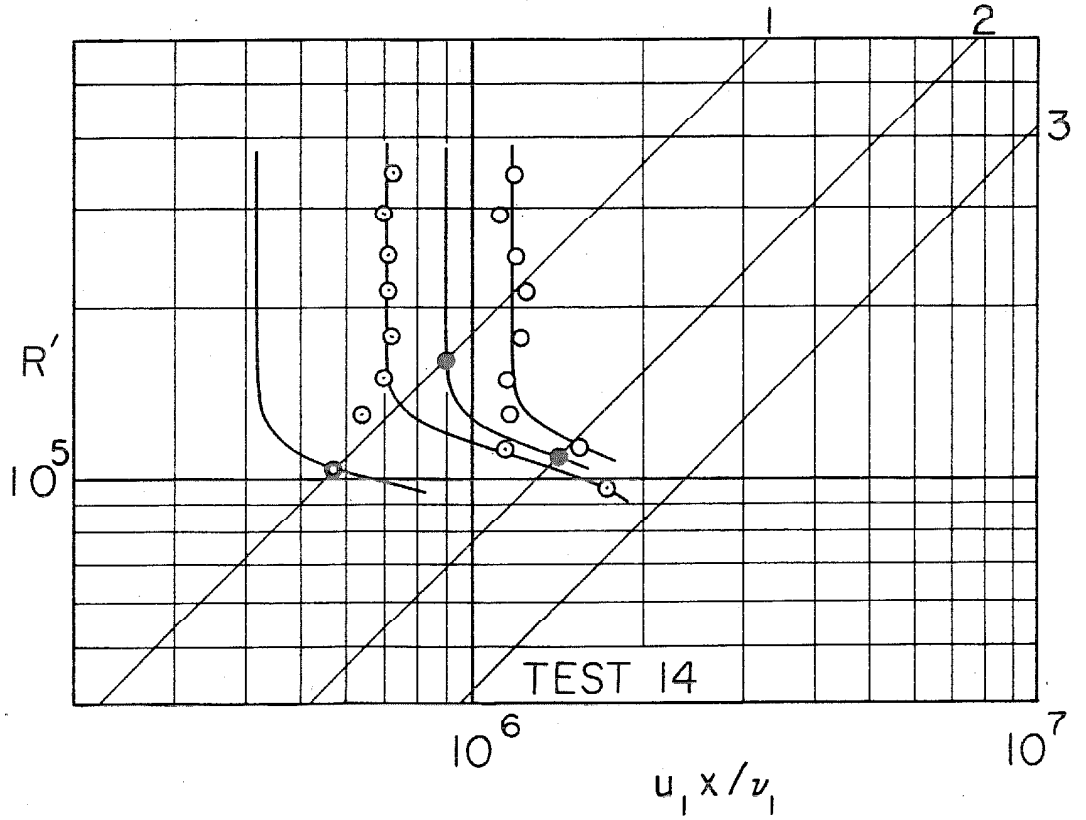

FIGURE 60. TRANSITION WITH FENCE TRIP, M = 3.70

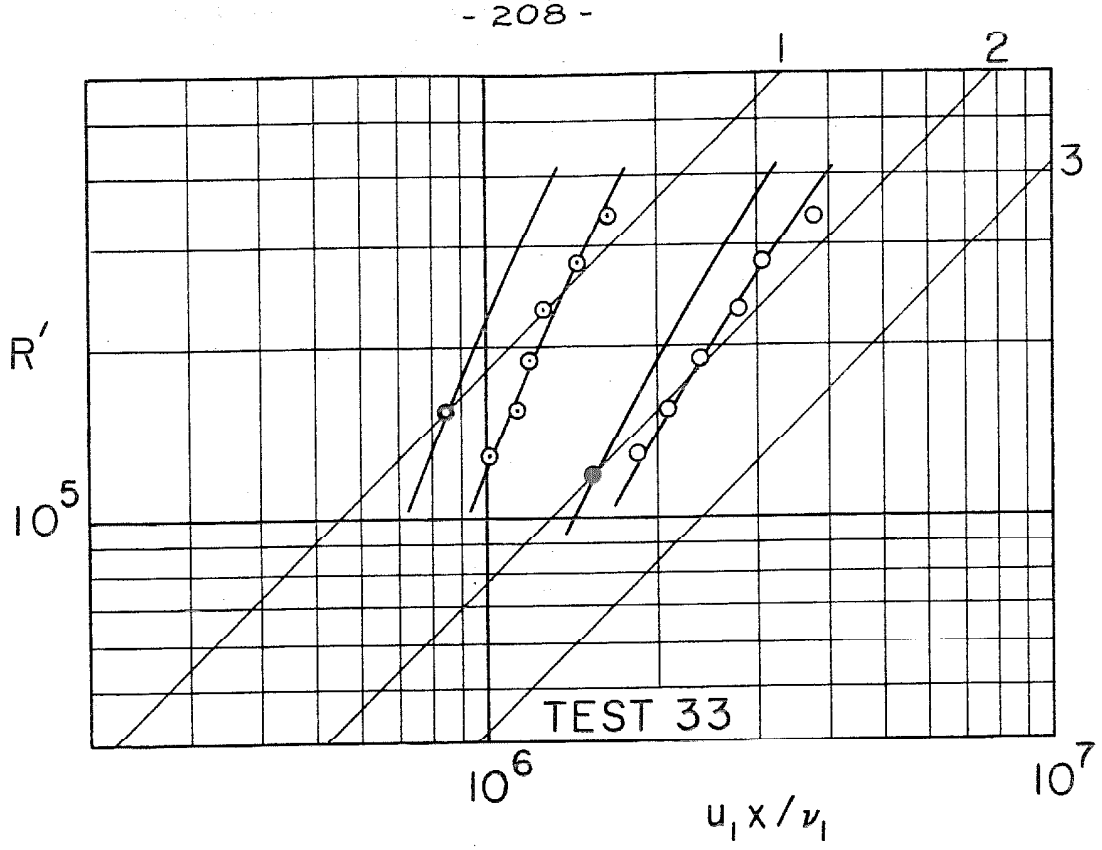

FIGURE 61. NATURAL TRANSITION, M = 4.54

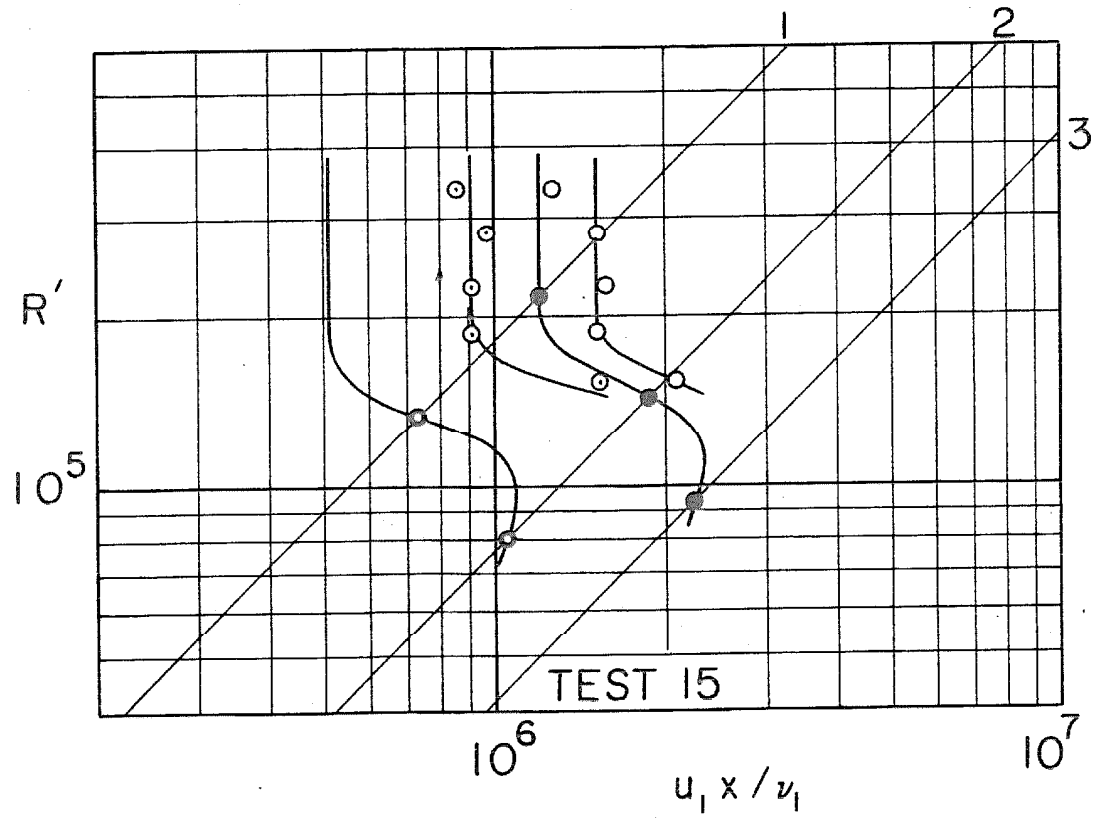

FIGURE 62. TRANSITION WITH FENCE TRIP, M = 4.54

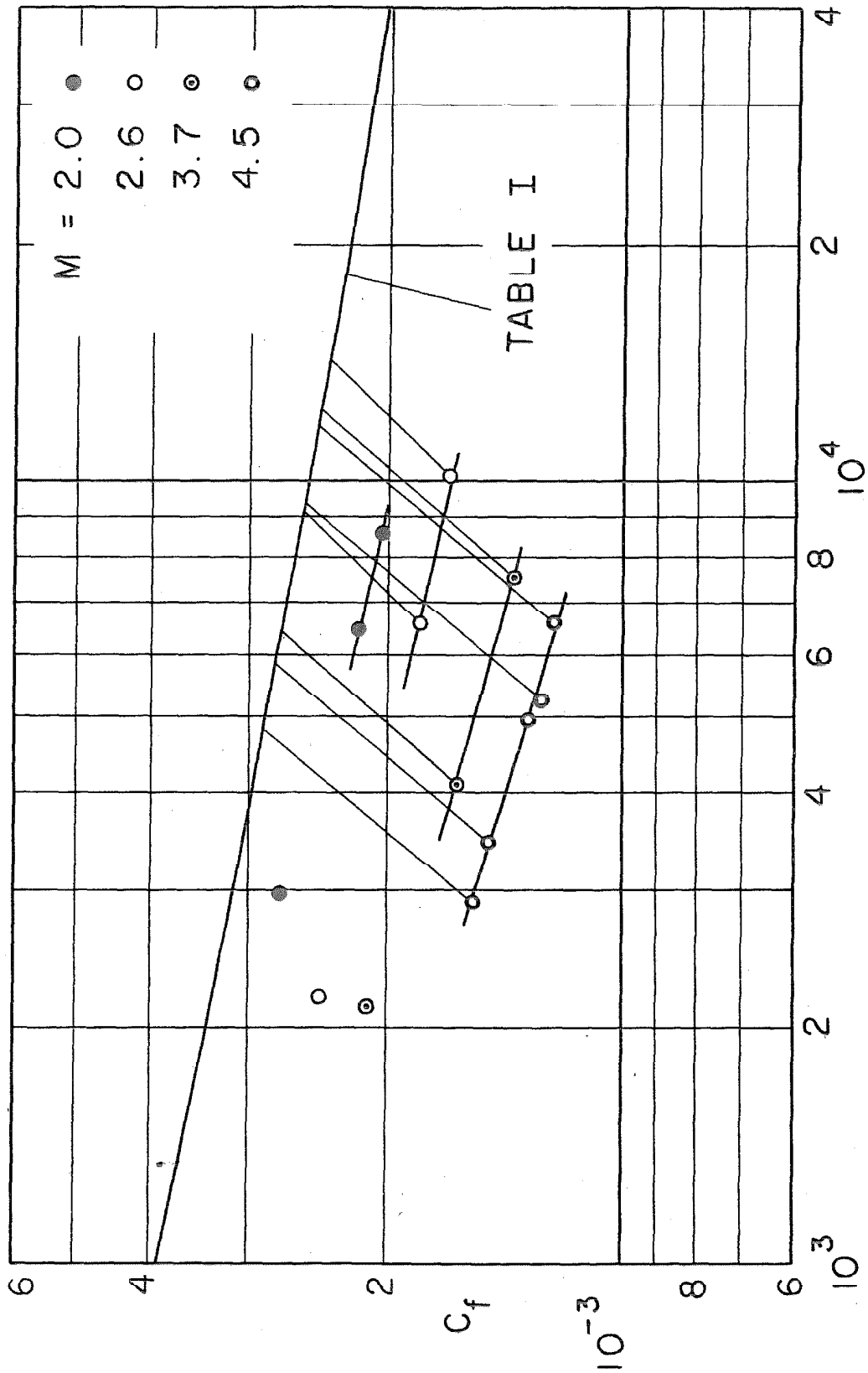

FIGURE 63. TEST OF EXPERIMENTAL DATA FOR UNIQUENESS

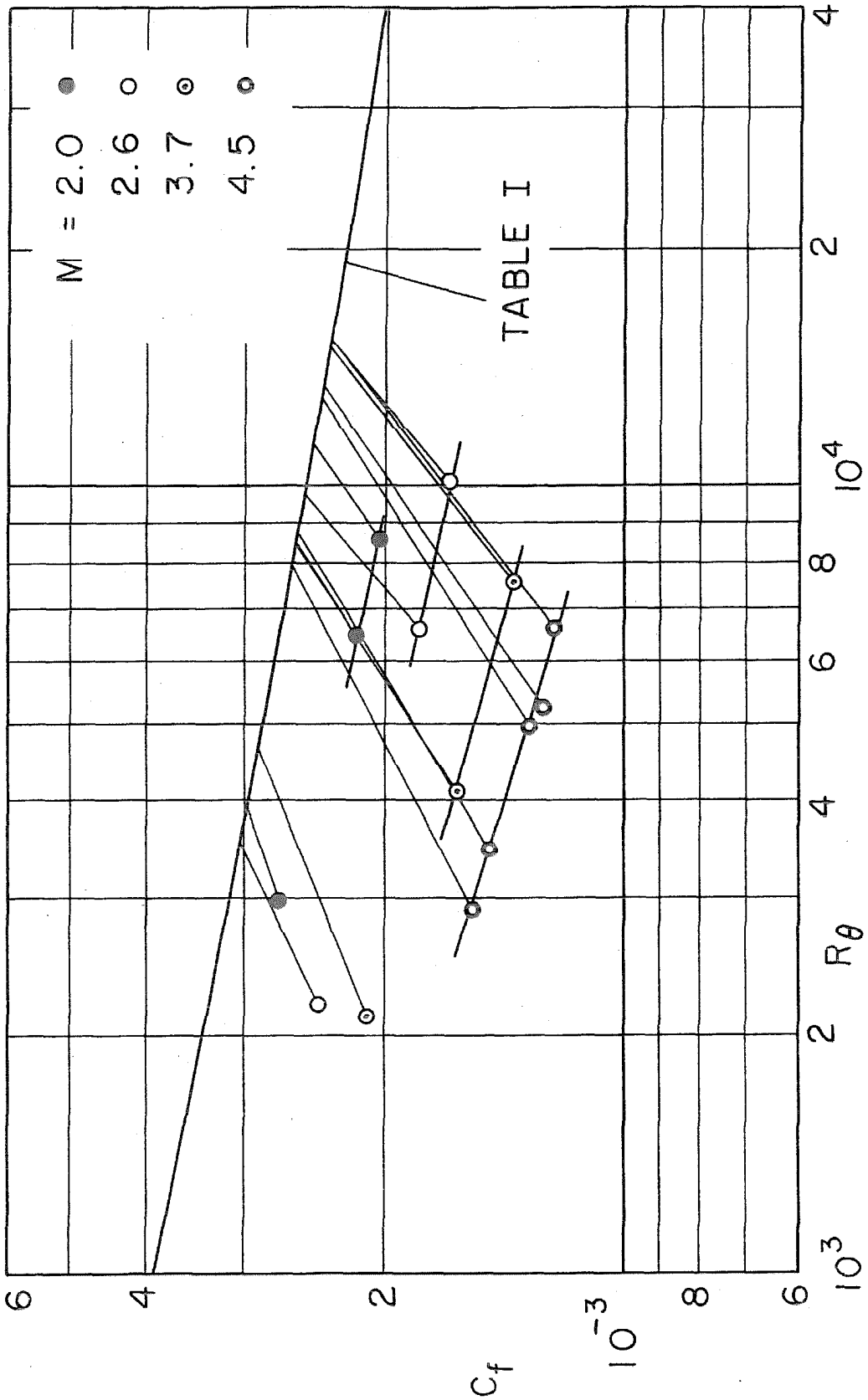

FIGURE 64. COMPARISON WITH LOW-SPEED FLOW FOR CONSTANT R_δ

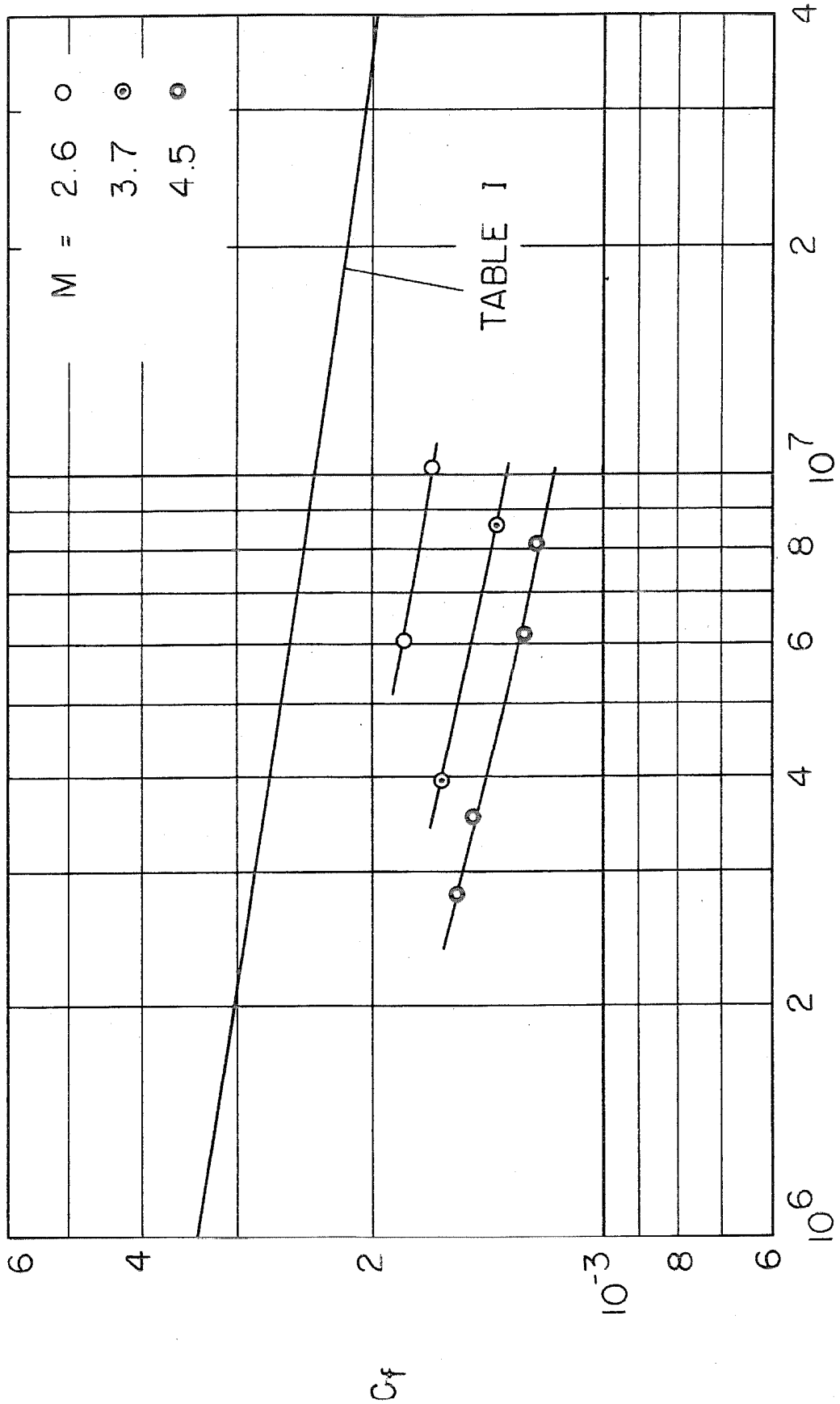

FIGURE 65. CORRECTED LOCAL FRICTION COEFFICIENTS

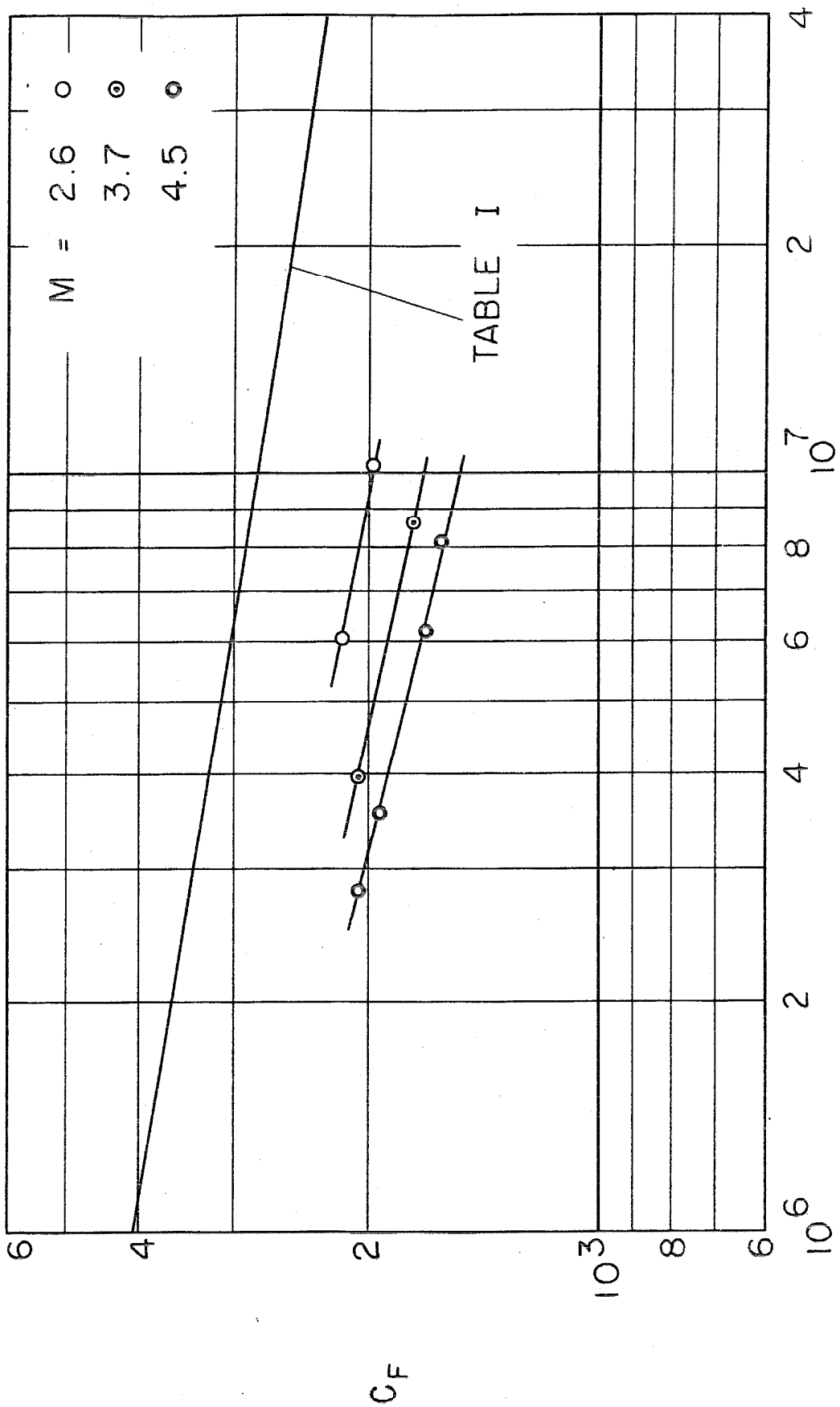

FIGURE 66. CORRECTED MEAN FRICTION COEFFICIENTS

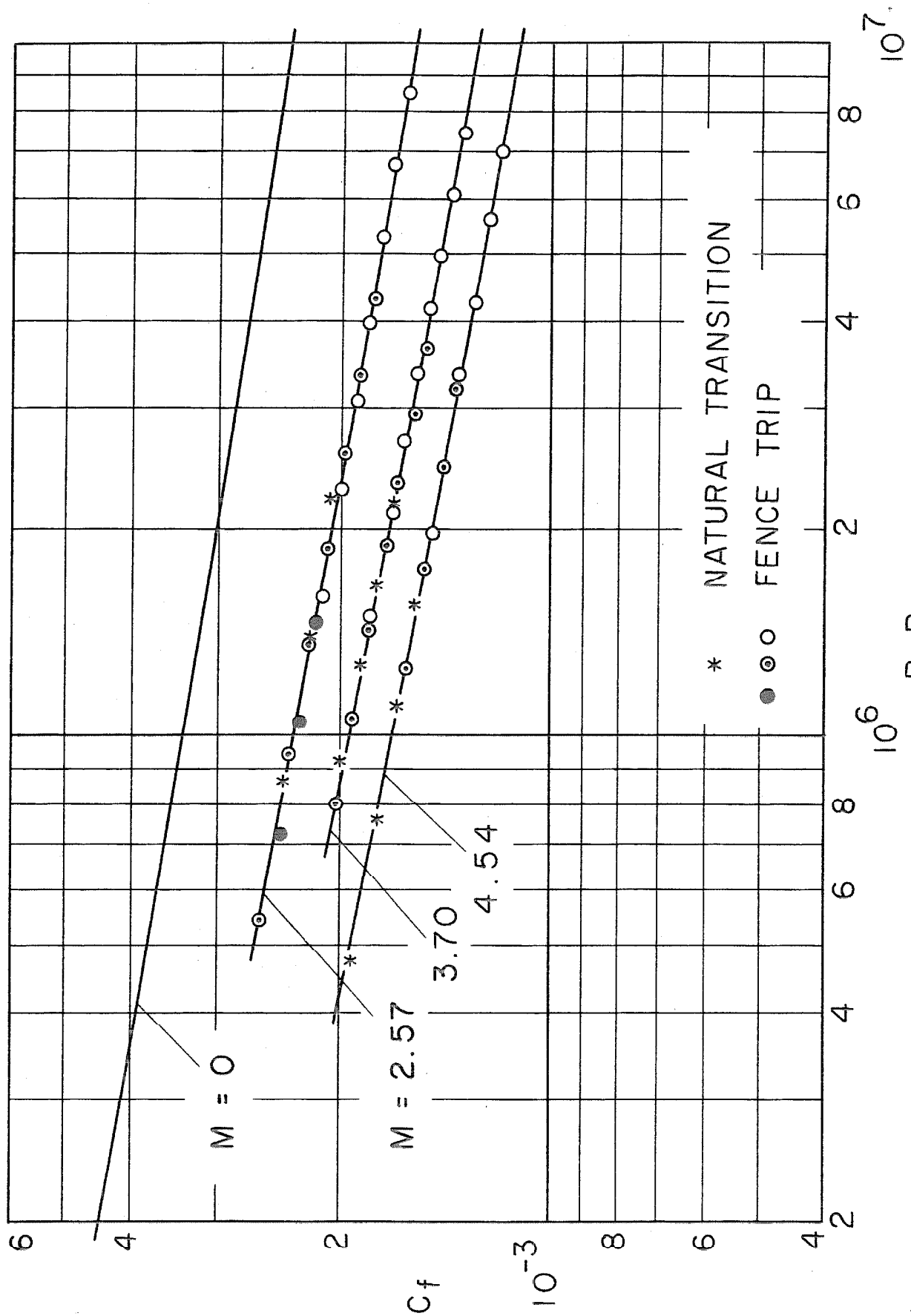

FIGURE 67 EQUIVALENCE OF NATURAL AND FORCED TRANSITION

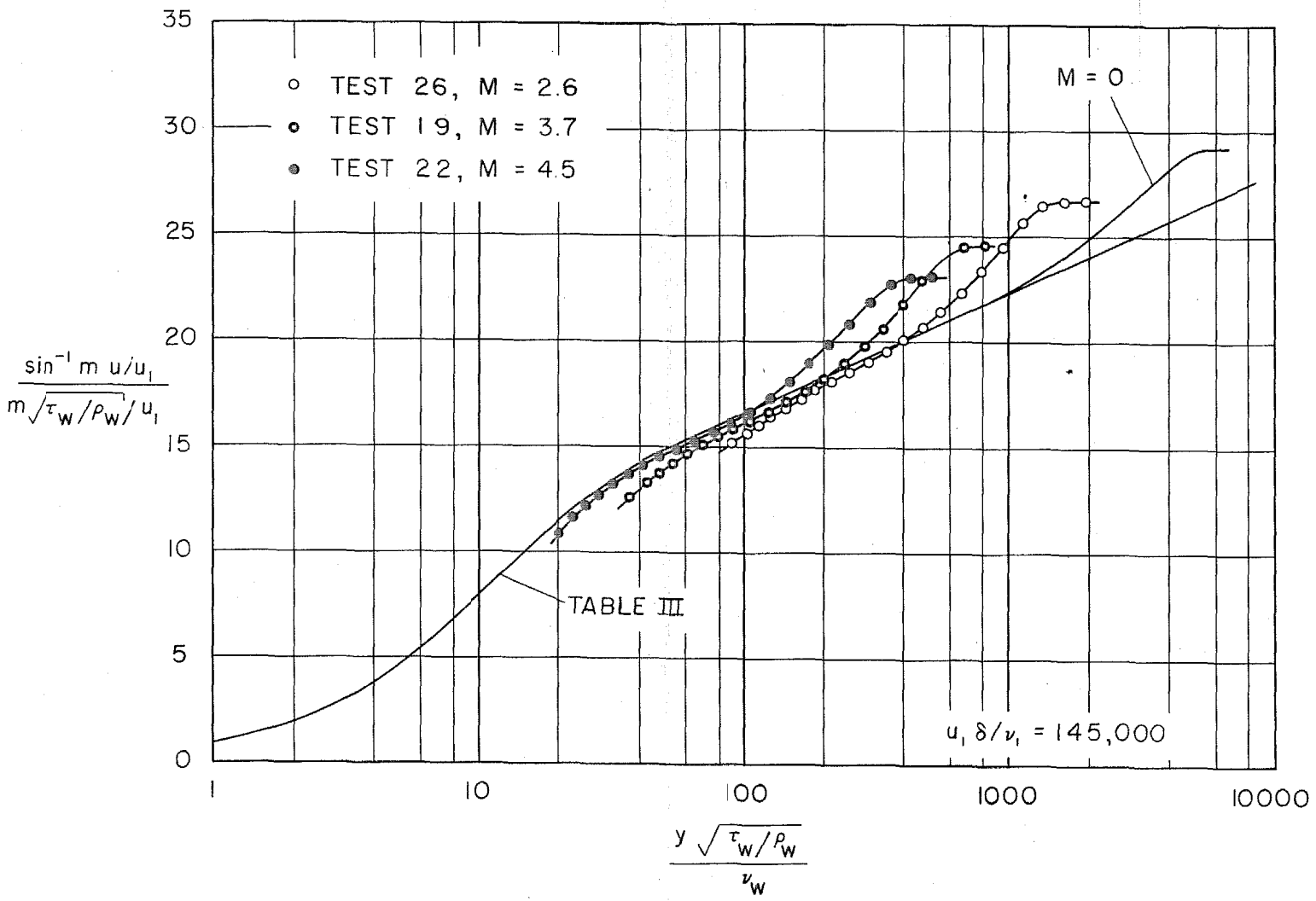

FIGURE 68 PROFILES ACCORDING TO GENERALIZED MIXING LENGTH THEORY

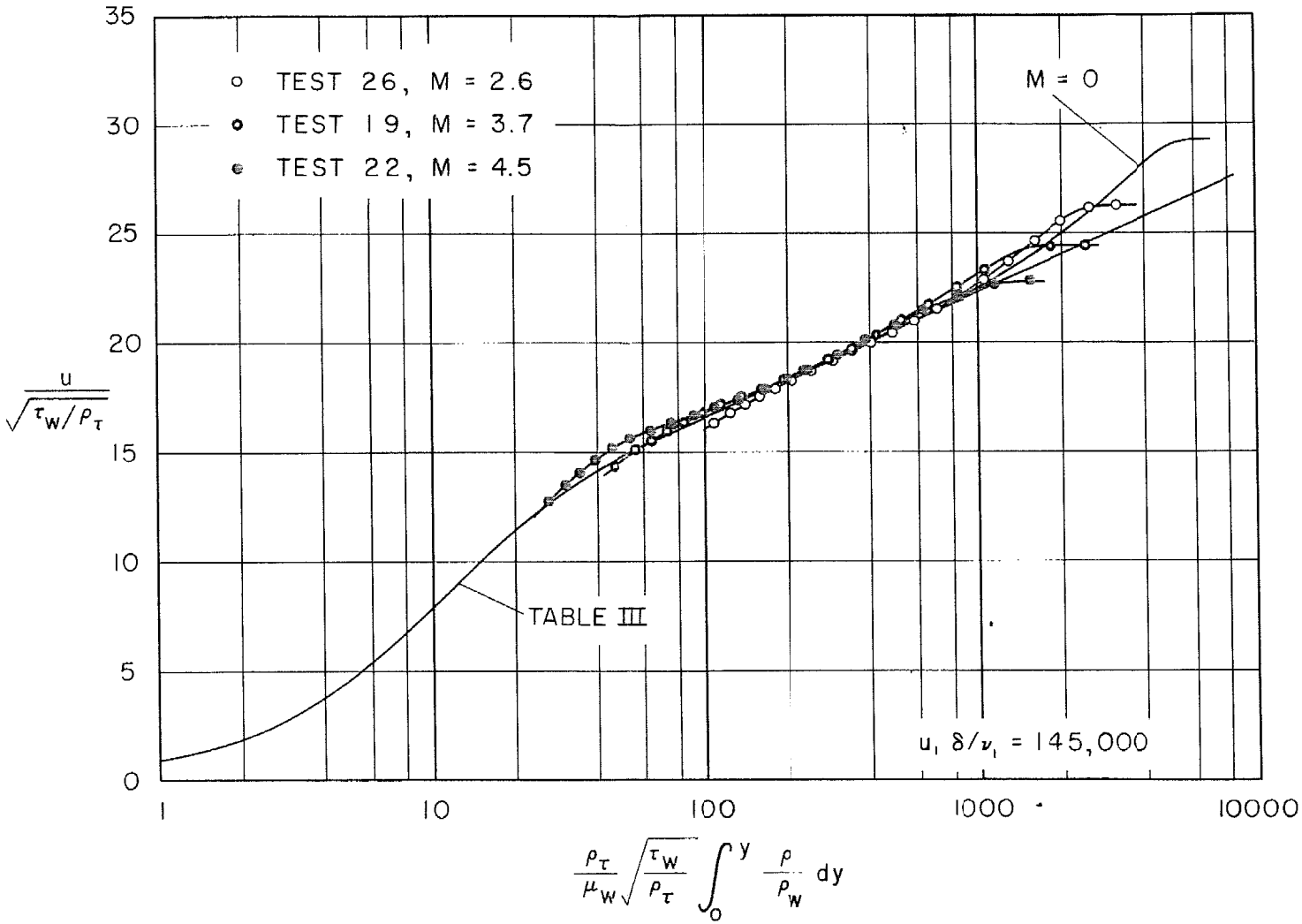

FIGURE 69 PROFILES ACCORDING TO GENERALIZED FUNCTIONAL SIMILARITY

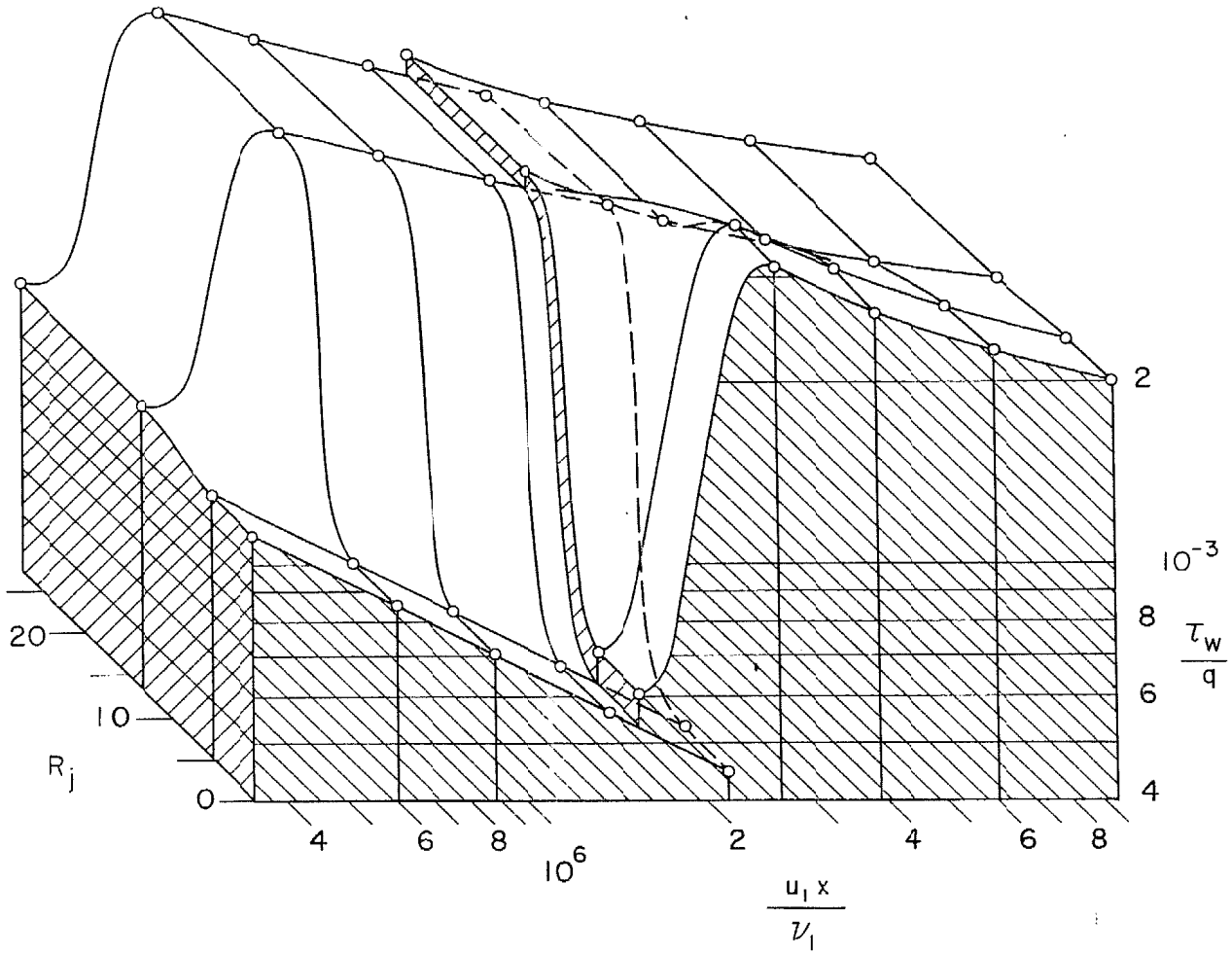

FIGURE 70. EFFECTIVENESS OF AIR JETS, M = 2.0

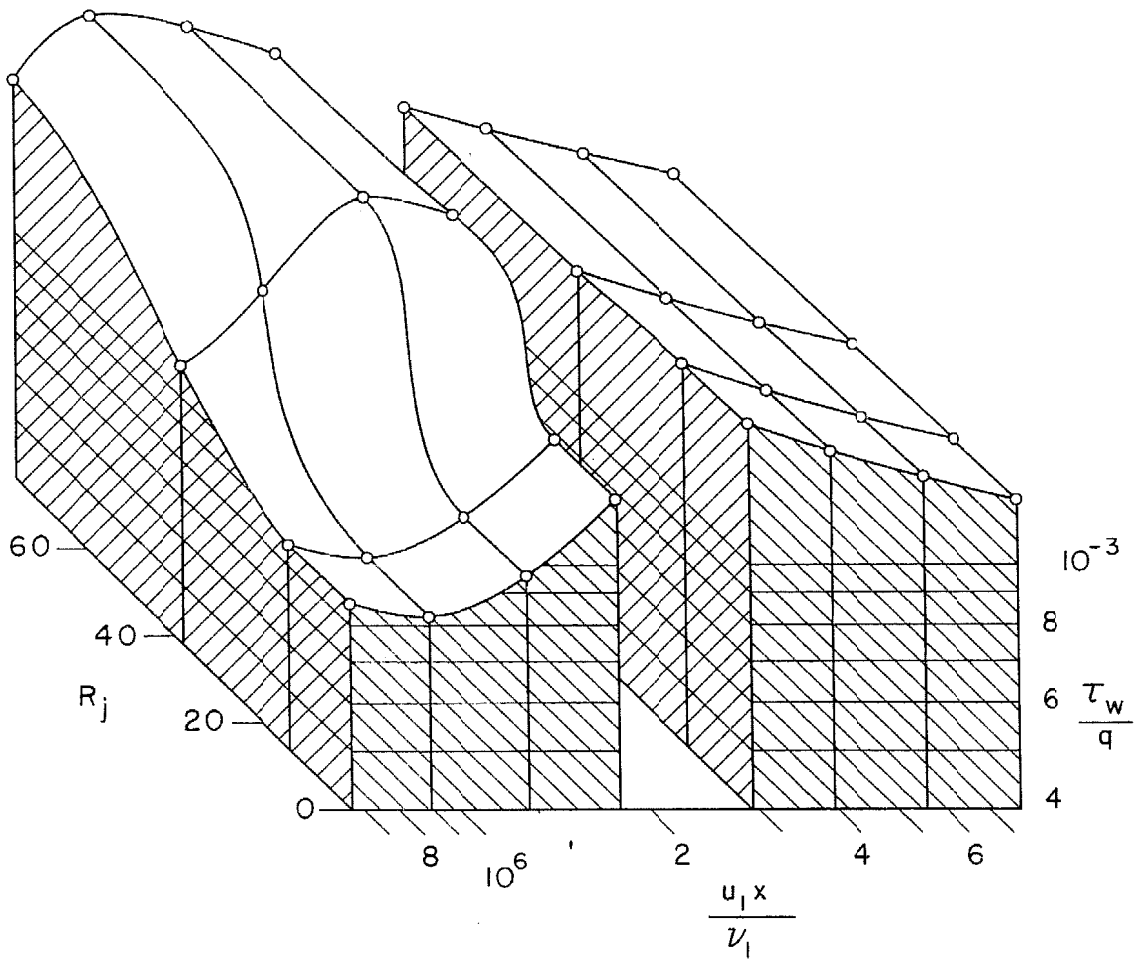

FIGURE 71. EFFECTIVENESS OF AIR JETS, M = 4.5

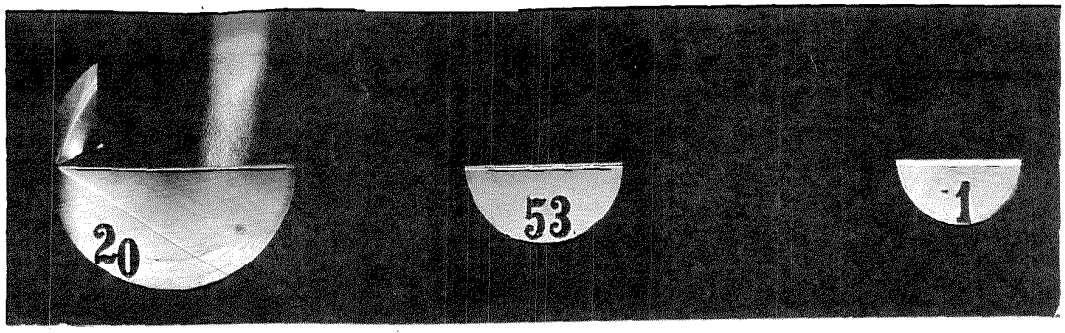

$R_j = 0$

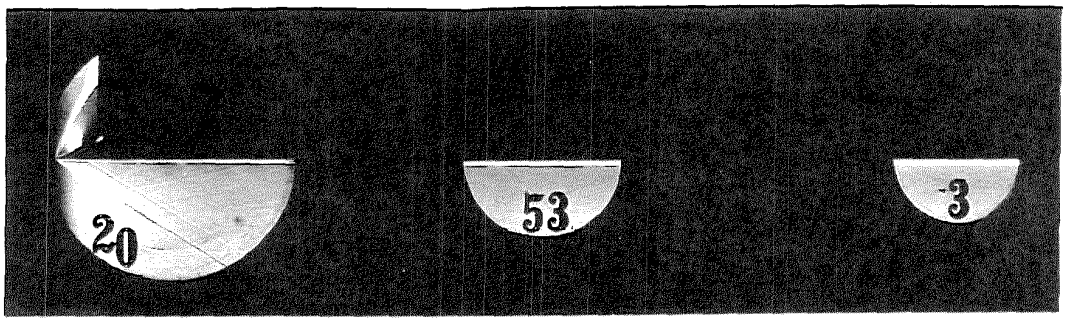

$R_j = 5$

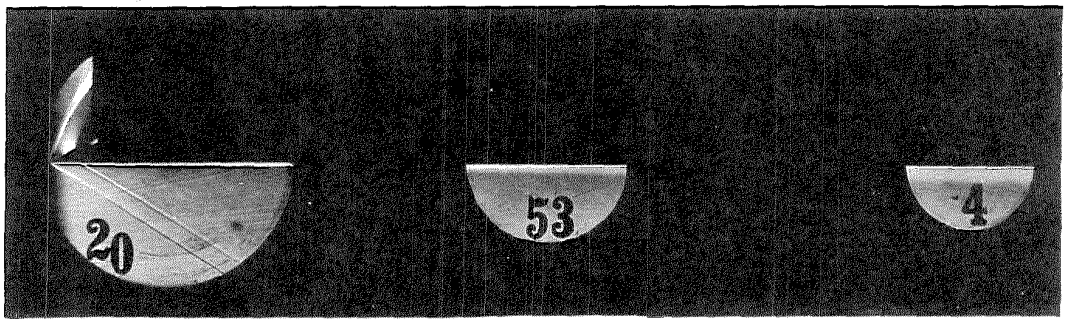

$R_j = 13$

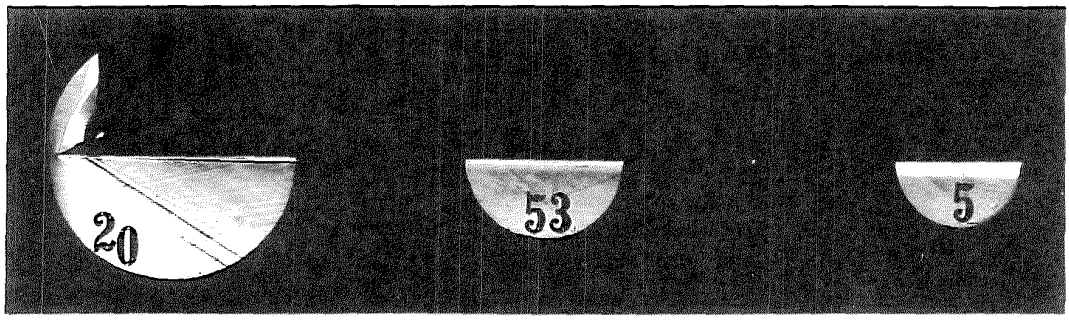

$R_j = 27$

FIGURE-72

M = 2.0 R' = 65,000 / IN.

AMBIGUOUS STATE OF BOUNDARY LAYER IN TRANSITION REGION

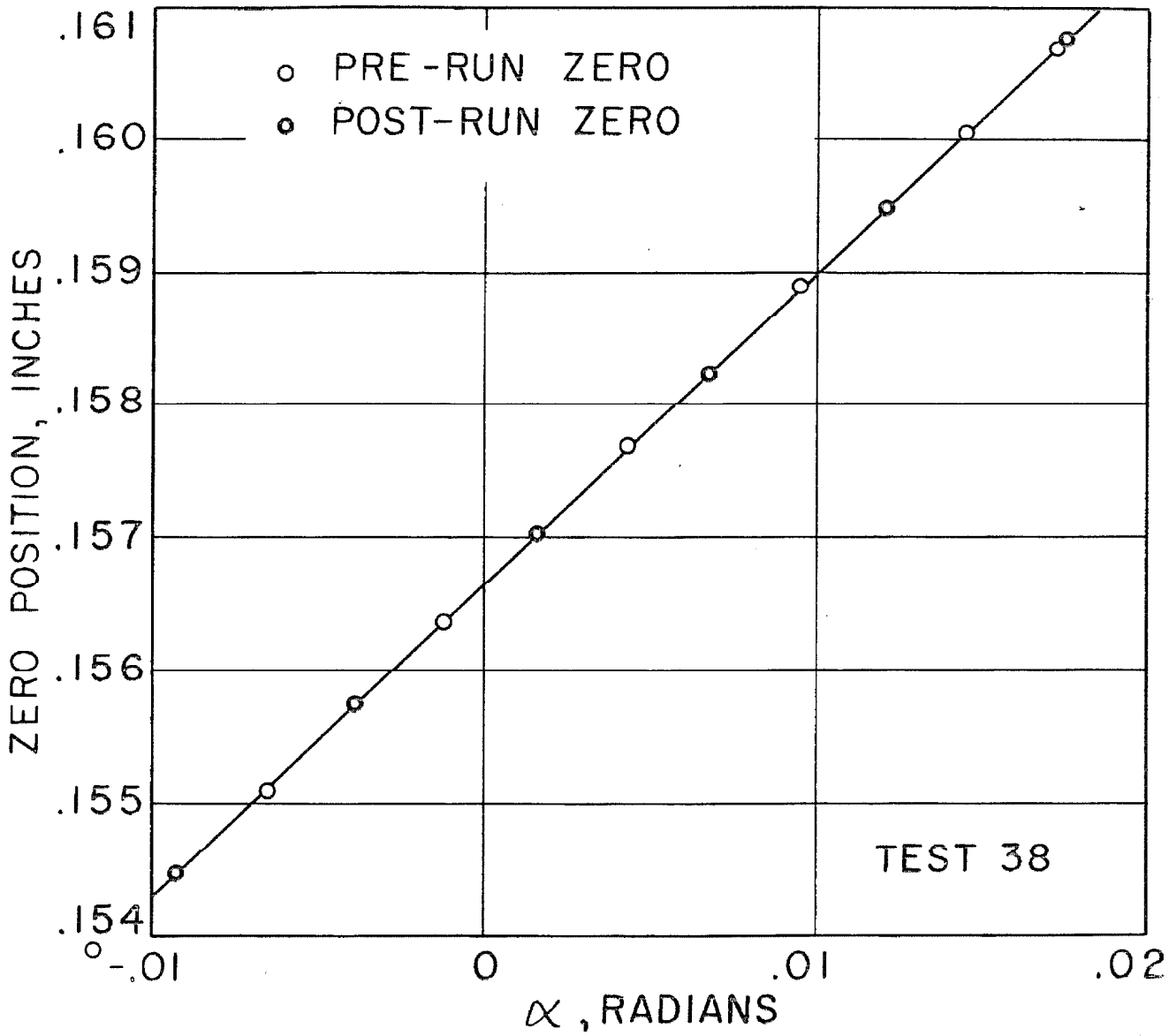

FIGURE 73. ELEMENT ZERO SHIFT WITH ANGLE OF ATTACK

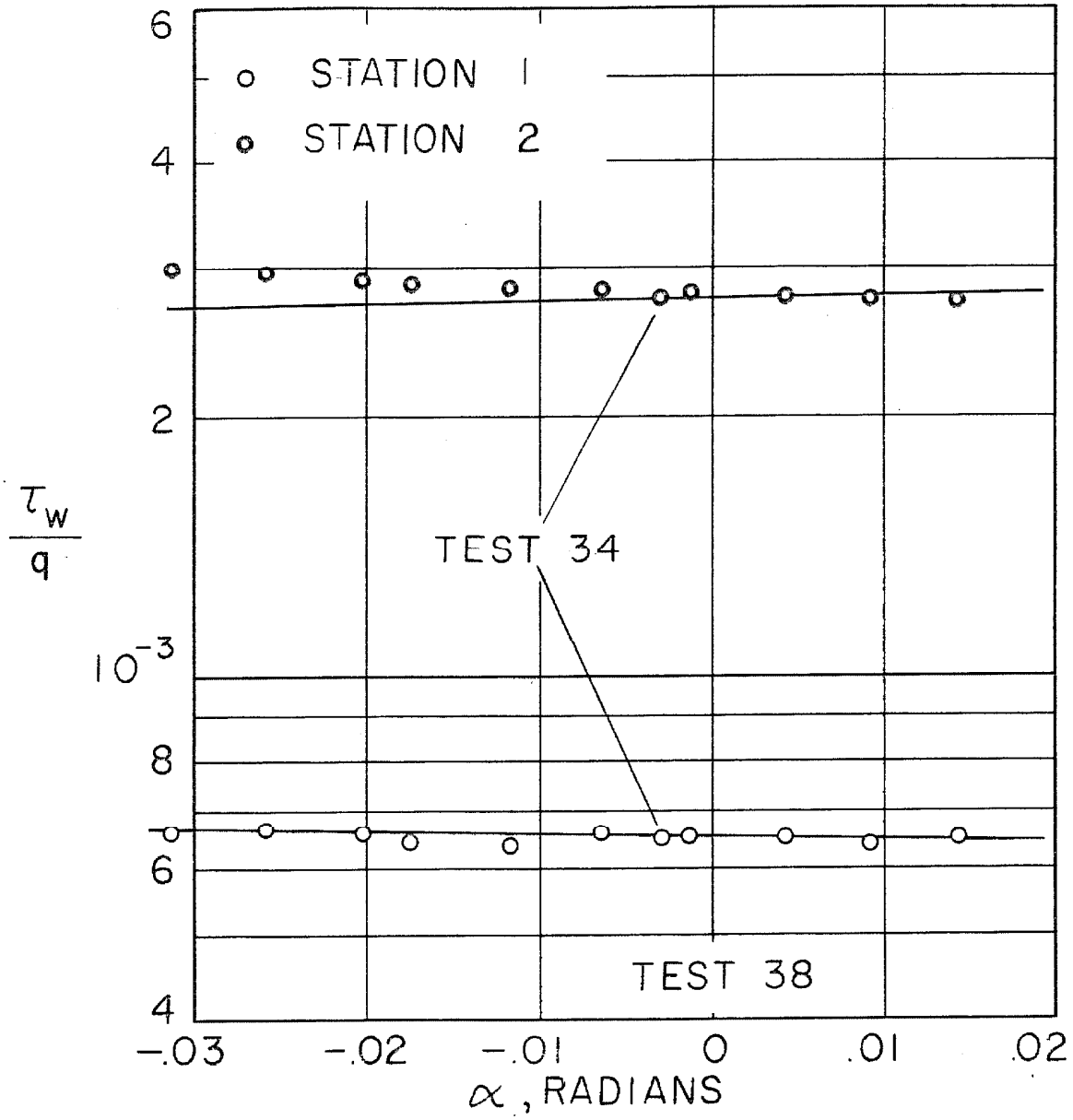

FIGURE 74. INDEPENDENCE OF FRICTION AND ANGLE OF ATTACK

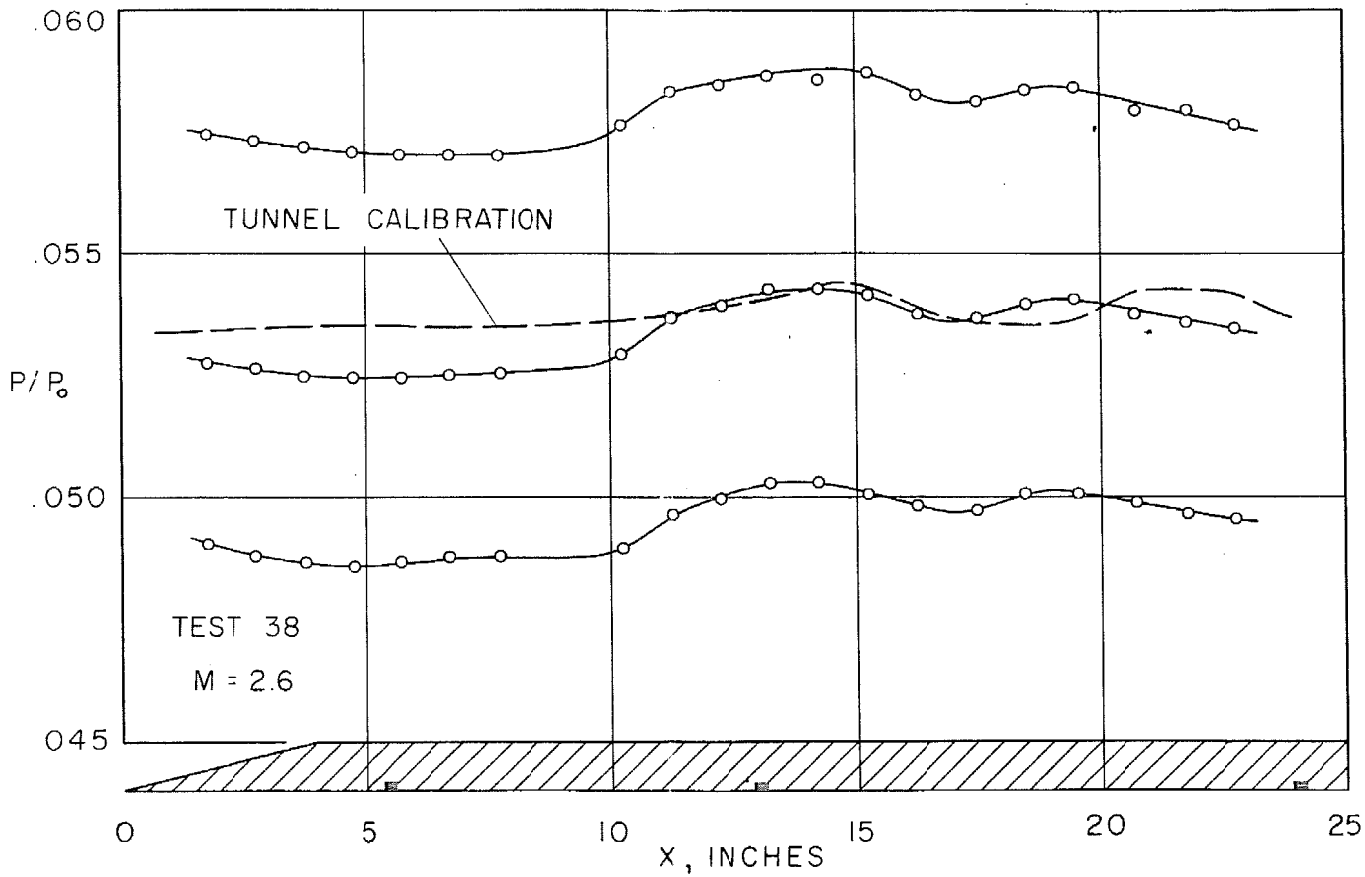

FIGURE 75 INDEPENDENCE OF PRESSURE DISTRIBUTION AND ANGLE OF ATTACK

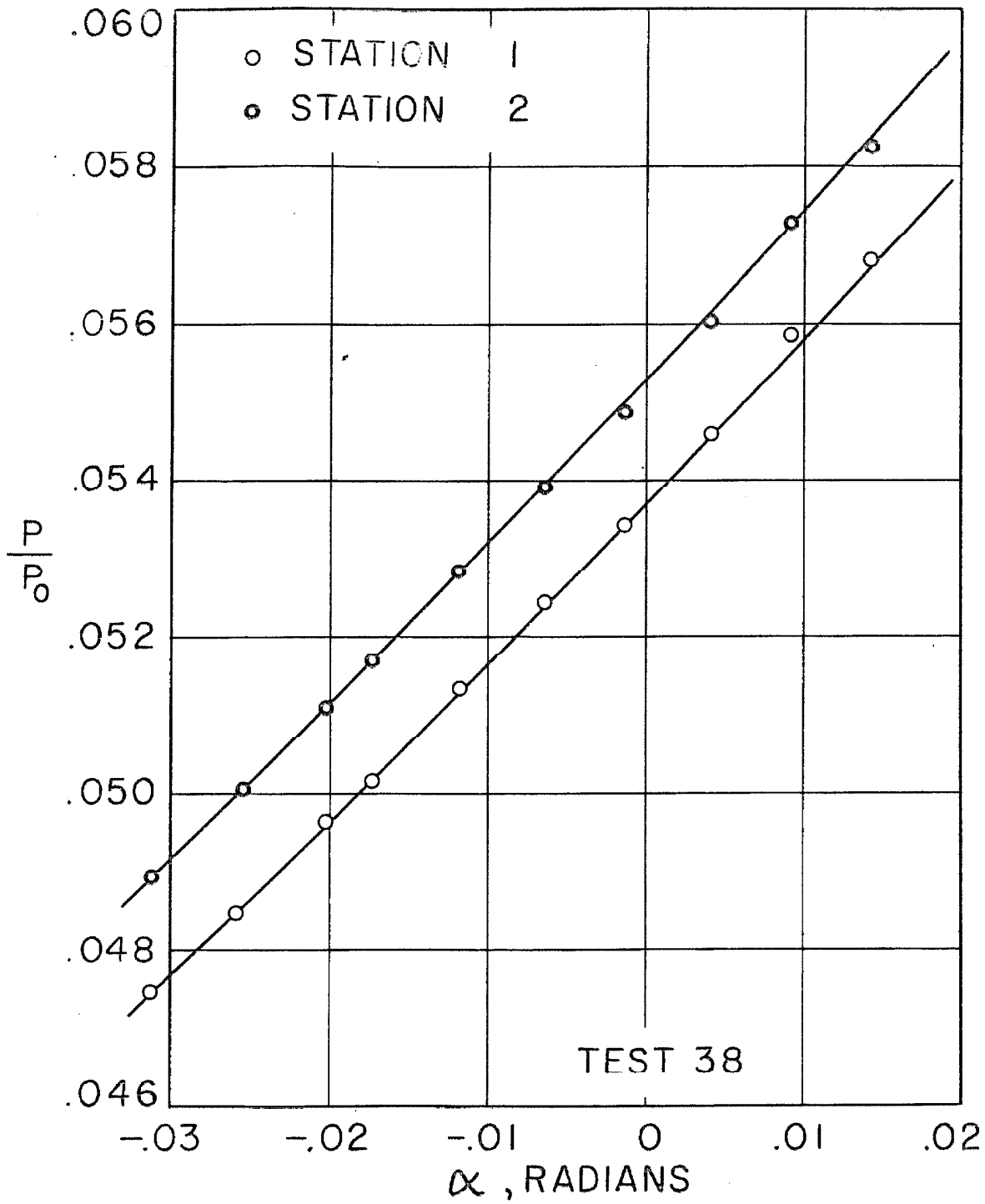

FIGURE 76. VERIFICATION OF PRANDTL-MEYER RELATIONSHIP

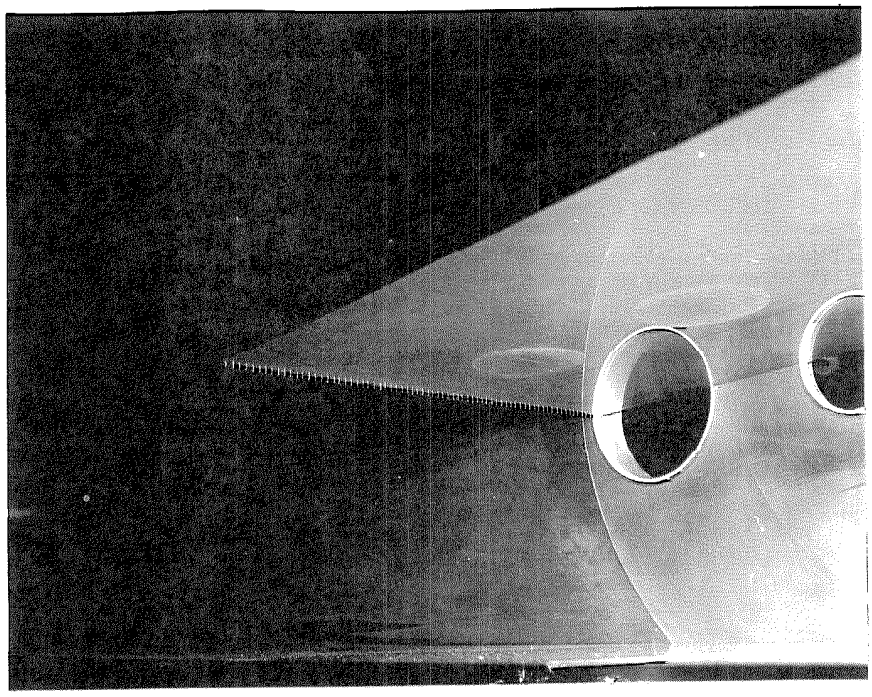

Figure 77 - Detail of the Leading Edge Fence

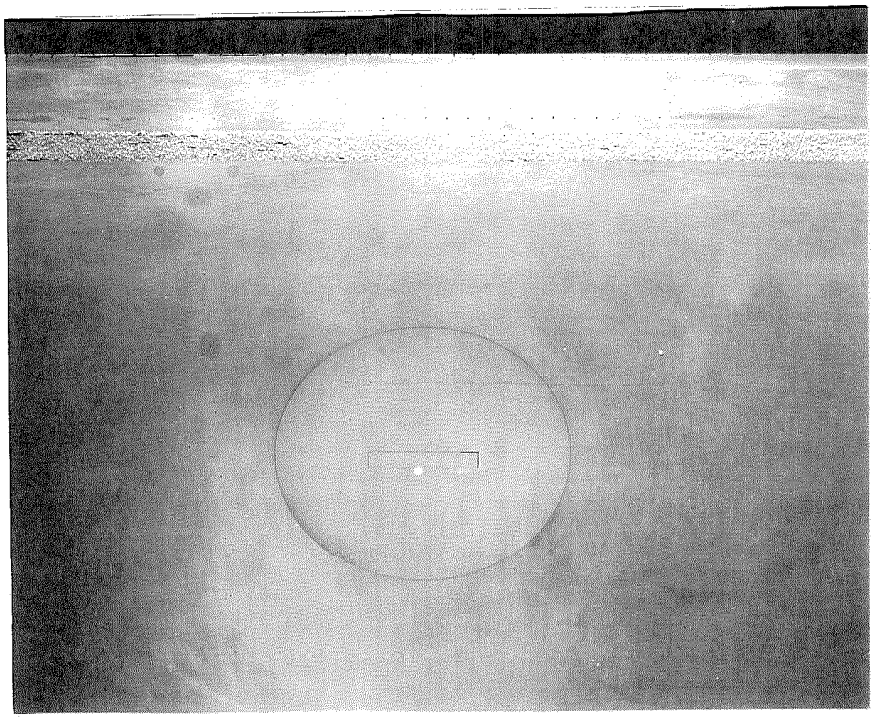

Figure 78 - Detail of the Sand Strip and Air Jets

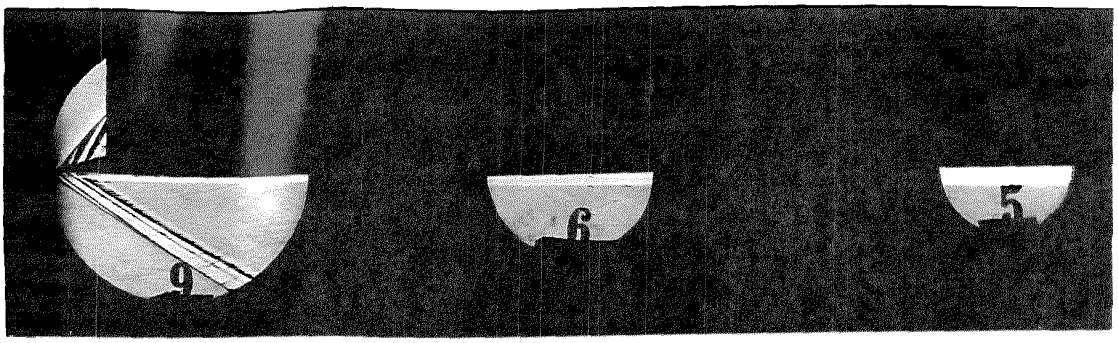

M = 2.0 R' = 188,000 / IN.

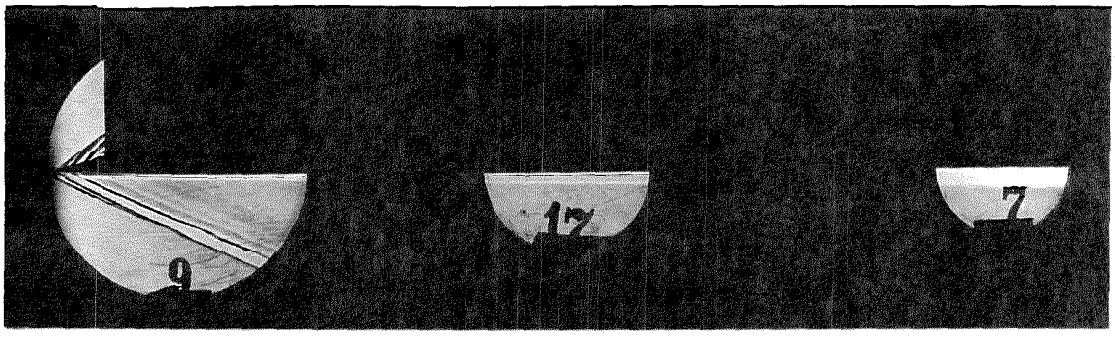

M = 2.6 R' = 192,000/IN.

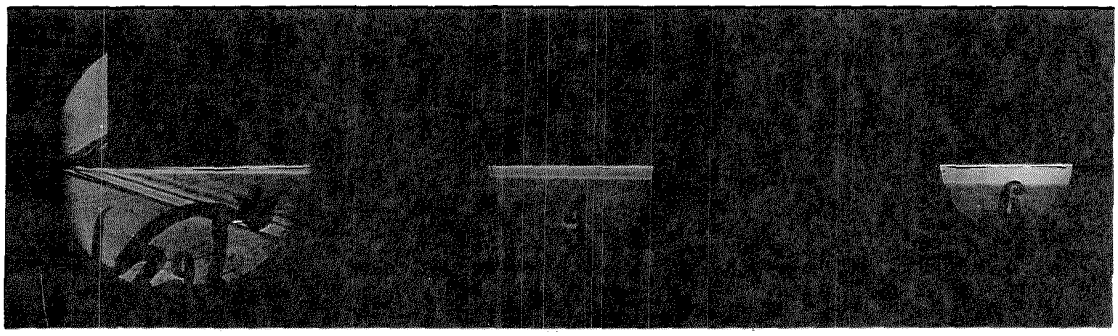

M = 3.7 R' = 211,000/IN.

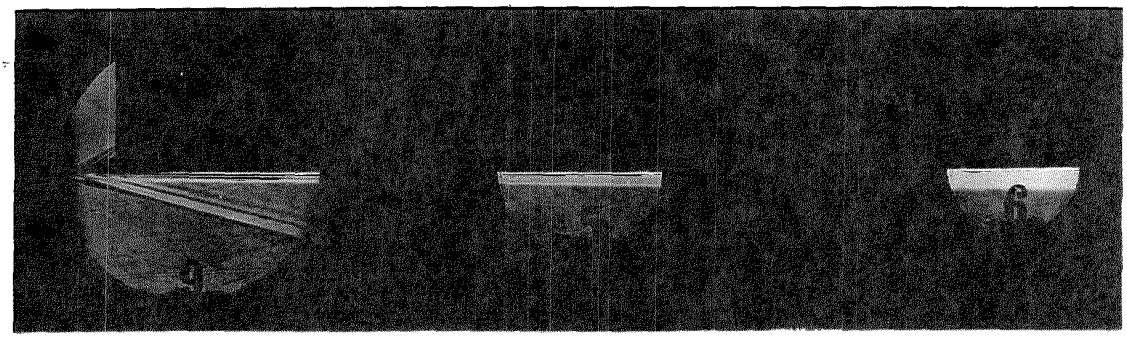

M = 4.5 R' = 188,000/IN.

EFFECT OF FENCE AT VARIOUS MACH NUMBERS

FIGURE -79

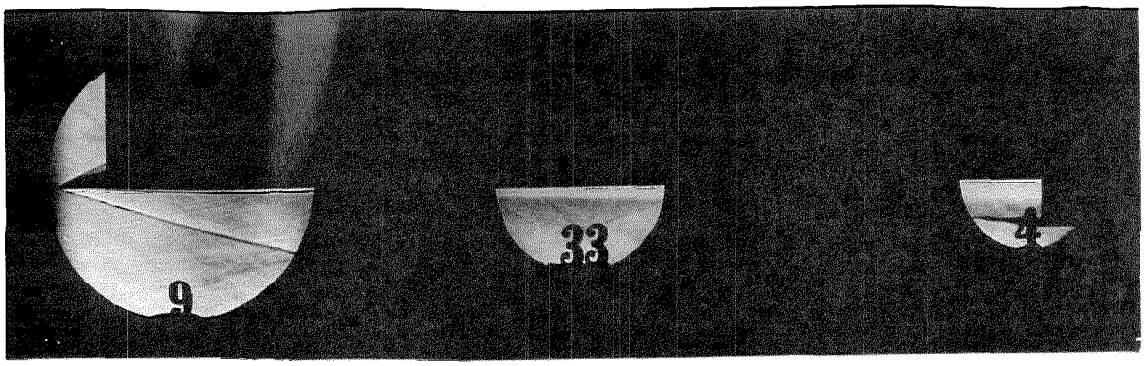

NATURAL TRANSITION $R' = 130,000$ / IN.

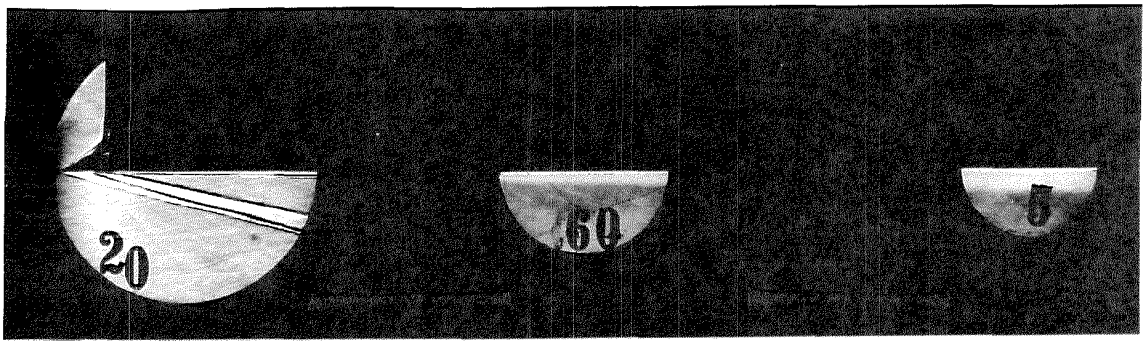

SAND TRIP $R' = 131,000$ / IN.

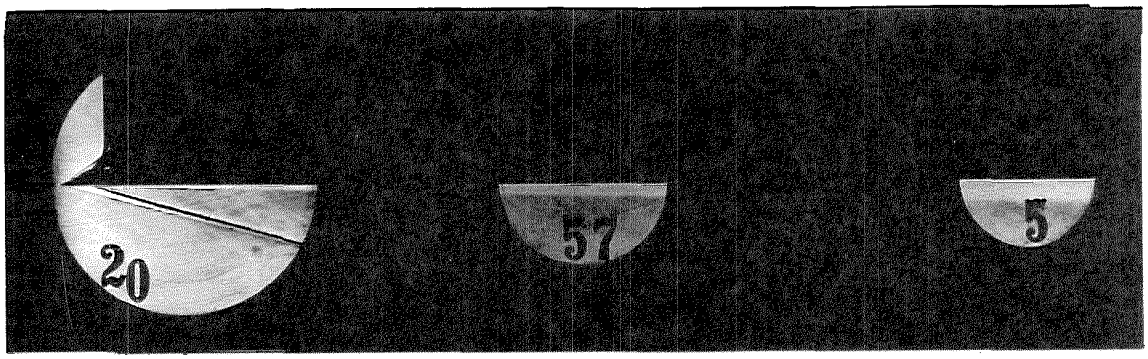

AIRJET TRIP ($R_j = 75$) $R' = 130,000$ / IN.

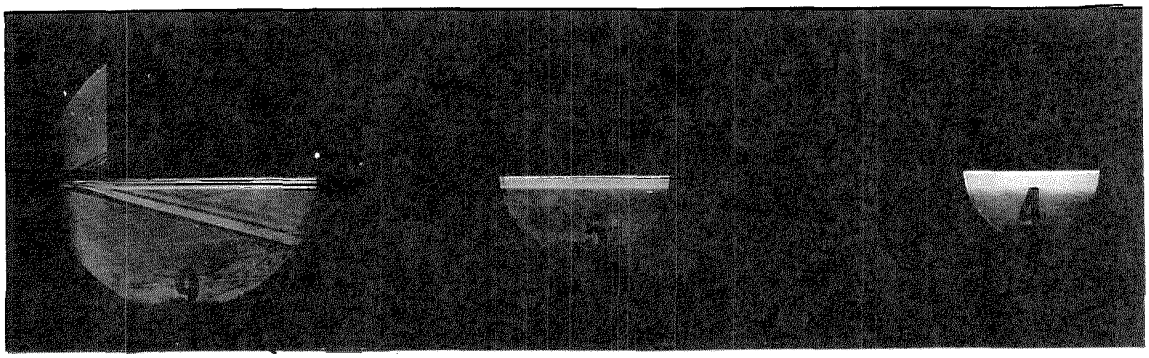

FENCE TRIP $R' = 127,000$ / IN.

COMPARISON OF TRIPPING DEVICES AT $M = 4.5$

FIGURE-80

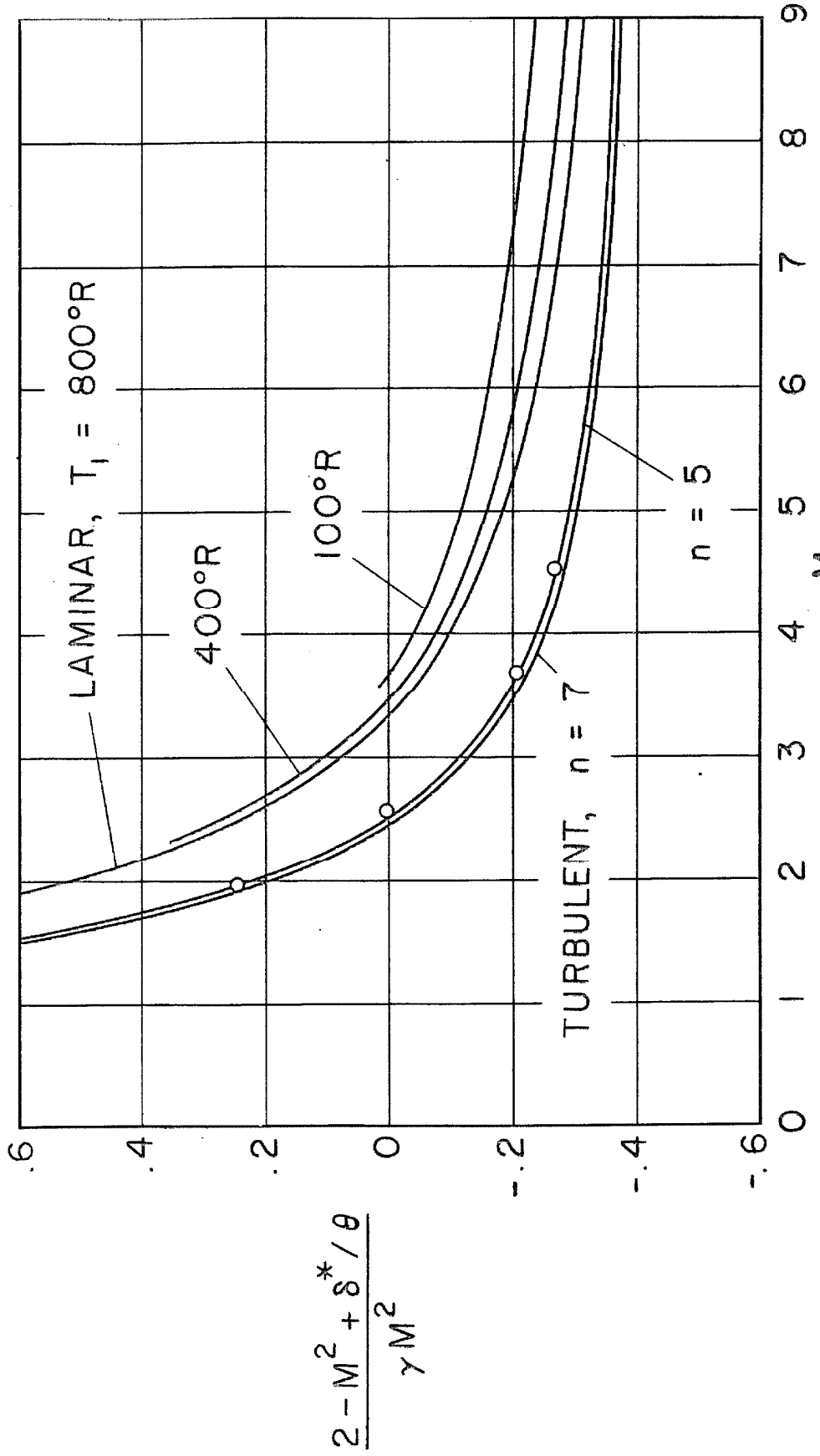

FIGURE 81 THE PRESSURE GRADIENT PARAMETER

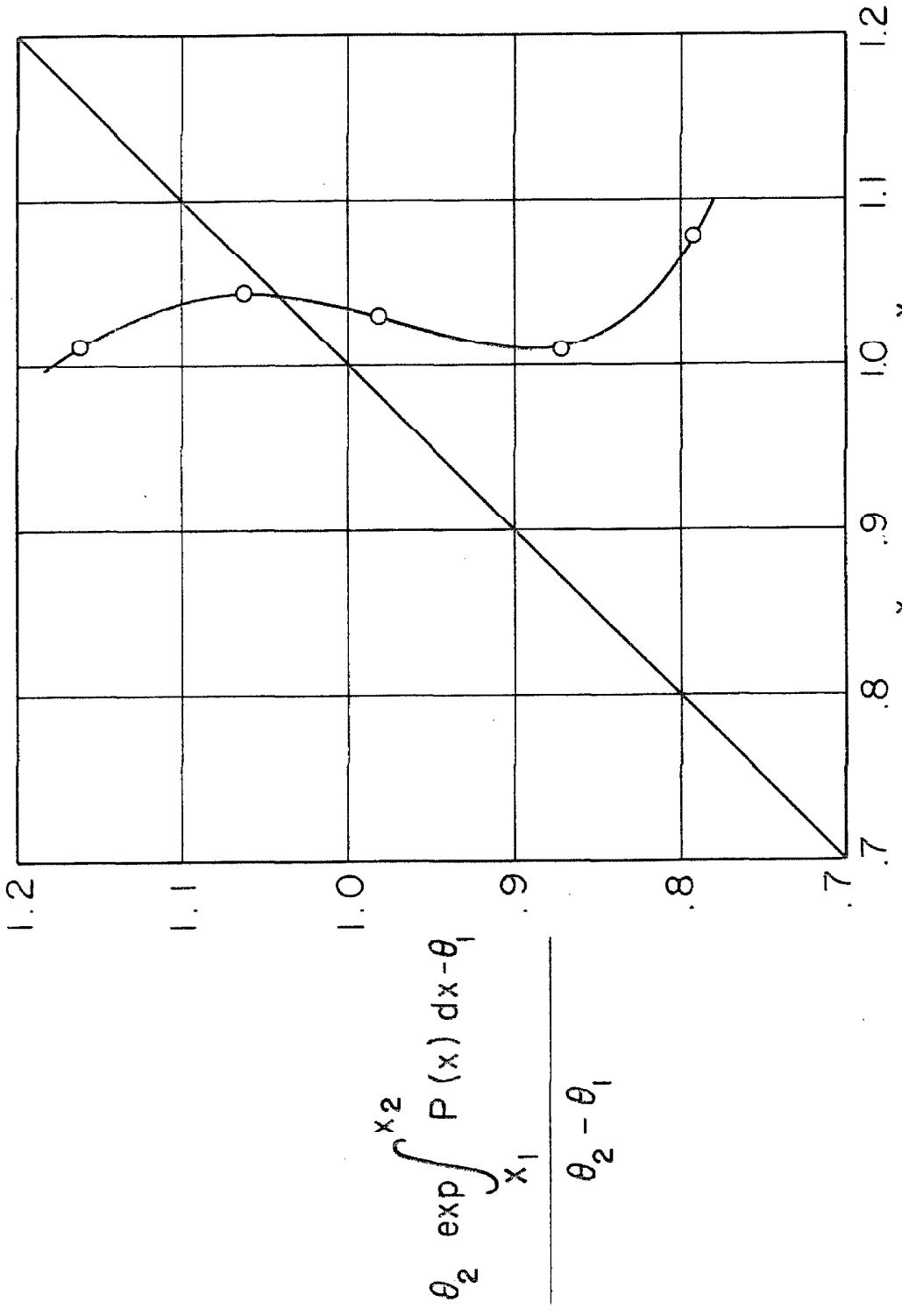

FIGURE 82 EVALUATION OF THE MOMENTUM INTEGRAL EQUATION

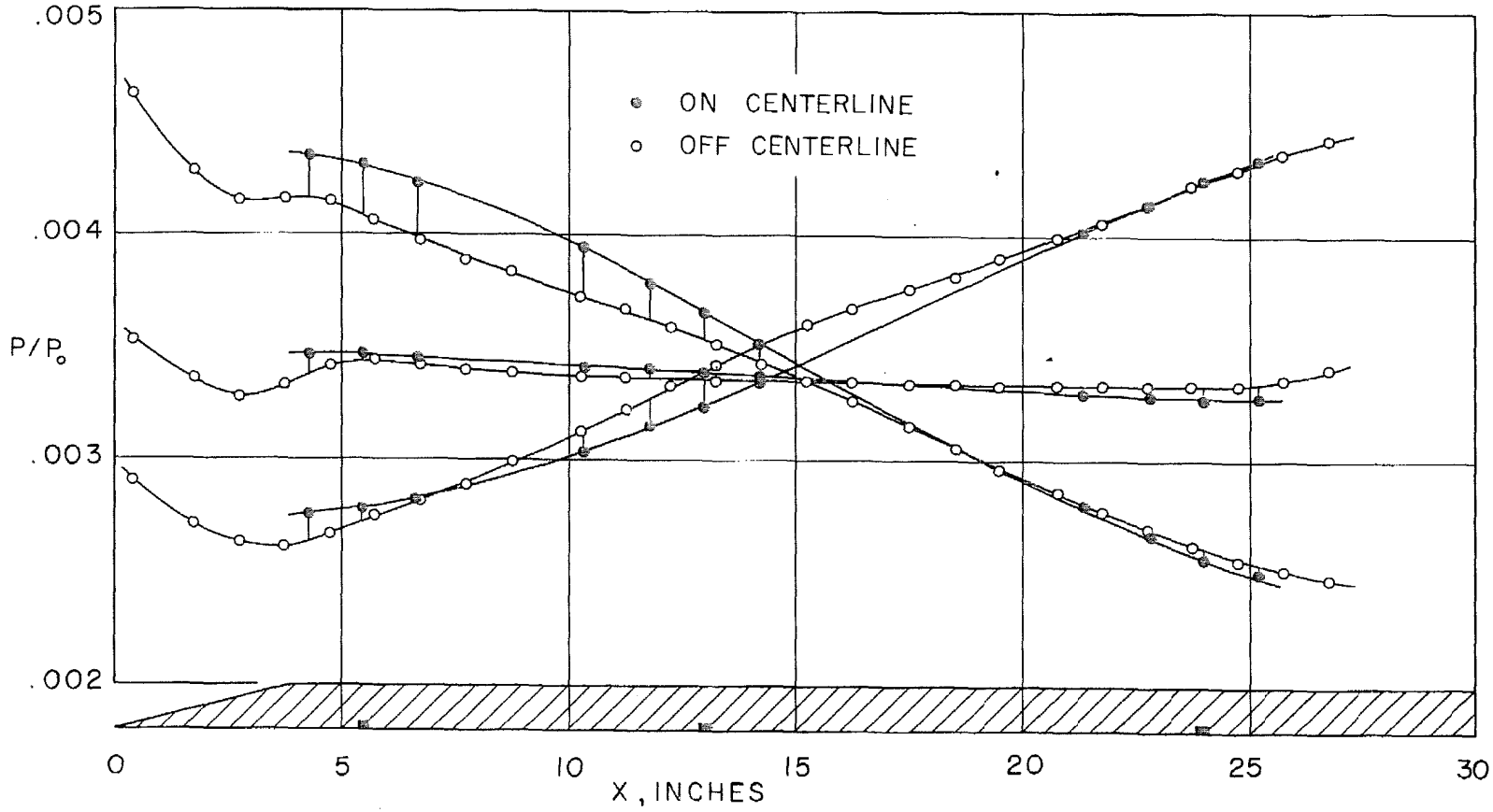

FIGURE 83 EVIDENCE OF THREE-DIMENSIONAL AMBIENT FLOW

Table A
Measured Local Friction Coefficients

Test No.	Station 1		Station 2		Station 3	
	$u_1 x/\nu_1 \cdot 10^{-6}$	$\tau_w/q \cdot 10^3$ $(R-R_t) \cdot 10^{-6}$	$u_1 x/\nu_1 \cdot 10^{-6}$	$\tau_w/q \cdot 10^3$ $(R-R_t) \cdot 10^{-6}$	$u_1 x/\nu_1 \cdot 10^{-6}$	$\tau_w/q \cdot 10^3$ $(R-R_t) \cdot 10^{-6}$
		A1 Natural Transition, M = 1.97				
35	.362	1.01	.852	.852		
	.447	.923	1.05	.731		
	.591	.812	1.39	.620		
	.755	.736	1.78	.567		
	1.02	.638	2.39	.623		
	1.31	.568	3.08	1.88		
	1.70	.501	4.03	2.83		
	2.20	.444	5.21	2.41		
		A2 Fence Trip, M = 1.97				
16	.360	1.19	.852	3.38	1.57	2.81
	.467	3.48	1.11	2.91	2.04	2.60
	.599	3.24	1.42	2.72	2.62	2.44
	.784	3.02	1.85	2.53	3.39	2.31
	1.03	2.84	2.45	2.36	4.50	2.18
	1.34	2.67	3.16	2.22	5.81	2.06
	1.75	2.51	4.11	2.09	7.61	1.95
	2.24	2.39	5.26	1.98	9.70	1.86
28	.450	3.37	1.06	2.94		
29	1.14	2.74	2.68	2.31		
30	1.60	2.52	3.75	2.12		

Table A
Measured Local Friction Coefficients

Test No.	Station 1		Station 2		Station 3	
	$\tau_w/q \cdot 10^3$		$\tau_w/q \cdot 10^3$		$\tau_w/q \cdot 10^3$	
	$u_1 x/\nu_1 \cdot 10^{-6}$	$(R-R_t) \cdot 10^{-6}$	$u_1 x/\nu_1 \cdot 10^{-6}$	$(R-R_t) \cdot 10^{-6}$	$u_1 x/\nu_1 \cdot 10^{-6}$	$(R-R_t) \cdot 10^{-6}$
A3 Natural Transition, M = 2.57						
34	.260	1.24	.615	.830		
	.311	1.15	.744	.772		
	.404	.983	.955	.853		
	.513	.879	1.21	1.14		
	.640	.790	1.51	2.10		
	.827	.713	1.99	2.95		
	1.02	.650	2.44	2.75		
	1.34	.603	3.19	2.41	.86	
	1.66	.674	3.94	2.22	1.39	
	2.08	1.28	4.95	2.08	2.20	
A4 Fence Trip, M = 2.57						
17	.419	1.12	.987	2.24	1.83	2.32
	.523	1.91	1.24	2.60	.54	2.29	2.12	1.59
	.669	3.05	1.58	2.38	.94	2.91	2.00	2.27
	.846	2.76	2.00	2.22	1.36	3.69	1.90	3.05
	1.06	2.57	2.51	2.10	1.87	4.61	1.83	3.97
	1.36	2.43	.72	3.20	1.98	2.56	5.90	1.75	5.26
	1.69	2.29	1.05	3.98	1.89	3.34	7.35	1.69	6.71
	2.10	2.17	1.46	4.94	1.80	4.30	9.11	1.61	8.47
25	.432	1.09		1.02	2.61				
26	2.08	2.19		4.91	1.78				
27	1.24	2.51		2.92	1.99				
32	2.12	2.16		5.01	1.78				

Table A
Measured Local Friction Coefficients

Test No.	Station 1		Station 2			Station 3		
	$\tau_w/q \cdot 10^3$		$\tau_w/q \cdot 10^3$			$\tau_w/q \cdot 10^3$		
	$u_1 x/\nu_1 \cdot 10^{-6}$	$(R-R_t) \cdot 10^{-6}$	$u_1 x/\nu_1 \cdot 10^{-6}$	$(R-R_t) \cdot 10^{-6}$		$u_1 x/\nu_1 \cdot 10^{-6}$	$(R-R_t) \cdot 10^{-6}$	
A5 Natural Transition, M = 3.70								
37	.551	.855	1.32	2.57				
	.618	.828	1.47	2.63				
	.708	.822	1.69	2.46				
	.833	.820	1.99	2.29				
	.986	.872	2.36	2.12				
	1.15	.976	2.76	2.00	.92			
	1.37	1.18	3.28	1.88	1.26			
	1.63	1.47	3.85	1.79	1.65			
	1.94	1.89	4.61	1.69	2.16			
A6 Fence Trip, M = 3.70								
14	.536	1.02	1.25	1.69		2.30	1.98	
	.627	1.03	1.47	2.22		2.68	1.81	1.49
	.714	1.42	1.70	2.03	.80	3.09	1.69	2.19
	.828	2.26	1.96	1.93	1.06	3.56	1.63	2.66
	.993	2.27	2.33	1.83	1.43	4.25	1.56	3.35
	1.18	2.17	2.79	1.72	1.89	5.06	1.50	4.16
	1.37	2.07	3.23	1.66	2.33	5.88	1.45	4.98
	1.61	1.93	3.83	1.57	2.93	6.94	1.39	6.04
	1.92	1.84	4.54	1.51	3.64	8.32	1.34	7.42
20	.919	2.35	2.17	1.83				
21	.548	1.06	1.29	1.63				
31	1.96	1.79	4.60	1.48				

Table A
Measured Local Friction Coefficients

Test No.	Station 1		Station 2			Station 3		
	$u_1 x/\nu_1 \cdot 10^{-6}$	$\tau_w/q \cdot 10^3$ $(R-R_t)\cdot 10^{-6}$	$u_1 x/\nu_1 \cdot 10^{-6}$	$\tau_w/q \cdot 10^3$ $(R-R_t)\cdot 10^{-6}$		$u_1 x/\nu_1 \cdot 10^{-6}$	$\tau_w/q \cdot 10^3$ $(R-R_t)\cdot 10^{-6}$	
A7 Natural Transition, M = 4.54								
33	.416	1.01	.988	1.59				
	.498	.958	1.18	1.97				
	.584	.892	1.40	2.18				
	.708	.829	1.69	2.18				
	.852	.808	2.05	2.10				
	1.04	.838	2.48	1.93	.47			
	1.27	.931	3.03	1.77	.75			
	1.53	1.14	3.65	1.66	1.10			
	1.86	1.38	4.44	1.57	1.54			
A8 Fence Trip, M = 4.54								
15	.384	1.09	.873	.909		1.63	1.52	
	.482	.999	1.13	.886		2.12	1.76	
	.577	.942	1.37	1.00		2.54	1.73	
	.698	.886	1.63	1.63		3.06	1.60	
	.842	.950	1.99	1.80		3.66	1.48	1.96
	1.03	1.70	2.45	1.61	1.25	4.51	1.36	3.31
	1.25	1.87	2.95	1.52	1.75	5.44	1.29	4.24
	1.54	1.77	3.65	1.43	2.45	6.77	1.23	5.57
	1.86	1.66	4.39	1.37	3.19	8.17	1.18	6.97
22	1.79	1.66	4.20	1.37				
23	.901	1.13	2.14	1.72				
24	.511	.966	1.20	.908				

Table A
Measured Local Friction Coefficients

Test No.	Station 1		Station 2		Station 3	
	$u_1 x/\nu_1 \cdot 10^{-6}$	$\tau_w/q \cdot 10^3$ $(R-R_t) \cdot 10^{-6}$	$u_1 x/\nu_1 \cdot 10^{-6}$	$\tau_w/q \cdot 10^3$ $(R-R_t) \cdot 10^{-6}$	$u_1 x/\nu_1 \cdot 10^{-6}$	$\tau_w/q \cdot 10^3$ $(R-R_t) \cdot 10^{-6}$
		A9 Sand Trip, M = 4.54				
60	.456	1.05	1.11	1.77	1.97	1.99
	.569	.967	1.38	2.24	2.46	1.82
	.719	.900	1.73	2.13	3.12	1.65
	.902	.914	2.18	1.95	3.92	1.54
	1.12	1.05	2.73	1.78	4.88	1.43
	1.42	1.35	3.41	1.64	6.12	1.35
	1.79	1.83	4.28	1.53	7.84	1.28
61	1.80	1.83	4.29	1.53		
		A10 Air Jet Trip, M = 4.54				
57	.448	1.21	1.02	2.14	2.02	1.76
	.575	1.53	1.35	1.94	2.50	1.62
	.722	1.86	1.71	1.82	3.10	1.53
	.891	2.18	2.13	1.70	3.92	1.42
	1.14	2.19	2.66	1.59	4.91	1.34
	1.43	2.06	3.35	1.51	6.12	1.29
	1.80	1.92	4.24	1.43	7.73	1.22
62	1.80	1.94	4.26	1.45		
76	1.79	1.92				

TABLE B

Summary of Major Parameters

During Boundary Layer Profile Measurements

Test Number Trip	28 Fence	29 Fence	30 Fence	25 Fence	27 Fence	26 Fence	21 Fence	20 Fence	19 Fence	23 Fence	22 Fence	61 Sand	76 Jets	62 Jets
M	1.966	1.978	1.982	2.540	2.568	2.578	3.690	3.701	3.697	4.512	4.554	4.545	4.504	4.544
n	.660	.665	.665	.751	.754	.755	.855	.856	.856	.896	.898	.897	.896	.897
P_o, cm Hg	20	50	71	26	76	131	59	103	214	148	232	301	301	302
T_o, ^oR	550	543	545	551	556	568	552	561	562	552	554	561	564	563
x, in.	21.48	21.48	21.48	21.48	21.48	21.48	21.48	21.48	21.48	21.48	21.48	21.35	10.35	21.35
$\nu_w \times 10^3$, ft^2/sec	4.54	1.839	1.293	8.64	3.08	1.846	20.06	11.78	5.67	23.90	12.33	11.96	11.56	12.00
$u_1 x/\nu_1 \times 10^{-6}$	1.72	4.33	6.18	1.68	4.84	8.32	2.07	3.54	7.25	3.52	6.83	6.87	3.37	6.91
θ, in.	.0372	.0321	.0298	.0279	.0295	.0263	.0220	.0249	.0224	.0212	.0207	.0155	.0089	.0162
δ^*, in.	.119	.102	.098	.123	.130	.121	.168	.198	.175	.230	.222	.171	.101	.181
δ, in.	.436	.390	.368	.397	.405	.377	.436	.478	.428	.498	.466	.382	.227	.396
R_θ	2980	6470	8570	2190	6600	10200	2120	4100	7560	3470	6590	4980	2900	5240
R_{δ^*}	9540	20700	28200	9620	29200	46800	16200	32600	58900	37600	70800	54800	32800	58600
R_δ	34900	78700	106000	31100	91200	146000	42100	78800	144000	81600	14800	123000	74000	128000
δ^*/θ	3.20	3.19	3.29	4.40	4.42	4.59	7.62	7.94	7.80	10.83	10.74	11.01	11.32	11.18
θ/δ	.0852	.0824	.0810	.0703	.0724	.0698	.0505	.0521	.0524	.0425	.0444	.0406	.0392	.0409
δ^*/δ	.273	.263	.267	.309	.320	.320	.384	.414	.408	.461	.477	.448	.443	.457
$\delta\sqrt{\tau_w/\rho_w}/\nu_w$	651	1290	1672	378	947	1427	242	397	682	237	392	344	228	349
r	.897	.889	.898	.898	.895	.890	.911	.896	.892	.907	.901	.899	.899	.895
ρ_T/ρ_w	1.36	1.29	1.24	1.26	1.26	1.26		1.46	1.42	1.58	1.51	1.48		1.45

Corrected Data

$R \times 10^{-6}$					6.08	10.26		3.98	8.63	3.57	8.17		2.81	6.20
C_f	.00272	.00218	.00202	.00242	.00181	.00166	.00211	.00162	.00138	.00148	.00122	.00131	.00155	.00126
C_F					.00217	.00199		.00206	.00175	.00194	.00161		.00206	.00169

Effect of Mach Number for Constant R

C_f/C_{fi}					.705	.700		.595	.570	.560	.500		.385	.495
C_F/C_{F_i}					.715	.710		.635	.610	.590	.560		.300	.560

Effect of Mach Number for Constant R_δ

C_f/C_{f_i}	.910	.838	.818	.796	.713	.710	.730	.625	.587	.571	.521	.546	.592	.525

Table C
Boundary Layer Profiles

y inches	u ft/sec	M	$\frac{u}{\sqrt{\tau_w/\rho_w}}$	$\frac{y\sqrt{\tau_w/\rho_w}}{\nu_w}$	$\frac{\sin^{-1} mu/u_1}{m\sqrt{\tau_w/\rho_w}/u_1}$	$\frac{u}{\sqrt{\tau_w/\rho_T}}$	$\frac{\eta \rho_T}{\mu_w}\sqrt{\frac{\tau_w}{\rho_T}}$
		C1	Test 28	M = 2.0			
.0239	1001	.945	12.28	35.7	12.62	14.31	43.4
.0270	1033	.981	12.68	40.4	13.05	14.77	49.6
.0299	1058	1.010	12.99	44.7	13.39	15.13	56.9
.0336	1079	1.033	13.24	50.2	13.67	15.43	64.3
.0380	1104	1.063	13.55	56.8	14.00	15.78	73.2
.0434	1128	1.092	13.84	64.9	14.34	16.13	84.4
.0496	1156	1.126	14.19	74.2	14.72	16.53	97.4
.0572	1178	1.153	14.46	85.5	15.02	16.85	113.3
.0663	1204	1.185	14.78	99.1	15.38	17.21	132.5
.0776	1233	1.222	15.13	116.0	15.78	17.63	156.7
.0908	1266	1.265	15.54	135.8	16.25	18.10	186.2
.1068	1298	1.308	15.93	159.7	16.71	18.56	221.6
.1260	1336	1.360	16.40	188.4	17.25	19.10	265.0
.1492	1379	1.421	16.92	223.1	17.87	19.72	319
.1766	1421	1.483	17.44	264.0	18.49	20.32	384
.2102	1476	1.568	18.11	314	19.30	21.10	466
.2507	1534	1.662	18.82	375	20.17	21.93	569
.2978	1597	1.773	19.60	445	21.16	22.84	709
.3566	1653	1.877	20.28	533	22.04	23.60	874
.4257	1690	1.950	20.74	636	22.64	24.16	1074
.5108	1694	1.966	20.79	764	22.75	24.21	1325

Table C
Boundary Layer Profiles

y inches	u ft/sec	M	$\frac{u}{\sqrt{\tau_w/\rho_w}}$	$\frac{y\sqrt{\tau_w/\rho_w}}{\nu_w}$	$\frac{\sin^{-1} mu/u_1}{m\sqrt{\tau_w/\rho_w}/u_1}$	$\frac{u}{\sqrt{\tau_w/\rho_r}}$	$\frac{\eta \rho_r}{\mu_w}\sqrt{\frac{\tau_w}{\rho_r}}$
		C2 Test 29 M = 2.0					
.0239	1050	1.009	14.39	7 79.0	14.83	16.33	95.3
.0270	1075	1.038	14.73	89.3	15.20	16.72	108.8
.0299	1095	1.062	15.00	98.9	15.51	17.02	121.6
.0336	1116	1.087	15.29	111.1	15.82	17.35	138.1
.0380	1139	1.114	15.61	125.6	16.18	17.72	158.0
.0434	1163	1.144	15.93	143.5	16.54	18.08	182.4
.0496	1188	1.175	16.28	164.0	16.93	18.48	210.4
.0572	1214	1.208	16.63	189.1	17.33	18.88	245.6
.0663	1241	1.244	17.00	219.2	17.75	19.30	288.5
.0776	1274	1.287	17.46	256.6	18.27	19.82	342
.0908	1307	1.332	17.91	300	18.80	20.32	406
.1068	1342	1.381	18.39	353	19.36	20.87	485
.1260	1379	1.434	18.89	417	19.96	21.44	582
.1492	1423	1.501	19.50	493	20.68	22.13	701
.1766	1468	1.571	20.11	584	21.43	22.82	847
.2102	1521	1.658	20.84	695	22.32	23.65	1031
.2507	1578	1.758	21.62	829	23.31	24.54	1262
.2978	1635	1.864	22.40	985	24.31	25.42	1545
.3566	1680	1.952	23.02	1179	25.12	26.13	1909
.4257	1692	1.978	23.18	1408	25.34	26.31	2349

Table C
Boundary Layer Profiles

y inches	u ft/sec	M	$\frac{u}{\sqrt{\tau_w/\rho_w}}$	$\frac{y\sqrt{\tau_w/\rho_w}}{\nu_w}$	$\frac{\sin^{-1} mu/u_1}{m\sqrt{\tau_w/\rho_w}/u_1}$	$\frac{u}{\sqrt{\tau_w/\rho_T}}$	$\frac{\eta \rho_T}{\mu_w}\sqrt{\frac{\tau_w}{\rho_T}}$
		C3 Test 30 M = 2.0					
.0239	1074	1.032	15.25	108.5	15.73	16.97	127.5
.0270	1098	1.063	15.59	122.6	16.11	17.35	145.7
.0299	1119	1.088	15.89	135.8	16.44	17.69	162.9
.0336	1142	1.116	16.21	152.6	16.81	18.04	185.4
.0380	1165	1.144	16.54	172.6	17.17	18.41	212.1
.0434	1189	1.174	16.88	197.1	17.55	18.79	244.9
.0496	1214	1.205	17.24	225.2	17.96	19.19	283.6
.0572	1240	1.240	17.60	259.8	18.38	19.59	331
.0663	1269	1.277	18.02	301	18.85	20.06	389
.0776	1300	1.320	18.46	352	19.36	20.55	462
.0908	1333	1.365	18.92	412	19.90	21.06	549
.1068	1364	1.410	19.36	485	20.43	21.55	656
.1260	1405	1.469	19.95	572	21.12	22.20	787
.1492	1446	1.532	20.53	678	21.82	22.85	950
.1766	1492	1.605	21.18	802	22.62	23.57	1148
.2102	1542	1.690	21.89	955	23.50	24.36	1398
.2507	1601	1.794	22.73	1138	24.56	25.30	1712
.2978	1655	1.897	23.50	1352	25.55	26.16	2095
.3566	1688	1.965	23.96	1620	26.17	26.67	2590
.4257	1696	1.979	24.08	1933	26.32	26.80	3180
.5108	1697	1.982	24.09	2320	26.34	26.81	3920

Table C
Boundary Layer Profiles

y inches	u ft/sec	M	$\frac{u}{\sqrt{\tau_w/\rho_w}}$	$\frac{y\sqrt{\tau_w/\rho_w}}{\nu_w}$	$\frac{\sin^{-1} mu/u_1}{m\sqrt{\tau_w/\rho_w}/u_1}$	$\frac{u}{\sqrt{\tau_w/\rho_T}}$	$\frac{\eta \rho_T}{\mu_w}\sqrt{\frac{\tau_w}{\rho_T}}$
		C4 Test 25 M = 2.6					
.0239	1138	1.104	11.53	22.8	11.94	12.96	27.3
.0270	1200	1.178	12.15	25.7	12.65	13.65	31.2
.0299	1236	1.225	12.52	28.5	13.06	14.07	35.2
.0336	1283	1.286	13.00	32.0	13.61	14.61	40.3
.0380	1320	1.337	13.37	36.2	14.04	15.02	46.3
.0434	1355	1.386	13.72	41.3	14.56	15.42	53.9
.0496	1387	1.432	14.05	47.2	14.84	15.79	63.0
.0572	1418	1.477	14.36	54.5	15.22	16.14	74.1
.0663	1449	1.525	14.68	63.1	15.59	16.50	87.7
.0776	1481	1.575	15.00	73.9	15.99	16.86	104.8
.0908	1514	1.629	15.34	86.5	16.40	17.24	125.4
.1068	1550	1.689	15.70	101.7	16.85	17.64	150.8
.1260	1592	1.762	16.13	120.0	17.39	18.13	182.4
.1492	1641	1.853	16.62	142.1	18.03	18.68	221.5
.1766	1690	1.950	17.12	168.2	18.68	19.24	269.4
.2102	1745	2.065	17.68	200.2	19.43	19.87	331
.2507	1804	2.200	18.27	238.8	20.25	20.53	411
.2978	1859	2.339	18.83	283.6	21.05	21.16	508
.3566	1904	2.462	19.28	340	21.72	21.67	636
.4257	1926	2.528	19.51	405	22.05	21.92	793
.5108	1930	2.540	19.55	487	22.11	21.97	990

Table C
Boundary Layer Profiles

y inches	u ft/sec	M	$\frac{u}{\sqrt{\tau_w/\rho_w}}$	$\frac{y\sqrt{\tau_w/\rho_w}}{\nu_w}$	$\frac{\sin^{-1} mu/u_1}{m\sqrt{\tau_w/\rho_w}/u_1}$	$\frac{u}{\sqrt{\tau_w/\rho_r}}$	$\frac{\eta \rho_r}{\mu_w}\sqrt{\frac{\tau_w}{\rho_r}}$
		℄ Test 27 M = 2.6					
.0239	1196	1.167	13.81	56.0	14.36	15.47	66.9
.0270	1228	1.207	14.18	63.3	14.77	15.88	76.7
.0299	1254	1.241	14.49	70.1	15.12	16.23	85.8
.0336	1283	1.278	14.82	78.7	15.50	16.60	97.8
.0380	1311	1.316	15.14	89.0	15.88	16.96	112.1
.0434	1340	1.356	15.48	101.7	16.27	17.34	130.4
.0496	1370	1.397	15.82	116.2	16.67	17.72	151.5
.0572	1400	1.441	16.17	134.0	17.09	18.11	177.8
.0663	1431	1.487	16.53	155.4	17.52	18.51	210.0
.0776	1465	1.539	16.92	181.8	18.00	18.95	250.5
.0908	1500	1.593	17.32	212.8	18.49	19.40	299.3
.1068	1537	1.654	17.76	250.3	19.02	19.89	359
.1260	1579	1.725	18.24	295.3	19.62	20.43	434
.1492	1629	1.815	18.82	350	20.36	21.08	527
.1766	1677	1.913	19.36	414	21.07	21.68	642
.2102	1735	2.034	20.04	493	21.97	22.44	790
.2507	1805	2.182	20.85	588	23.08	23.35	980
.2978	1871	2.344	21.60	698	24.09	24.19	1214
.3566	1924	2.494	22.23	836	25.07	24.90	1530
.4257	1948	2.562	22.49	998	25.47	25.19	1917
.5108	1950	2.568	22.52	1197	25.51	25.22	2405

Table C
Boundary Layer Profiles

y inches	u ft/sec	M	$\frac{u}{\sqrt{\tau_w/\rho_w}}$	$\frac{y\sqrt{\tau_w/\rho_w}}{\nu_w}$	$\frac{\sin^{-1} mu/u_1}{m\sqrt{\tau_w/\rho_w}/u_1}$	$\frac{u}{\sqrt{\tau_w/\rho_t}}$	$\frac{\eta \rho_t}{\mu_w}\sqrt{\frac{\tau_w}{\rho_t}}$
		C6 Test 26 M = 2.6					
.0239	1226	1.189	14.61	90.5	15.21	16.39	108.5
.0270	1261	1.234	15.03	102.3	15.68	16.86	124.3
.0299	1287	1.267	15.34	113.3	16.03	17.21	139.2
.0336	1317	1.306	15.70	127.3	16.45	17.62	158.6
.0380	1344	1.343	16.02	143.9	16.82	17.97	182.6
.0434	1374	1.384	16.37	164.4	17.24	18.37	212.3
.0496	1406	1.430	16.76	187.9	17.69	18.80	246.7
.0572	1437	1.474	17.12	216.7	18.13	19.21	289.4
.0663	1467	1.519	17.48	251.1	18.56	19.61	341
.0776	1501	1.572	17.89	294.0	19.05	20.07	408
.0908	1536	1.627	18.30	344	19.57	20.53	488
.1068	1574	1.690	18.76	405	20.13	21.05	587
.1260	1617	1.764	19.27	477	20.78	21.62	709
.1492	1670	1.860	19.89	565	21.60	22.33	862
.1766	1722	1.963	20.52	669	22.41	23.02	1052
.2102	1784	2.093	21.26	796	23.40	23.85	1295
.2507	1852	2.251	22.07	950	24.53	24.76	1608
.2978	1917	2.418	22.84	1128	25.65	25.63	1998
.3566	1961	2.544	23.37	1351	26.43	26.22	2520
.4257	1972	2.578	23.50	1612	26.63	26.37	3155

Table C
Boundary Layer Profiles

y inches	u ft/sec	H	$\frac{u}{\sqrt{\tau_w/\rho_w}}$	$\frac{y\sqrt{\tau_w/\rho_w}}{\nu_w}$	$\frac{\sin^{-1} mu/u_1}{m\sqrt{\tau_w/\rho_w}/u_1}$	$\frac{u}{\sqrt{\tau_w/\rho_T}}$	$\frac{\eta \rho_T}{\mu_w}\sqrt{\frac{\tau_w}{\rho_T}}$
		C7	Test 21	M = 3.7			
.0229	1151	1.117	8.62	12.7		8.94	
.0270	1247	1.238	9.34	15.0		9.76	
.0299	1327	1.345	9.94	16.6		10.45	
.0336		Impact pressure not recorded					
.0380	1492	1.590	11.18	21.1		11.93	
.0434	1558	1.700	11.67	24.1		12.54	
.0496	1613	1.797	12.08	27.5		13.06	
.0572	1662	1.890	12.45	31.7		13.54	
.0663	1703	1.972	12.75	36.8		13.94	
.0776	1736	2.042	13.00	43.0		14.28	
.0908	1768	2.114	13.24	50.4		14.61	
.1068	1804	2.195	13.51	59.2		14.98	
.1260	1845	2.296	13.82	69.9		15.42	
.1492	1891	2.420	14.16	82.8		15.92	
.1766	1938	2.558	14.52	97.9		16.44	
.2102	1994	2.736	14.94	116.6		17.09	
.2507	2051	2.948	15.36	139.0		17.78	
.2978	2108	3.188	15.79	165.2		18.51	
.3566	2158	3.439	16.16	197.8		19.18	
.4257	2189	3.615	16.40	236.1		19.61	
.5108	2200	3.681	16.48	283.3		19.77	
.6126	2202	3.690	16.49	340		19.80	

Table C
Boundary Layer Profiles

y inches	u ft/sec	M	$\frac{u}{\sqrt{\tau_w/\rho_w}}$	$\frac{y\sqrt{\tau_w/\rho_w}}{\nu_w}$	$\frac{\sin^{-1} mu/u_1}{m\sqrt{\tau_w/\rho_w}/u_1}$	$\frac{u}{\sqrt{\tau_w/\rho_T}}$	$\frac{\eta \rho_T}{\mu_w}\sqrt{\frac{\tau_w}{\rho_T}}$
		C8 Test 20 M = 3.7					
.0229	1188	1.153	10.12	19.0	10.51	12.22	24.0
.0270	1271	1.256	10.83	22.4	11.31	13.08	28.9
.0299	1328	1.332	11.31	24.8	11.87	13.66	32.4
.0336	1387	1.414	11.81	27.9	12.46	14.27	37.2
.0380	1439	1.491	12.26	31.6	12.99	14.81	43.1
.0434	1487	1.564	12.67	36.1	13.48	15.30	50.5
.0496	1529	1.631	13.02	41.2	13.93	15.73	59.1
.0572	1567	1.695	13.35	47.5	14.33	16.13	70.0
.0663	1605	1.761	13.67	55.1	14.74	16.51	83.2
.0776	1642	1.827	13.99	64.5	15.14	16.90	100.5
.0908	1677	1.894	14.28	75.4	15.53	17.25	121.4
.1068	1716	1.972	14.61	88.7	15.97	17.65	148.2
.1260	1761	2.066	15.00	104.7	16.49	18.12	181.7
.1492	1812	2.183	15.43	123.9	17.11	18.64	222.6
.1766	1867	2.318	15.90	146.7	17.75	19.21	273.7
.2102	1930	2.492	16.44	174.6	18.54	19.86	341
.2507	2002	2.712	17.05	208.2	19.48	20.60	429
.2978	2070	2.959	17.63	247.4	20.42	21.30	544
.3566	2138	3.256	18.21	296.2	21.41	22.00	703
.4257	2198	3.559	18.72	354	22.34	22.61	917
.5108	2217	3.690	18.88	424	22.66	22.81	1204
.6126	2219	3.701	18.90	509	22.69	22.83	1556

Table C
Boundary Layer Profiles

y inches	u ft/sec	M	$\frac{u}{\sqrt{\tau_w/\rho_w}}$	$\frac{y\sqrt{\tau_w/\rho_w}}{\nu_w}$	$\frac{\sin^{-1} mu/u_1}{m\sqrt{\tau_w/\rho_w}/u_1}$	$\frac{u}{\sqrt{\tau_w/\rho_t}}$	$\frac{\eta \rho_t}{\mu_w}\sqrt{\frac{\tau_w}{\rho_t}}$
		C9 Test 19 M = 3.7					
.0229	1311	1.307	12.10	36.5	12.60	14.41	46.5
.0270	1370	1.388	12.65	43.0	13.32	15.07	56.3
.0299	1409	1.444	13.01	47.6	13.75	15.49	63.5
.0336	1452	1.506	13.40	53.5	14.22	15.96	72.7
.0380	1491	1.567	13.76	60.5	14.66	16.39	83.8
.0434	1527	1.624	14.10	69.1	15.07	16.79	98.2
.0496	1560	1.678	14.40	79.0	15.45	17.15	114.5
.0572	1595	1.738	14.72	91.1	15.86	17.53	135.5
.0663	1628	1.798	15.03	105.6	16.24	17.90	161.0
.0776	1663	1.864	15.35	123.6	16.66	18.28	193.7
.0908	1701	1.938	15.70	144.6	17.12	18.70	233.7
.1068	1744	2.027	16.10	170.1	17.65	19.18	283.3
.1260	1792	2.131	16.54	200.7	18.26	19.70	346
.1492	1850	2.268	17.08	237.7	19.01	20.34	426
.1766	1909	2.423	17.62	281.3	19.80	20.99	527
.2102	1975	2.620	18.23	335	20.71	21.71	660
.2507	2048	2.866	18.91	399	21.78	22.52	838
.2978	2118	3.151	19.55	474	22.86	23.28	1067
.3566							
.4257	2217	3.662	20.47	678	24.52	24.38	1839
.5108	2222	3.697	20.51	814	24.61	24.43	2390

Table C
Boundary Layer Profiles

y inches	u ft/sec	M	$\frac{u}{\sqrt{\tau_w/\rho_w}}$	$\frac{y\sqrt{\tau_w/\rho_w}}{\nu_w}$	$\frac{\sin^{-1} mu/u_1}{m\sqrt{\tau_w/\rho_w}/u_1}$	$\frac{u}{\sqrt{\tau_w/\rho_t}}$	$\frac{\eta \rho_t}{\mu_w}\sqrt{\frac{\tau_w}{\rho_t}}$
		C10 Test 23 M = 4.5					
.0380	1444	1.515	10.57	18.1	11.22	13.28	25.8
.0434	1522	1.640	11.14	20.7	11.92	14.00	30.3
.0496	1587	1.750	11.61	23.6	12.51	14.59	35.7
.0572	1643	1.853	12.02	27.3	13.04	15.11	42.5
.0663	1688	1.941	12.35	31.6	13.47	15.52	51.3
.0776	1730	2.030	12.66	37.0	13.88	15.91	62.6
.0908	1770	2.116	12.95	43.3	14.28	16.28	76.2
.1068	1808	2.206	13.23	50.9	14.67	16.63	93.3
.1260	1850	2.312	13.54	60.0	15.10	17.02	114.8
.1492	1903	2.455	13.92	71.1	15.67	17.49	142.3
.1766	1957	2.617	14.32	84.1	16.27	18.00	177.2
.2102	2021	2.832	14.79	100.2	17.01	18.59	223.3
.2507	2089	3.107	15.28	119.4	17.83	19.20	285.4
.2978	2157	3.431	15.78	141.9	18.71	19.83	368
.3566	2223	3.830	16.27	169.9	19.64	20.45	486
.4257	2278	4.246	16.67	202.8	20.46	20.95	650
.5108	2304	4.484	16.86	243.4	20.88	21.19	877
.6126	2306	4.512	16.87	291.9	20.91	21.20	1162

Table C
Boundary Layer Profiles

y inches	u ft/sec	M	$\frac{u}{\sqrt{\tau_w/\rho_w}}$	$\frac{y\sqrt{\tau_w/\rho_w}}{\nu_w}$	$\frac{\sin^{-1} mu/u_1}{m\sqrt{\tau_w/\rho_w}/u_1}$	$\frac{u}{\sqrt{\tau_w/\rho_T}}$	$\frac{\eta \rho_T}{\mu_w}\sqrt{\frac{\tau_w}{\rho_T}}$
		C11 Test 22 M = 4.5					
.0239	1295	1.298	10.40	20.1	10.90	12.77	26.4
.0270	1372	1.404	11.02	22.7	11.62	13.53	30.4
.0299	1427	1.485	11.46	25.2	12.15	14.07	34.3
.0336	1485	1.574	11.93	28.3	12.71	14.65	39.2
.0380	1537	1.659	12.35	32.0	13.23	15.17	45.5
.0434	1583	1.738	12.72	36.5	13.69	15.62	53.4
.0496	1624	1.812	13.05	41.7	14.11	16.03	63.2
.0572	1664	1.887	13.37	48.1	14.53	16.42	75.4
.0663	1698	1.955	13.64	55.8	14.89	16.75	90.6
.0776	1735	2.032	13.94	65.3	15.29	17.12	109.6
.0908	1772	2.113	14.24	76.4	15.69	17.49	133.2
.1068	1813	2.209	14.56	89.8	16.16	17.88	162.6
.1260	1860	2.326	14.94	106.0	16.69	18.35	199.3
.1492	1916	2.479	15.39	125.5	17.35	18.90	246.7
.1766	1974	2.658	15.86	148.5	18.06	19.48	307
.2102	2041	2.892	16.40	176.8	18.92	20.14	388
.2507	2112	3.188	16.97	210.9	19.88	20.84	498
.2978	2181	3.537	17.52	250.5	20.88	21.51	644
.3566	2248	3.969	18.06	299.9	21.93	22.18	858
.4257	2297	4.373	18.45	358	22.77	22.66	1153
.5108	2315	4.554	18.60	430	23.09	22.84	1556

Table C
Boundary Layer Profiles

y inches	u ft/sec	M	$\frac{u}{\sqrt{\tau_w/\rho_w}}$	$\frac{y\sqrt{\tau_w/\rho_w}}{\nu_w}$	$\frac{\sin^{-1} mu/u_1}{m\sqrt{\tau_w/\rho_w}/u_1}$	$\frac{u}{\sqrt{\tau_w/\rho_t}}$	$\frac{\eta \rho_t}{\mu_w}\sqrt{\frac{\tau_w}{\rho_t}}$
		C12	Test 61	M = 4.5			
.0176	1331	1.333	10.30	15.9		12.53	20.7
.0201	1393	1.420	10.78	18.1		13.12	24.3
.0239	1470	1.535	11.38	21.5		13.85	30.0
.0286	1550	1.662	12.00	25.8		14.60	37.2
.0346	1624	1.792	12.57	31.2		15.30	47.0
.0415	1690	1.916	13.08	37.4		15.92	58.9
.0500	1749	2.038	13.54	45.0		16.48	73.9
.0600	1799	2.149	13.92	54.0		16.94	92.5
.0726	1842	2.252	14.26	65.4		17.35	117.3
.0877	1887	2.365	14.60	79.0		17.76	148.2
.1062			Impact pressure not recorded				
.1288	1994	2.685	15.43	116.0		18.78	242.3
.1562	2056	2.907	15.91	140.6		19.36	318
.1888	2120	3.169	16.41	170.0		19.97	411
.2278	2182	3.480	16.89	204.8		20.55	536
.2771	2247	3.883	17.39	249.5		21.16	722
.3355	2300	4.296	17.80	302		21.66	977
.4078	2323	4.521	17.98	367		21.88	1332
.4958	2324	4.545	17.99	446		21.90	1784

Table C
Boundary Layer Profiles

y inches	u ft/sec	M	$\frac{u}{\sqrt{\tau_w/\rho_w}}$	$\frac{y\sqrt{\tau_w/\rho_w}}{\nu_w}$	$\frac{\sin^{-1} mu/u_1}{m\sqrt{\tau_w/\rho_w}/u_1}$	$\frac{u}{\sqrt{\tau_w/\rho_T}}$	$\frac{\eta \rho_T}{\mu_w}\sqrt{\frac{\tau_w}{\rho_T}}$
		C13	Test 76	M = 4.5			
.0174	1453	1.501	10.41	17.5			
.0205	1537	1.633	11.01	20.7			
.0243	1618	1.771	11.59	24.5			
.0290	1696	1.916	12.15	29.2			
.0350	1773	2.076	12.70	35.2			
.0419	1843	2.237	13.20	42.2			
.0504	1906	2.400	13.65	50.7			
.0604	1959	2.549	14.03	60.9			
.0730	2007	2.704	14.38	73.5			
.0881	2060	2.891	14.76	88.7			
.1066	2118	3.131	15.17	107.3			
.1292	2198	3.418	15.60	130.2			
.1566	2239	3.774	16.04	157.7			
.1892	2292	4.161	16.42	190.6			
.2282	2321	4.438	16.63	229.8			
.2775	2328	4.504	16.68	279.4			

Table C
Boundary Layer Profiles

y inches	u ft/sec	M	$\frac{u}{\sqrt{\tau_w/\rho_w}}$	$\frac{y\sqrt{\tau_w/\rho_w}}{\nu_w}$	$\frac{\sin^{-1} mu/u_1}{m\sqrt{\tau_w/\rho_w}/u_1}$	$\frac{u}{\sqrt{\tau_w/\rho_T}}$	$\frac{\eta \rho_T}{\mu_w}\sqrt{\frac{\tau_w}{\rho_T}}$
		C14	Test 62	M = 4.5			
.0167	1290	1.273	10.17	14.7		12.23	19.0
.0198	1365	1.375	10.76	17.4		12.93	23.0
.0236	1445	1.490	11.40	20.8		13.71	28.0
.0283	1523	1.612	12.01	24.9		14.43	34.5
.0343	1597	1.736	12.59	30.2		15.14	43.5
.0412	1663	1.856	13.12	36.3		15.77	54.6
.0497	1722	1.972	13.58	43.8		16.33	68.6
.0597	1771	2.078	13.97	52.6		16.79	86.1
.0723	1815	2.177	14.31	63.7		17.20	109.1
.0874	1859	2.284	14.66	77.0		17.62	138.3
.1059	1910	2.418	15.06	93.2		18.11	175.6
.1285	1968	2.586	15.52	113.1		18.65	225.2
.1559	2031	2.797	16.02	137.3		19.26	290.4
.1885	2098	3.052	16.55	166.0		19.89	376
.2275	2165	3.362	17.07	200.3		20.52	491
.2768	2234	3.763	17.62	243.7		21.18	661
.3352	2294	4.216	18.09	295.2		21.75	899
.4075	2326	4.508	18.34	359		22.05	1240
.4955	2327	4.544	18.35	436		22.06	1676

References

The following abbreviations are used:

Reports of government agencies:

ARC, R & M; CP Aeronautical Research Council, Great Britain, Reports and Memoranda; Current Papers

NACA, TN; TM; TR; RM; ACR (WR) National Advisory Committee for Aeronautics, Technical Note; Technical Memorandum; Technical Report; Research Memorandum; Advance Confidential Report (Wartime Report)

ZWB, KWI, U & M; FB Zentrale für wissenschaftliches Berichtswesen der Luftfahrtforschung des Generalluftzeugmeisters, Kaiser Wilhelm Institut für Strömungsforschung, Untersuchungen und Mitteilungen; Forschungsbericht

Reports of research laboratories:

CAL, CU Cornell Aeronautical Laboratory, Buffalo

DRL, UT Defense Research Laboratory, University of Texas, Austin

GALCIT Guggenheim Aeronautical Laboratory, California Institute of Technology, Pasadena

Technical journals:

Ing.-Arch. Ingenieur-Archiv

JAS Journal of the Aeronautical Sciences

PRSA Proceedings of the Royal Society, Series A, Mathematical and Physical Sciences

ZAMM Zeitschrift für angewandte Mathematik und Mechanik

Colloquia and congresses:

HTFMI Heat Transfer and Fluid Mechanics Institute

Proc. X Cong. Proceedings of the Xth International Congress for Applied Mechanics (or Theoretical and Applied Mechanics)

REFERENCES

(1) Prandtl, L., Über Flüssigketisbewegung bei sehr kleiner Reibung, Proceedings of the Third International Congress for Mathematics, Heidelberg, pp. 484-491, 1904; also in Vier Abhandlungen zur Hydrodynamik und Aerodynamik, Göttingen, 1927, reprinted by Edwards Bros., Ann Arbor, 1943; translated as Motion of fluids with very little viscosity, NACA, TM 452, March 1928

(2) Weyl, H., On the differential equations of the simplest boundary layer problems, Annals of Mathematics, 2nd Series, Vol. 43, pp. 381-407, 1942

(3) von Mises, R., and Friedrichs, K. O., Fluid dynamics, Lecture notes, Brown University, Providence, 1942

(4) Latta, G. E., Singular perturbation problems, California Institute of Technology, Pasadena, Thesis, May 1951; abstracted in Proc. VIII Cong., Istanbul, Aug. 1952

(5) Lagerstrom, P., and Liepmann, H. W., Laminar Flow, High Speed Aerodynamics and Jet Propulsion, Vol. IV, Section A (to be published)

(6) Goldschmied, F. R., Skin Friction of incompressible turbulent boundary layers under adverse pressure gradients, NACA, TN 2431, Aug. 1951

(7) Blasius, H., Grenzschichten in Flüssigkeiten mit kleiner Reibung, Göttingen, Thesis, 1907; also in Zeitschrift für Mathematik und Physik, Vol. 56, No. 1, pp. 1-37, 1908; translated as The boundary layer in fluids with little friction, NACA, TM 1256, Feb. 1950

(8) Kuerti, G., The laminar boundary layer in compressible flow, Advances in Applied Mechanics, Vol. II, pp. 21-92, New York, Academic Press, 1951

(9) Dryden, H. L., Air flow in the boundary layer near a plate, NACA, TR, 562, 1936

(10) Liepmann, H. W., Investigations on laminar boundary layer stability and transition on curved boundaries, NACA, ACR 3H30 (W-107), Aug. 1943

(11) Liepmann, H. W., and Dhawan, S., Direct measurements of local skin friction in low-speed and high-speed flow, Proceedings, First U.S. National Congress of Applied Mechanics, pp. 869-874, Chicago, 1951; see also Dhawan, S., Direct measurements of skin friction, GALCIT, Thesis, 1951, or NACA, TN 2567, Jan. 1952

(12) Maydew, R. C., and Pappas, C. C., Experimental investigation of the local and average skin friction in the laminar boundary layer on a flat plate at a Mach number of 2.4, 1952 HTFMI, Los Angeles, pp. 95-109, June 1952; also NACA, TN 2740, July 1952

(13) Dalitz, R. H., The effect of a sharp-nosed leading edge on the boundary layer of a flat plate, Australia, Council for Scientific and Industrial Research, Division of Aeronautics, Rep. No. A.40, Dec. 1945

(14) Hansen, M., Die Geschwindigkeitsverteilung in der Grenzschicht an einer eingetauchten Platte, ZAMM, Vol. 8, No. 3, pp. 185-199, 1928; also in Abhandlungen aus dem Aerodynamischen Institut an der Technischen Hochschule, Aachen, No. 8, pp. 31-45, 1928; translated as Velocity distribution in the boundary layer of a submerged plate, NACA, TM 585, Oct. 1930

(15) Prandtl, L., Über die ausgebildete Turbulenz, Proc. II Cong., Zurich, pp. 62-74, 1926; translated as Turbulent flow, NACA, TM 435, Oct. 1927; see also Bericht über Untersuchungen zur ausgebildeten Turbulenz, ZAMM, Vol. 5, No. 2, pp. 136-139, April 1925; translated as Report on investigation of developed turbulence; NACA, TM 1231, Sept. 1949

(16) von Kármán, T., Mechanische Ähnlichkeit und Turbulenz, Nachrichten von der Gesellschaft der Wissenschaften zu Göttingen, Fachgruppe I (Mathematik), No. 5, pp. 58-76, 1930; also in Proc. III Cong., Stockholm, pp. 85-93, 1930; translated as Mechanical similitude and turbulence, NACA, TM 611, March 1931

(17) Taylor, G. I., The transport of vorticity and heat through fluids in turbulent motion, PRSA, Vol. 135, No. 828, pp. 685-702, April 1932

(18) Rotta, J., Das in Wandnähe gültige Geschwindigkeitsgesetz turbulenter Strömungen, Ing.-Arch., Vol. 18, No. 4, pp. 277-280, 1950

(19) Liepmann, H. W., and Laufer, J., Investigation of free turbulent mixing, NACA, TN 1257, Aug. 1947

(20) Batchelor, G. K., Note on free turbulent flows with special reference to the two-dimensional wake, JAS, Vol. 17, No. 7, pp. 441-445, July 1950

(21) Prandtl, L., The mechanics of viscous fluids, Article G, Vol. III, Aerodynamic Theory (W. F. Durand, ed.), Berlin, 1934; reprinted, Pasadena, 1943

(22) von Kármán, T., Some aspects of the turbulence problem, Proc. IV Cong., Cambridge (Eng.), pp. 54-91, 1934

(23) Goldstein, S. (ed.), Modern developments in fluid dynamics, Oxford, 1938

(24) Schubauer, G. B., Turbulent Flow, High Speed Aerodynamics and Jet Propulsion, Vol. IV, Section E (to be published)

(25) Laufer, J., The structure of turbulence in fully developed pipe flow, U. S. Department of Commerce, National Bureau of Standards, Washington, Rep. No. 1974, Sept. 1952 (to be published as NACA TN)

(26) Klebanoff, P. S., and Diehl, Z. W., Some features of artificially thickened fully developed turbulent boundary layers with zero pressure gradient, NACA TN 2475, Oct. 1951

(27) Townsend, A. A., The structure of the turbulent boundary layer, Proceedings of the Cambridge Philosophical Society, Vol. 47, Part 2, pp. 375-395, 1951

(28) Townsend, A. A., Measurements in the turbulent wake of a cylinder, PRSA, Vol. 190, No. 1023, pp. 551-561, Sept. 1947

(29) Townsend, A. A., Local isotropy in the turbulent wake of a cylinder, Australian Journal of Scientific Research, Series A, Physical Sciences, Vol. 1, No. 2, pp. 161-174, June 1948; see also Diffusion in the turbulent wake of a cylinder, Proc. VII Cong., London, Vol. 2, Part I, pp. 227-248, 1948

(30) Townsend, A. A., Momentum and energy diffusion in the turbulent wake of a cylinder, PRSA, Vol. 197, No. 1048, pp. 124-140, May 1949

(31) Townsend, A. A., The fully developed turbulent wake of a circular cylinder, Australian Journal of Scientific Research, Series A, Physical Sciences, Vol. 2, No. 4, pp. 451-468, Dec. 1949

(32) Townsend, A. A., The eddy viscosity in turbulent shear flow, Philosophical Magazine, 7th Series, Vol. 41, No. 320, pp. 890-906, Sept. 1950

(33) Laufer, J., Investigation of turbulent flow in a two-dimensional channel, NACA, TN 2123, July 1950: TR 1053, 1951

(34) Schubauer, G. B., and Klebanoff, P. S., Investigation of separation of the turbulent boundary layer, NACA, TN 2133, Aug. 1950; TR 1030, 1951

(35) Corrsin, S., and Uberoi, M. S., Spectra and diffusion in a round turbulent jet, NACA, TN 2124, July 1950; TR 1040, 1951

(36) Millikan, C. B., A critical discussion of turbulent flows in channels and circular tubes, Proc. V Cong., Cambridge (Mass.), pp. 386-392, 1938

(37) von Mises, R., Some remarks on the laws of turbulent motion in tubes, Applied Mechanics, Theodore von Kármán Anniversary Volume, pp. 317-327, 1941

(38) Kampé de Fériet, J., Sur l'écoulement d'un fluide visquex incompressible entre deux plaques parallèles indéfines, Houille Blanche, Vol. 3, No. 6, pp. 509-517, Nov.-Dec. 1948

(39) von Kármán, T., Theorie des Reibungswiderstands, Hydromechanische Probleme des Schiffsantriebs, Hamburg, pp. 50-73, May 1932

(40) Fage, A., Profile and skin friction aerofoil drags, ARC, R & M 1852, April 1938

(41) Squire, H. B., and Young, A. D., The calculation of the profile drag of aerofoils, ARC, R & M 1838, Nov. 1937

(42) Schoenherr, K. E., Resistance of flat surfaces moving through a fluid, Transactions of the Society of Naval Architects and Marine Engineers, Vol. 40, pp. 279-313, 1932

(43) Schoenherr, K. E., Progress in the computation of the frictional resistance of ships, Massachusetts Institute of Technology, Cambridge, Symposium, Hydrodynamics in Modern Technology, pp. 101-110, June 1951

(44) Sheppard, P. A., The aerodynamic drag of the earth's surface and the value of von Kármán's constant in the lower atmosphere, PRSA, Vol. 188, No. 1013, pp. 208-222, Jan. 1947

(45) Kempf, G., Neue Ergebnisse der Widerstandsforschung, Werft-Reederei-Hafen, Vol. 10, No. 11, pp. 234-239; No. 12, pp. 247-253, 1929

(46) Falkner, V. M., A new law for calculating drag, Aircraft Engineering, Vol. 15, No. 169, pp. 65-69, March 1943

(47) Schultz-Grunow, F., Neues Reibungswiderstandsgesetz für glatte Platten, Luftfahrtforschung, Vol. 17, No. 8, pp. 239-246, Aug. 1940; translated as New frictional resistance law for smooth plates, NACA, TM 986, Sept. 1941

(48) Wieghardt, K., Erhöhung des turbulenten Reibungswiderstandes durch Oberflächenstörungen, ZWB, KWI, FB 1563, March 1942; translated as Increase of the turbulent frictional resistance caused by surface irregularities, British Reports and Translations No. MAP-VG-129T, June 1946

(49) Tillmann, W., Neue Widerstandsmessungen an Oberflächenstörungen in der turbulenten Reibungsschicht, ZWB, KWI, U & M 6619, Dec. 1944; translated as Additional measurements of the drag of surface irregularities in turbulent boundary layers, NACA, TM 1299, Jan. 1951

(50) Wieghardt, K., Zum Reibungswiderstand rauher Platten, ZWB, KWI, U & M 6612, Sept. 1944; see also Über die turbulente Strömung im Rohr und längs einer Platte, ZAMM, Vol. 24, No. 5/6, pp. 294-296, 1944

(51) Wieghardt, K., Über die Wandschubspannung in turbulenten Reibungsschichten bei veränderlichem aussendruck, ZWB, KWI, U & M 6603, Dec. 1943

(52) Wieghardt, K., and Tillmann, W., Zur turbulenten Reibungsschicht bei Druckanstieg, ZWB, KWI, U & M 6617, Nov. 1944; translated as On the turbulent friction layer for rising pressure, NACA, TM 1314, Oct. 1951

(53) Tillmann, W., Untersuchungen über Besonderheiten bei turbulenten Reibungsschichten an Platten, ZWB, KWI, U & M 6627, 1945; translated as Investigations of some particularities of turbulent boundary layers on plates, British Reports and Translations No. MAP-VG-34-45T, 1946; also as Interrogation Report BIGS-19 (CGD 497), Washington, D. C., 1946

(54) Tillmann, W., Über die Wandschubspannung turbulenter Reibungsschichten bei Druckanstieg, Göttingen, Thesis, 1947

(55) Ludwieg, H., Ein Gerät zur Messung der Wandschubspannung turbulenter Reibungsschichten, Ing.-Arch., Vol. 17, No. 3, pp. 207-218, 1949; translated as Instrument for measuring the wall shearing stress of turbulent boundary layers, NACA, TM 1284, May 1950

(56) Ludwieg, H., and Tillmann, W., Untersuchungen über die Wandschubspannung in turbulenten Reibungsschichten, Ing.-Arch., Vol. 17, No. 4, pp. 288-299, 1949; translated as Investigations of the wall shearing stress in turbulent boundary layers, NACA, TM 1285, May 1950

(57) Hama, F. R., The turbulent boundary layer along a flat plate, I and II (in Japanese), Reports of the Institute of Science and Technology, Tokyo Imperial University, Vol. 1, No. 1, pp. 13-16, No. 3-4, pp. 49-50, 1947

(58) Nikuradse, J., Gesetzmässigkeiten der turbulenten Strömung in glatten Rohren, VDI Forschungsheft 356, 1932; translated as Regularity of turbulent flow in smooth pipes, U.S. Navy Dept., Project Squid, Purdue University, Lafayette, Tech. Memo. Pur-11, Aug. 1949; summarized in Über turbulente Wasserströmungen in geraden Rohren bei sehr grossen Reynoldsschen Zahlen, Vorträge aus dem Gebiete der Aerodynamik und verwandte Gebiete, Aachen, pp. 63-69, 1929; translated as On turbulent hydraulic flow in straight pipes at very large Reynolds numbers, U.S. Navy Dept., David W. Taylor Model Basin, Translation 173

(59) Ross, D., Turbulent flow in smooth pipes; a re-analysis of Nikuradse's experiments, Ordnance Research Laboratory, Pennsylvania State College, Contract NOrd 7958, Sept. 1952

(60) Peters, H., A study in boundary layers, Proc. V Cong., Cambridge (Mass.), pp. 393-395, 1938

(61) Baines, W. D., An exploratory investigation of boundary layer development on smooth and rough surfaces, State University of Iowa, Iowa City, Thesis, Aug. 1950

(62) Nikuradse, J., Turbulente Reibungsschichten an der Platte, Monograph, ZWB, published by Oldenbourg, München and Berlin, 1942

(63) Ashkenas, H., Riddell, F., and Rott, N., An investigation of the turbulent boundary layer on a flat plate, Cornell University, Ithaca, Contract Rep. NAw-6014, June 1952 (to be published as NACA TN)

(64) van der Hegge Zijnen, B. G., Measurements of the velocity distribution in the boundary layer along a plane surface, Delft, Thesis, 1924; see also Burgers, J. M., The motion of a fluid in the boundary layer along a plane smooth surface, Proc. I Cong., Delft, pp. 113-128, 1924

(65) Landweber, L., A review of the theory of the frictional resistance of a smooth flat plate with turbulent boundary layers, U.S. Navy Dept., David W. Taylor Model Basin, Rep. 726, pp. 4-9, Sept. 1950

(66) Rotta, J., Über die Theorie der turbulenten Grenzschichten, Mitteilungen aus dem Max-Planck-Institut für Strömungsforschung, Göttingen, No. 1, 1950; translated as On the theory of the turbulent boundary layer, NACA, TM 1344, Feb. 1953; see also Beitrag zur Berechnung der turbulenten Grenzschichten, Ingenieur-Archiv, Vol. 19, No. 1, pp. 31-41, 1951; translated as Contribution to the calculation of turbulent boundary layers, U.S. Navy Dept., David W. Taylor Model Basin, Translation 242, Nov. 1951

(67) Baines, W. D., A literature survey of boundary layer development on smooth and rough surfaces at zero pressure gradient, State University of Iowa, Iowa City, Contract N8onr-500, 1951

(68) Deissler, R. G., Analytical and experimental investigation of adiabatic turbulent flow in smooth tubes, NACA, TN 2138, July 1950

(69) Wattendorf, F. L., and Kuethe, A. M., Investigations of turbulent flow by means of the hot-wire anemometer, Physics, Vol. 5, pp. 153-164, June 1934

(70) Corrsin, S., and Kistler, A. L., The free stream boundaries of turbulent flows, The Johns Hopkins University, Baltimore, Contract NAw-6093, Jan. 1953 (to be published as NACA TN)

(71) von Kármán, T., The problem of resistance in compressible fluids, Reale Accademia d'Italia, V Convegno della Fondazione Allesandro Volta, Rome, pp. 226-290, 1935

(72) Tucker, M., Approximate turbulent boundary layer development in plane compressible flow along thermally insulated surfaces with application to supersonic tunnel contour correction, NACA, TN 2045, March 1950

(73) Tucker, M., Approximate calculation of turbulent boundary layer development in compressible flow, NACA, TN 2337, April 1951

(74) Cope, W. F., The turbulent boundary layer in compressible flow, Great Britain, National Physical Laboratory, Rep. ARC 7634, 1943

(75) Monaghan, R. J., and Johnson, J. E., The measurement of heat transfer and skin friction at supersonic speeds, Part II. Boundary layer measurements on a flat plate at M = 2.5 and zero heat transfer, ARC, CP 64, Dec. 1949

(76) Monaghan, R. J., Comparison between experimental measurements and a suggested formula for the variation of turbulent skin friction in compressible flow, ARC, CP 45, Feb. 1950

(77) Kalikhman, L. E., The gas dynamic theory of heat transfer, Prikladnaia Matematika i Mekhanika, Vol. 10, pp. 449-474, 1946; translated as Gas dynamic theory of heat, Air Materiel Command, Dayton, Ohio, Rep. F-TS-1211-1A, Jan. 1949; also translated as Heat transmission in the boundary layer, NACA, TM 1229, April 1949

(78) Eckert, H. U., Characteristics of the turbulent boundary layer on a flat plate in compressible flow from measurements of friction in pipes, Engineering Division, Air Materiel Command, Dayton, Ohio, Oct. 1949; also in JAS, Vol. 17, No. 9, pp. 573-585, Sept. 1950

(79) Prandtl, L., Über den Reibungswiderstand strömender Luft, Ergebnisse der aerodynamischen Versuchsanstalt zu Göttingen, III Lieferung, pp. 1-5, 1927

(80) Wilson, R. E., Turbulent boundary layer characteristics at supersonic speeds - theory and experiment, DRL, UT, Rep. DRL221 (CM-569), Nov. 1949; also in JAS, Vol. 17, No. 9, pp. 585-594, Sept. 1950

(81) Frankl, F., and Voishel, V., Turbulent friction in the boundary layer of a flat plate in a two-dimensional compressible flow at high speeds, Central Aero-Hydrodynamical Institute, Moscow, Rep. 321, 1937; translated as NACA, TM 1053, Dec. 1943

(82) Rubesin, M. W., Maydew, R. C., and Varga, S. A., An analytical and experimental investigation of the skin friction of the turbulent boundary layer on a flat plate at supersonic speeds, NACA, TN 2305, Feb. 1951

(83) Clemmow, D. M., The turbulent boundary layer flow of a compressible fluid along a flat plate, British Directorate, Guided Weapons Research and Development, Rep. 50/6, Aug. 1950 (available from Collection and Dissemination Section, ORDGU-IN, OCO, Department of the Army, Rm. 1-C-460, Washington 25, D.C., as ID 753660)

(84) Van Driest, E. R., Turbulent boundary layer for compressible fluids on an insulated flat plate, North American Aviation Rep. AL-958, Sept. 1949; also The turbulent boundary layer for compressible fluids on a flat plate with heat transfer, North American Aviation Rep. AL-997, Jan. 1950; combined in Turbulent boundary layer in compressible fluids, JAS, Vol. 18, No. 3, pp. 145-160, March 1951

(85) Young, A. D., The equations of motion and energy and the velocity profile of a turbulent boundary layer in a compressible fluid, College of Aeronautics, Cranfield, Rep. 42, Jan 1951

(86) Wilson, R. E., Turbulent boundary layer flow on a smooth flat plate at supersonic speeds (with Discussion by E. R. Van Driest), unclassified paper in NavOrd Rep. 1651 (CONFIDENTIAL), Nov. 1951

(87) Li, T.-Y. and Nagamatsu, H. T., Effects of density fluctuations on the turbulent skin friction of an insulated flat plate at high supersonic speeds, GALCIT, Contract DA-04-495-Ord-19, Memo. 5, May 1951; abstracted in JAS, Vol. 18, No. 10, pp. 696-697, Oct. 1951

(88) Ferrari, C., Study of the boundary layer at supersonic speeds in turbulent flow; case of flow along a flat plate, CAL, CU, Rep. CAL/CM 507, Nov. 1948; also in Quarterly of Applied Mathematics, Vol. 8, No. 1, pp. 33-57, April 1950

(89) Ferrari, C., Comparison of theoretical and experimental results for the turbulent boundary layer in supersonic flow along a flat plate, CAL, CU Rep. CAL/CM 562, Sept. 1949; also in JAS, Vol. 18, No. 8, pp. 555-564, Aug. 1951

(90) Ferrari, C., The turbulent boundary layer in a compressible fluid with positive pressure gradient, CAL, CU, Rep. CAL/CM 560, Sept. 1949; also in JAS, Vol. 18, No. 7, pp. 460-477, July 1951

(91) Gompf, G., Supersonic nozzle design for viscous fluids, GALCIT, Thesis, 1949

(92) Jeffreys, H. and Jeffreys, B., Methods of mathematical physics, 2nd ed., Cambridge, 1950

(93) Thompson, M. J., A comparison of turbulent boundary layer characteristics in supersonic flow with the theories of von Kármán and Ferrari, DRL, UT, Rep. DRL 230 (CM-637), Sept. 1950

(94) Moretti, G., La teoria del trasporto turbolento, L'Aerotecnica, Vol. 27, No. 1, pp. 44-50, Feb. 1947

(95) Hirschfelder, J. O., Bird, R. B., and Spotz, E. S., Properties of gases and gas mixtures, Naval Ordnance Laboratory, Symposium on Aerothermodynamics, pp. 1-50, June 1949;

see also Viscosity and other physical properties of gases and gas mixtures, Transactions of the American Society of Mechanical Engineers, Vol. 71, pp. 921-937, Nov. 1949

(96) Kirkwood, T. F., Integral methods applied to a compressible boundary layer on an insulated flat plate parallel to the wind, GALCIT, Thesis, 1947

(97) Amano, T., On the turbulent boundary layer along the surface of a heated flat plate in a high-speed air flow (in Japanese), Central Aeronautical Research Institute, Japan, date unknown; translated as Wright-Patterson Air Force Base Rep. F-TS-5160-RE (ATI 58162)

(98) Donaldson, C duP., Skin friction and heat transfer through turbulent boundary layers for incompressible and compressible flows, 1952 HTFMI, Los Angeles, pp. 19-35, June 1952; see also On the form of the turbulent skin friction law and its extension to compressible flows, NACA, TN 2692, May 1952

(99) Squire, H. B., Reconsideration of the theory of free turbulence, Philosophical Magazine, 7th Series, Vol. 39, No. 288, pp. 1-20, Jan. 1948

(100) Lin, C. C. and Shen, S. F., Studies of von Kármán's similarity theory and its extension to compressible flows. A critical examination of similarity theory for incompressible flows, NACA, TN 2541, Nov. 1951

(101) Skinner, G. T., Mean speed measurements in two-dimensional, incompressible, fully developed turbulent channel flow, GALCIT, Thesis, 1951

(102) Ross, D. and Robertson, J. M., A superposition analysis of the turbulent boundary layer in an adverse pressure gradient, Journal of Applied Mechanics, Vol. 18, No. 1, pp. 95-100, March 1951

(103) Howarth, L., Concerning the effect of compressibility on laminar boundary layers and their separation, PRSA, Vol. 194, No. 1036, pp. 16-42, July 1948

(104) Ginsburgh, A. S., Supersonic skin friction drag measurements at a Mach number of 1.72, United Aircraft Corporation, Project Meteor, Rep. UAC-17, Feb. 1948

(105) Hakkinen, R. J., Measurements of skin friction in turbulent boundary layers at transsonic speeds, GALCIT, Thesis, 1953

(106) Weiler, J. E. and Hartwig, W. H., The direct determination of local skin friction coefficient, DRL, UT, Rep. DRL-295 (CF-1747), Jan. 1952

(107) Eimer, M., Experimental skin friction at hypersonic Mach numbers, GALCIT, Thesis, 1953

(108) Bradfield, W. S., DeCoursin, D. G., and Blumer, C. B., Characteristics of laminar and turbulent boundary layer at supersonic velocity, Institute of Technology, University of Minnesota, Minneapolis, Research Rep. 83, July 1952

(109) Chapman, D. R. and Kester, R. H., Direct force measurements of turbulent skin friction on cylinders in axial flow at subsonic and supersonic velocities, NACA, Jan. 1953 (paper presented at Institute of the Aeronautical Sciences Annual Meeting, New York, Jan 1953)

(110) Schaevitz, H., The linear variable differential transformer, Proceedings of the Society for Experimental Stress Analysis, Vol. 4, No. 2, pp. 79-88, 1947

(111) Eastman, F. S., Flexure pivots to replace knife edges and ball bearings, Engineering Experiment Station, University of Washington, Seattle, Bulletin No. 86, Nov. 1935

(112) Shires, G. L., The viscid flow of air in a narrow slot, ARC, CP13, Dec. 1948

(113) Spivack, H. M., Experiments in the turbulent boundary layer of a supersonic flow, North American Aviation Rep. AL-1052, Jan. 1950

(114) Wegener, P. P., Winkler, E. M., and Sibulkin, M., A measurement of turbulent boundary layer profiles and heat transfer coefficient at M = 7, JAS, Vol. 20, No. 3, pp. 221-222, March 1953

(115) Monaghan, R. J. and Cooke, J. R., The measurement of heat transfer and skin friction at supersonic speeds, Part III. Measurements of overall heat transfer and of the associated boundary layers on a flat plate at M = 2.43, Royal Aircraft Establishment, Farnborough, Tech. Note Aero. 2129, Dec. 1951

(116) Wildhack, W. A., A versatile pneumatic instrument based on critical flow, Reviews of Scientific Instruments, Vol. 21, No. 1, pp. 25-30, Jan. 1950

(117) Blackshear, P. L., Sonic flow orifice temperature probe for high gas temperature measurements, NACA, TN 2167, Sept. 1950

(118) Wilson, R. E. and Young, E. C., Aerodynamic interference of pitot tubes in a turbulent boundary layer at supersonic speed, DRL, UT, Rep. DRL 228 (CM-1351), Dec. 1949

(119) Schurmeier, H. M. and Riise, H. N., Aerodynamic calibration of the flexible nozzle of the J.P.L. 20-inch supersonic wind tunnel, Jet Propulsion Laboratory, California Institute of Technology, Pasadena, Rep. 20-68 (to be published)

(120) Fage, A. and Sargent, R. F., An air-injection method of fixing transition from laminar to turbulent flow in a boundary layer, ARC, R & M 2106, June 1944

(121) Pfenninger, W., Untersuchungen über Reibungsverminderungen an Tragflügeln, insbesondere mit Hilfe von Grenzschichtabsaugung, Institut für Aerodynamik, Eidgenössische Technische Hochschule, Zürich, Mitteilungen 13, 1946; translated as Investigations on reductions of friction on wings, in particular by means of boundary layer suction, NACA, TM 1181, Aug. 1947

(122) Hall, A. A. and Hislop, G. S., Experiments on the transition of the laminar boundary layer on a flat plate, ARC, R & M 1813, Aug. 1938

(123) Stanton, T. E., On the effect of air compression on drag and pressure distribution on cylinders of infinite aspect ratio, ARC, R & M 1210, 1928

(124) Busemann, A. and Walchner, O., Profileigenschaften bei Überschallgeschwindigkeit, Forschung auf dem Gebiete des Ingenieurwesens, Vol. 4, No. 2, pp. 87-92, 1933; translated as Airfoil characteristics at supersonic speeds, Ministry of Aircraft Production, RTP Translation 1786

(125) Eula, A., L'influenza del numero di Reynolds ai grandi numeri di Mach, L'Aerotecnica, Vol. 20, No. 1, pp. 20-29, 1940

(126) Alperin, M., A study of detached shock waves in two dimensions, GALCIT, Thesis, 1950

(127) Young, G. B. W. and Janssen, E., The compressible boundary layer, Rand Corporation, Rep. P-214, June 1951; also in JAS, Vol. 19, No. 4, pp. 229-236, April 1952

(128) Coles, D., Direct measurement of supersonic skin friction, JAS, Vol. 19, No. 10, p. 717, Oct. 1952